THE UNIVERSITY
of EDINBURGH

Inter-organ signalling by hepatocyte-derived microRNA-122

Olivia Fay Matthews

Doctor of Philosophy (PhD)

The University of Edinburgh

2020

Declaration

I declare that the work presented in this thesis is entirely my own with the exception of:

- Chapter 3 and 4- Timothy Kendall provided blinded assessments of the liver and spleen and Graeme Reid provided blinded assessments of the kidney histology.
- Chapter 3 and 4 - ALT assays were carried out by the University specialist assay service facilities.

This work has not previously been submitted for any degree or professional qualification

Olivia Fay Matthews

Acknowledgments

I would like to thank the many people who have contributed to the work presented in this thesis. A special thank you to:

- Medical Research Scotland and AstraZeneca for the financial and material support of my PhD studentship.
- CVS students and staff, particularly the BDD group, for their support and advice. It has been a pleasure working with you.
- Dominic Williams, Rebecca Sargeant, Abhishek Srivastava, Helen Rollison and colleagues for the opportunity to work in your lab and supporting my research.
- Professor Neil Henderson, my second supervisor and Dr Laura Denby for their technical help, scientific knowledge and pastoral support.
- Finally, my supervisor James Dear for his optimism, encouragement and support throughout my PhD. I am forever grateful for the guidance and opportunities he has provided me to develop as a scientist.

I would like to dedicate my work to:

- My parents and brother who have supported me and believed in me from the beginning. Thank you for your understanding and encouragement.
- Fraser, for the endless support from listening to my practice presentations to keeping me sane as I wrote my thesis.
- My friends, for cheering me on and being great company.

Abstract

MicroRNAs (miRNAs) are small non-protein coding RNA species involved in the regulation of gene expression. Bound to either protein or encapsulated in extracellular vesicles (EVs), miRNA are released from the cell and found within biological fluids. Following release, miRNAs have shown to play a role in cellular communication *in vitro* and to a lesser extent *in vivo*. The studies described in this thesis aimed to investigate the organ uptake of the hepatocyte enriched miRNA, miR-122, *in vivo* during in the absence and presence of paracetamol-related drug induced liver injury (DILI). As it is known that kidney tubules can internalise EVs containing miRNA, it was hypothesised that miR-122 released from the liver during paracetamol-related DILI, enters the kidney and has a protective role against subsequent injury.

The production of miRNA is reliant on the activity of the cytoplasmic enzyme Dicer. To induced Dicer1 knockdown, *Dicer1* $^{flox/flox}$ mice were treated with a hepatotropic Cre-AAV8 or its negative control Null-AAV8. In this model, investigation of Dicer expression via western blotting and RT-qPCR indicated a significant loss of Dicer in the liver one week following Cre-AAV8 treatment. Consequently, a time dependent loss of total hepatic miRNA was observed using RT-qPCR and *in situ* hybridisation. Cre-recombinase delivery was confirmed to be liver-specific with stable Dicer and organ-enriched miRNA expression in the spleen, kidney, heart, lung and brain.

In the absence of DILI, It was found that the loss of total miRNA in the liver resulted in a significant reduction of miR-122 expression in the spleen and kidney. During paracetamol-induced liver injury, the well described increase of miR-122 in the circulation was not observed in the Cre-AAV8 treated mice. Subsequently, the increase of miR-122 expression in the spleen, kidney and heart was significantly diminished with the loss of hepatic miRNA production. Depletion of miR-122 resulted in an increase of CYP2E1 expression and activity in the liver and kidney following 300mg/kg paracetamol.

Therefore, these findings show that under normal physiological conditions, expression of miR-122 in the spleen and kidney is reliant on miRNA transfer from the

liver. During paracetamol induced hepatotoxicity, the mechanism of miR-122 signalling is upregulated and extends to the heart. Lastly, the observed upregulation of CYP2E1 following a loss of miR-122 in the kidneys indicates hepatic miRNA plays a role in regulating drug metabolism in the kidney.

Lay summary

Liver injury is a disease which can develop into liver failure and can be life-threatening. Paracetamol, also known as acetaminophen, is the leading cause of liver injury in the western world. To diagnose paracetamol toxicity, blood samples are taken and analysed for markers of liver injury. Previous studies have shown that molecules called microRNA are released from the injured liver into the bloodstream. MicroRNAs are important in the body because they block the conversion of DNA into a functional product, for example a protein.

MicroRNA-122 (miR-122) is normally found in the liver at very high concentrations, with little-to-none found in other organs. Previous studies have shown that during a paracetamol overdose, patients have a 100 times greater concentration of miR-122 in their bloodstream than a healthy patient. Due to this, miR-122 can be measured in patients to determine whether they require treatment for liver injury. However, it is unknown what happens to miR-122 after it is released into the bloodstream. Thus, this thesis explored which organs are responsible for the uptake of miR-122 from the bloodstream. Furthermore, it was investigated whether miR-122 impacts the gene function following its uptake into other organs.

From the experiments described in this thesis, it was discovered that in health and during a paracetamol overdose, the kidney and spleen were responsible for the uptake of miR-122 from the bloodstream. In addition, once transferred from the liver to the kidney, miR-122 was found to decrease the concentration and activity of enzymes involved in the breakdown of drugs. This highlights that liver-derived miR-122 plays a role in the metabolism of drugs and response to drug toxicity in the kidney.

List of Achievements

- Member of the CVS BHF Fundraising Team. 2017-2020
- Student demonstrator and tutor at the University of Edinburgh 2017-2020.
- STEM ambassador and a member of the BHF Scotland School Outreach Programme 2017-2020.
- Social secretary of Little France Postgraduate Society 2017-2019

Publications

Matthews O, Morrison EE, Tranter JD, Starkey Lewis P, Toor IS, Srivastava A, Sargeant R, Rollison H, Matchett KP, Kendall TJ, Gray GA, Goldring C, Park K, Denby L, Dhaun N, Bailey MA, Henderson NC, Williams D, Dear JW. Transfer of hepatocellular microRNA regulates cytochrome P450 2E1 in renal tubular cells. EBioMedicine. 2020 Dec; 62:103092. doi: 10.1016/j.ebiom.2020.103092. Epub 2020 Nov 21. PMID: 33232872; PMCID: PMC7689533.

Conference presentations

- *Transfer of hepatocellular microRNA regulates cytochrome P450 enzymes in renal tubular cells*. Oral presentation at the SOT 59th Annual meeting 2020, Society of Toxicology (cancelled due to Covid-19).
- *Transfer of hepatocellular microRNA regulates cytochrome P450 2E1 in renal tubule*s. Oral presentation at Pharmacology 2019, British Pharmacological Society.
- *Hepatocyte-renal signalling of miR-122*". Poster presentation at the ediRNA Meeting 2019.
- *MicroRNA-122 is transferred from liver to kidney and spleen in vivo: a new signalling mechanism and biomarker clearance pathway*. Oral presentation at the Pharmacology 2018, British Pharmacological Society.

Awards and funding

- Awarded the 2020 CVS Public Engagement Award for involvement in the BHF-STEM outreach program.
- Awarded Associate Fellow of the Higher Education Academy, 2020.

- Graduate Student Travel Support from the Society of Toxicology 59th Annual meeting 2020.
- Oral Communications Prize at the Pharmacology 2019, British Pharmacological Society.
- Travel grants from British Pharmacological Society for attendance at Pharmacology 2018 and 2019.

List of Tables

List of Figures

Abbreviations

ΔCT	Delta cycle threshold
°C	Degrees Celsius
α-SMA	alpha smooth muscle actin
AAV8	Adeno-associated virus serotype-8
ADAM10	A distintegrin and metalloprotease family 10
Ago2	Argonaute 2
Aldoa	Aldolase A
ALF	Acute liver failure
ALI	Acute liver injury
ALT	Alanine transaminase
ANOVA	Analysis of variance
AST	Aspartate transaminase
ATP	Adenosine triphosphate
AUC	Area under the curve
BCA	Bicinchoninic acid assay
CCl_4	Carbon tetrachloride
CCNG1	Cyclin G1
cDNA	Complementary DNA
COL1A1	α1 type I collagen
CUTL1	Cut-like homeobox 1
Cre-AAV8	Cre containing AAV8
Ct	Cycle threshold

CYP450	Cytochrome P450
DAMPS	Damage-associated molecular patterns
DILI	Drug-induced liver injury
DGCR8	DiGeorge Syndrome Critical Region 8
DNA	Deoxyribonucleic acid
Epo	Erythropoietin
EVs	Extracellular vesicles
FN1	Fibronectin 1
FOXO3	Forkhead box O3
HCC	Hepatocellular carcinoma
HCV	Hepatitis C virus
HDL	High density lipoprotein
HMGB1	High mobility group box 1
Hmgcr	3-hydroxy-3-methylglutaryl-CoA-reductase
HSC	Hepatic stellate cells
IGF-1R	Insulin-like growth factor 1 receptor
IHC	Immunohistochemistry
ISH	In situ hybridisation
KIM1	Kidney injury marker 1
LDL	Low density lipoprotein
miR-122	MicroRNA-122
miRNA	MicroRNA

mRNA	Messenger ribonucleic acid
NAC	N-acetylcysteine
NAPQI	N-acetyl-p-benzoquinone-imine
NDRG3	N-myc downstream-regulated gene 3 protein
NPM1	Nucleophosmin-1
NPV	Negative predictive value
Null-AAV8	Empty AAV8
nSMase2	Neutral sphingomyelinase 2
OCT	Optimal cutting temperature
PACT	Protein activator of dsRNA-dependent protein kinase
Pol II/III	RNA polymerase II/III
Pre-miRNA	Precursor miRNA
Pri-miRNA	Primary miRNA
PPV	Positive predictive value
RISC	RNA-induced silencing complex
RLC	RISC loading complex
ROC	Receiver Operator Characteristic
ROS	Reactive oxygen species
RNA	Ribonucleic acid
RT-qPCR	Real-Time Quantitative Reverse Transcription PCR
SD	Standard deviation
SRF	Serum response factor

TBG	Thyroid hormone-binding globulin
TMED3	Transmembrane P24 Trafficking Protein 3
TRBP2	Trans-activation response RNA-binding protein

Contents

Chapter 1 Introduction

1.1 Liver function

The liver performs a wide variety of vital functions for the maintenance of normal homeostasis. It plays a major role in the metabolism of key nutrients including carbohydrates (gluconeogenesis) and lipids (fatty acid oxidation) [1]. The liver also synthesises key proteins comprising of albumin and most clotting factors including prothrombin, fibrinogen and factors V, VII, VIII, IX, X, XI and XII [1, 2]. Bile acids are synthesised and secreted from the liver to aid digestion [3]. Furthermore, the liver is important for the modification (biotransformation) of endogenous and exogenous compounds into water soluble compounds for excretion in the bile and urine[1]. Thus, it is unsurprising that the disruption and decline of normal liver function is associated with high morbidity and mortality.

1.2 Acute liver failure

Acute liver failure (ALF) is the severe clinical manifestation of acute hepatocyte injury, that has evolved over days or weeks, in the absence of chronic liver disease [4]. ALF is a rare event, with an incidence between 1 to 6 cases per million people each year in the western world [5, 6]. Historically, ALF had a fatality rate of around 80% [4]. However, with improvements in intensive care support and access to liver transplantation, short-term survival has increased to 67% [7].

ALF is characterised by an unexpected and rapid loss of hepatic function (metabolic and immunological) that regularly progresses into hepatic encephalopathy, coagulopathy and multi-organ failure [8]. Hence, to help distinguish the cause of disease, potential complications and patient prognosis, ALF has been divided into three groups based on the onset of jaundice and encephalopathy. These groups are: hyperacute (0-7 days), acute (1-4 weeks) and subacute (4-12 weeks) [8, 9]. There are several important factors for the prognosis of patients with ALF. The most widely accepted criteria are the King's College criteria which factors age, cause, duration of jaundice, INR and serum bilirubin levels [10, 11]. Hyperacute cases are identified by high aminotransferase and low bilirubin concentrations, whereas the acute and subacute have lower aminotransferase and higher bilirubin levels [4, 8, 9]. In general, hyperacute

patients have a greater chance of short-term survival than the patients with slower progressing liver injury [4, 8, 9].

The onset of ALF has been linked to multiple causes including drug induced liver injury (DILI), viral hepatitis, ischemia and autoimmunity [4, 8]. However, the main causes of ALF varies between the developing and developed world. In the developing world, the main cause of ALF is believed to be viral hepatitis A, B and E [4, 8]. Whereas, in the developed world, including USA and UK, the main causes of ALF is paracetamol (also known as acetaminophen, APAP) toxicity and DILI [4, 8, 12, 13].

1.3 Drug-induced liver injury

DILI describes the abnormalities in liver function tests associated with the intake of medication [14, 15]. The histological phenotypes of DILI are diverse and have been stratified into 12 patterns [16]. However, accounting for around 80% of observed cases in a large study, the most frequently observed phenotypes of DILI are presented as: acute and chronic hepatitis, acute and chronic cholestasis, and cholestatic hepatitis [17]. Hence, DILI frequently resembles acute and chronic liver disease. There are two forms of DILI based on their predictability and dose-dependency: idiosyncratic and intrinsic [14].

Idiosyncratic DILI is regularly described to be an unpredictable and unpreventable form of DILI [16, 18]. Its pathogenesis is not well understood as it has an unclear and complex dose-response relationship, with a variable latency period from weeks to months [19]. Additionally, it has been observed that the risk of developing idiosyncratic liver injury varies between individuals and is influenced by environmental (including lifestyle and alcohol consumption), host (such as age, race, genetics and sex) and drug factors (for example dosage and drug-drug interactions) [18]. However, some drugs cause idiosyncratic DILI more than often than others. Cases have been observed across an array of drugs with differing drug actions including antibiotics, anticonvulsants and analgesics in current use. These include: amoxicillin-clavulanic acid, valproic acid, isoniazid and minocycline [20, 21].

In the UK, around 10% of DILI cases are due to idiosyncratic injury [20]. Nevertheless, the cases of idiosyncratic DILI are rare, occurring in 13.9-19.1 cases in 100,000 patients per year [22, 23]. Due to this, it is infrequently detected in pre-clinical and clinical trials due to the limited number of subjects in the studies [18, 24]. Thus, this form of DILI has a major impact on the drug development industry, with it being a reason for implementing regulatory actions, such as black box warnings and drug withdrawals [25, 26].

On the other hand, intrinsic DILI is predictable, reproducible in preclinical models and appears after a short latency period (hours to days) [16, 27]. Examples of drugs that can induce intrinsic DILI include aspirin, methotrexate and paracetamol at high doses[24]. However, paracetamol is the leading cause of DILI and ALF in the UK and USA [12, 21, 28-30]. With it accounting for 38,000 hospital admissions in England alone (2010-2011), paracetamol surpasses cases of idiosyncratic DILI reaching ALF by four fold [31].

1.4 Mechanism of paracetamol-induced liver injury

Paracetamol is the most commonly used antipyretic and analgesic in the western world [32]. It is widely available, found in more than 600 different prescriptions and over-the-counter medications including pain relievers, cough, cold and anti-allergy medication [33]. Although considered safe at therapeutic doses (4g/day), an unintentional (multiple moderate) or intentional (single severe) overdose can cause significant liver injury and in some cases progress to ALF [29].

Following therapeutic administration, around 25% of the dose undergoes “first pass” metabolism, predominantly in the liver [34]. Upon entering the liver, paracetamol enters the hepatocytes mainly via passive diffusion and subsequently forms conjugates with glucuronic acid (40-67%) and sulfate (20-46%)[35, 36] (Figure 1.1). This in turn leads to the formation of an inactive metabolite for excretion [32, 37]. However, a small percentage (<5%) is converted to a reactive metabolite, N-acetyl-*p*-benzoquinone-imine (NAPQI) via cytochrome P450 (CYP450) oxidation [36]. Nonetheless, the small fraction of NAPQI produced is detoxified through glutathione conjugation and eliminated in the urine and bile [32].

The mechanism of paracetamol toxicity is well defined (Figure 1.1). In excess, paracetamol overwhelms the conjugation pathway and oxidisation by the CYP450 enzymes becomes the leading route of metabolism [38, 39]. Subsequently, excessive NAPQI production leads to the depletion of glutathione stores [38, 39]. Hepatocyte injury occurs when glutathione stores are depleted to 30%, allowing the reactive metabolite to react with alternative targets [40]. NAPQI has been described to react with nucleophilic macromolecules, proteins, DNA and unsaturated lipids [40]. Additionally, these cellular events lead to mitochondrial dysfunction following NAPQI binding to mitochondrial proteins, production of reactive oxygen species (ROS), inhibition of mitochondrial respiration and a loss in ATP production [41, 42]. Furthermore, the reduction in mitochondrial function is associated with oxidative stress, resulting in necrosis and programmed cell death (apoptosis) [37, 43]. An inflammatory response then follows cell death which can determine the extent of tissue necrosis and risk of organ failure [43]. The CYP450 enzymes are concentrated in the centrilobular zone (zone III) of the liver [40, 44]. Hence, this is the most affected area of paracetamol-induced liver injury due to the greater oxidative capacity of hepatocytes in this zone. However, in extreme doses of paracetamol, necrosis can spread to the pericentral zone (zone I) and midlobular zone (zone II)[40].

The antidote for paracetamol toxicity is N-acetylcysteine (NAC) which replenishes glutathione stores and neutralises NAPQI present in the liver [37, 40](Figure 1.1). When administered within around 8 hours of drug ingestion, NAC is highly effective at preventing hepatic injury [45]. However, delayed treatment significantly reduces its efficacy [45].

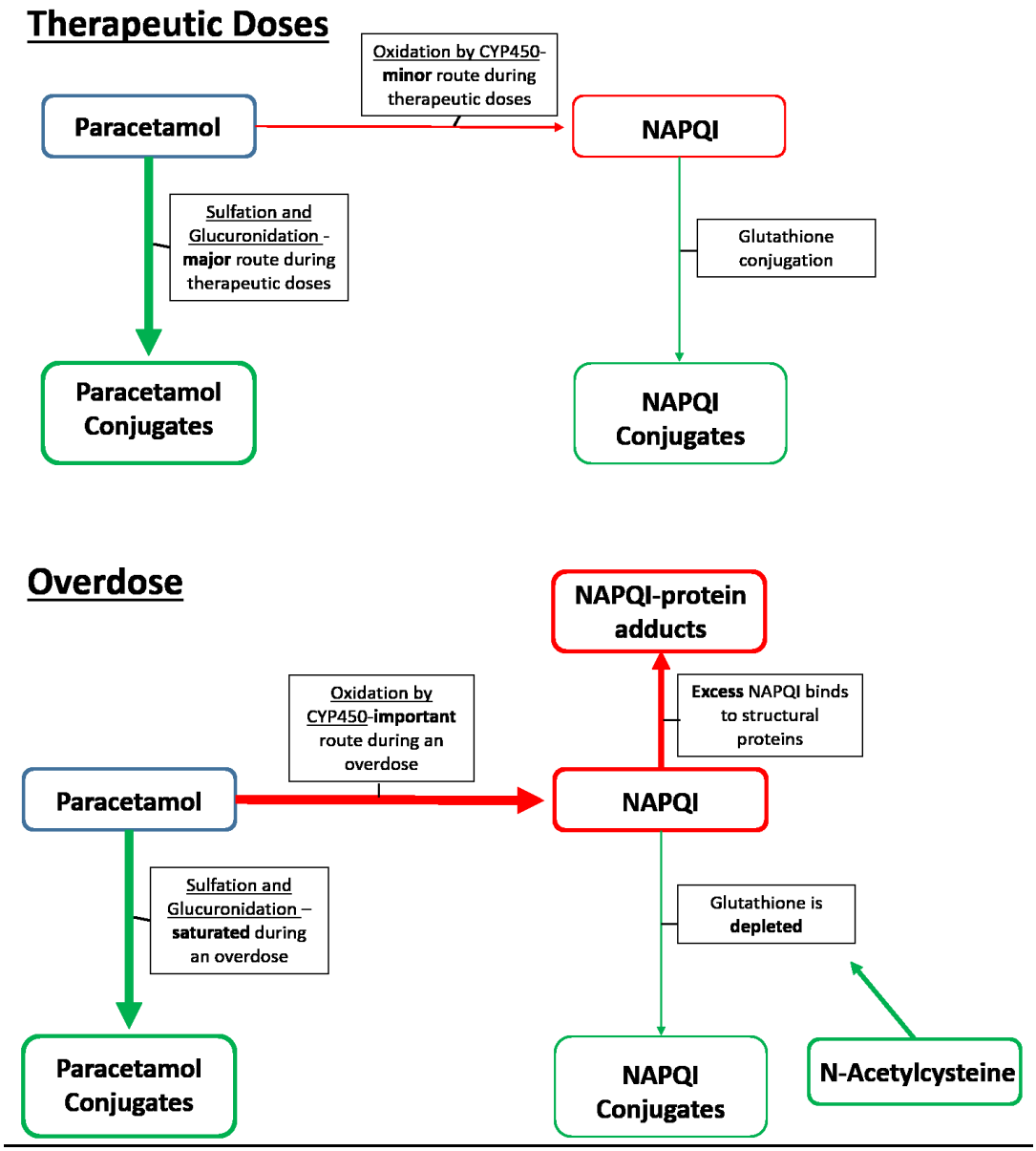

Figure 1.1 Mechanism of paracetamol metabolism and toxicity following a therapeutic dose and an overdose.

Following therapeutic doses, the major pathways of paracetamol metabolism are glucoronidation and sulfation. The non-toxic products are then eliminated in the bile and urine. However, a small percentage is converted to the toxic metabolite NAPQI, which is detoxified by glutathione conjugation. During an overdose, the primary pathway of metabolism is saturated and the glutathione stores are depleted.

Furthermore, the accumulation of NAPQI leads to oxidative stress, liver injury and cell death. Diagram adapted from Vliegenthart et al. [46].

1.5 Cytochrome P450 (CYP450) enzymes

CYP450 enzymes are a superfamily of haem-containing enzymes classified by similar gene sequence, then assigned into family number (e.g. CYP2), subfamily letter (e.g. CYP2E) and differentiated by isoform number (e.g. CYP2E1) [47]. Different members of the CYP450 superfamily have distinct, but often overlapping substrate specificities [47]. CYP450 enzymes are predominantly found in the liver, but have been described to be expressed throughout the body, including the lung and kidney [48-52]. Here, they play an important role in the oxidation of endogenous compounds, environmental xenobiotics and pharmacological agents [53]. However, not all of the 57 human CYP450 enzymes are involved in drug metabolism [54]. In humans, it has been reported that six CYP450 enzymes: 1A2, 2C9, 2C19, 2D6, 2E1 and 3A4/5 account for around 75% of drug metabolism [54, 55].

Intrinsic and extrinsic factors have been described to influence the expression and activity of the CYP450 enzymes. While genetic polymorphisms have been recognised to play a major role in the variability of a few CYP450 enzymes, most are controlled by sex, age, hormonal and diurnal factors [55]. Extrinsic factors such as xenobiotic exposure and environmental factors can inhibit and induce CYP450 activity [54]. Furthermore, it has been identified that xenobiotic receptors, AhR (aryl hydrocarbon receptor), PXR (pregnane X receptor) and CAR (constitutive androstane receptor) are activated in the presence of toxic compounds derived from endogenous and exogenous xenobiotics [56]. Once activated, they have been observed to regulate the expression of drug metabolising enzymes, including the CYP450 enzymes. AhR has been described to regulate CYP1A1 and CYP1B1, whilst CAR and PXR have been reported to regulate multiple CYP450 enzymes including CYP2B and 3A subfamilies [57-60].

1.5.1 CYP450 enzymatic activity following paracetamol administration

The CYP450 isoforms described to have a central role in the oxidation of paracetamol are: CYP2E1, CYP1A2, CYP3A4 and CYP2A6 [61, 62]. CYP2E1 is frequently described to have the greatest influence on the metabolism of paracetamol into NAPQI. Multiple studies have highlighted that changes in CYP2E1 expression and activity can significantly alter the rate of paracetamol oxidation [63, 64]. Additionally, the knockdown of CYP2E1 has been observed to induce resistance to paracetamol toxicity [65, 66]. Hence, it was hypothesised that inhibiting CYP2E1 could be a promising therapy in minimising NAPQI formation and liver toxicity following a paracetamol overdose. This hypothesis was tested in a study using fomepizole (4-methylpyrazole, 4MP), a direct inhibitor of CYP2E1, alongside a treatment of 300mg/kg paracetamol in C57/BL6 mice [67]. Here, the inhibition of CYP2E1 was shown to prevent the depletion of GSH, reduce the formation of ROS and thus paracetamol toxicity [67]. In addition, these findings have been confirmed in humans, demonstrating that fomepizole treatment prevents the biotransformation of paracetamol to NAPQI [68]. However, fomepizole needs to be administered as early as possible to inhibit the drug metabolism phase and has limited benefits to patients presenting with significant liver injury [67].

Nonetheless, the importance of CYP1A2 during paracetamol toxicity has been demonstrated by CYP2E1 and CYP1A2 knockout mice displaying a significant resistance to paracetamol toxicity [38]. The contribution of CYP3A4 in paracetamol toxicity has also been indicated in alcohol-enhanced paracetamol toxicity studies[69]. Furthermore, it has been suggested that with increasing doses of paracetamol, the contribution of CYP2E1 in the formation of NAPQI decreases, indicating CYP1A2 and CYP3A4, significantly contributes to NAPQI production at higher doses [70].

1.6 ALT as a biomarker of paracetamol-induced liver injury

During hepatocyte injury, alanine aminotransferase (ALT) is released into the circulation following the leakage and rupture of hepatocytes [71, 72]. Currently, serum ALT is the most commonly used diagnostic measure for suspected hepatotoxicity, including paracetamol toxicity [73, 74]. ALT has never been formally qualified as a

biomarker, however, it has been validated by decades of clinical use [75]. Despite this, ALT is unable to prognosticate early onset DILI due to its lack of specificity and sensitivity to hepatotoxicity [46, 74].

The majority of patients (90%) present to the emergency department within 12 hours of drug overdose [76]. However, ALT on average takes 12-24 hours to significantly increase during paracetamol-induced hepatotoxicity [77]. Hence, to confidently exclude the development of hepatic injury using ALT, it is required to delay the measurement of ALT for at least 24 hours after the time of overdose [74]. As a consequence, there is an increase in the length of hospital stays and it limits patient stratification in an emergency care setting [74]. In addition, elevation of ALT is not limited to DILI. Circulating ALT rises in a range of acute and chronic liver diseases and in co-morbidities such as diabetes, heart failure and alcohol excess [46, 78]. Therefore, these limitations have highlighted the clinical need for new and improved biomarkers of DILI to be used in conjunction with or instead of the current biomarkers. Recently, new mechanistic and predictive biomarkers of DILI have been identified. These include keratin-18 (K18), high-mobility group box-1 (HMGB1) and microRNA-122 (miR-122)(Table 1.1) [46].

Table 1.1 Current and emerging biomarkers of paracetamol-induced liver injury

Biomarker	Biomarker utility	Advantages	Disadvantages	Ref
Current biomarkers				
Alanine transaminase (ALT)	Elevations associated with hepatocellular injury	• Reflects hepatocellular necrosis. • Abundant in the liver. • Prognostic value	• Doesn't provide mechanistic understanding of injury. • Increase occurs during myocardial infarction and exercise. • Long half-life.	[75, 79]
Aspartate transaminase (AST)	Elevations associated with hepatocellular injury	• Reflects hepatocellular necrosis. • Prognostic value	• Not liver specific. Abundant in the heart, kidneys and brain. • Long half-life.	[46, 73]
Emerging biomarkers				
Alpha-fetoprotein (AFP)	Loss of circulating ALF is associated with poor prognosis	• Highly enriched in liver progenitor cells. • Indicative of DILI prognosis.	• Doesn't provide mechanistic understanding of injury	[80, 81]
Caspase cleaved cytokeratin 18 /cytokeratin 18 (ccK18/K18)	Elevations represent liver inflammation and their ratio could be used to assess extent of hepatocellular apoptosis and necrosis	• Early detection during DILI • Indicative of DILI prognosis • Provides information on mechanism of cell death	• Ubiquitously expressed-not liver specific • Increases in other diseases	[82, 83]

Biomarker	Biomarker utility	• Advantages	• Disadvantages	Ref
Glutamate dehydrogenase (GLDH)	Elevations associated with mitochondrial dysfunction and hepatocellular injury.	• Liver enriched • Early detection of DILI • Not influenced by age and gender (low intra- and inter- subject variation)	• Elevated levels have been observed in absence of hepatocellular injury.	[82, 84]
High mobility group box-1 (HMGB1)	Acts as a mediator of inflammation and its acetylated form acts as a biomarker of liver injury	• Early detection of DILI • Indicative of DILI prognosis • Quick clearance	• Ubiquitous expression	[82, 85]
MicroRNA-122 (miR-122)	Elevations associated with hepatocellular necrosis.	• Liver enriched • Early detection of DILI • Quick clearance • Doesn't increase following muscular injury	• Doesn't provide mechanistic understanding of injury.	[86, 87]
Osteopontin (OPN)	Acts as a pro-inflammatory cytokine, attracting neutrophils, lymphocytes and macrophages to sites of hepatic injury.	• Indicative of DILI prognosis • Associated with the degree of liver necrosis	• Broad localisation	[88]
Sorbitol dehydrogenase (SDH)	Elevated during acute and mild liver injury.	• Early recognition of DILI • Abundant in the liver • Short half-life	• Not liver specific- high expression in the kidney and testis • Not indicative of DILI prognosis	[89]

Table adapted from Fu et al. [73]

1.6.1 Biomarkers of paracetamol-induced kidney injury

Injury induced by paracetamol toxicity is predominantly found in the liver [37]. Nevertheless, a paracetamol overdose can induce renal insufficiency in 1-2% of patients [43]. This has a significant clinical impact as it leads to a substantial increase in mortality in this subset of patients [90]. Hence, kidney function, determined by serum creatinine concentration, is included in the Kings College Criteria for liver transplantation [91]. Additionally, kidney injury marker-1 (KIM-1), a kidney specific biomarker with greater sensitivity than serum creatinine, has been newly proposed as a biomarker, enhancing prognosis studies in patients with paracetamol-induced liver injury [92].

1.7 MicroRNA

MicroRNA's (miRNA's) are a class of small (~22 nucleotides), non-protein coding RNA species conserved in their sequence across mammals, plants and viruses [93]. MiRNA's role in the regulation of post-transcriptional gene expression is well recognised and estimated to modulate over half of human genes [94-96]. In addition to their role inside the cell, miRNA are found extracellularly, within the human circulation.

1.7.1 MicroRNA biogenesis

Within the genome, miRNA transcripts are primarily found in the exonic and intronic regions [97]. The remaining transcripts are intergenic, transcribed and regulated independently from a host gene [98]. The initial steps of miRNA processing occurs within the nucleus of the cell. Then, the precursors are exported into the cytoplasm for further processing into its mature functional form [97, 98](Figure 1.2).

1.7.2 MicroRNA processing in the nucleus

The transcription of miRNA has shown to be coordinated by transcription factors or upon the methylation of their promotor sequences [99, 100]. MiRNA biogenesis starts with the RNA polymerase II (Pol II) or RNA polymerase III (Pol III) mediated transcription of the miRNA gene into primary transcript (pri-miRNA), a long hairpin structure containing the mature sequence [95, 101, 102]. Next, the pri-miRNA is processed by the microprocessor complex composed of the ribonuclease, Drosha, and RNA-binding protein, DiGeorge Syndrome Critical Region 8 (DGCR8). DGCR8

recognises the N6-methyladenosine motif within the pri-miRNA, while Drosha is responsible for the cleavage at the base of the pri-miRNA [103]. This results in the removal of its 5'- cap and 3'- poly A tail and the formation of the precursor miRNA (pre-miRNA) with a two-nucleotide-long 3' overhang [104](Figure 1.2).

1.7.3 MicroRNA processing and maturation in the cytoplasm

The subsequent shorter miRNA strand, pre-miRNA, (~60-70 nucleotides) is exported into the cytoplasm by exportin 5-Ran-GTP complex and undergoes further processing by the RNase III endonuclease Dicer [94, 105]. Dicer, along with its cofactors TRBP2 (trans-activation response RNA-binding protein) and PACT (protein activator of dsRNA-dependent protein kinase), preferentially binds to the two-nucleotide-long 3' overhang of the pre-miRNA and cuts out the duplex RNA (~22 nucleotides) from the pre-miRNA. As a result, mature miRNA is formed. The miRNA-5p strand derives from the 5' end of the pre-miRNA hairpin and a miRNA-3p end from the 3' end [100, 105, 106] (Figure 1.2).

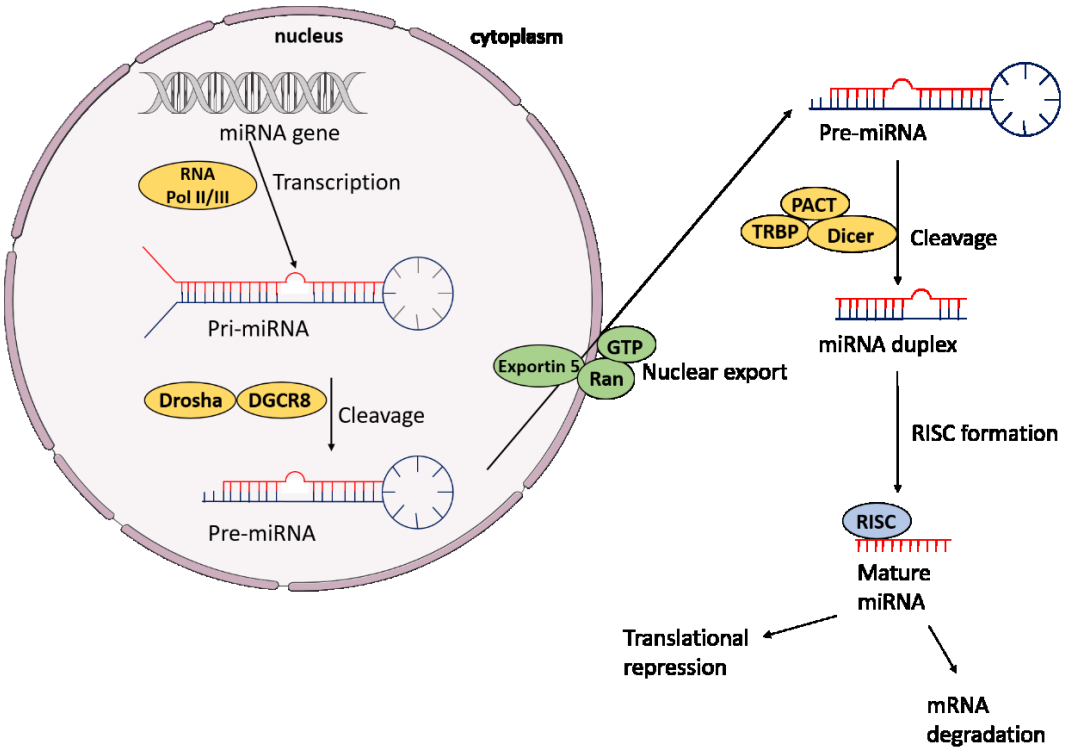

Figure 1.2 Biogenesis pathway of microRNA

In the nucleus the first steps of miRNA biogenesis involves the transcription of the pri-miRNA by RNA polymerase II/III (Pol II/III) and the nuclear processing of pri-miRNA to pre-miRNA by the microprocessor complex (Drosha and DGCR8). Pre-miRNA is exported out of the nucleus by the exportin 5-Ran-GTP complex and undergoes cleavage by the RNase III endonuclease Dicer and its cofactors TRBP2 and PACT, to form the miRNA duplex. Finally, one strand of the miRNA duplex is loaded onto the Ago protein to form the RISC complex and mediate mRNA repression and degradation. Figure adapted from Winter et al. and created using Servier Medical Art, Les Laboratoires Servier.

1.8 MicroRNA function

During RNA silencing, either strand (5p or 3p) from the mature miRNA duplex can be loaded onto the Argonaute (Ago) proteins to form the ribonuclease complex, RNA-induced silencing complex (RISC)[107]. For each miRNA, the proportion of 5p or 3p strands loaded onto Ago, varies greatly and depends on the cell state, type and developmental stage [108]. Furthermore, RISC, directed by complementary base

pairing of miRNA (6-8 nucleotides), mediates post-transcriptional messenger RNA (mRNA) repression, resulting in the inhibition of protein translation or induction of mRNA degradation [93, 107, 109] (Figure 1.2). Thus, miRNA plays an important role in the homeostasis of physiological processes such as differentiation, proliferation, stress response and immunity [96, 104, 110, 111]. In eukaryotic cells, miRNA have shown to primarily repress gene expression [112]. A single miRNA is believed to target and repress hundreds of distinct mRNA targets [113]. The dysregulation of miRNA has been associated with multiple pathological disorders including cancer, cardiovascular and metabolic diseases [114, 115].

1.9 Extracellular microRNA

Extracellular miRNA have been identified in a range of biological fluids including: plasma, saliva, tears, urine, amniotic fluid and cerebrospinal fluid [116]. Cell-free miRNA are sensitive to RNase degradation within the circulation [117]. Hence, for stability and protection from degradation, circulating miRNA are bound to RNA-binding proteins, encapsulated in extracellular vesicles or within high lipid density proteins [117-119]

1.9.1 MicroRNA associated with HDL

The lipid based particles found in the plasma, low lipid density proteins (LDLs, 22nm) and high lipid density proteins (HDLs, 8-12nm) have been described to contain endogenous microRNA in human plasma [119]. HDLs isolated from familial hypercholesterolemia patients were demonstrated to have significantly distinct profiles of miRNA content compared to healthy patients [119]. Furthermore, the HDL-miRNA isolated from the familial hypercholesterolemia patients were shown to induce differential gene expression of mRNA targets in hepatocyte cells *in vitro* [119]. Together, these results indicate that HDLs participate in the transport and cellular communication of extracellular miRNA.

1.9.2 MicroRNA associated with protein complexes

Through various size exclusion methods it was discovered that approximately 90% of miRNAs circulating in the plasma are associated with a ribonuclease complex [117, 120]. *In vivo*, it has been reported that circulating miRNA is primarily associated with

Argonaute 2 (Ago2), a key component of the RISC complex [117, 120]. Additionally, Wang *et al.* supported the theory that extracellular miRNA were predominantly associated with protein complexes. They discovered that Nucleophosmin-1 (NPM1), a nuclear protein involved in the shuttling of RNA and ribosomal proteins to the cytosol, is also involved in exporting and protecting of miRNA in the extracellular space [121]. However, the exact role NPM1 plays *in vivo* has yet to be described.

It has been proposed that circulating protein-bound miRNA are a product of passive release from its cell of origin upon necrosis and apoptosis [120, 122]. This is supported by observations of circulating miRNA following cell toxicity and death [87, 123].

1.9.3 MicroRNA encapsulated in extracellular vesicles

Extracellular vesicles (EVs) are small membrane bound vesicles that are secreted by various cells [124]. They can be detected in various biological fluids, including blood and urine [125-127]. Based on their size, origin and identifying markers, EVs are divided into three groups: apoptotic bodies, microvesicles and exosomes [128, 129] (Table 1.2).

Table 1.2 Extracellular vesicles characteristics

Extracellular vesicles	Size	Biogenesis
Apoptotic bodies	500-2000nm	Outward blebbing of the apoptotic cell membrane
Microvesicles	50-1000nm	Outward budding of the cell membrane
Exosomes	30-100nm	Endosomal pathway

Table adapted from Andaloussi et al. [130] and Braicu et al. [131]

Originally, EVs were regarded as cell debris with no significant biological role [130]. However, multiple studies have shown that exosomes and microvesicles encapsulate protein, lipids, mRNA and miRNA specific to the host cell [132, 133]. Furthermore, EVs have been observed to play an important role during intercellular communication, via the transfer of their contents [134]. In particular, miRNA have been observed to be selectively packaged and transported within EVs to neighbouring and distant cells [134]. Subsequently, this EV mediated transfer of miRNA results in extensive gene regulation in the recipient cell [134-137].

Interestingly, Arroyo *et al*, discovered that the profile of miRNA encapsulated in EVs differs from the Ago2 bound miRNA population. Indicating, that the circulating form of miRNA depends on the cell type of origin and its mechanism of release [117, 121]

1.10 MicroRNA as a signalling molecule

The presence of miRNA in the extracellular environment raised the hypothesis that the selective release of miRNA contributes to endocrine and paracrine cellular communication [134]. Following this hypothesis, it has since been well established that extracellular miRNA can be transported to recipient cells, altering gene expression and cell function [138-140]. MiRNA mediated cellular communication has been observed *in vivo* and *in vitro* via EVs, HDLs and Argo2 (Table 1.3).

Numerous studies have shown that EVs mediate the transfer of miRNA from one cell to another under various physiological and pathological states. A considerable interest has been taken in exosomes as a cell signalling mediator. Exploration into the mechanism of release and uptake of exosomes has been extensive. Evidence suggests that exosomal secretion via the endosomal pathway is initiated by the neutral sphingomyelinase 2 (nSMase2) enzyme [141, 142]. This was further confirmed when the treatment of an nSMase2 inhibitor, GW4869, decreased both exosome and miRNA secretion [141, 142].

Cell targeting and miRNA uptake has been demonstrated to be through the interaction of exosomal surface proteins and receptors on recipient cells [120]. It has previously been described the hormonal regulation of EV uptake and transfer in cells, mice and humans. They observed that desmopressin, a vasopressin analogue, stimulated a significant uptake of EVs into kidney collecting duct cells ($mCCD_{C11}$) and primary cortical collecting duct cells [143]. In mice, when vasopressin activity was inhibited by tolvaptan (a selective vasopressin V2 receptor antagonist), EV numbers significantly increased in the urine and significantly reduced in the kidney [143]. This highlighted that uptake and excretion of EVs is regulated by vasopressin *in vivo*. Lastly, these findings were consistent in patients with central diabetes insipidus, where desmopressin resulted in the reduced excretion of EVs from the glomerular and proximal tubular cells [143]. Furthermore, the functional transfer of exosomes and

small EVs miRNA has been demonstrated in a large number of *in vitro* and *in* vivo studies, influencing tumour development, cardiovascular disease and diabetes (Table 1.3).

In addition, it has been reported that isolated HDL-miRNA complexes found within the plasma can transmit their contents to other cells (Table 1.3). Unlike EVs, the export of HDL containing miRNA was observed to be negatively regulated by nSMase2 [144]. The delivery of HDL-miRNA was also dependent on the membrane bound receptor SR-BI [144]. Moreover, it was revealed that the HDL-miRNA content was influenced by disease states including atherosclerosis and cardiovascular diseases [144, 145]. The transport and delivery of miRNA, specifically miR-223, was shown to regulate gene expression and in turn have anti-inflammatory properties in endothelial cells and hepatocytes [145]. However, subsequent evaluation of HDL-miRNA content has demonstrated that HDLs contain a small percentage of total circulating miRNA, with HDL-miR-223 contributing to only 8% of total circulating miR-223 [146]. In addition, the study was unable to replicate the significant uptake of HDL-miRNA observed in Vickers *et al.* study. Here, they found there was a non-significant uptake of HDL bound miRNA in endothelial, smooth muscle and peripheral mononuclear cells *in vitro* [146]. Hence, the importance of HDL-miRNA mediated cellular communication remains uncertain.

As mentioned above, miRNA bound to protein complexes are believed to be passively released during cell death. Until recently, there was no indication of active release of Ago2-miRNA or selective uptake from recipient cells. However, Wang *et al.* uncovered that the passive release of Ago2-miR-122 from injured hepatocytes resulted in its significant uptake in alveolar macrophages [122]. Not only did this indicate selective uptake of protein bound miRNA for the first time, it also highlighted miRNA in this form induce a biological function *in vivo* (Table 1.3).

Table 1.3 Functional miRNA in intercellular communication

microRNA	Carrier	Donor cell	Recipient cell	Target gene	Biological function	Reference
miR-223 miR-105	HDL	Unknown*- macrophages**	Endothelial Cells (HCAEC)	ICAM-1	Unknown- inhibits vascular inflammation**	[145]
miR-223	HDL	Macrophages	Hepatocytes (Huh7)	RhoB, EFNA1	Unknown	[144]
miR-122	Ago2	Hepatocytes	*In vivo*: Alveolar macrophages	TLR7	Activates inflammatory responses	[122]
miR-155	Exosomes	Adipose Tissue Macrophages	L6 skeletal myoblast, primary hepatocytes	PPARγ	Promotes insulin resistance during obesity	[147]
miR-125b	EVs	Breast cancer cells- 4T1 and 4TO7	Primary fibroblasts	Tp53inp1	Fibroblast activation	[148]
miR-27 miR-28	Exosomes	Primary fibroblasts	Primary cardiomyocytes	Nrf2	Promotes oxidative stress during chronic heart failure	[149]
miR-132	Exosomes	Primary cortical neurons	Brain microvascular endothelial cells (b.End3)	eEF-2K	Maintains vascular integrity	[150]

microRNA	Carrier	Donor cell	Recipient cell	Target gene	Biological function	Ref
miR-21	Exosomes	Bone marrow–derived macrophages (BMDM)	Gastric cancer cells (MFC,MGC-803)	PTEN	Suppresses cell apoptosis and enhances activation of PI3K/AKT signalling pathway	[151]
miR-133a	Exosomes	Primary muscle fibres	Fibroblasts (NIH3T3)	Smarcd1, Runx2	Promote skeletal muscle myogenesis	[152]
miR-486	Exosomes	Endothelial colony-forming cells	Endothelial cells (HUVEC) and *in vivo*	caspase-3, PTEN	Inhibits hypoxia-induced apoptotic responses via Akt activation	[153]
miR-27a miR-22 miR-221	EVs	Tumour-associated macrophages	Glioma stem cells	CHD7	Promotes proneural-to-mesenchymal transition and radiotherapy resistance	[154]
miR-210	EVs	Bronchial epithelial cells (HBECs)	Lung fibroblasts	ATG7	Regulates autophagy processes	[155]
miR-1	EVs	Primary glioblastomal cells	Brain microvascular endothelial cells (HBMVEC)	ANXA2	Tumour suppressor	[156]

**Isolated from whole blood, **hypothesised source/function*

1.11 MicroRNA as a biomarker of DILI

In addition to their stability in the circulation, miRNA have shown to be highly conserved across mammalian genomes, making them translational from pre-clinical to clinical studies [157]. Furthermore, some miRNA species are tissue enriched meaning the dysregulation of certain miRNA can reflect a specific cell activity and disease state [158]. Hence, the application of miRNAs as a non-invasive biomarker has become a focus in research. Circulating miRNAs were first assessed as a diagnostic biomarker in the serum of diffuse B cell lymphoma patients [159]. Since then, the dysregulation of miRNA has been described in various diseases including: cancer, diabetes, viral infections, autoimmune diseases and DILI [157].

In the search for new and improved biomarkers of DILI, miRNA expression profiles were assessed in the circulation of mice with paracetamol toxicity [123]. It was first noted that there were significant changes in the profile of miRNA in the circulation of mice following an overdose of paracetamol, compared to healthy controls [123]. From this study, several miRNA species were identified as biomarkers of paracetamol-induced liver injury: miR-122, miR-192, miR-148a and miR-193 [123]. Out of the numerous miRNA species identified, miR-122 and miR-192 were the most abundant circulating miRNAs following liver injury. Furthermore, it was determined that their release into the circulation was dose and exposure dependent, paralleling liver degeneration. In addition, unlike ALT, both miRNA biomarkers could be detected prior to significant liver injury [86, 123].

MiR-192 is highly expressed in other organs including the kidney and gastrointestinal tract [160]. Consequently, an increase in miR-192 is also associated with kidney dysfunction [87]. MiR-122, on the other hand, is highly enriched in the liver and has little-to-no expression elsewhere [160-162]. MiR-122 has been observed to remain stable in the presence of exercise-induced muscular injury and kidney dysfunction [87, 163]. Moreover, the increase of miR-122 during DILI has been replicated in humans. A study has observed a 100-fold increase of miR-122 in the bloodstream of patients with paracetamol-induced liver injury, compared to a control population [82]. Again,

as observed in the mice, this increase in miR-122 return to baseline more rapidly, has greater sensitivity and comparable specificity compared to ALT activity (Table 1.4). Therefore, enabling greater confidence of prognosis and patient stratification, reduction in hospital bed occupancy and reduction in adverse drug reactions from unnecessary NAC treatment [82].

Table 1.4 Receiver Operator Characteristic (ROC) Curve Analysis of ALT and miR-122

Biomarker	ROC-AUC (95% CI)	Sens (95% CI)	PPV	NVP	P value
ALT	0.81 (0.65-0.97)	0.69 (0.39-0.91)	64	92	0.0006
miR-122	0.95 (0.9-1.0)	0.62 (0.32-0.86)	62	91	<0.0001

ROC analysis determining plasma miR-122 and ALT activity to predict to development of ALI at first presentation to hospital following acetaminophen overdose (n=67). Table includes: ROC-AUC (area under the curve with 95% confidence interval), sensitivity (SENS at 90% specificity, with 95% confidence interval) at 90% specificity, positive (PPV) and negative (NPV) predictive value and statistical significance. MiR-122 normalised by miR-1287. Data taken from Vliegenthart et al. [87].

1.12 Hepatic function of miR-122

Within the liver, miR-122 is the most abundant miRNA, accounting for around 70% of hepatocyte's total miRNA (66,000 copies/hepatocytes) [164]. MiR-122 is translational, found in humans, rodents, zebrafish, dogs, pigs and cynomolgus monkeys [82, 160, 165-170]. In these species, miR-122, primarily bound to Ago2, is released into the bloodstream, accurately acting as a circulating predictive biomarker for DILI [117, 171]. However, miR-122 alone cannot distinguish between different etiologies of hepatocyte damage [172]. Thus, it has been frequently recommended to be used in combination with the biomarkers previously discussed in Section 1.6. Furthermore, miR-122 has shown to be a multifunctional RNA species involved in various physiological and pathological processes in the liver (Figure 1.3).

Through antisense targeting of miR-122, it was observed that the loss of miR-122 resulted in the reduction of plasma cholesterol, increased hepatic fatty acid metabolism and a decrease in hepatic fatty acid and cholesterol synthesis [173]. Moreover, miR-122 has been shown to downregulate genes such as 3-hydroxy-3-methylglutaryl-CoA-reductase (Hmgcr), a rate-limiting enzyme of endogenous cholesterol biosynthesis [173, 174]. Therefore, it has been indicated that miR-122 acts as a key regulator of cholesterol and fatty acid metabolism in the adult liver.

MiR-122 has been suggested to play a central role in the development and differentiation in the liver. During mouse liver development, miR-122 has shown to gradually silence the transcription factor cut-like homeobox 1 (CUTL1), initiating terminal differentiation in multiple cell lines, including hepatocytes [150]. In addition, the loss of miR-122 in developing zebrafish resulted in delayed maturation of hepatocytes *in vivo* [175].

The characterisation of miR-122 knockout mice has revealed that a reduction in miR-122 expression is associated with various diseases in the liver. MiR-122 knockout mice have been shown to develop steatohepatitis, fibrosis and hepatocellular carcinoma (HCC) [176]. Additional studies have investigated this further, indicating miR-122 functions as a tumour suppressor in the liver. During HCC, miR-122 has been shown to mediate the repression of genes involved in the tumour progression such as cyclin G1 (CCNG1), a distintegrin and metalloprotease family 10 (ADAM10), insulin-like growth factor 1 receptor (IGF-1R) and serum response factor (SRF) [177-179]. Furthermore, a decrease in miR-122 expression has been linked with poor prognosis and metastasis in hepatocellular carcinoma (HCC) [180]. Replenishing miR-122 in HCC has shown to reverse the tumourigenic properties of the cells and inhibit HCC

progression *in vivo* [165].

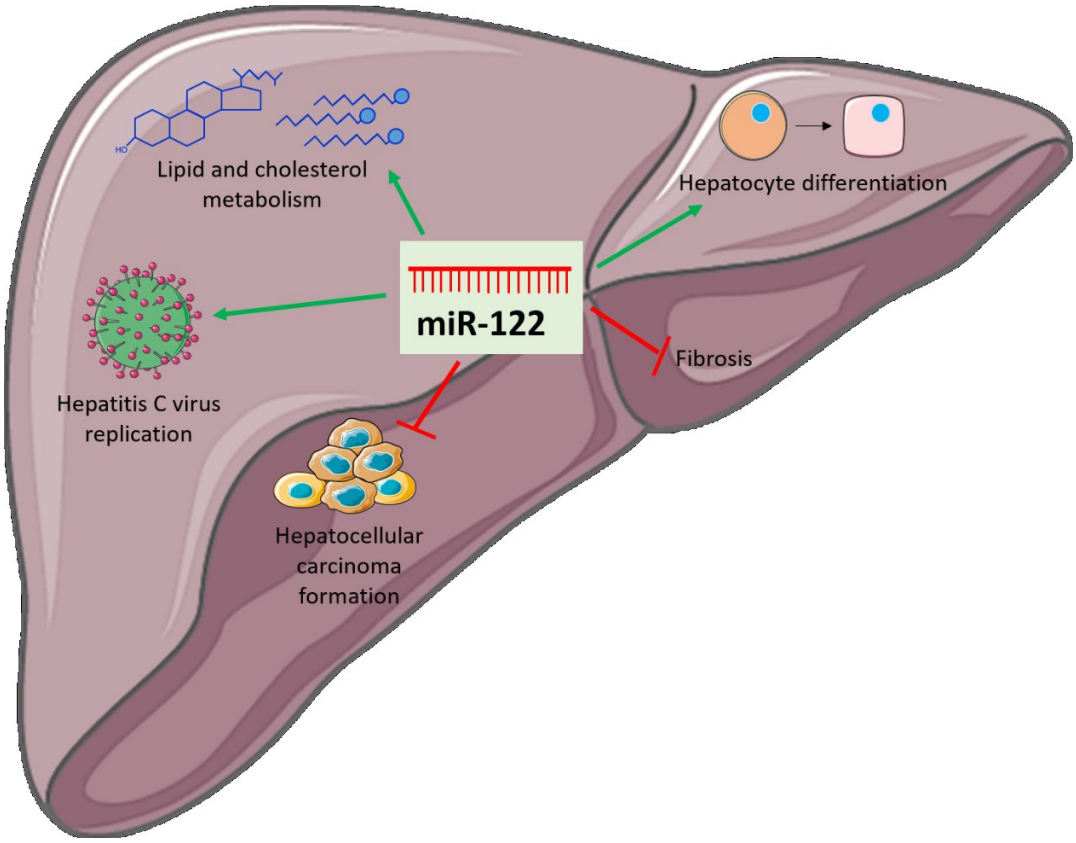

Figure 1.3 Physiological and pathological roles of miR-122 in the liver

In physiological conditions, miR-122 regulates cholesterol and lipid metabolism, hepatocyte differentiation and maintenance. Under pathological conditions, it has shown to mediate hepatitis virus replication, inhibit the formation of hepatocellular carcinomas and progression of fibrosis. Figure adapted from Hornby et al. and Bandiera et al. [181, 182] and created using Servier Medical Art, Les Laboratoires Servier.

Additionally, miR-122 has been revealed to negatively regulate the production of collagen and progression of fibrosis in hepatic stellate cells (HSCs). During carbon tetrachloride (CCl_4)-induced fibrosis, miR-122 was observed to significantly decrease with an inverse correlation of its mRNA target prolyl 4-hydroxylase (P4HA1- a key enzyme in collagen maturation) in HSCs [183]. The overexpression of miR-122 led to the reduction of P4HA1, collagen and excessive cellular matrix protein production [183]. Moreover, miR-122 has been described to repress fibrosis related genes: alpha

smooth muscle actin (α-SMA), fibronectin 1 (FN1) and α1 type I collagen (COL1A1), in HSCs and fibroblasts [184].

Whilst examining hepatitis C virus (HCV) infection and replication, it was observed that there was a marked loss of viral replication following the loss of miR-122 in the liver cells [185]. Thus, further investigation determined that miR-122 directly binds to HCV, enhancing the stability and replication of viral RNA [185, 186]. As a result, miR-122 is being investigated as a drug target for the treatment of HCV.

1.13 Regulation of miR-122

MiR-122 is significantly upregulated during embryogenesis and reaches maximal expression prior to birth [164, 187]. Upon investigation, it was identified that the expression of miR-122 is activated by the CCAAT/enhancer-binding protein, C/EBPα and the liver enriched transcriptional factors: HNF1α, HNF3α and HNF3β [187]. Furthermore, it was discovered that under circadian control, the orphan nuclear receptor, REV-ERBα, governs the transcription of the miR-122 gene [188]. Subsequently, the expression of pri-miR-122 and pre-miR-122 fluctuates, with its highest expression during the day [188]. Nonetheless, as mature miR-122 has an estimated half-life of 10.2 days in the liver, its expression remains stable over the circadian cycle [188, 189]. Within the circulation, the half-life of circulating miR-122 is uncertain, however, it has been described as significantly shorter than ALT which has an average half-life of 48 hours[86].

1.14 Cellular communication of miR-122

In addition to acting as a biomarker for DILI, there have been a number of studies investigating extracellular miR-122 as a cell signalling molecule. Recent studies have highlighted the transfer of miR-122 during physiological and pathological diseases including: cancer, alcohol-related liver disease and DILI.

In breast cancer, the promotion of metastasis has been shown to be mediated by the transfer of miR-122 enriched exosomes from breast cancer cells to neighbouring and distant cells. This transfer of miR-122 was described to promote metastasis and facilitate disease progression via the downregulation of pyruvate kinase and glucose consumption in the pre-metastatic niche, *in vivo* and *in vitro* [137]. Furthermore, the use of miR-122 antagonists were shown to significantly reduce the development of metastasis in the brain and lung *in vivo* [137]. Suggesting, targeted therapy to dampen miR-122 signalling in breast cancer patients may be of benefit.

Additionally, miR-122 transfected adipose tissue-derived MSCs (AMSCs) have shown to effectively package and deliver exosomal miR-122 to hepatocellular carcinoma (HCC) cells [190]. However, unlike breast cancer, an increase of miR-122 in the HCC cells has been shown to result in cell cycle arrest and increased apoptosis via the downregulation of ADAM10, CCNG1 and IGF-1R [190]. Furthermore, the HCCs with greater miR-122 content had increased sensitivity to the anti-tumour drug sorafenib [190]. Therefore, this study suggests that miR-122 export via AMSCs highlights a novel therapy to enhance HCC sensitivity to chemotherapy.

In alcohol-related liver disease, hepatocyte derived exosomal miR-122 were exhibited to undergo horizontal transfer to monocytes. Consequently, the increase of miR-122 in the monocytes was described to inhibit the HO-1 pathway, increase sensitivity to LPS stimulation and enhance the production of pro-inflammatory cytokines.[191] Following ConA-induced acute hepatitis, *Wang et al* recently noted that miR-122 released from the liver enters the lung, activates alveolar macrophage TLR7/8 and in turn pulmonary inflammation [122]. Furthermore, the depletion of miR-122 in the liver and circulation abolished lung damage and pulmonary inflammation [122].

MiR-122 signalling has also been implicated during physiological conditions involving the synthesis of triglycerides. Free fatty acids have been described to activate the retinoic acid-related orphan receptor alpha (RORα) and in turn enhance primary, precursor and mature miR-122 expression in the liver [192]. Subsequently, this activation has been observed to induce liver secretion of miR-122 into the bloodstream and its uptake into skeletal muscle and white adipose tissue [192]. This increase in miR-122 expression was shown to significantly reduce miR-122 mRNA targets involved in triglyceride synthesis: AldoA, Agpat1 and Cpt1a in all three tissues [192]. Moreover, this study also demonstrated that fasting causes an increase in free fatty acids and miR-122 expression, which in turn reduces triglyceride synthesis and α-oxidation, utilising lipid accumulation as an energy source [192].

1.15 miR-122 in the kidney

The main function of the kidney is to maintain physiological homeostasis by eliminating waste products and maintaining volume, electrolyte content and pH of the extracellular fluid [54]. In addition, the kidney is also involved in the synthesis of erythropoietin (Epo), renin and vitamin D [54]. Recently Rivkin *et al.* highlighted that miR-122 released from the liver enters the kidney and targets Epo expression. During LPS-induced liver inflammation, a significant increase in mature miR-122 was observed in the circulation and the kidney [193]. Alongside known miR-122 targets, Aldoa and AGPAT1, Epo expression was demonstrated to be inversely correlated with an increase in miR-122 [193]. Moreover, a prolonged increase of miR-122 and loss of Epo expression in the kidney, linked to liver inflammation, resulted in a reduction of bone marrow erythropoiesis and the development of inflammation-induced anaemia [193]. Thus, this study suggests that hepatocyte derived miR-122 can regulate gene expression in the kidney.

A high oxygen demand paired with a low oxygen tension leaves the kidney vulnerable to hypoxia and acute kidney injury [194]. In addition, toxicity can be heightened in the proximal tubule cells due to their exposure to circulating chemicals and its role in extensive cellular uptake and clearance [195]. Examples of drugs that induce proximal

tubule injury include aminoglycosides, cisplatin and paracetamol [196, 197]. Cisplatin is a chemotherapeutic agent used for the treatment of solid-organ tumours [198]. Despite its high success rate, nephrotoxicity is a prevalent event associated with the intake of cisplatin [199]. Downregulation of miR-122 has been observed to contribute to tubular cell injury following cisplatin treatment [200]. Replenishing miR-122 expression was shown to reduce cisplatin-induced tubular injury through inhibition of FOXO3, a core protein involved in the activation of the p53 cascade and initiation of apoptosis [200]. Recent studies have revealed that EVs isolated from the plasma of liver injured mice, containing a high concentration of miR-122, induced resistance to cisplatin-induced injury in mouse primary proximal tubule cells [201]. Together, these findings suggest that miR-122 may function as a mediator of cell viability during tubular injury.

1.16 Hypothesis and aims

ALF is often accompanied by acute kidney injury (AKI). Due to this, renal function is an important measure of patient prognosis during ALI and ALF. However, the mechanism behind the renal response to liver injury is poorly understood. It is well recognised that following a paracetamol overdose, the injured liver releases large amounts of miRNA. MiR-122, a miRNA highly expressed in the hepatocytes of the liver, displays the greatest release into the circulation in humans and murine models following a paracetamol overdose. In addition, miRNA, including hepatic miR-122, has shown to enter recipient cells, modulate RNA targets *in vivo* and promote cell viability in the kidney *in vitro.* Therefore, the studies in this thesis were carried out to explore whether hepatic miRNA, particularly miR-122, is transferred from the liver to the kidney. In addition, an investigation into whether liver-derived miRNA can modulate kidney mRNA expression and in turn nephrotoxic tubular injury was carried out. Thus, it was hypothesised that the large release of miR-122 from the liver to the circulation, during DILI, enters the kidney and induces resistance to subsequent injury.

To address this hypothesis, the aims of the studies were to:

1. Optimise and define an inducible model of liver-specific Dicer deletion *in vivo*.
2. Investigate which organs are responsible for the uptake of miR-122 after its abundant release during paracetamol-induced liver injury.
3. Investigate if the loss of miR-122 signalling from the liver to the kidney has a functional effect.

Chapter 2 Methods

2.1 Location

All experiments were performed in the Centre for Cardiovascular Science, Queen's Medical Research Institute, apart from the *in situ* hybridisation (ISH) of miR-122 (Section 2.9.3), immunohistochemistry (IHC) of CYP2E1 (Section 2.9.2) and mass spectrometry of the CYP450 enzymes (Section 2.12) which were carried out at AstraZeneca, Cambridge.

2.2 Experimental Animals

All studies carried out meet the following requirements as appropriate of the Animals (Scientific Procedures) Act 1986 / ASPA Amendment Regulations 2012 for work performed in the UK, or under the EU Directive 2010/EU/63.

The animals were housed in groups of 4-8 with free access to standard chow and water at 22°C ± 1°C, 55% humidity. They were kept to a 12 hour light-dark cycle (lights on 07:00 and off at 19:00). The mice were allowed to acclimatise to this environment for at least a week before each study. Wild-type C57BL/6J mice were purchased from Charles River Laboratories, UK.

2.3 *in vivo* model: Liver specific DICER knockdown

Homozygous *Dicer1* $^{flox/flox}$ mice (B6.Cg-*Dicer1*^{tm1Bdh}/J strain, The Jackson Laboratory, ME, USA) express *loxP* sites on either side of exon 23 of the *Dicer1* gene. Cre-mediated recombination leads to the loss of the *Dicer1* gene and in turn ceases the production of mature miRNA.

The homozygous *Dicer1* $^{flox/flox}$ mice (both sexes, aged 8-12 weeks) were injected with a single tail vein injection of a hepatocyte-specific adeno-associated virus serotype 8 (AAV8). To induce liver specific *Dicer1* knockdown, a Cre-containing AAV8 with the promoter for the thyroxine binding globulin (TBG) was used (Table 2.1). An empty AAV8, Null-AAV8, was used as a negative control (Table 2.1).

Similar to previous experiments carried out by Kylie Matchett (Centre for Inflammation Research, CIR) and Victoria Gadd (Centre for Regenerative Medicine, CRM), both AAV8 vectors were diluted to either $2.5x10^{11}$ or $6.25x10^{10}$ viral genomes

dose. Each dose was limited to 100µl in sterile PBS to limit hydrodynamic effects [202]. Mice were randomly selected to be injected with either the Cre-AAV8 or Null-AAV8. Untreated *Dicer1* $^{flox/flox}$ (baseline) mice were used as controls where indicated. The mice were left under normal housing conditions for a maximum of four weeks where they were either humanely culled or underwent further treatment with paracetamol.

Table 2.1 Adeno-associated virus serotype-8 (AAV8) name and gene expression

AAV8	Gene expression
Null-AAV8	AAV8.TBG.PI.Null.bGH
Cre-AAV8	AAV8.TBG.PI.Cre.rBG

AAV8 vectors were purchased from Penn Vector Core, PA, USA.

2.4 Paracetamol toxicity model

Using methods previously described, paracetamol was used to induce acute DILI in male *Dicer1* $^{flox/flox}$ mice [203]. First, mice were fasted for 12 hours (overnight) prior to paracetamol dosing with free access to water. This was done to deplete ATP and glutathione levels to ensure the mice had comparable conditions of paracetamol metabolism in humans [204]. Additionally, the act of fasting prior to drug treatment has shown to reduce variability and induce a greater extent of centrilobular injury, compared to non-fasted mice [205, 206].

On the day of treatment, paracetamol (4-Acetamindophenol; ACROS organics, Geel, Belgium) was prepared in sterile PBS (Sigma Aldrich, MO, USA) in an ultrasonic bath (37°C). Mice were randomly selected and administered with either sterile PBS (control), 150mg/kg paracetamol or 300mg/kg paracetamol via a single intraperitoneal injection and placed in a hot box (34°C) with free access to food (mash and standard chow) and water. Mice were euthanized 6 hours following dosing, as miR-122 has been shown to peak in the circulation at this time point [207].

2.5 Carbon Tetrachloride (CCl_4) toxicity model

Male C57BL/6 mice (8 weeks old) were injected with a single dose of CCl_4 as described previously [208-210]. After a 12 hour overnight fast, mice underwent an intraperitoneal

injection of 1ml/kg CCl_4 (sterile CCl_4 in a 1:3 ratio with olive oil) or with olive oil (control) at the equivalent volume.

2.6 Blood and tissue sampling

The mice were humanely culled via rising concentration of CO_2 before exsanguinations according to the Humane Killing of Animals Under Schedule 1 to the Animals (Scientific Procedures) 1 Act 1986.

Following blood collection via cardiac puncture, buffered sodium citrate solution (1.09mM) was immediately added as a 1:6 dilution. Whole blood was stored on ice until it was centrifuged for 10 minutes at 8000 x *g* at 4°C. Plasma was isolated and stored at -80°C. Tissue (brain, lung, heart, liver, kidney and spleen) were macroscopically dissected and placed in 4% paraformaldehyde (Sigma Aldrich), RNAlater (Sigma Aldrich) and dry ice. This prepared and maintained the integrity of the samples for histology, RT-qPCR and protein analysis respectively.

2.7 RT-qPCR

2.7.1 RNA extraction

2.7.1.1 Blood

Total RNA was extracted and purified from plasma using the miRNeasy Serum/Plasma Kit (Qiagen, Hilden, Germany). As recommended by the manufacturer, *C. elegans* miR-39 miRNA mimic (Qiagen) was added to each sample at $4x10^7$ copies/µl as an external control. Following the manufacturing instructions RNA was eluted in 14µl of RNase-free water and stored at -80°C.

2.7.1.2 Tissue

Following manufacturing instructions no more than 25mg of tissue was used to isolate RNA. The tissue was thoroughly homogenised in Qiazol (Qiagen) using sterile stainless steel beads on the TissueLyser II (Qiagen). Total RNA was extracted and purified from the homogenised tissue using the miRNeasy Mini Kit (Qiagen). Using the NanoDrop® ND-1000 UV-Vis Spectrophotometer (Thermo Fisher Scientific, MA, USA) RNA quality and concentration was determined and consequently diluted to 250ng.

2.7.2 Reverse Transcription

cDNA was synthesised using the miScript II RT kit (Qiagen) according to the manufacturer instructions. Alongside each cDNA generation, a no RT control was included. The following volumes were used for tissue and plasma:

Table 2.2 Reverse Transcription components and volumes used for plasma and tissue

	Volumes	
Component	**Plasma**	**Tissue**
5x miScript HiSpec Buffer or 5x miScript HiFlex Buffer*	4µl HiSpec Buffer	4µl HiFlex Buffer
10x miScript Nucleics Mix	2µl	2µl
RNase-free water	7µl	Variable**
miScript Reverse Transcriptase Mix	2µl	2µl
Template RNA	5µl	Variable**
Total Volume	20µl	

**5x HiFlex Buffer generated cDNA for the investigation of miRNAs and mRNA in the tissue. 5x HiSpec Buffer was used for the quantification of mature miRNA only in the plasma.*

*** Variable template RNA and RNase-free water per tissue cDNA synthesis to generate a final concentration of 250ng.*

Samples were incubated for 1 hour at 37°C and then for 5 minutes at 95°C. Every sample was diluted 1:10 with RNase-free water and stored at -20°C.

2.7.3 RT-qPCR analysis

Real time PCR (RT-qPCR) detection was carried out on the Lightcycler 480 (Roche Diagnosis, Basel, Switzerland). For the quantification of mRNA and miRNA miScript SYBR green PCR kit (Qiagen) was used. As per the manufacturing instructions, 1µl of sample was added to 9 µl of the SYBR green components. To measure miRNA, the

sample was added to 1µl of 10x miScript Universal Primer, 1µl 10x miScript Primer Assay, 5µl 2x QuantiTect SYBR Green PCR Master Mix and 2µl RNase-free water. For the quantification of mRNA, the sample was added to 1µl 10x QuantiTect Primer Assay, 5µl 2x QuantiTect SYBR Green PCR Master Mix and 3µl RNase-free water.

The Taqman Gene Expression Mix was used for the detection of primary miRNA (pri-miRNA) transcripts (Life Technologies, CA, USA). For quantification, 5µl Taqman Gene Expression Master Mix, 0.5µl TaqMan Pri-miRNA Primer and 3.5µl RNase-free water was added to the 1µl sample.

The real-time PCR cycles were set up according to the miScript (Qiagen), QuantiTect (Qiagen) and Taqman (Life Technologies) gene expression manuals. Melt curve analysis was completed to determine that there was no primer dimer formation and non-specific amplification. All samples were analysed in duplicate.

2.7.4 Relative quantification

All tissue samples miRNA and mRNA Ct values were translated by the $2^{-\Delta CT}$ method [211]. The Ct values were normalised by an internal control using the following equation:

$$2^{-\Delta CT} = [\,(Ct\ gene\ of\ interest - Ct\ internal\ control)] \quad [211]$$

2.7.5 Absolute quantification

Plasma sample miRNA concentrations were determined using standard curves containing known 1:10 dilutions of miScript miRNA Mimics: Syn-hsa-miR-122-5p, Syn-mmu-miR-192-5p and Syn-mmu-miR-151-3p (#219600, Qiagen). Standard curves were run three times, in duplicate and averaged. The raw Ct values were translated to copy number by absolute quantification analysis using linear interpolation.

2.7.6 Primer details

2.7.6.1 miScript Primer Assay

Table 2.3 miScript primers used for the quantification of miRNA

Primer name	Target	Catalogue number	Target Sequence
Hs_SNORD68_11	SNORD68	MS00033712	
Hs_SNORD95_11	SNORD95	MS00033726	
Hs_RNU6-2_11	RNU6-6P	MS000033740	
Ce_miR-39_1	cel-miR-39-3p	MS00019789	5'UCACCGGGUGUAAAUCAGCUUG
Hs-miR-122a-1	hsa-miR-122-5p	MS00003416	5'UGGAGUGUGACAAUGGUGUUUG
Mm_miR-151-3p_1	mmu-miR-151-3p	MS00032340	5'CUAGACUGAGGCUCCUUGAGG
Mm_miR-192_2	mmu-miR-192-5p	MS00011354	5'CUGACCUAUGAAUUGACAGCC
Mm_miR-124_1	mmu-miR-124-3p	MS0002921	5'UAAGGCACGCGGUGAAUGCC
Mm_miR-196a_2	mmu-miR-196a-5p	MS00032515	5'UAGGUAGUUUCAUGUUGUUGGG
Mm_miR-1-2*_1	mmu-miR-1a-2-5p	MS00011004	5'ACAUACUUCUUUAUGUACCCAUA
Mm_miR-195_1	mmu-miR-195a-5p	MS00001792	5'UAGCAGCACAGAAAUAUUGGC
Mm_miR-146_1	mmu-miR-146a-5p	MS00001638	5'UGAGAACUGAAUUCCAUGGGUU

The pre-designed miScript primers were purchased from Qiagen, Hilden, Germany.

2.7.6.2 QuantiTect Primer Assay

Table 2.4 QuantiTect primers used in the measurements of mRNA in the tissue samples

Primer name	Target	Catalogue number
Mm_Gapdh_3_SG	Glyceraldehyde-3-phosphate dehydrogenase (mouse)	QT01658692
Mm_Rn18s_3_SG	18S ribosomal RNA (mouse)	QT02448075
Mm_Actb_1_SG	Beta actin (mouse)	QT00095242
Mm_Hprt_1_SG	hypoxanthine guanine phosphoribosyl transferase (mouse)	QT00166768
Mm_Dicer1_1_SG	Dicer 1, ribonuclease type III (mouse)	QT00114702
Mm_Cyp1a2_1_SG	cytochrome P450, family 1, subfamily a, polypeptide 2 (mouse)	QT00100674
Mm_Cyp2e1_1_SG	cytochrome P450, family 2, subfamily e, polypeptide 1 (mouse)	QT00112539
Mm_Aldoa_1_SG	aldolase A, fructose-bisphosphate (mouse)	QT00291753
Mm_Tmed3_1_SG	transmembrane emp24 domain containing 3 (mouse)	QT00256907
Mm_Ndrg3_1_SG	N-myc downstream regulated gene 3 (mouse)	QT00165767
Mm_Foxo3_1_SG	forkhead box O3 (mouse)	QT00168623
Mm_Havcr1_1_SG	hepatitis A virus cellular receptor 1	QT00112427

The pre-designed QuantiTect primers were purchased from Qiagen, Hilden, Germany

2.7.7 Taqman Gene Expression Assay

Table 2.5 Taqman Gene Expression Assay primers used for the quantification of pri-miRNA 122

Primer name	Target	Catalogue number
Mm99999915_g1	Gapdh	4331182
Mm03024075_m1	Hprt	4331182
Mm02619580_g1	Actb	4331182
Mm03306556_pri	mmu-mir-122	4427012

The pre-designed Taqman primers were purchased from Thermo Fisher Scientific, MA, USA

2.7.8 Data evaluation and statistical analysis

Data were analysed and presented as mean ±SD in Graphpad Prism (Version 8, CA, USA). For the experiments described in Chapter 3, linear regression was used to calculate the Cre-AAV8 treatment slope (expression/time) and determine whether it was significantly different from the control slope (Null-AAV8) and zero. For the variables of AAV8 treatment and paracetamol treatment (described in Chapter 4), statistical comparisons between the main effect and interaction of the treatments were assessed using a two-way analysis of variance (ANOVA, Tukey's multiple comparison test). For data sets comparing two unmatched treatment groups a Mann Whitney U test or t-test were used to determine statistical significance. The p value for each statistical test was set at 0.05. A Pearson's correlation was carried out to assess the correlation between two variables. The correlation coefficient, r, was used to interpret the strength and nature of the correlation. The confidence interval (set at 0.05) value was used to determine whether the correlation observed is not due to random sampling.

2.8 Quantification of plasma ALT levels

Mouse plasma ALT measurements were determined using methods previously described by The University of Edinburgh specialist assay service facilities [212]. To achieve this, a commercial ALT plasma kit (Alpha Laboratories Ltd., Eastleigh, UK) was adapted for use on either a Cobas Fara or Cobas Mira analyser (Roche Diagnostics Ltd, Welwyn Garden City, UK). Settings were set with a run precision of CV < 4% and an intra-batch precision of CV < 8%.

2.9 Histology and immunohistochemistry of toxicity

2.9.1 Formalin-Fixed Paraffin-Embedded (FFPE) tissue

During sample collection, a portion of each tissue was fixed for overnight in 4% paraformaldehyde (Sigma Aldrich) at 4°C. Following fixation, the tissue was placed in 70% ethanol ready for paraffin embedding. The tissue was then dehydrated, placed in paraffin-filled blocks and allowed to cool (carried out by the SURF histology team, The University of Edinburgh).

2.9.1.1 Haematoxylin and Eosin staining

FFPE spleen, liver and kidney blocks were cut in 3µm sections. Once the sections were cut, they were baked on the Superfrost Plus Slides for 40 minutes at 70°C (Thermo Fisher Scientific). The tissue was rehydrated with 25% xylene (4x 5mins), 100% ethanol (2x 2mins) and 95% ethanol (1x 2mins). After this, the slides were washed with running water (1min) ready for staining.

After rehydration, the slides were placed sequentially in haematoxylin (6mins), diH2O (1min), 1% acid alcohol (hydrochloric acid in 70% ethanol, 5mins), diH2O (1min), Scott's tap water (1min), diH2O (1min) and aqueous eosin (4mins). Finally, the slides had their last wash with diH2O (1min) and were then dehydrated with the following protocol: 95% ethanol (30s), 100% ethanol (30s and 45s) and 25% xylene (4x 1min). DPX mounting media and coverslips were placed over the tissue ready for imaging.

2.9.2 Immunohistochemistry (IHC) of cytochrome P450 2E1 in the liver and kidney

FFPE liver and kidney blocks were cut at 3µm, placed on Superfrost Plus slides (Thermo Fisher Scientific) and baked at 70°C for 40 minutes. Staining was executed on the Discovery ULTRA Staining Module (Roche Diagnostics) with the following program using Roche Diagnostic's reagents:

First, the slides were deparaffized again (2x4 minutes, 70°C). For further staining preparation, the temperature was increased to 100°C (4 minutes) and incubated with Ventana Cell Conditioner 1 (5x 8 minutes). To enhance the specificity of the signal, the sections were exposed to 150µl of Ventana DISCOVERY inhibitor (8 minutes). This was followed by another incubation with casesin (1:10 dilution, 8 minutes). With the slides warmed up to 37°C, 150µl of the CYP2E1 antibody was added (Table 2.6, 60 minutes). For the second time, the slide was exposed to a casesin (1:10 dilution, 1x 8 minutes). Next, the slides were exposed to 150µl of anti-Rb HRP (Table 2.6, 10 minutes). To initiate the signal, 150µl of the HRP-activated chromagen, DISCOVERY purple was added (40 minutes). Finally, 150µl of haemotoxylin (12 minutes) followed by 150µl of bluing reagent (4mins) was used as the counterstain.

Before adding DPX mountant, the slides were dehydrated by placing and agitating in 70% ethanol (1 minutes), 100% ethanol (2x 1 minutes) and 100% xylene (3x 1 minutes).

Table 2.6 Primary and secondary antibodies used for CYP2E1 IHC

Target	**Host and Conjugate**	**Source (catalogue no.)**	**Dilution for IHC**
Cytochrome P450 2E1	Rabbit	Abcam, Cambridge UK (Ab 28146)	1:100
Rabbit	anti-rabbit IgG HRP	Roche, Basel, Switzerland Roche DISCOVERY UltraMap (760-4315)	

2.9.3 *In situ* hybridisation (ISH) of miRNA-122

MiRNA-122 localisation was determined using the miRCURY LNA miRNA Detection Probes (Qiagen). FFPE blocks of liver and kidney were cut at 5µm, placed on Superfrost Plus slides (Thermo Fisher Scientific). The deparaffization and staining procedure was completed on Discovery ULTRA Staining Module (Roche Diagnostics). The programme was set according to methods established in AstraZeneca (Rebecca Sargeant, due for publication).

During the staining programme, the miRCURY LNA miRNA Detection probes and controls were prepared using the miRCURY LNA miRNA ISH Buffer Set (FFPE) (Qiagen) mixed 1:1 with UltraPure DEPC water (Thermo Fisher Scientific) (Table 2.7). Alongside the miR-122-5p slides, the U6 probe was used to assess the sample quality, the scramble-miR and buffer mix alone acted as negative controls (Table 2.7).

Table 2.7 miRCURY LNA miRNA Detection probe and controls for miRNA-122 ISH

Target	Source (catalogue no.)	Probe Sequence (target sequence)	Concentration for ISH
mmu-miR-122-5p	Qiagen (YD00615338)	CAAACACCATTGTCACACTCC (UGGAGUGUGACAAUGGUGUUUG)	40nM (1:625)
U6	Qiagen (YD00699002)	CACGAATTTGCGTGTCATCCTT	40nM (1:625)
Scramble-miR	Qiagen (YD00699004)	GTGTAACACGTCTATACGCCCA	0.5nM (1:1000)

2.9.4 Imaging and scoring of histological slides

Brightfield imaging of the H&E, IHC and ISH slides was achieved on the ZEISS Axio Scan.Z1 (ZEISS, Oberkochen, Germany). The Zen Blue edition software (ZEISS) was used for tissue visualisation. The Fiji (Fiji is just ImageJ, [213])software was used to assess the level of injury in the kidney and liver.

The percentage of necrosis/staining in the centrilobular zone of the liver was calculated by:

$$100x\frac{\text{distance }(\mu m)\text{between the central vein and edge of the necrotic/staining zone}}{\text{total distance }(\mu m)\text{between the central vein and portal triad}}$$

For each sample, ten measurements were chosen at random, measured and averaged. The average measurements of the Cre-AAV8 and Null-AAV8 treatment groups were then compared.

2.10 *in vivo model:* visualisation of Cre-recombination

mT/mG mice (B6.129(Cg)-Gt(ROSA)26Sor$^{tm4(ACTB-tdTomato,-EGFP)Luo/J}$, The Jackson Laboratory) globally express *loxP*-tdTomato (mT)-*loxP* (red fluorescence) at the cell membrane of all cell and tissue types. Following the exposure of a Cre-recombinase, the *floxed* tdTomato is deleted, enabling the downstream expression of the EGFP (mG) at the cell membrane. This results in the red fluorescent membrane to emit

green fluorescence. Untreated mT/mG mice were used as controls. Three weeks following a single AAV8 treatment as above (Section 2.3, $6.25x10^{10}$ viral genomes/100µl dose), the mice were sacrificed (as described in Section 2.6) and the tissue was harvested. mT/mG tissue (brain, lung, heart, liver, spleen and kidney) was fixed and imaged to visualise and assess the recombination of the Cre and Null-AAV8

2.10.1 mT/mG tissue preparation and cryopreservation with sucrose

Tissue was harvested, immersed in methanol free 4% PFA and placed on a roller (Thermo Fisher Scientific, 2 hours, 4°C in the dark). The tissue was drained of PFA, washed twice with PBS and placed in 18% sucrose solution on a roller in the dark (overnight, 4°C). For cryopreservation, the tissue was drained of sucrose solution, dabbed dry and placed in a mould containing optimal cutting temperature compound (OCT, VWR, PA, USA). Tissue was allowed to acclimatise to the OCT (30mins, room temperature). During acclimatisation bubbles were removed for even preservation. The OCT-immersed tissue was flash frozen using a slurry (absolute ethanol and dry ice) and stored at -80°C

2.10.2 Imaging of fluorescent tissue

Two hours before sectioning, the OCT embedded tissues were transferred from -80°C to -20°C. Each tissue was cut in 10µM sections and stored in the dark at -80°C. To prepre for imaging the slides were left at room temperature to air dry for 30mins. Once dry, ProLong™ Diamond Antifade Mountant with DAPI (Invitrogen, CA, USA) was added alongside a coverslip. Slides were again stored in the dark (overnight, 4°C) for imaging the next day.

Fluorescent imaging of the mT/mG mouse sections was achieved on the ZEISS Axio Scan.Z1 (ZEISS). The green and red fluorescence was measured on the eGFP and Alexofluor555 channel. The DAPI counterstain (blue fluorescence, DAPI channel) was used to focus the microscope on the tissue. The Zen Blue edition software (ZEISS) was used for tissue visualisation.

2.11 Western Blotting

Western Blotting analysis of CYP2E1 protein expression was investigated in the liver and kidney. Dicer protein expression was measured in the liver, spleen and kidney. Due to the differing molecular weights, western blotting of Dicer ~218kDa and CYP2E1 ~50-55kDa required different gel and transfer conditions.

2.11.1 Protein extraction

To keep dephosphorylation and protein denaturing to a minimum, snap frozen tissue (⅓ of the left lateral lobe of the liver, ⅓ of the spleen and ½ of the kidney) were homogenised (as per section 2.7.1.2) in ice cold lysis buffer containing protease inhibitors. The lysis buffer was composed of filtered 250mM sucrose and 10mM triethanolamine in diH2O (7.6pH). After filtration, Merck cocktail III protease inhibitor (Calibochem, Merck-Millipore, CA, USA) was added to the lysis buffer at 10µl/ml. Following homogenisation, the samples were centrifuged for 2 minutes at 2000rpm and left to rest on ice for 15 minutes. The supernatant was placed in aliquots and stored at -80.

2.11.2 Bicinchoninic acid assay (BCA) assay and tissue preparation

Protein concentrations were determined for gel electrophoresis (Section 2.11.3) and microsomal preparation (Section2.12) by adding samples (1:10 dilution in milliQ water) to the prepared Pierce BCA Protein assay in duplicate (Thermo Fisher Scientific). The assay was completed following the manufacturing instructions. The plate's absorbance was read after incubation (37°C, 30 minutes) at 562nm. The samples were then diluted to 1µg/µl of protein in DTT (final concentration of 50mM), LDS sample buffer (NuPAGE™ x4, ThermoFisher Scientific, final concentration of x1) and deionised water. The sample preparation was vortexed, denatured at 70°C for 15 minutes and centrifuged briefly before loading

2.11.3 Gel Electrophoresis

For CYP2E1 expression, ten well, 4-20% gradient tris-glycine precast gels (Novex™, Wedgewell™, Invitrogen) were rinsed and placed in a Mini Gel Tank (Life Technologies). The tank was filled with electrophoresis running buffer (SDS-PAGE running buffer: 250mM trizma base, 190mM glycine and 0.1% SDS, pH 8.6). A protein

load of 30µg was added to each well alongside a PageRuler™ Plus Prestained Protein Ladder (ThermoFisher Scientific). The samples underwent gel electrophoresis at a constant voltage of 150V for 110 minutes.

For the investigation of Dicer protein expression, ten well, 4-12% gradient tris-glycine precast gels (Novex™, Wedgewell™, Invitrogen) were used following the instructions above and ran at 150V for 80 minutes.

2.11.4 Protein transfer

The 0.45µM PVDF membrane (Immobilon-P, Merck, NJ, USA) was cut and prepared for protein transfer by immersion in absolute methanol for 15 seconds, several washes in diH_2O and in the transfer buffer (480µM Trizma Base, 3.84mM Glycine and 10% v/v methanol, pH8.8) for 5 minutes. Taking care to avoid bubbles, the PVDF membrane was then placed on top of the gel, along with a sheet of blotting paper (Cytiva, Sheffield, UK) pre-soaked in transfer buffer. The gel was then flipped over and another pre-soaked sheet of electrode paper was added on top. For the wet protein transfer, the gel sandwiched with the PVDF membrane in between 2 sheets of electrode paper was placed in the XCell II Blot Module (XCell SureLock™, Invitrogen with sponges (pre-soaked in transfer buffer) on either side. The transfer was left at 30V for 2 hours at room temperature.

Using the same methods as above, protein transfer for Dicer was completed using chilled methanol-free transfer buffer (480µM Trizma Base, 3.84mM Glycine). Following the membrane preparation, the wet protein transfer was left at 90mA for 16 hours at 4°C

2.11.5 Immunoblotting

The membrane was removed from the transfer module and incubated (1 hour at room temperature) in 20mls of blocking buffer (5% milk in wash buffer (TBS-T, 20mM Trizma base, 150mM NaCl and 0.1% v/v Tween-20, pH 7.6)). The primary antibody for Dicer or CYP2E1 (Table 2.8) was added to 1% milk (dissolved in TBS-T) and incubated with the membrane (overnight, 4°C). The membrane was washed with wash buffer (3x 10 minutes). The membrane was then transferred into 5mls of the HRP-secondary antibody (Table 2.8) diluted in 1% milk and placed on a roller (1 hour at room temperature). The membrane was washed as previously described and incubated with ECL reagent (Pierce™, ThermoFisher Scientific) (5 minutes at room temperature). Excess ECL was removed, the membrane placed in a plastic wallet, exposed to X-Ray film (CL-Xposure film, ThermoFisher Scientific), developed (Compact 4x, Xograph) and scanned.

Table 2.8 Primary and secondary antibodies used for western blotting

Target (immunogen)	**Host and Conjugate**	**Source and Catalogue no.**	**Dilution factor**
Primary antibodies			
Dicer	Rabbit, -	Sigma Aldrich, SAB004200087	1:200
Cytochrome P450 2E1	Rabbit,-	Abcam, ab28146	1:5000
β-actin	Mouse,-	Sigma Aldrich, A2228	1:20,000
Secondary antibodies			
Rabbit IgG	Goat, HRP	Vector Laboratories , PI-1000-1	1:3000
Mouse IgG	Horse, HRP	Vector Laboratories, PI-2000-1	1:3000

2.11.6 Stripping and re-probing

After the film development and analysis of Dicer or CYP2E1 expression, the membrane was stripped and re-probed for β-actin. To remove the antibodies on the membrane, the membrane was incubated 2x30 minutes in acid stripping buffer (30g glycine, 2g SDS, 20ml Tween-20 in 1L diH_2O, pH 2.2). The membrane pH was then neutralised by 3x3 minute washes with PBS and placed into the blocking buffer (5% milk). The steps from Section 2.11.5 (immunoblotting) were repeated with the β-actin primary and secondary antibodies.

2.11.7 Quantification of protein bands

Western blot analysis was achieved using ImageJ (National Institutes of Health, MD, USA). Images were converted to 8-bit and each lane density (intensity) was measured [214]. The relative density of each peak was then calculated from the baseline control sample on each gel.

2.12 Determination of CYP450 enzymatic activity

2.12.1 Microsomal preparation

Snap frozen kidney and liver from the tissue sampling (described in Section 2.6) were used for the microsomal preparation. To ensure there was sufficient protein for the detection of cytochrome P450 (CYP450) activity, five ½'s of kidney were pooled for each group and homogenised together. As the CYP450 expression is high in the liver [215], these samples were not pooled. Consequently, there was an n=3 for livers and an n=1 for the kidneys per group.

Tissues were weighed and added to buffer 1 (154 mM KCl, 50 mM Tris (Base) pH 7.4 buffer) until the buffer and tissue combined was 4 times greater than the tissue alone. The tissues were then homogenised using sterile stainless steel beads on a TissueLyser II (Qiagen). The homogenate was centrifuged at 9000 x*g* (4°C, 20mins) and the supernatant transferred to ultracentrifuge tubes topped up with buffer 1. The supernatant was centrifuged at 100,000 x*g* (4°C, 1 hour). The pellet was reconstituted in 0.5ml of buffer 2 (50 mM potassium phosphate/20% glycerol, pH 7.4) per g of starting sample weight. Samples were aliquoted and stored at -80°C.

To determine protein content, the samples were diluted 1:20 with milliQ water and added to the Pierce BCA Protein assay in duplicate (Thermo Fisher Scientific) (Section 2.11.2)

2.12.2 Cytochrome P450 enzyme assay using liquid chromatography- mass spectrometry (LC-MS)

First, the liver and kidney samples were diluted to 1mg/ml and 3mg/ml respectively in phosphate buffer (pH 7.4) to make a total volume of 188µl. To set up the metabolism, a cocktail of 7 CYP450 substrates (x100) (As previously described [216, 217], Table 2.9) and 20nM of the reducing agent NADPH was added to the samples (in duplicate). The plate was incubated on a plate shaker at 450rpm, 38°C for 10 minutes.

To halt the activity of the CYP450 enzymes, 40µl of the sample was added to 160µl of a quench solution (200nM of benzoxazol and 4nM of verapamil). Again, the samples were left to shake at 650rpm, 38°C for 10 minutes. After that, the plate was centrifuged down for 5 minutes and 50µl of supernatant was added to 150µl of ultrapure water. The individual plate wells were then analysed on a mass spectrometer (Xevo TQ-S, Waters, Milford, MA, USA). Data were collected on the Water's Masslynx software (Waters Corporation, MA, USA).

Activity of each CYP450 was determined by:

$$\frac{area\ under\ the\ curve\ (AUC) of analyte}{AUC\ of\ internal\ control}$$

For each CYP450 assessed (Table 2.9), a fixed concentration of verapamil was used as the internal control.

Table 2.9 Mass Spectrometry components and read settings to measure CYP450 activity

Substrate	Metabolite	MRM (Parent→Daughter) m/z	Dwell (s)	Cone voltage (V)	Collision energy (V)
Phenacetin	Acetaminophen	152.02→109.96	0.02	15	15
Bupropion	Hydroxybupropion	256.06→139.02	0.02	15	30
Amodiaquine	n-Desethylamodiaquine	328.10→283.13	0.02	75	15
Diclofenac	4-Hydroxydiclofenac	312.13→230.09	0.02	15	40
Bufuralol	1-Hydroxybufuralol	278.16→186.12	0.02	55	20
Midazolam	1-Hydroxymidazolam	342.05→168.24	0.02	75	40
Chlorzoxazone	6-Hydroxychlorzoxazone	183.93→119.87	0.05	10	20

Chapter 3 Characterisation of Dicer knockdown in the liver

3.1 Introduction

3.2 Background

MiR-122 has shown to be the miRNA with the greatest organ specificity [164]. It accounts for around 72% of hepatocytes total miRNA, with little-to-no expression in other organs [160-162]. This specificity has enabled studies to confidently determine that miR-122 measured in circulation of healthy and DILI patients has derived from the liver [86, 122]. Additionally, miR-122 has been shown to be trafficked between cells and organs eliciting an effect [121, 122, 137]. Thus, it has been indicated that miR-122 acts as a short and long distant cell-cell signalling molecule in physiological and pathological events.

It was previously observed that the increase of miR-122 in the circulation, following paracetamol-induced liver injury, was paired with an increase in miR-122 in the kidney cortex and medulla of C57BL/6 mice [218]. Furthermore, the role of hepatic-derived EV-bound miR-122 in the kidney proximal tubule cell was investigated *in vitro*. Replicating Lee *et al.* findings, Morrison found that isolated miR-122 enriched EV's were taken up by primary kidney proximal tubule cells and reduced a known miR-122 mRNA target, FOXO3[200, 218]. Furthermore, incubation with miR-122 enriched EV's significantly protected the kidney proximal tubule cells from subsequent cisplatin-induced nephrotoxicity, compared to cells incubated with EV's from control mice and mice with cardiac injury [218]. To explore this further, the aim of the studies in this chapter was to optimise and define an inducible model of liver-specific Dicer deletion. In addition, exploration into the organs responsible for the uptake and clearance of liver-derived miR-122 was carried out in a non-DILI mouse.

In the cytoplasm of the cell, Dicer, within the RISC loading complex (RLC), is involved in the cleavage and processing of pre-miRNA into mature miRNA [94, 219]. Encoded by a single locus, studies have shown that disruption of Dicer results in the loss of almost all miRNA, indicating Dicer is essential for miRNA production [220-222]. The global loss of *Dicer1* and in turn miRNA is detrimental during the early stages of embryo development [223, 224]. Additionally, the use of *Albumin-Cre; Dicer1$^{flox/flox}$* [225] or *AlfpCre;Dicer1$^{flox/flox}$* mice [226] as a model of hepatocyte specific *Dicer1* knockdown

resulted in postnatal inflammation, liver damage and necrosis. However, inducing hepatocyte specific *Dicer1* knockdown in adult *Dicer1*$^{flox/flox}$ mice has been shown to successfully abolish Dicer enzymatic activity and miRNA production, without disrupting hepatocyte proliferation prior to weaning [227]. Moreover, inducing *Dicer1* knockdown in the liver is not associated with chronic steatohepatitis, liver fibrosis and spontaneous hepatocellular carcinoma seen in the germline knockout of miR-122 (*miR-122*$^{-/-}$) [165, 176].

As the inducible model of *Dicer1*$^{flox/flox}$ mice was previously shown to display no signs of injury [227], *Dicer1* $^{flox/flox}$ mice were used as an *in vivo* model to investigate the transfer of hepatocyte-derived microRNA to other organs .Homozygous *Dicer1* $^{flox/flox}$ mice have a global expression of *loxP* sites on either side of exon 23 of the *Dicer1* gene. Cre-mediated recombination leads to the loss of the *Dicer1* gene and in turn ceases the production of mature miRNA. With AAV8s known to preferentially direct themselves to hepatocytes [228], an AAV8-Tbg-Cre was used to induce Cre-recombination in the liver of the *Dicer1*$^{flox/flox}$ mice. To further ensure liver specific *Dicer1* deletion, the Cre-AAV8 used contained a thyroid hormone-binding globulin (TBG) promoter.

3.3 Experimental plan

3.3.1 mT/mG mice

The double-fluorescent Cre reporter mouse strain, mT/mG [229], were used to visualise and assess the Cre-recombination efficiency of the hepatocyte specific Cre-AAV8 and its negative control (Null-AAV8). As described in Section 2.10, tissues were harvested 3 weeks post Cre and Null-AAV8 injection ($6.25x10^{10}$ viral genomes/100µL dose).

3.3.2 Dicer1 $^{flox/flox}$ mice

Homozygous *Dicer1* $^{flox/flox}$ mice (male and female) underwent a single tail vein injection of a hepatocyte-specific AAV8 ($2.5x10^{11}$ viral genomes/100µL dose, Table 2.1). Mice were randomly selected for an injection with either the Cre-AAV8 or its negative control, Null-AAV8 (Section 2.3). After injection, tissue and blood were collected weekly, for up to four weeks (n=20, n=5 per time point) (Figure 3.1). To assess the basal level of expression without the influence of an AAV8, tissue and plasma from baseline (untreated) mice (n=5) were used as a control (Figure 3.1). Dicer mRNA and protein expression were measured by RT-qPCR and western blotting respectively (as per methods). MiRNA expression was determined using RT-qPCR as described in Section 2.7.

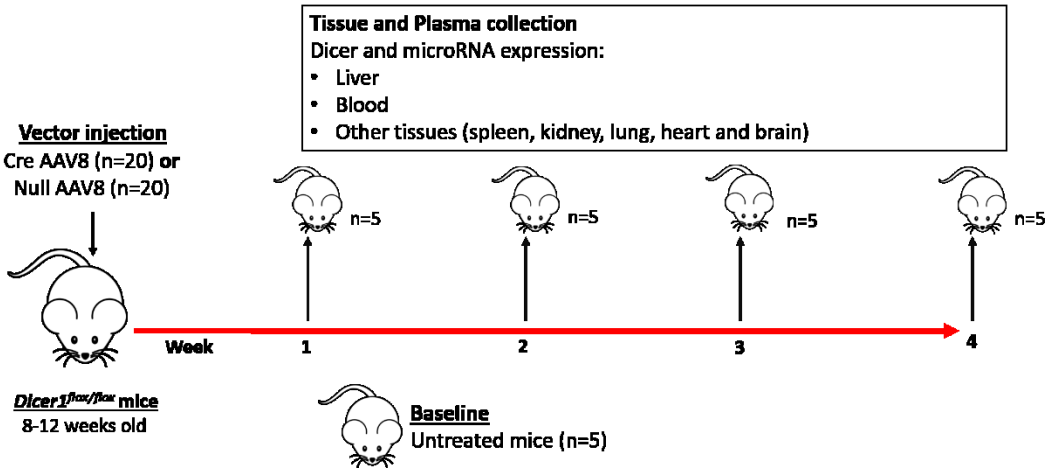

Figure 3.1 Schematic of the experimental plan used to determine the time course of *Dicer1* and miRNA deletion following a single tail vein injection of an AAV8 vector.

3.4 Results

3.4.1 Successful Cre-recombination observed in the hepatocytes following Cre-AAV8 treatment

In the liver, 3 weeks post AAV8 injection, the Cre-AAV8 treated mT/mG mice primarily displayed positive recombination in the hepatocytes (green fluorescent membranes)(Figure 3.2C). Whereas, the baseline (untreated) and Null-AAV8 treated mT/mG mice globally expressed red fluorescent membranes in the liver, reflecting negative Cre-recombination (Figure 3.2A and B).

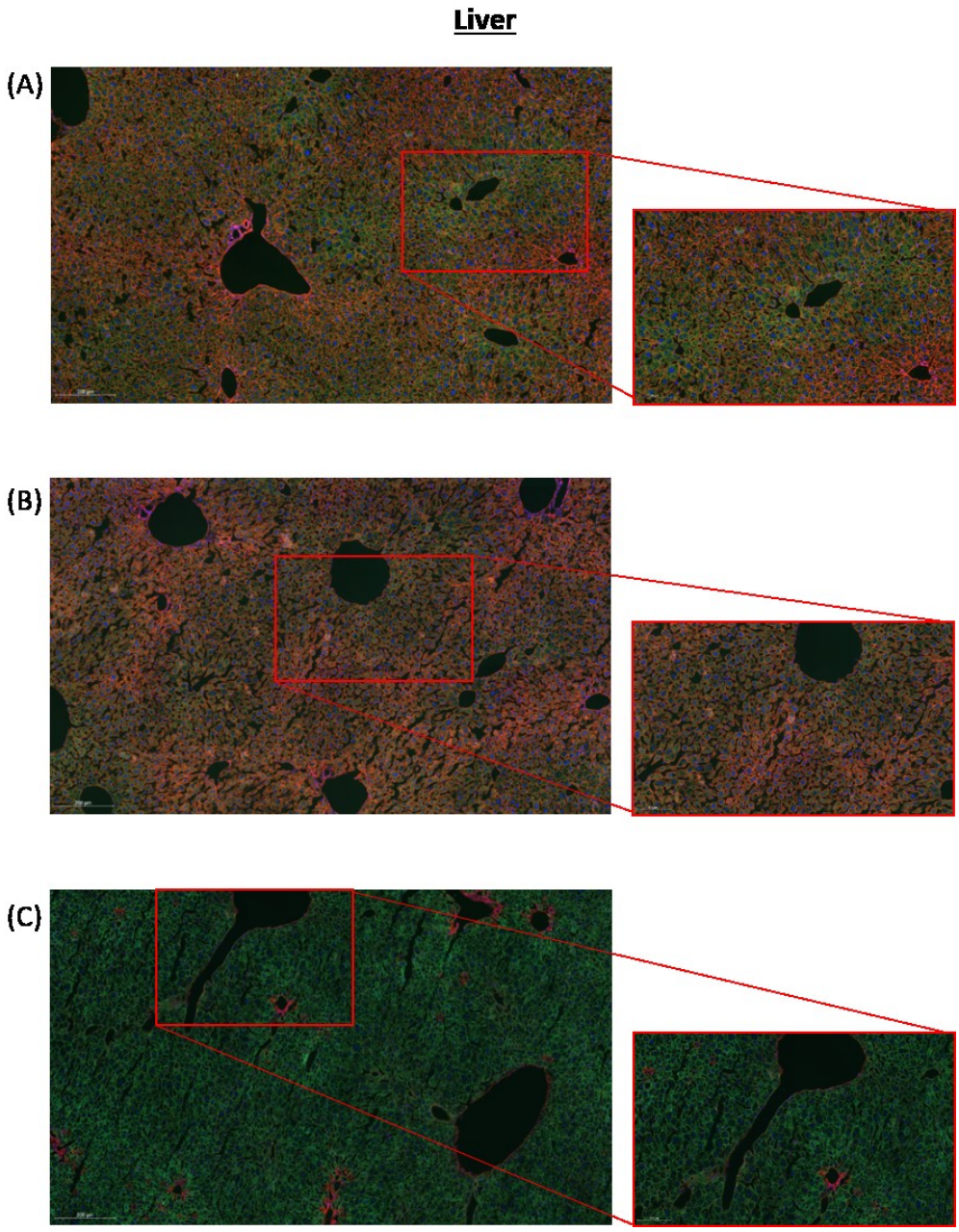

Figure 3.2 Fluorescent imaging of mT/mG livers following Null-AAV8 and Cre-AAV8 treatment

Liver sections of (A) baseline (untreated), (B) Null-AAV8 injected and (C) Cre-AAV8 injected mT/mG mice. Images taken 3 weeks after a single AAV8 treatment (Null or Cre-AAV8). Negative Cre-recombination shown with the global expression of red fluorescence (tdTomato) at the cell membranes (A and B). Whilst, in the Cre-AAV8 treated mice (C) the hepatocytes primarily express green fluorescence (EGFP),

reflecting positive Cre-recombination. Blue fluorescence is DAPI. Scale bar represents 300µm, 20x magnification. Images representative of n=2.

After visually assessing Cre-recombination in the mT/mG mice, the activity of the Null-AAV8 and Cre-AAV8 were investigated in the *Dicer1*$^{flox/flox}$ mice (Figure 3.1). Western blotting was carried out to determine if the Cre-AAV8 treatment resulted in the successful knockdown of Dicer protein expression in the hepatocytes. One week following Cre-AAV8 treatment, a total loss of Dicer protein was observed and maintained until week 4 (Figure 3.3A and B). Baseline (untreated) mice and the AAV8 negative control, Null-AAV8, exhibited bands representing Dicer expression at ~218kDa (Figure 3.3A and B). It can be seen in Figure 3.3A and B that the loading control, β-actin (~42kDa), remains consistent across each well. Relative density analysis of each band (Figure 3.3C and D) supported these findings further.

Moreover, Dicer mRNA was measured in the liver to further define the activity of the AAV8 treatments. Interestingly, Cre-recombination following Cre-AAV8 treatment did not influence the expression of Dicer mRNA, in contrast to the Null-AAV8 treated mice (Appendix I).

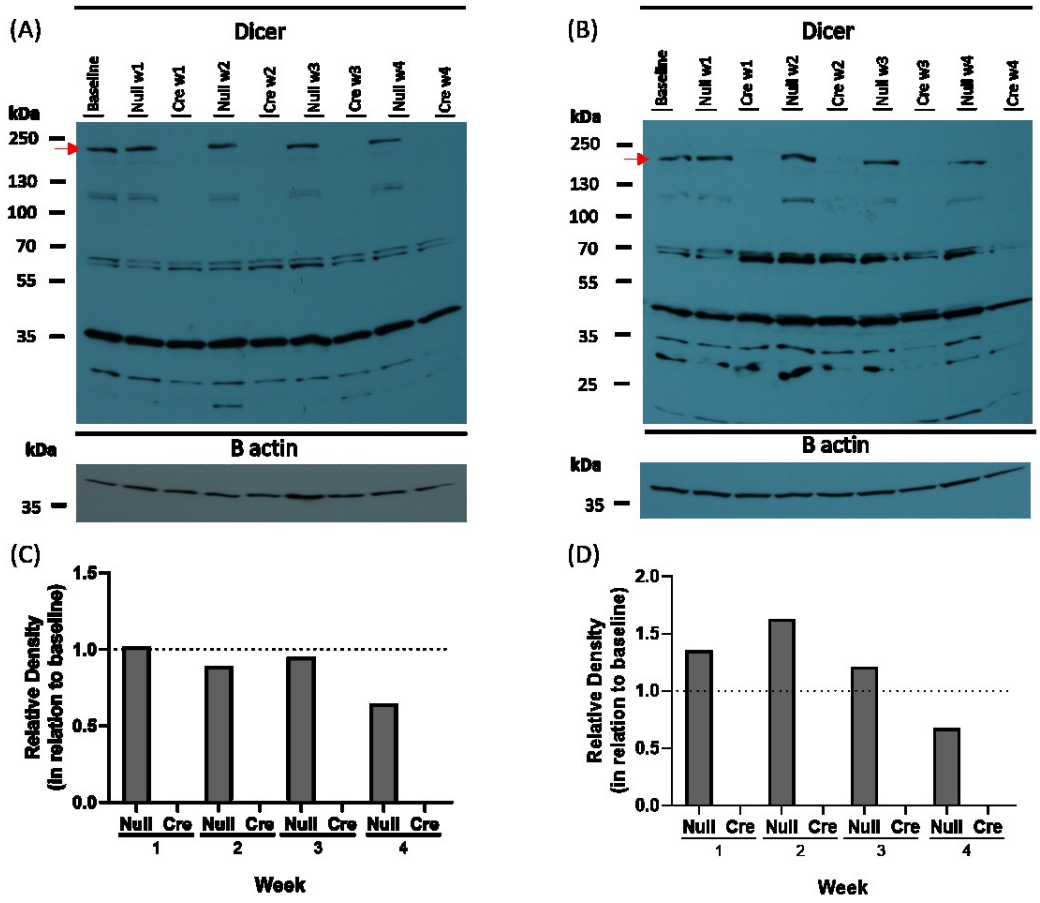

Figure 3.3 Dicer protein expression in the liver post Null-AAV8 and Cre-AAV8 treatment

(A and B) Protein expression of Dicer (~218kDa, indicated by the red arrows) in the liver of the baseline (untreated) and week 1-4 of the Null-AAV8 and Cre-AAV8 treated Dicer1$^{flox/flox}$ mice, was determined by western blotting. For each western blot, β-actin (~42kDa) was used as a loading control. (C and D). To quantify Dicer protein expression, relative density of the ~218 kDa band was calculated in the Null (light grey) and Cre-AAV8 (dark grey) treated mice (week 1 to 4, post injection), normalised to the baseline control Dicer band (dotted line). Each western blot represents an n=1 from each treatment group.

After confirmation that Dicer protein was knocked down in the liver, mature miRNA was measured using RT-qPCR. In the liver, previously described hepatocyte enriched miRNA species: miR-122, miR-192 and miR-151 were measured [86, 87, 123](Figure 3.4A). Two weeks post Cre-AAV8 treatment, all 3 miRNAs decreased in comparison to the Null-AAV8 treated mice (Linear Regression: miR-122: Cre slope=-24 week^{-1},Cre slope vs zero, p<0.0001; miR-192: Cre slope=-24 week^{-1}, Cre slope vs zero p<0.0001; miR-151**:** Cre slope -9.4 week^{-1}, Cre slope vs zero p=0.014) (Figure 3.4A, Table 6.1). In the Cre-AAV8 treated mice, the loss of miR-122 and miR-192 was significantly different than the Null-AAV8 treated mice (Linear regression: miR-122: Null vs Cre p<0.0001; miR-192: Null vs Cre p=0.0004 (Figure 3.4A)). miR-151 did not significantly change in the Cre-AAV8 mice, compared to the Null-AAV8 mice (Linear Regression: Null vs Cre p=0.08).

Three housekeeping genes: SNORD68, SNORD95 and U6 were assessed for the normalisation of miRNA in the liver. It was observed that all three housekeeping genes had significantly different Ct values in the Cre-AAV8 liver, when compared to the Null-AAV8 mice. Due to this, Figure 3.4 shows miR-122 normalised by SNORD68 (B), SNORD95 (C) and U6 (D). Here, the loss of miR-122 was observed following the normalisation with each housekeeping gene (Figure 3.4). When comparing the means of the Null-AAV8 and Cre-AAV8 mice, SNORD68 exhibited the smallest difference (ANOVA: Null vs Cre difference in means=0.4). Due to this, Figure 3.4A is normalised to SNORD68.

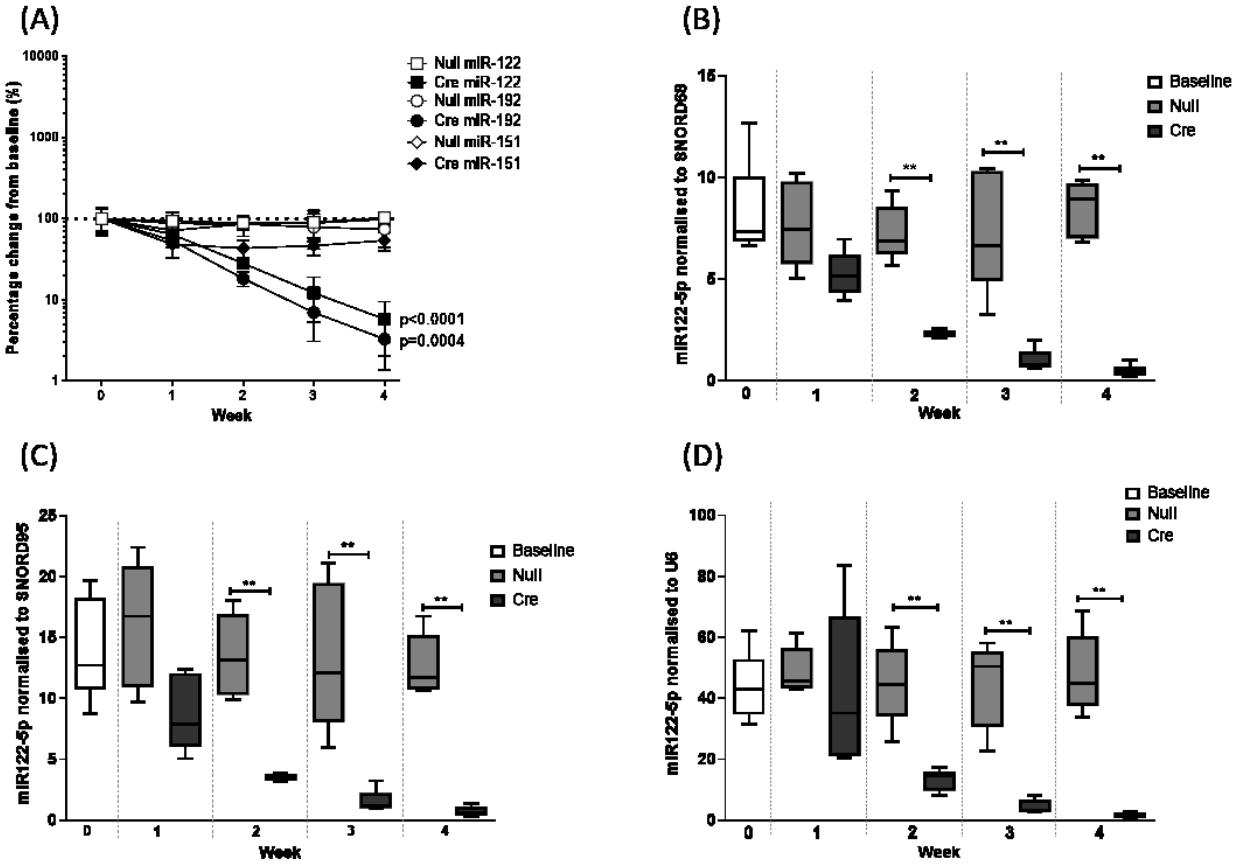

Figure 3.4 Hepatocyte enriched miRNA in the liver of the AAV8 treated mice

*Mature miRNA were measured in the liver by RT-qPCR and presented as $2^{-\Delta T}$. (A) miR-122, miR-192 and miR-151 in the liver of the Null-AAV8 (white) and Cre-AAV8 (black) treated mice, first normalised to SNORD68, and then converted as a percentage to the baseline mice (untreated, week 0, dotted line). Data represented as mean ±SD n=5. P values were calculated by linear regression, comparing the slopes of the Null-AAV8 and Cre-AAV8 treated Dicer1 $^{flox/flox}$ mice (B-D) miR-122 normalised to SNORD68, SNORD95 and U6 respectively in the baseline (white), Null-AAV8 (light grey) and Cre-AAV8 (dark grey) treated Dicer1$^{flox/flox}$ mice. Data are represented as mean ±SD, n=5. Significant differences were calculated from an unpaired Mann Whitney U test, comparing the expression of miR-122 in the Null-AAV8 and Cre-AAV8 treated mice at each week **p≤0.01.*

Next, H&E staining was carried out in the liver sections to assess whether the Null or Cre-AAV8 induced liver injury (Figure 3.5). Baseline (untreated, A) and week 1-4 post Null-AAV8 (B-E) and Cre-AAV8 (F-I) treatments were assessed blindly. A skilled subjective opinion of histological appearances was provided without a formal scale. Across each treatment group it was determined that there were no signs of liver injury with: normal portal-central vascular relationships, uninflamed portal tracts, no bile duct inflammation, damage or loss, no interface inflammation or ductular reaction, no lobular inflammation, hepatocellular injury or loss and lastly, no steatosis (Figure 3.5).

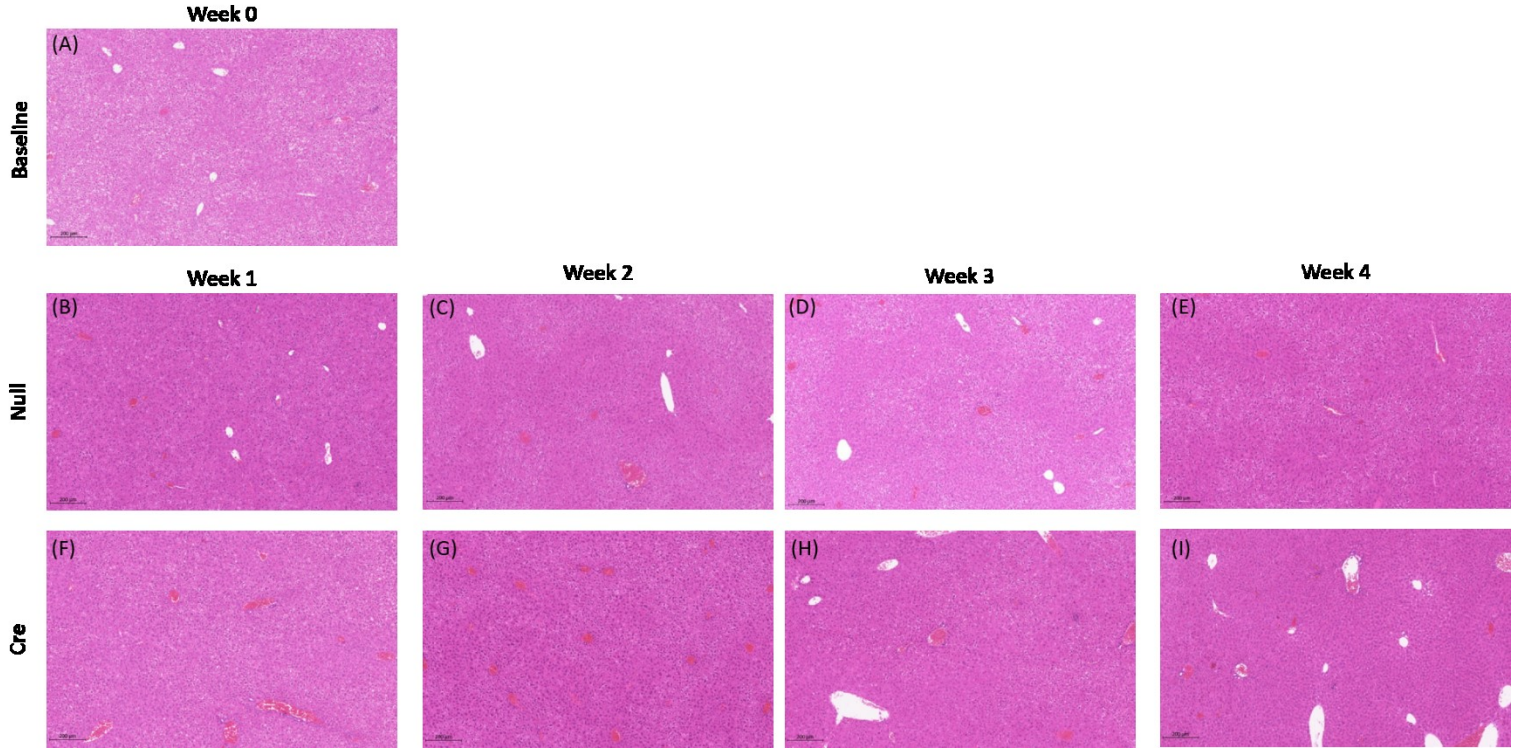

Figure 3.5 H&E stained livers following AAV8 treatment

H&E stained liver sections of baseline (untreated, A), Null-AAV8 (B-E) and Cre-AAV8 (F-I) treated Dicer1 $^{flox/flox}$ mice from week 1 to 4. Scale bar represents 200µm, 20x magnification. Images representative of an n=2.

After assessing the H&E stained livers for injury, ALT was measured in the plasma of each treatment group described in Figure 3.1. This was carried out to determine if a single treatment of the AAV8 (Null or Cre) induced liver injury. It was observed that the Null-AAV8 and Cre-AAV8 treatments were not significantly different from eachother, with both inducing an increase in circulating ALT (ANOVA of each treatment mean, $p>0.05$).

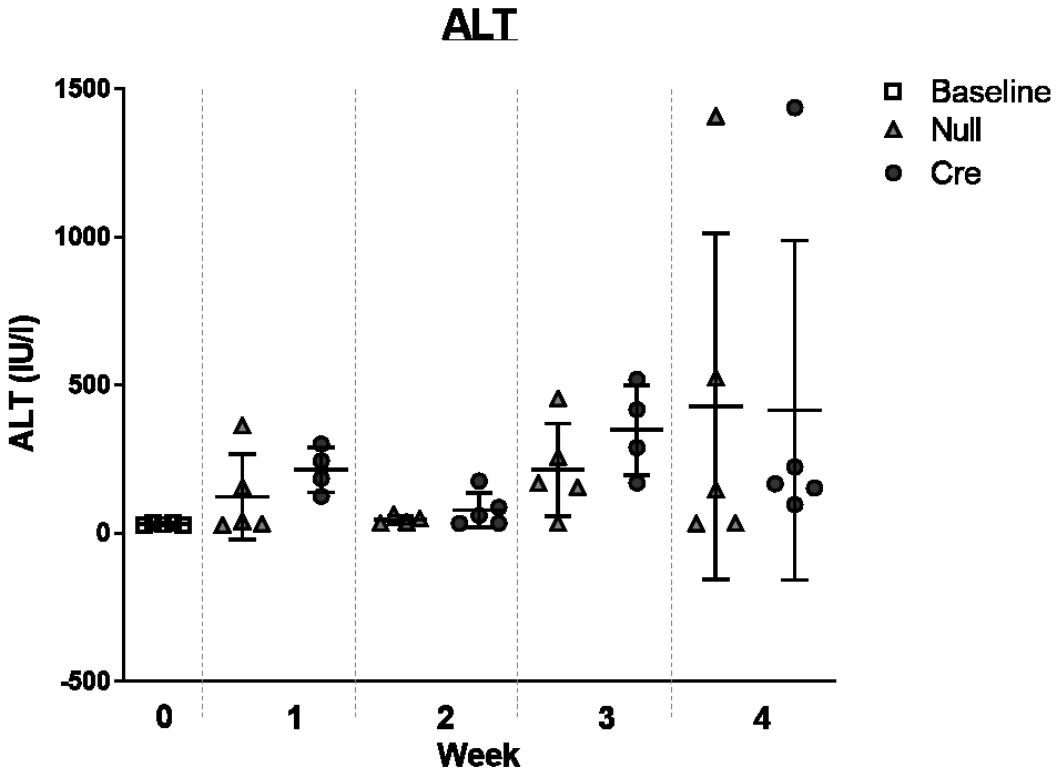

Figure 3.6 Plasma ALT levels after a single Null and Cre-AAV8 injection

Plasma ALT activity (IU/l) was measured in the baseline (untreated, white squares), Null-AAV8 (light grey triangles) and Cre-AAV8 (dark grey circles) treated mice 1-4 weeks post injection. Error bars represent mean ±SD, n=5. (Cre-AAV8 week 1 and 3 and Null week 2, n=4). Multiple comparison two-way ANOVA determined there were no significant difference between the means of each treatment group and time point (p>0.05).

3.4.2 Mature miR-122 is decreased in the spleen following hepatocyte specific *Dicer1* knockdown

The mT/mG mice spleens were assessed following Null-AAV8 and Cre-AAV8 injection. This was carried out to determine if the hepatocyte specific AAV8s displayed off-target *Dicer1* knockdown in the spleen. Figure 3.7 confirms negative Cre-recombination (global expression of red fluorescence at the cell membranes) in both the Null-AAV8 (A) and the Cre-AAV8 (B) treated mT/mG mice.

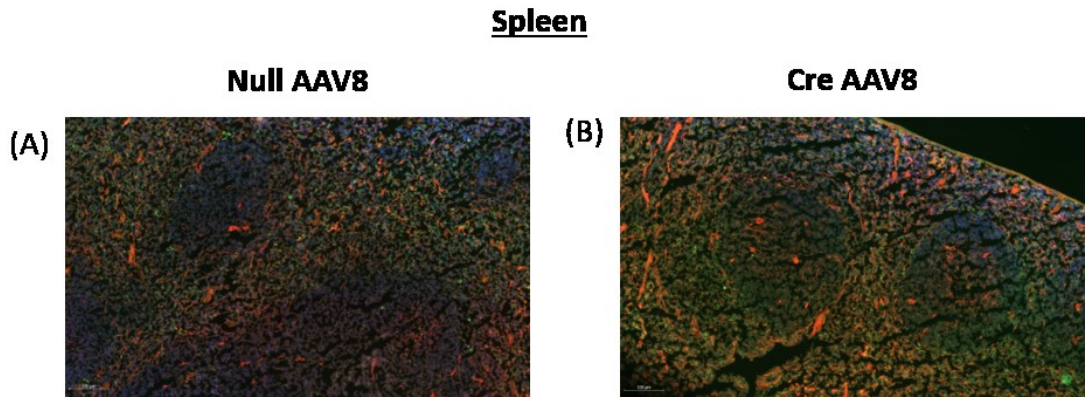

Figure 3.7 Fluorescent imaging of the spleen following AAV8 treatment

mT/mG spleen sections 3 weeks after Null-AAV8 (A) and Cre-AAV8 (B) treatment. Negative Cre-recombination shown with the global expression of red fluorescence (tdTomato) at the cell membranes (A, B). Blue fluorescence is DAPI. Scale bar represents 100µm, 20x magnification. Images representative of n=2.

For each time point and treatment group outlined in the experimental plan (shown in Figure 3.1), Dicer protein expression was measured in the *Dicer1* $^{flox/flox}$ spleens by Western blotting. Figure 3.8A and B highlights a consistent expression of Dicer protein (~218kDa) across each treatment group: baseline (untreated) and Null-AAV8 and Cre-AAV8 treated mice from week 1 to 4. For both western blots, the loading control, β-actin (~42kDa), remains stable across each well (Figure 3.8A and B). Relative density analysis of each band (Figure 3.8C and D) quantified and validated these findings further. In addition to this, a non-significant difference in Dicer mRNA expression was observed between the Cre-AAV8 and Null-AAV8 treated mice (Figure 6.2).

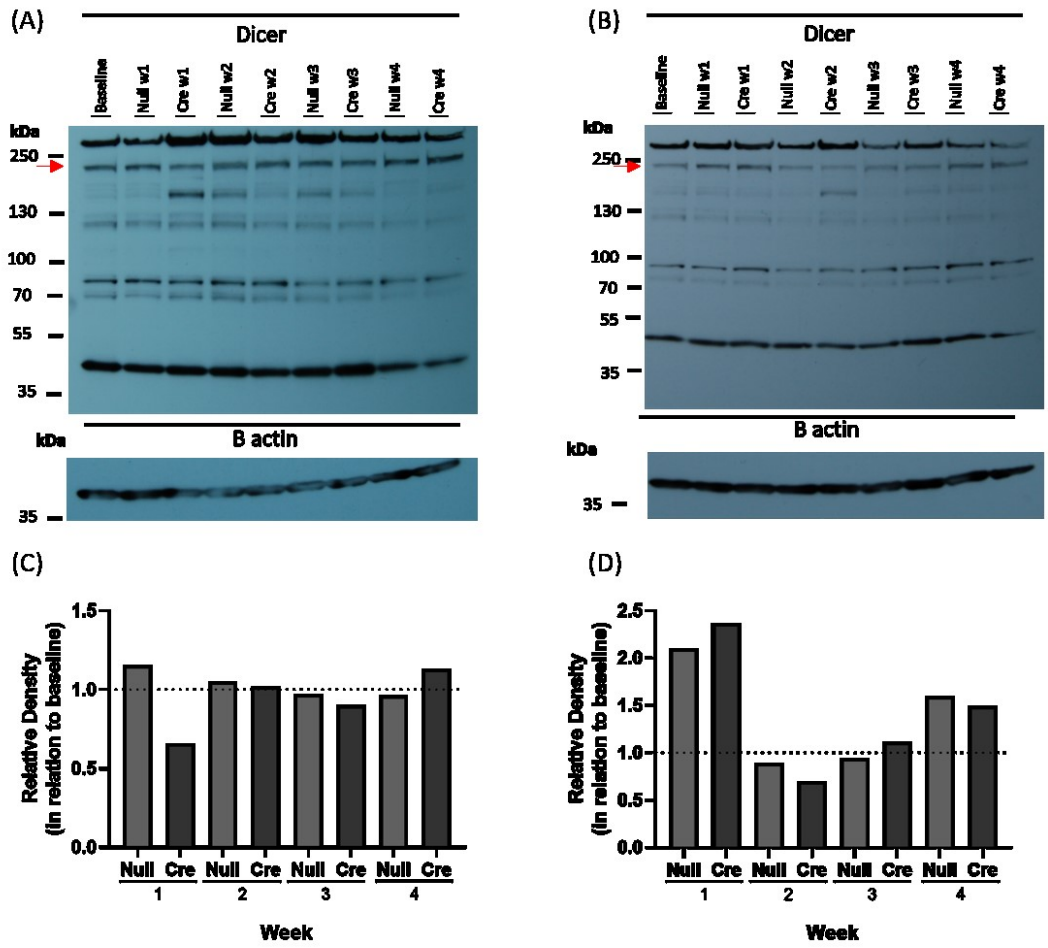

Figure 3.8 Dicer protein expression in the spleen after Null and Cre-AAV8 injection

(A and B) Protein expression of Dicer (~218kDa, indicated by the red arrows) in the spleen of the baseline (untreated) and week 1 to 4 of the Null-AAV8 and Cre-AAV8 treated mice, was determined by western blotting. For each western blot, β-actin (~42kDa) was used as a loading control. (C and D)To quantify Dicer protein expression, relative density of the ~218 kDa band was calculated in the Null (light grey) and Cre-AAV8 (dark grey) treated mice (week 1 to 4, post injection), normalised to the baseline control Dicer band (dotted line). Each western blot represents an n=1 from each treatment group.

Subsequently, mature miRNA was measured in the spleen to determine its involvement in the uptake of circulating hepatocyte-derived miR-122. MiR-146a, a miRNA described to be enriched in the splenocytes [230, 231], was measured alongside the hepatocyte enriched miR-122 (Figure 3.9A). As reflected in the liver (Figure 3.4A), miR-122 decreased from week 2 to 4 in the Cre-AAV8 treated group when compared to the Null-AAV8 treated group (Linear Regression: Cre slope=-24.8 $week^{-1}$, Cre slope vs zero p=0.0003, Null vs Cre p=0.1). Furthermore, miR-122 was significantly lower in the Cre-AAV8 treated mice, in contrast to the Null-AAV8 mice at 2, 3 and 4 weeks post injection (Whitney U test: Null vs Cre $p<0.01$) (Figure 3.9B-C). Additionally, the evaluation of the raw Ct values of miRNA in the spleen highlights the loss of miR-122 expression in the Cre-AAV8, in comparison to the Null-AAV8 treated mice (Table 6.2.).

On the other hand, the slope of miR-146a expression was significantly greater in the Cre-AAV8 treated mice compared to the Null-AAV8 mice (Linear Regression: Cre slope= 15 $week^{-1}$, Cre slope vs zero p=0.014, Null vs Cre p=0.005) (Figure 3.9A). Despite this, each AAV8 treatment displayed similar levels of miR-146a expression in comparison to the baseline (untreated mice, dotted line) (Figure 3.9A and Table I.2.).

Three housekeepers were used in the measurement of miRNA in the spleen. When used as a normaliser, SNORD68 (B), SNORD95 (C) and U6 (D) displayed the same trend in miR-122 expression (Figure 3.9B-D). Nonetheless, it was determined that U6 was the gene with the greatest stability across the Null-AAV8 and Cre-AAV8 treatments. Hence, U6 was used as the normaliser for Figure 3.9A.

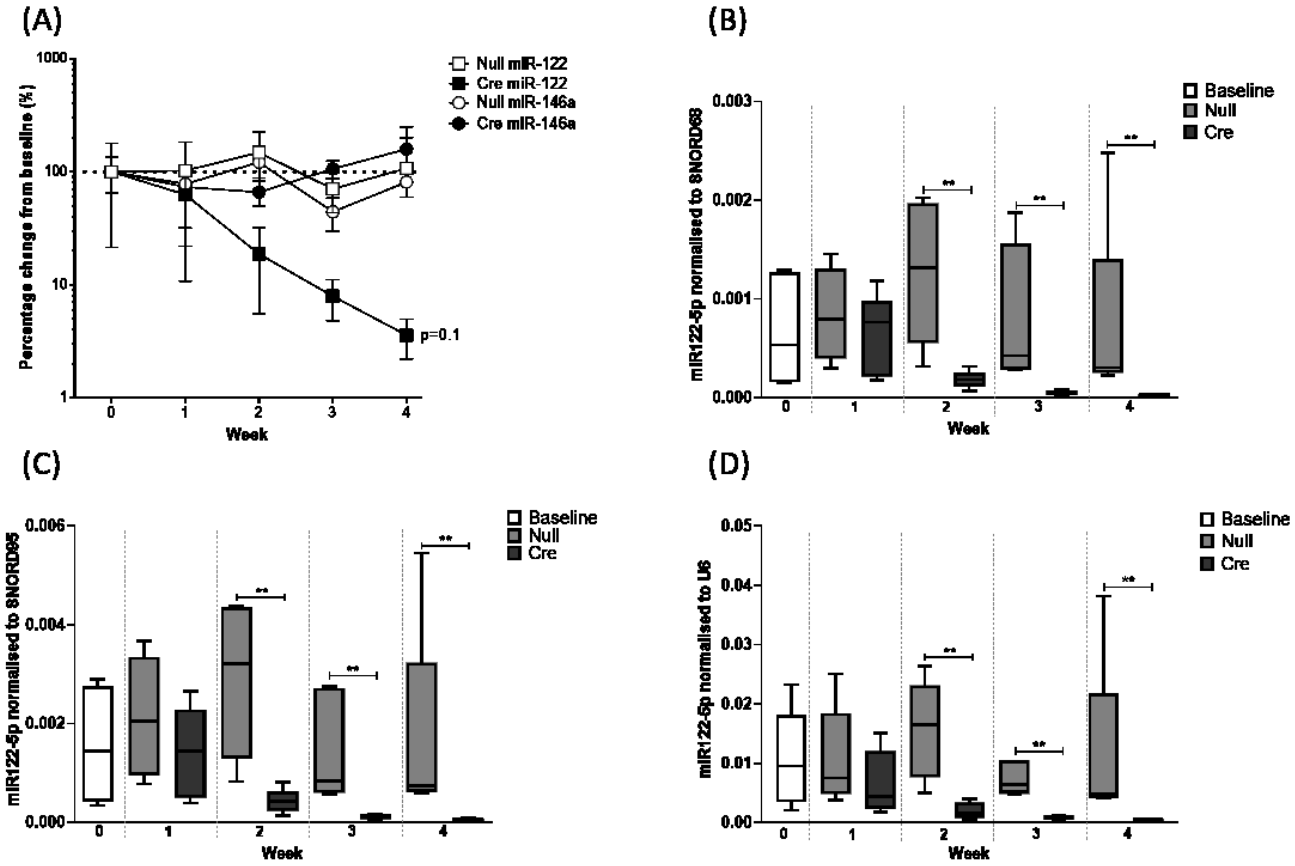

Figure 3.9 miR-122 and miR-146a expression in the spleen following a single Null-AAV8 and Cre-AAV8 treatment

*Mature miRNA was measured in the spleen by RT-qPCR and presented as $2^{-\Delta T}$. (A) miRNA-122 and miRNA-146a in the spleen of the Null-AAV8 (white) and Cre-AAV8 (black) Dicer1$^{flox/flox}$ mice, first normalised to U6, then converted as a percentage to the baseline mice (untreated, week 0, dotted line). Data represented as mean ±SD n=5. P values were calculated by linear regression, comparing the slopes of the Null-AAV8 and Cre-AAV8 mice. (B to D) miRNA-122 normalised to SNORD68, SNORD95 and U6 respectively in the baseline (white), Null-AAV8 (light grey) and Cre-AAV8 (dark grey) mice. Data were represented as mean ±SD, n=5. Significant differences were calculated from an unpaired Mann Whitney U test, comparing the expression of miR-122 in the Null-AAV8 and Cre-AAV8 treated mice at each week. ** p≤0.01.*

To investigate whether the loss of miR-122 had a detrimental effect on the health and morphology of the spleen, H&E stained spleens were evaluated in the Cre-AAV8 mice and the baseline and Null-AAV8 treated controls (Figure 3.10). Whilst blinded, a skilled subjective opinion indicated that all the spleens, regardless of treatment and time point, displayed no signs of injury with normal red and white pulp (Figure 3.10).

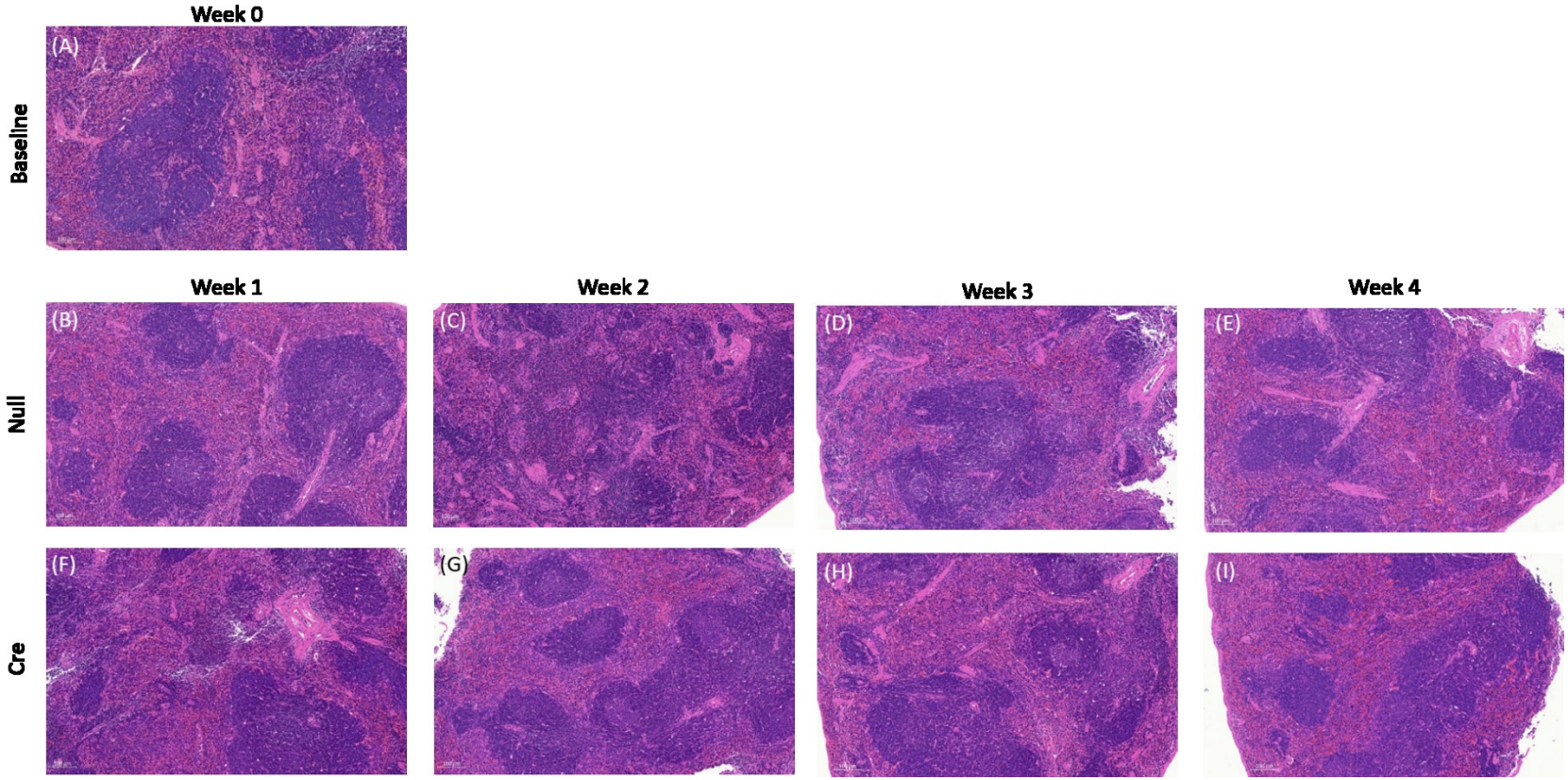

Figure 3.10 Spleen H&E sections in the baseline, Null and Cre-AAV8 treated mice

H&E stained spleen sections of the baseline (untreated, A), Null-AAV8 (B-E) and Cre-AAV8 (F-I) treated Dicer1$^{flox/flox}$ mice from week 1 to 4. Scale bar represents 100µm, 20x magnification*. Images representative of an n=2. Each image displays normal red and white pulp suggesting a lack of injury in the spleens.*

3.4.3 Mature miR-122 is lost in the kidney cortex and medulla following hepatocyte specific *Dicer1* knockdown

The whole kidney of the reporter mT/mG mice were visually assessed 3 weeks following Null-AAV8 and Cre-AAV8 injection. This was carried out to determine if the Null and Cre-AAV8 displayed any off-target *Dicer1* knockdown. Confirmation of negative Cre-recombination (global expression of red fluorescence at the cell membranes) in both the kidney cortex and medulla of the Null-AAV8 (A and C) and the Cre-AAV8 (B and D) treated mT/mG mice (Figure 3.11).

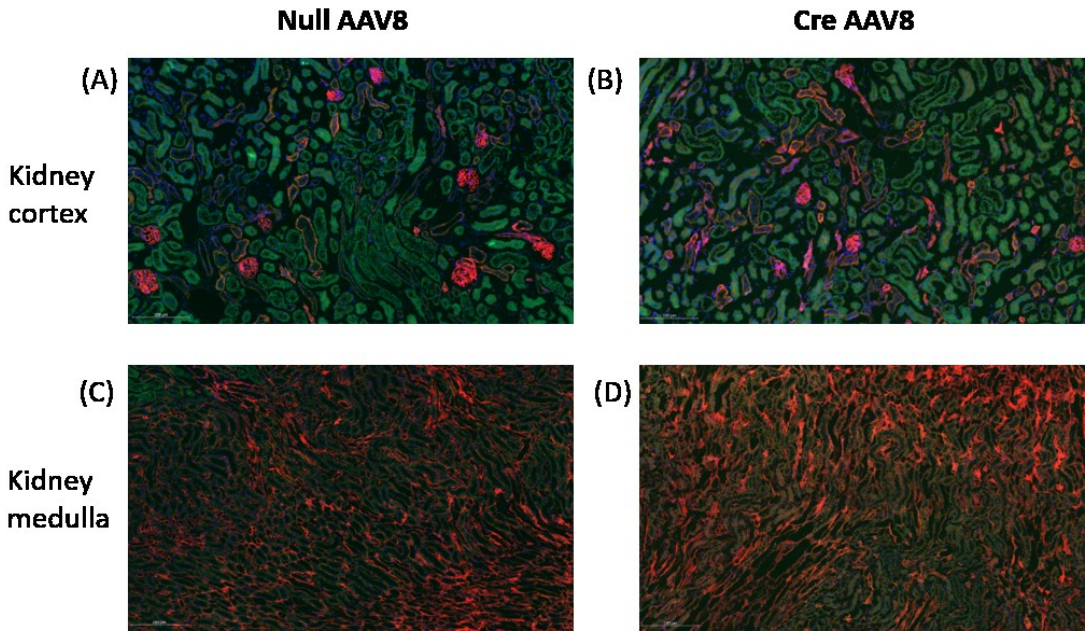

Figure 3.11 Fluorescent images of the kidney cortex and medulla following Cre-AAV8 and Null-AAV8 treatment.

Null-AAV8 injected (A and C) and Cre-AAV8 injected (B and D) mT/mG mice kidney cortex and medulla sections. Images taken 3 weeks post AAV8 injection. Negative Cre-recombination shown with the global expression of red fluorescence (tdTomato) at the cell membranes (kidney cortex: A, B; kidney medulla: C and D). Blue fluorescence is DAPI. Scale bar represents 100µm, 20x magnification. *Images representative of n=2.*

Dicer mRNA expression in the kidney cortex and medulla indicates constant expression across each treatment group described in (Figure 6.3). To explore this further, Dicer protein expression was then measured in the whole kidney. In Figure 3.8A and B, the Dicer protein band (~218kDa) was stable across each treatment group: baseline (untreated) and Null-AAV8 and Cre-AAV8 treated mice from week 1 to 4. It can be seen in Figure 3.12A and B that the loading control, β-actin, remains consistent across each well. Relative density analysis of each band (Figure 3.12C and D) confirmed these findings further.

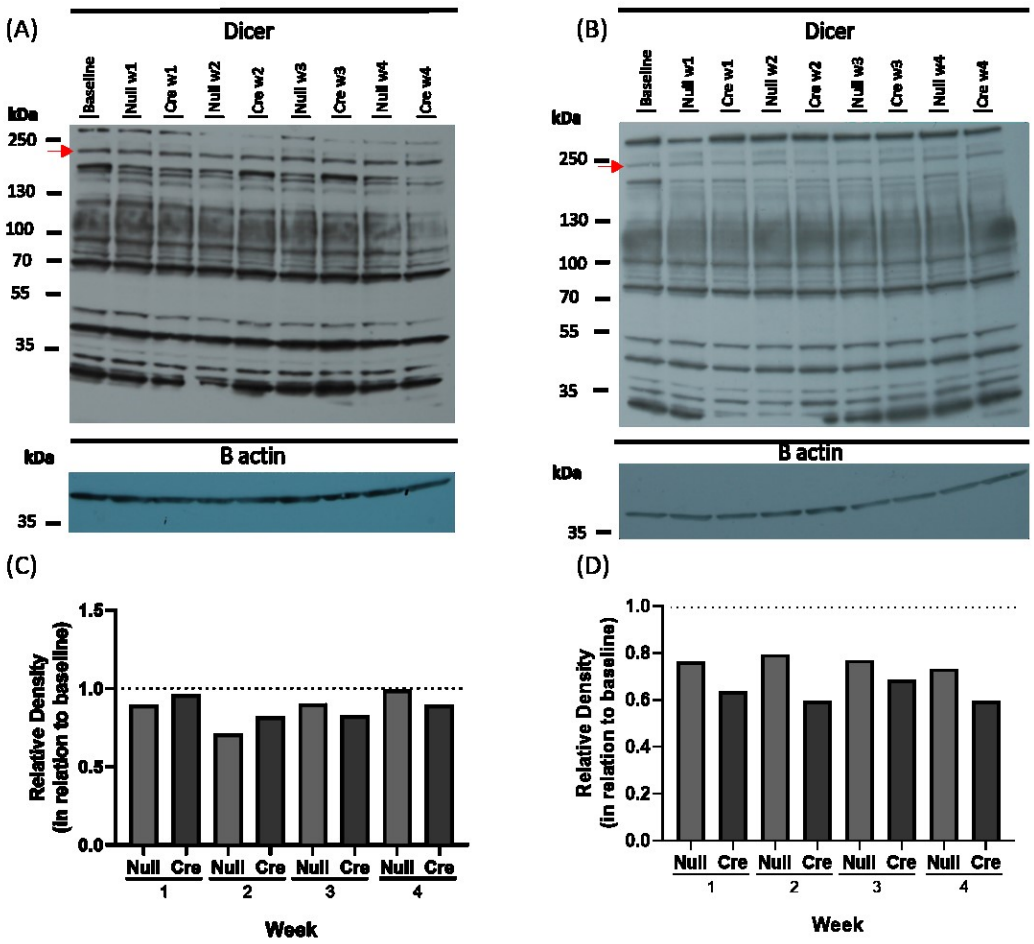

Figure 3.12 Dicer protein expression in the kidney following Cre-AAV8 and Null-AAV8 treatment

(A and B) Protein expression of Dicer (~218kDa, indicated by the red arrows) in the kidney of the baseline (untreated) and week 1 to 4 of the Null-AAV8 and Cre-AAV8 treated mice, was determined by Western blotting. For each Western blot, β-actin (~42kDa) was used as a loading control. (C and D) To quantify the protein Dicer expression, relative density of the ~218 kDa band was calculated in the Null (light grey) and Cre-AAV8 (dark grey) treated mice (week 1 to 4, post injection), normalised to the baseline control Dicer band (dotted line). Each western blot represents an n=1 from each treatment group

Similar to the spleen, mature miRNA were measured in the kidney cortex (Figure 3.13) and medulla (Figure 3.14) to determine their involvement in the uptake of circulating hepatocyte-derived miR-122. MiR-196a, a miRNA described to be highly enriched in the kidney [231, 232] was measured alongside the hepatocyte enriched miR-122 (Figure 3.13 and Figure 3.14). In addition to this, miR-192, a miRNA expressed in both the hepatocytes [86, 123] and the kidney was measured (Figure 3.13 and Figure 3.14)

In the kidney cortex, miR-192 and miR-196a were unaffected by the Cre-AAV8 treatment, when compared to the Null-AAV8 treatment (Linear Regression: miR-192: Cre slope=-5 week^{-1}, Cre slope vs zero p=0.018, Null vs Cre p=0.16; miR196a: Cre slope =-4 week^{-1}, Cre slope vs zero p=0.57, Null vs Cre p=0.9) (Figure 3.13A). Nevertheless, miR-122 expression declines in the Cre-AAV8 treated mice from week 2 to 4 (Linear Regression: Cre slope=-25.7 week^{-1}, Cre slope vs zero p=0.0004, Null vs Cre p=0.007) (Figure 3.13A-D). In Figure 3.13B-D, these findings were supported further, with a significant loss miR-122 expression in the Cre-AAV8 mice at week 3 and 4, compared to the Null-AAV8 controls (Mann Whitney U: Null vs Cre $p \leq 0.01$) (Table 6.3).

The same expression of miRNA can be seen in the kidney medulla (Figure 3.14). Medullary miR-192 and miR-196a are unchanged in the Cre-AAV8 treated mice (Linear Regression: miR-192: Cre slope= 19, Cre slope vs zero p=0.0001, Null vs Cre p=0.009; miR196a: Cre slope 1.75 week^{-1}, Cre slope vs zero p=0.7, Null vs Cre p=0.51) (Figure 3.14A). Furthermore, the Cre-AAV8 treated mice displayed a loss of miR-122 expression in the medulla, in contrast to the baseline and Null-AAV8 treated mice (Linear Regression: Cre slope=-22.6 week^{-1}, Cre vs zero p=0.0002, Null vs Cre p=0.15). This loss was deemed significant at week 2, 3 and 4 post Cre-AAV8 injection, when compared to the Null-AAV8 treated mice (Mann Whitney U: Null vs Cre $p<0.01$)(Figure 3.14B-D) (Table 6.4).

To ensure miRNA were normalised correctly in the kidney cortex and medulla, three housekeeping genes were used for the measurements of miRNA-122: SNORD68 (Figure 3.13B and Figure 3.14B), SNORD95 (Figure 3.13C and Figure 3.14C) and U6

(Figure 3.13 and Figure 3.14D). All three normalisers highlighted the same trend in miRNA expression. However, as U6 exhibited the greatest stability across each treatment group, U6 was carried forward as the internal control for all 3 miRNA (Figure 3.13A and Figure 3.14A).

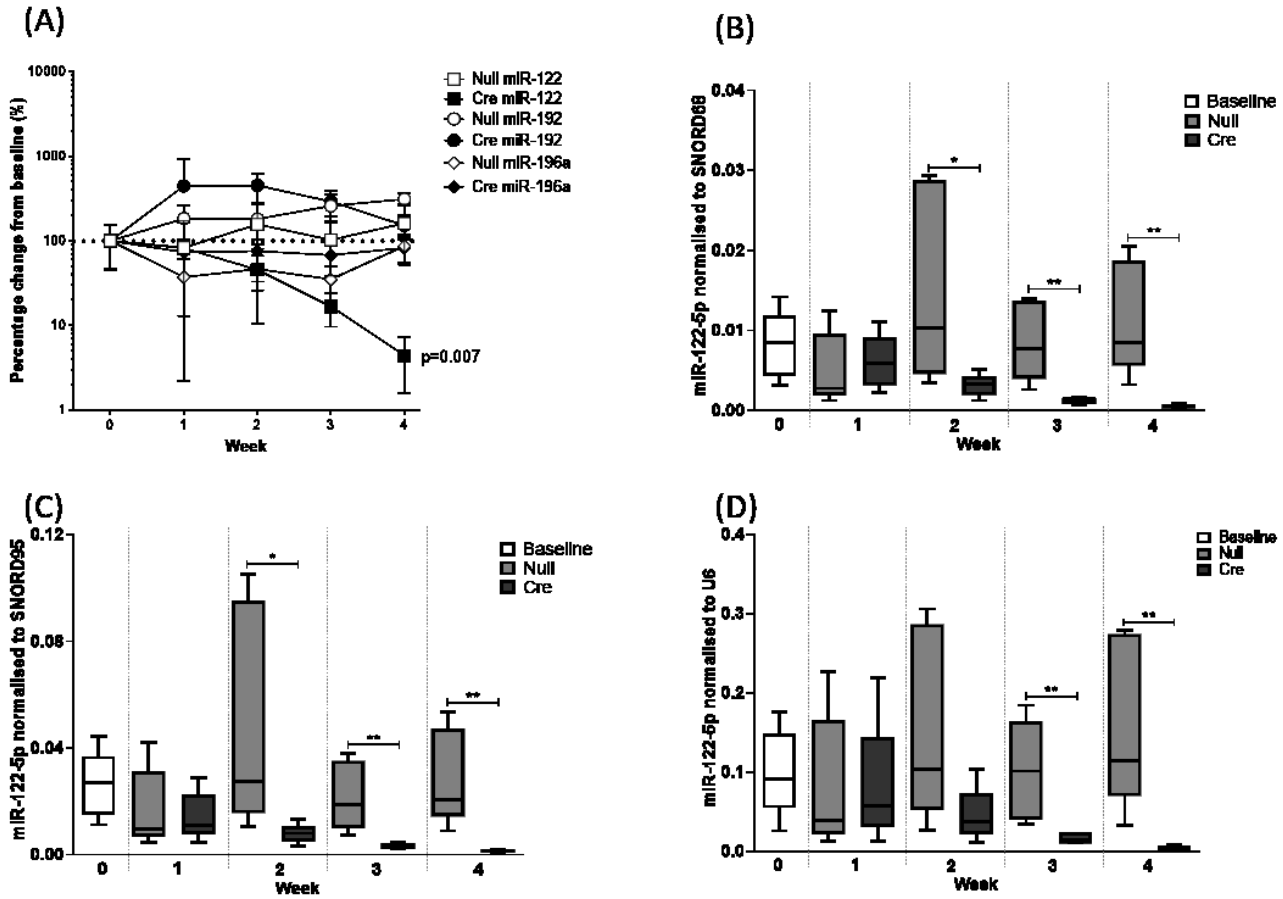

Figure 3.13 miR-122 and renal enriched miRNA measurements in the kidney cortex following AAV8 treatment

*RT-qPCR determined the expression of mature miRNA in the kidney cortex. (A) miR-122, miR-192 and miR-196a expression in the Null-AAV8 (white) and Cre-AAV8 (black) Dicer1flox/flox mice, first normalised to U6, then converted as a percentage to the baseline (untreated, week 0, dotted line) mice. Data presented as 2-ΔT (mean ±SD n=5). P values were calculated from linear regression comparing the slopes of the Null-AAV8 and Cre-AAV8 treated mice. (B-D) miRNA-122 normalised to SNORD68, SNORD95 and U6 respectively in the baseline (white), Null-AAV8 (light grey) and Cre-AAV8 (dark grey) mice. Data was represented as mean ±SD, n=5. Significant differences were calculated from an unpaired Mann Whitney U test, comparing the expression of miR-122 in the Null-AAV8 and Cre-AAV8 treated mice at each week. * p≤0.05, ** p≤0.01.*

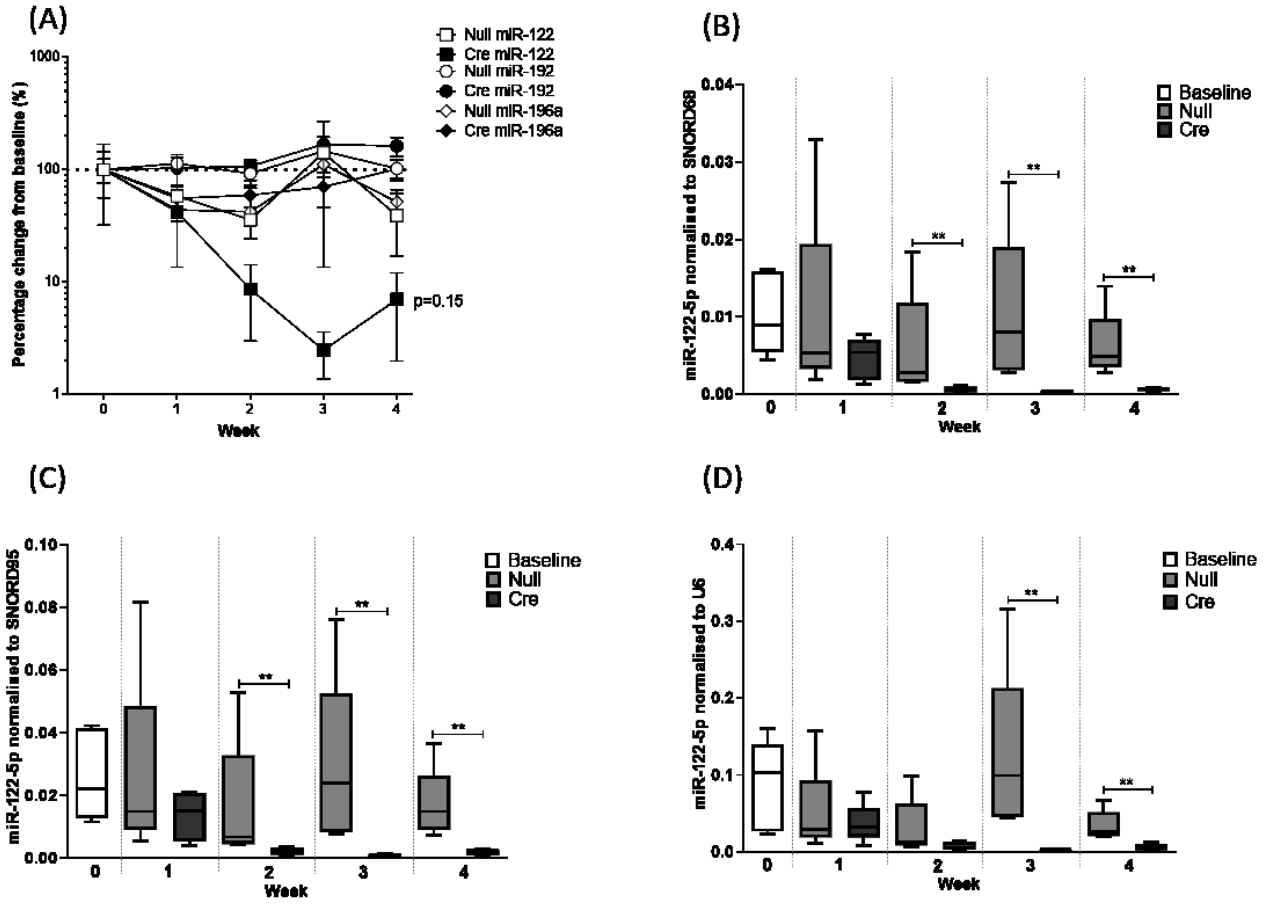

Figure 3.14 Measurements of miR-122 and renal enriched miRNA in the kidney medulla after a single AAV8 injection

*RT-qPCR determined the expression of mature miRNA in the kidney medulla. (A) miR-122, miR-192 and miR-196a expression in the Null-AAV8 (white) and Cre-AAV8 (black) Dicer1 $^{flox/flox}$ mice, first normalised to U6, then converted as a percentage to the baseline (untreated, week 0, dotted line) mice. Data presented as 2-ΔT (mean ±SD n=5). P values were calculated from linear regression comparing the slopes of the Null-AAV8 and Cre-AAV8 treated mice. (B-D) miR-122 normalised to SNORD68, SNORD95 and U6 respectively in the baseline (white), Null-AAV8 (light grey) and Cre-AAV8 (dark grey) mice. Data was represented as mean ±SD, n=5. Significant differences were calculated from an unpaired Mann Whitney U test, comparing the expression of miR-122 in the Null-AAV8 and Cre-AAV8 treated mice, ** p≤0.01.*

To evaluate whether the loss of miR-122 in the kidney was damaging, whole kidney sections were stained with H&E and assessed for any signs of injury. It was concluded from a skilled objective that the each kidney section regardless of treatment (baseline, Null-AAV8 and Cre-AAV8) and time point (week 0-4 post injection), that there were no signs of injury (Figure 3.15).

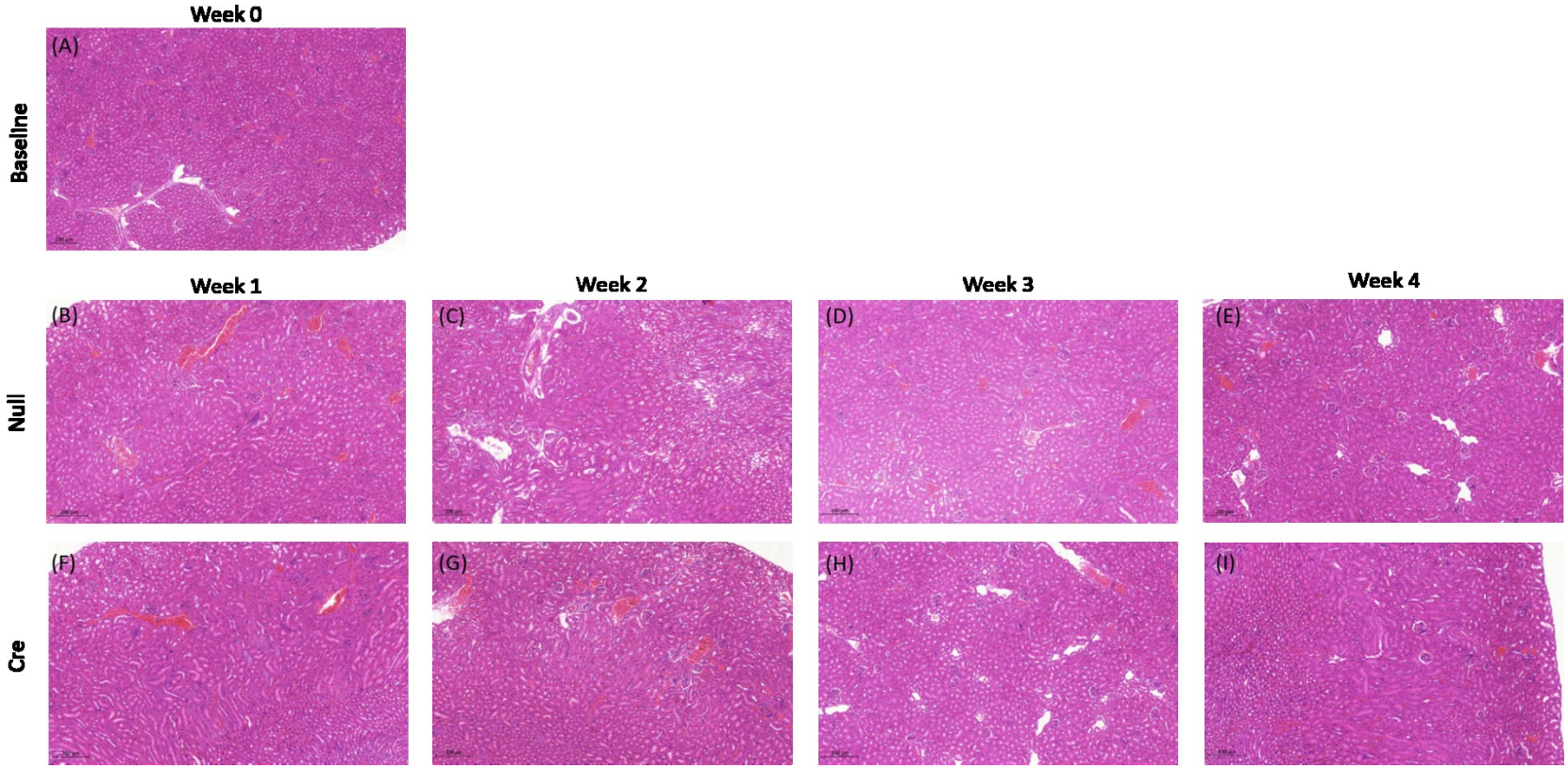

Figure 3.15 H&E stained kidneys after Null-AAV8 and Cre-AAV8 injections

H&E stained kidney sections of baseline (untreated, A), Null-AAV8 (B-E) and Cre-AAV8 (F-I) treated Dicer1$^{flox/flox}$ mice from week 1 to 4. Scale bar represents 200µm. Images representative of an n=2.

3.4.4 Expression of miRNA in the heart, lung and brain is unaltered following Cre-AAV8 injection.

The heart, lung and brain of the reporter mT/mG mice were visually assessed following Null-AAV8 and Cre-AAV8 injection. This was done to determine if the hepatocyte specific AAV8's induced an off-target *Dicer1* knockdown. Confirmation of negative Cre-recombination (global expression of red fluorescence at the cell membranes) in the heart (A, B), lung (C and D) and brain (E, F) of the Null-AAV8 and the Cre-AAV8 treated mT/mG mice (Figure 3.16).

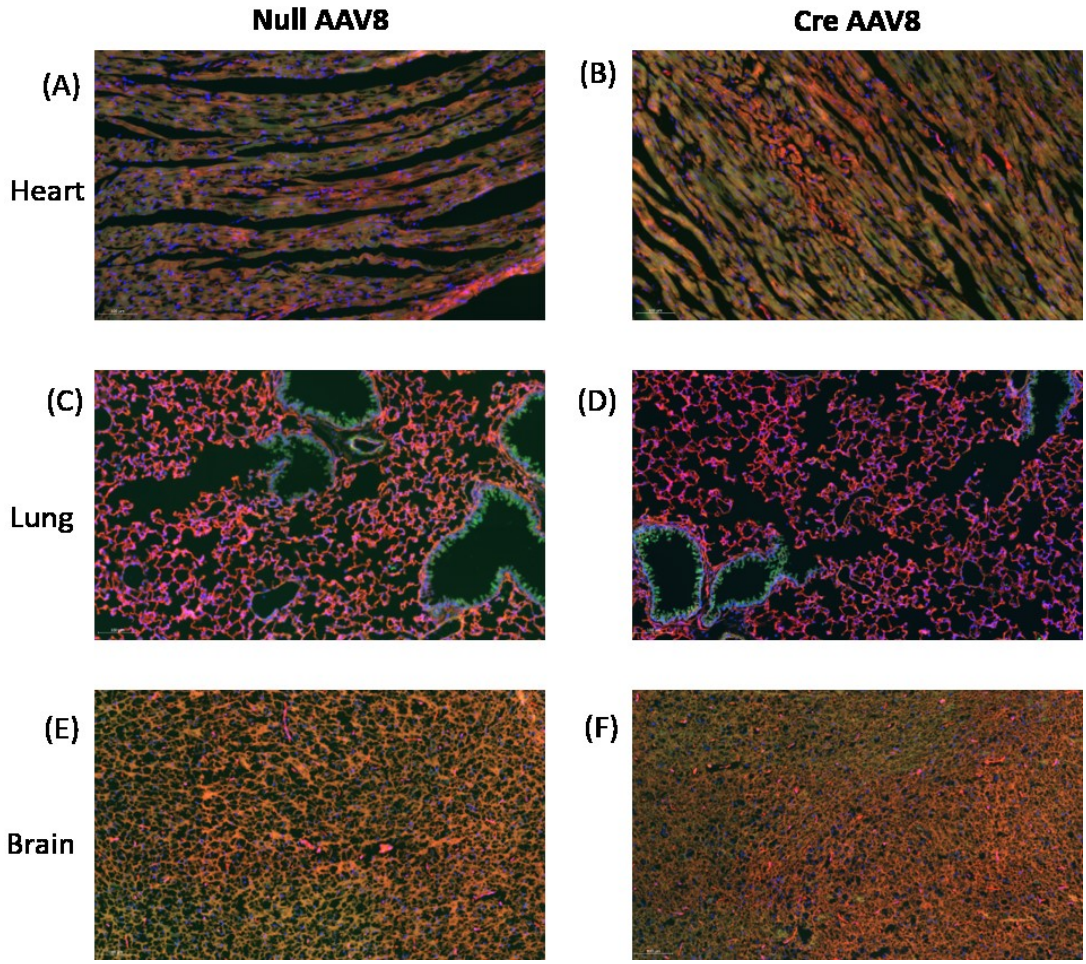

Figure 3.16 Fluorescent imaging in the heart, lung and brain after a single AAV8 injection

Null-AAV8 injected (A, C, E) and Cre-AAV8 injected (B, D, F) mT/mG heart (A, B), lung (C and D) and brain (E, F) sections. Negative Cre-recombination was visualised in all 3 tissues, with the global expression of red fluorescence (tdTomato) at the cell membranes. Blue fluorescence is DAPI. Scale bar represents 100µm, 20x magnification. Images representative of n=2.

After Dicer mRNA was assessed (Figure 6.4), mature miRNA was measured in the heart, lung and brain (Figure 3.17). MiR-122 expression was evaluated in all three tissues to determine if they play a role in its uptake and clearance from the circulation. Alongside this, miRNA known to be specific or highly enriched in the heart, lung and brain were assessed too. MiR-1 was measured in the heart, miR-195a in the lung and miR-124 in the brain (Figure 3.17). To ensure the tissue miRNA were normalised correctly, three housekeeping genes used: SNORD68, SNORD95 and U6. All three housekeepers highlighted the same trend in miRNA expression. However, SNORD95 in the heart and brain and U6 in the lung exhibited the greatest stability across each treatment group. Due to this, these housekeepers were used to normalise the data in Figure 3.17.

In the heart, miRNA-1 was unaffected following Cre-AAV8 injection (Cre slope= -12.7 $week^{-1}$, Cre slope vs zero p=0.73, Null vs Cre p=0.5). Cre-AAV8 treated mice displayed similar miR-122 expression to the baseline mice, with a non-significant difference in expression compared to the Null-AAV8 treated mice (Cre slope=-15.3 $week^{-1}$, Cre slope vs zero p=0.007, Null vs Cre p=0.42)(Figure 3.17A).

In the lung, miR-122 and miR-195a expression did not change following the Cre-AAV8 injection, in contrast to the Null-AAV8 treatment (Linear Regression: miR-122: Cre slope=-12.6 $week^{-1}$, Cre slope vs zero p=0.004, Null vs Cre p=0.6; miR-195a: Cre slope=-2.9 $week^{-1}$, Cre slope vs zero p=0.76, Null vs Cre p=0.6)(Figure 3.17B).

Figure 3.17C highlights miR-122 and miR-124 did not differ in the brain between the Null and Cre-AAV8 treated mice (Linear Regression: miR-122: Cre slope= -13.9 $week^{-1}$, Cre slope vs zero p=0.006, Null vs Cre p=0.8; miR-124: Cre slope=-12.7 $week^{-1}$, Cre slope vs zero p=0.004, Null vs Cre p=0.26)(Figure 3.17B).

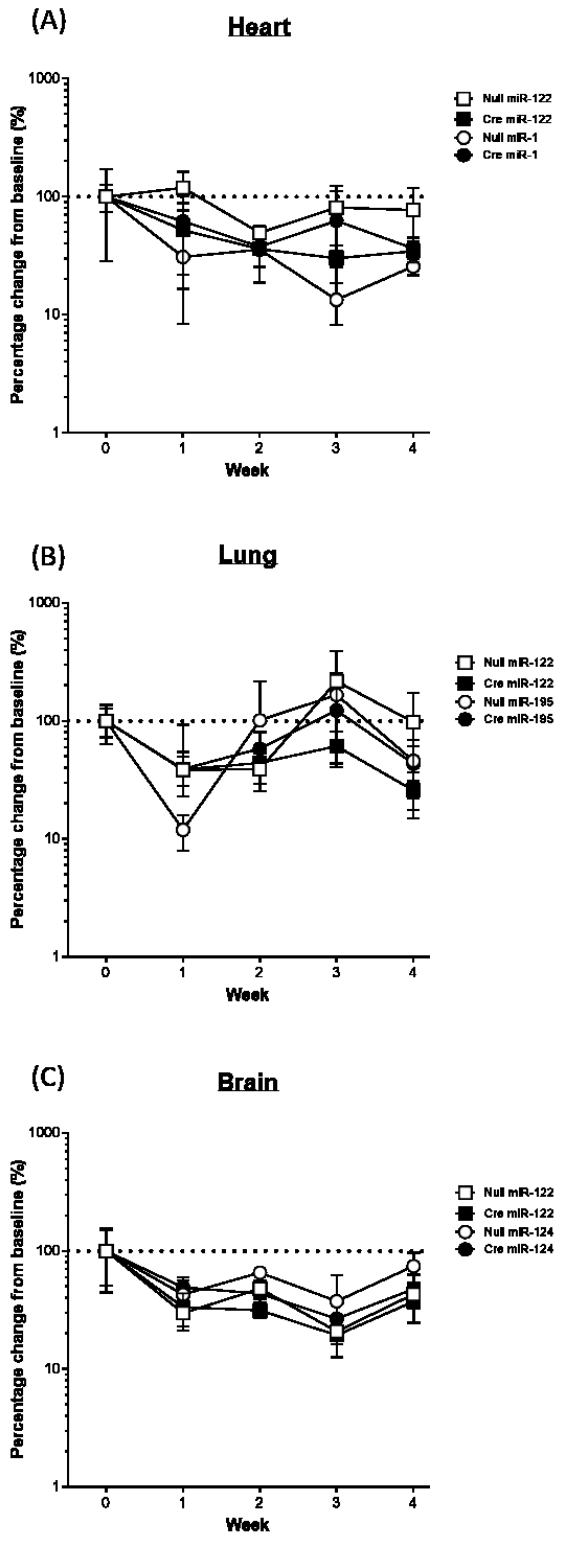

Figure 3.17 miRNA in the heart, lung and brain after Cre-AAV8 and Null-AAV8 treatments

RT-qPCR determined the expression of mature miRNA in the heart, lung and brain. (A) miR-122 and miR-1 expression in the heart, (B) miR-122 and miR-195a in the lung and (C) miR-122 and miR-124 in the brain of the baseline Null-AAV8 (white) and Cre-AAV8 (black) Dicer1$^{flox/flox}$ mice. MiRNA expression was first normalised to SNORD95 (heart and brain) or U6 (lung), then converted as a percentage to the baseline (untreated, week 0, dotted line) mice. Data represented as mean ±SD n=5. P values were calculated by linear regression between the Null-AAV8 and Cre-AAV8 slopes (p>0.05).

3.4.5 The primary transcript of miR-122 in the liver, spleen and kidney cortex and medulla is stable following Cre-AAV8 treatment

To ensure the loss of miRNA-122 observed in the liver, spleen, kidney cortex and medulla was not due to alterations in its *de novo* synthesis, the primary transcript of miR-122 (pri-miR-122) was measured.

The liver had the greatest expression of pri-miR-122 with an average Ct value of 24.8 (Table 6.8). Following the injections of the Null and Cre-AAV8 there was a slight incline in expression from week 1 to 4 (Figure 3.18A). When comparing between the Null and Cre-AAV8 treated mice, there was no significant difference in pri-miR-122 expression (Linear Regression: Cre slope=92 week^{-1}, Cre slope vs zero p=0.005, Null vs Cre p=0.13).

The spleen, had a minimal Ct levels of pri-miR-122 (Table 6.8). This expression was unchanged between the Cre-AAV8 and Null-AAV8 treated mice (Linear Regression Cre slope= -5.2 week^{-1}, Cre slope vs zero p=0.3, Null vs Cre p=0.2) (Figure 3.18B).

Low levels of pri-miR-122 were also observed in both the kidney cortex and medulla (average Ct=35) (Table 6.9). In both the kidney cortex and medulla, there was no significant difference between the Null-AAV8 and Cre-AAV8 treated groups (Linear Regression: kidney cortex: Cre slope=1.8 week^{-1}, Cre slope vs zero p=0.8, Null vs Cre p=0.8; kidney medulla: Cre slope=-8 week^{-1}, Cre slope vs zero p=0.24, Null vs Cre p=0.26)(Figure 3.18C). Lastly, pri-miR-122 was undetectable in the brain, heart and lung of the *Dicer1$^{flox/flox}$* mice, regardless of treatment.

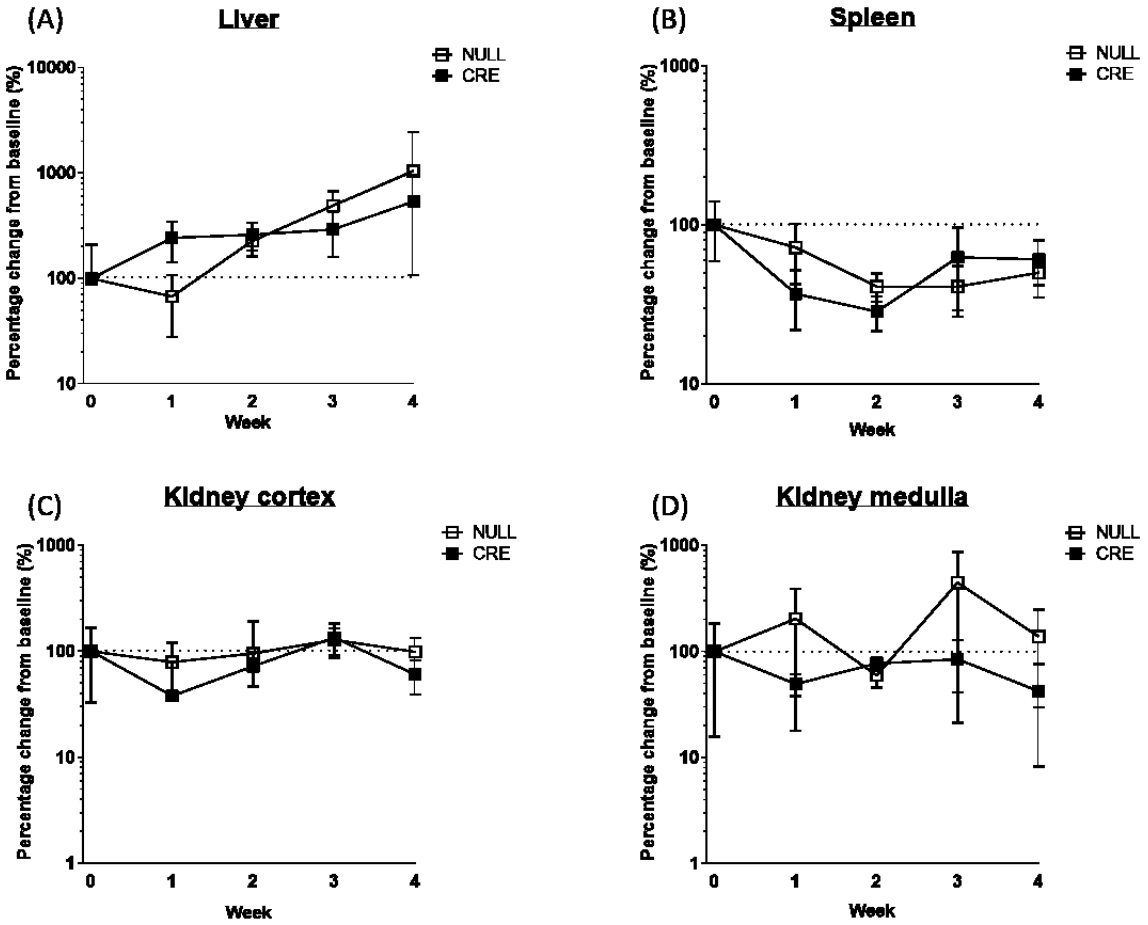

Figure 3.18 Primary transcript of miR-122 after Null-AAV8 and Cre-AAV8 treatment

Pri-miR-122 expression measured by RT-qPCR in the (A) liver, (B) spleen (C) kidney cortex and (D) kidney medulla. Pri-miR-122 expression of the Null-AAV8 (white) and Cre-AAV8 (black) treated Dicer1flox/flox mice were first normalised to GAPDH, then converted as a percentage to the baseline (untreated, week 0, dotted line) mice. Data represented as mean ±SD n=5. P values were calculated from a two-way ANOVA between the Null-AAV8 and Cre-AAV8 treated mice.

3.4.6 Circulating miRNA profile is altered in response to AAV8 treatment

Moreover, the circulating miRNA profile was investigated in the Null-AAV8 and Cre-AAV8 treated mice. MiRNA known to be released after a paracetamol overdose was measured [86, 87, 123]. Hence, Figure 3.19 shows the expression of miR-122 (A), miR-192 (B) and miR-151 (C) in the plasma. Measurements of the 3 miRNAs were taken at each time point for the baseline (untreated), Null-AAV8 and Cre-AAV8 treated mice (Figure 3.19, **Table 6.10**). With a high level of variability seen in the mice treated with either a Null or Cre-AAV8, the differences in their means was not significant (ANOVA $p>0.05$).

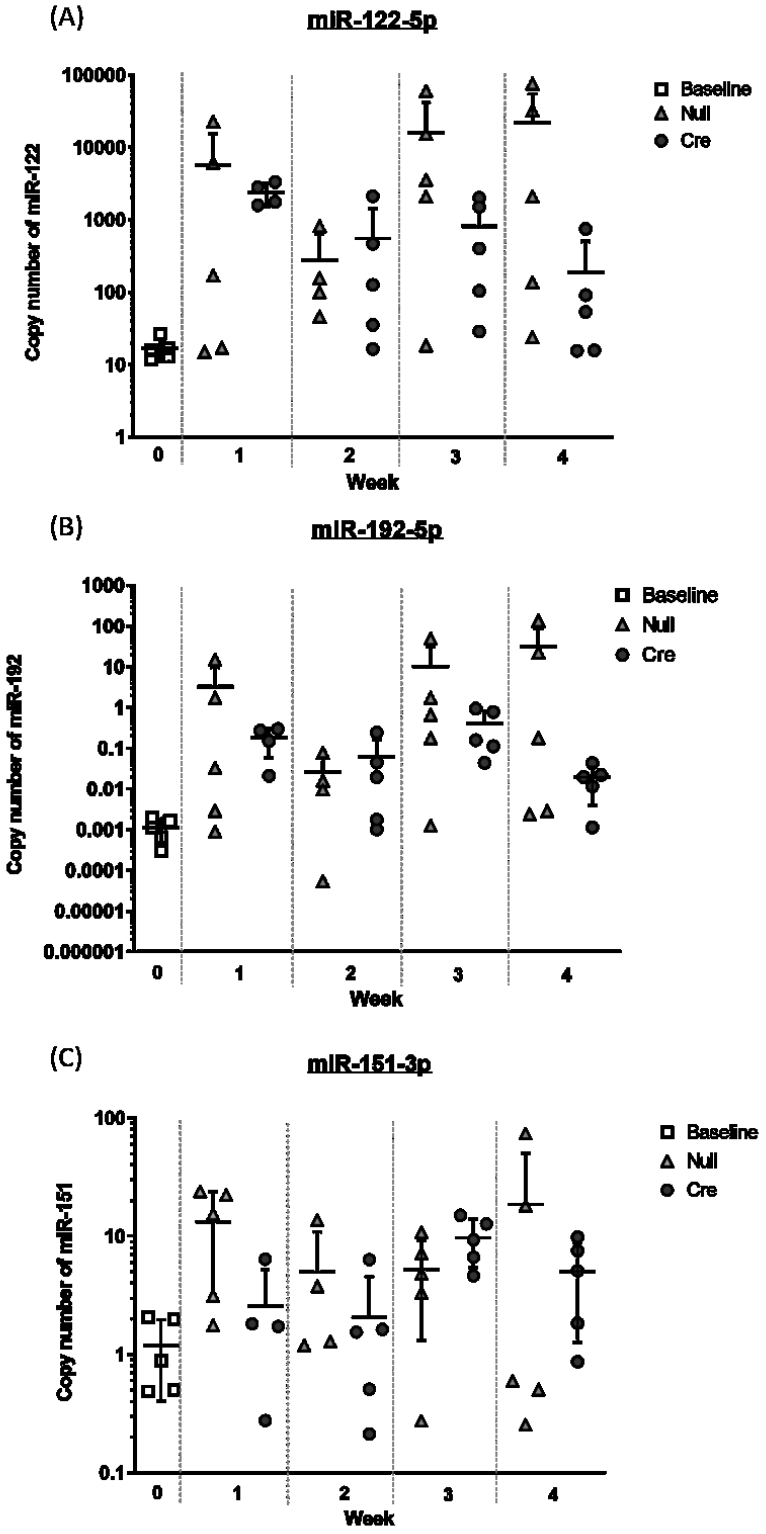

Figure 3.19 Circulating miR-122, miR-192 and miR-151 increases after AAV8 treatment

Circulating miRNA in the plasma were measured using RT-qPCR (Section 2.7). (A) miR-122, (B) miR-192 and (C) miR-151 were measured for each treatment group and time point. Copy number was determined by absolute quantification, error bars represent mean ±SD (n=5; Cre-AAV8 week 1 and 3 and Null week 2, n=4). For each miRNA measured, a multiple comparison two-way ANOVA was carried out to see if there were a significant differences between each treatment group and time point (p>0.05).

A Pearson's correlation coefficient analysis was carried out to determine if plasma miR-122 was correlated to known liver injury marker ALT and miR-122 expression in the liver. Both correlation analyses were calculated in the baseline, Null and Cre-AAV8 treated mice, week 0-4 post AAV8 injection. Plasma miR-122 expression and ALT activity displayed a significant positive correlation (Pearson's correlation: $r=0.6$, $p<0.0001$). Whereas, the correlation was not significant when plasma miR-122 expression was plotted against miR-122 expression in the liver (Pearson's correlation: $r=0.1$, $p=0.4$).

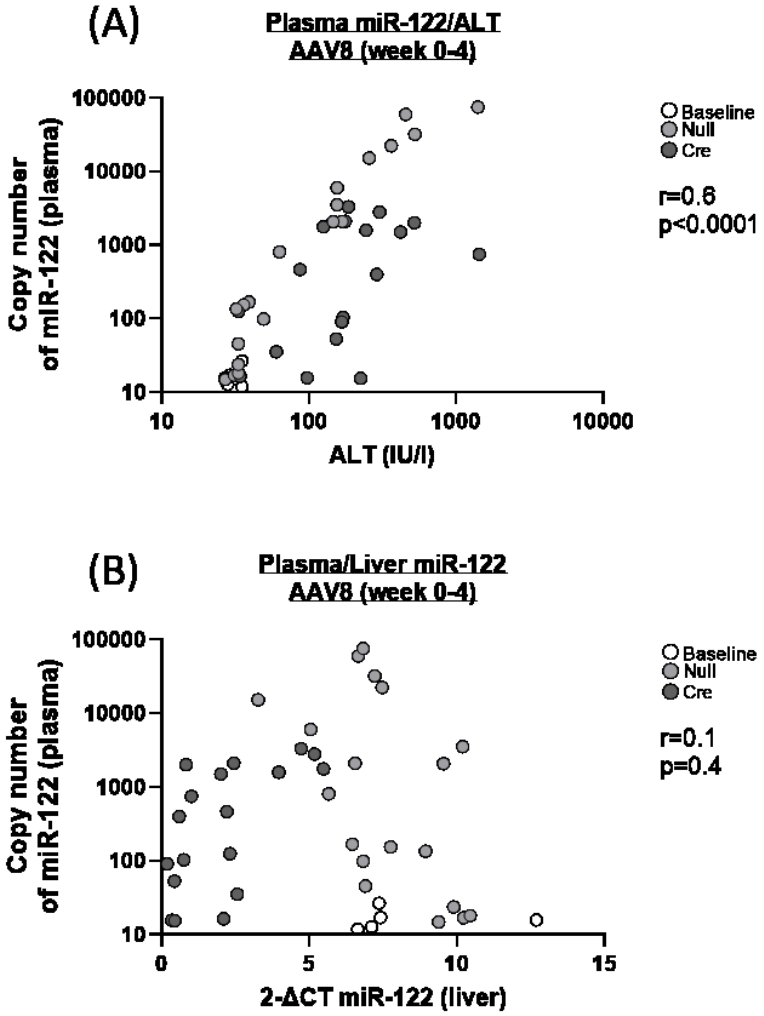

Figure 3.20 Plasma miR-122 correlation with ALT and liver miR-122 expression

Pearson's correlation was calculated to determine if there was a correlation between circulating miR-122 levels and (A) ALT, (B) liver miR-122 expression. This was assessed in the untreated AAV8 (week 0, baseline, white) mice and week 1-4 weeks post Null-AAV8 (light grey) and Cre-AAV8 (dark grey) treatment in the Dicer1$^{flox/flox}$. For each data set, correlation coefficient, r, and its confidence interval, p, was determined. Correlation was deemed significant if p≤ 0.05.

3.4.7 Main Findings

- Successful and sustained knockdown of Dicer was observed in the *Dicer1* $^{flox/flox}$ livers, 1 week after a single Cre-AAV8 injection.
- A loss of hepatocyte enriched miRNA was seen in the liver, 2 weeks after Cre-AAV8 injection.
- There was no histological evidence of liver injury, despite variability in circulating ALT and miR-122
- MiR-122 expression decreased in the spleen and kidney (cortex and medulla) from week 2 post Cre-AAV8 injection.
- MiR-122 was unchanged in the heart, lung and brain following Cre-AAV8 injection.
- Dicer expression in the spleen, kidney cortex and medulla, heart, lung and brain were unaffected by the Cre-AAV8 treatment.
- Other miRNA in the spleen, kidney cortex and medulla, heart, lung and brain were stable in all three treatment groups.

3.5 Discussion

Dicer, within the RISC loading complex (RLC), is essential for the cleavage and processing of pre-miRNA into mature miRNA [94, 219-222]. In this chapter, Dicer and mature miRNA were knocked down in the hepatocytes to determine which organs were responsible for the uptake of circulating miR-122 in a healthy mouse.

As previously described, Dicer expression was significantly reduced in the hepatocytes one week following a single Cre-AAV8 injection in the *Dicer1* $^{flox/flox}$ mice [227]. With the pri-miR-122 unchanged following Cre-AAV8 treatment, it was confirmed that the loss of miRNA was due to a knockdown of *Dicer1* only and not due to a disruption further upstream in its *de novo* synthesis [219, 233]. Subsequently, mirroring previous findings [227], the loss of *Dicer1* in the hepatocytes resulted in the significant loss of miR-122, miR-192 and miR-151 in the liver, two weeks post Cre-

AAV8 treatment. The delay in the loss of miRNA following Dicer knockdown indicates that miRNA is highly stable in quiescent hepatocytes of the adult liver [227]. Moreover, this result is consistent with miR-122 having a half-life of 10 days in adult hepatocytes[189]. Dicer expression was stable in the spleen, kidney cortex and medulla, heart, lung and brain. Additionally, across all 6 tissues, the organ enriched miRNAs remained consistent in expression. Therefore, the stable Dicer and miRNA production per time point and treatment, highlights the Cre-AAV8 activity is restricted to the hepatocytes.

Liver histology and measurements of known biomarkers of hepatocyte injury: ALT and miR-122, were assessed in each treatment group [86, 87, 123]. The blinded histological assessments determined that there was no evidence of liver injury. However, from week 1-4 post AAV8 injection, plasma miR-122 and ALT activity were variable in the Null-AAV8 and Cre-AAV8 treated mice. Despite the group means being non-significantly different from the untreated AAV8 mice (baseline), some individual mice, particularly in the Null-AAV8 treatment groups, displayed high levels of circulating ALT and miR-122. Moreover, the plasma miR-122 and ALT activity had a significant positive correlation in the baseline, Null-AAV8 and Cre-AAV8 treated mice, (Figure 3.20). Yet, there was a lack of correlation observed between miR-122 expression in the liver and plasma miR-122. Therefore, this data implies that the liver had a mild response to the AAV8 infection rather than a global knockdown of miRNA in the hepatocytes. (Figure 3.5).

Previous studies detailed that an injection of a Cre-AAV8, and consequently deletion of Dicer, does not cause liver injury, DNA damage, death, or abnormal proliferation in hepatocytes of *Dicer1* $^{flox/flox}$ mice [227]. Personal communications with Victoria Gadd (CRM) and Kylie Matchett (CIR), the AAV8 dose used in this study was higher than required to produce optimal Cre-recombination. Perhaps, with a lower dose of AAV8, the variability of ALT and miR-122 observed would be reduced or eliminated. Thus, for further experiments (Chapter 4), a lower dose was used in the hope that the mild response to the AAV8 injections would be reduced or eliminated.

MiR-122 is regularly described as an abundant, liver specific miRNA [164, 165, 193]. This chapter was consistent with these findings as even though miR-122 was detected in all seven tissues investigated, the expression was found to be at least 400 fold greater in the liver (Section I.4). Furthermore, as reflected in the lack of primary transcript in the other tissues, miR-122 production occurs almost exclusively in the liver. Nevertheless, it has been previously noted that genes enriched in cells and tissues such as macrophages, spleen, kidney, thymus and lung, are significantly altered during global miR-122 knockdown [189]. This suggests that miR-122 has a role in silencing and activating genes out with the liver. Due to this, miR-122 expression was measured in the plasma, heart, lung, brain, spleen and kidney cortex and medulla.

In the heart, lung and brain, miR-122 expression was unchanged following Cre-AAV8 treatment. However, the loss of hepatic miRNA was observed to cause a significant reduction in the expression of miR-122 in the spleen and kidney. For both organs, the primary transcript of miR-122 was lowly expressed. These findings demonstrate that in a healthy, uninjured mouse, miR-122 expression in the spleen and kidney is reliant on the transfer of miR-122 from the liver.

These findings are agreement with Rivkin *et al,* who found that the depletion of macrophages resulted in the loss of miR-122 expression in the kidney. Consequently, they proposed the primary source of kidney miR-122 is from circulating miR-122 originating from the liver [193]. Additionally, a previous study revealed the spleen displays a significant uptake of miR-122 during ConA-induced liver injury, implying that circulating miR-122 released from the liver is greater in the portal circulation compared to the systemic circulation [122]. Interestingly, the same study found that following ConA-induced liver injury, miR-122 preferential enters the lung causing acute pulmonary inflammation. Nevertheless, in this chapter, miR-122 levels were non-significantly reduced in the lung following Dicer knockdown in the liver, suggesting this mechanism of transfer does not occur during health. However, to investigate this further, Chapter 4 describes two models of acute liver injury to determine if the uptake and clearance of miR-122 alters following liver injury.

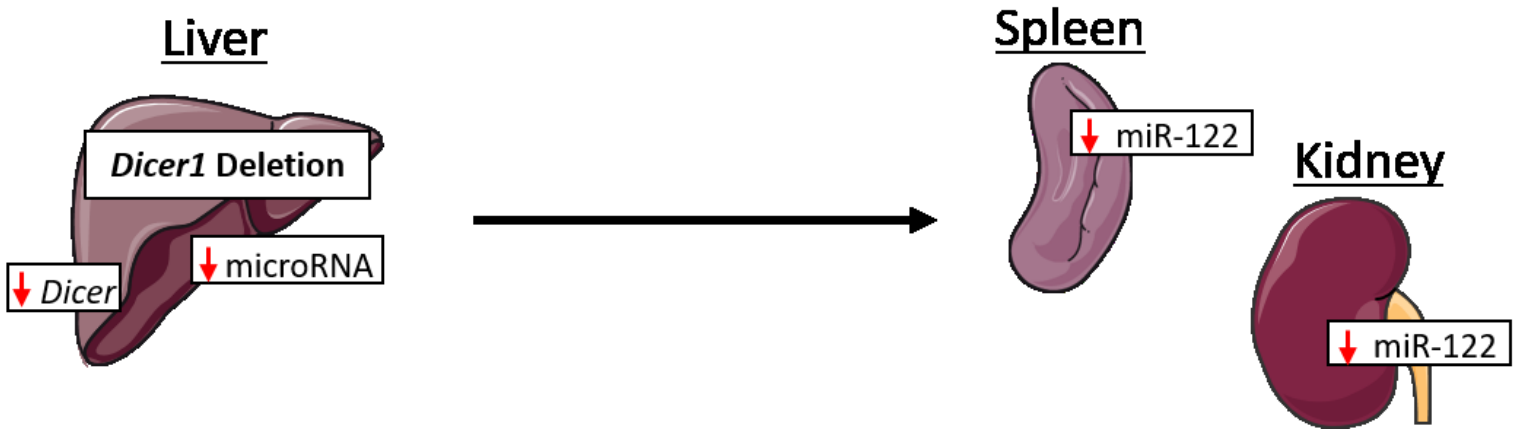

Figure 3.21 Diagram of main findings from Chapter 3

Hepatocyte specific Dicer1 knockdown resulted in the total loss of mature miRNA in the hepatocytes. This in turn led to the loss of mature miR-122 expression in the spleen and kidney (both the cortex and medulla). This highlights that in a healthy mouse, the spleen and kidney are involved in the uptake and clearance of circulating miR-122 released from the liver. Figure created using Servier Medical Art, Les Laboratoires Servier.

Chapter 4 The impact Dicer knockdown has on miRNA release and transfer during paracetamol-induced liver injury

4.1 Introduction

4.1.1 Background

Organ damage can result in the release of miRNA into the circulation and urine [234]. A range of miRNAs are released from the liver into the bloodstream during drug-induced liver injury (DILI) [87, 123]. In both humans and mice, miR-122 and miR-192 have been described to significantly increase in the circulation following paracetamol induced liver injury, compared to healthy controls [82, 86, 87]. Additionally, miR-122 and miR-192 have been shown to predict DILI earlier and at lower paracetamol doses than ALT [117, 123, 171]. Due to this, both miRNAs have been extensively researched as non-invasive biomarkers for the diagnosis and prognosis during a suspected paracetamol overdose [46, 82, 123].

In the previous chapter, I presented data demonstrating the involvement of the kidney and spleen in the uptake and clearance of circulating miR-122 in healthy mice. The studies presented in the current chapter aimed to determine if the mechanism of hepatic miR-122 uptake seen in chapter 3 is altered in the setting of paracetamol DILI. To achieve this, two well described models of acute liver toxicity were used in this investigation: paracetamol in the *Dicer1* $^{flox/flox}$ mice and carbon tetrachloride (CCl_4.) in wild type C57BL/6 mice.

4.2 Experimental plan

4.2.1 Dicer $^{flox/flox}$ mice

Compared to Chapter Chapter 3, a lower dose of the Cre-AAV8 and its control, Null-AAV8 ($6.25x10^{10}$ viral genomes/100µl dose), was used to induce *Dicer1* knockdown in the liver. This was based on unpublished studies (personal communications with Victoria Gadd, CRM) identifying the same level of Cre-recombination at $2.5x10^{11}$and $6.25x10^{10}$ viral genomes/dose. As described in Chapter Chapter 3, *Dicer1* and miRNA significantly decreased in the Cre-AAV8 treated mice two weeks post injection. Due to this, three weeks post AAV8 treatment was used for the paracetamol dosing and tissue collection time point.

Male homozygous *Dicer1* $^{flox/flox}$ mice (9 weeks old) had a single tail vein injection of the hepatotropic Cre-AAV8 or its negative control, Null-AAV8 ($6.25x10^{10}$ viral genomes/100µL dose, Table 2.1). Mice were randomly selected for either AAV8 treatment and left under normal conditions for 3 weeks (n=15 per group, Section 2.3). Running parallel, baseline (untreated) mice were used as a control to determine the response of DILI in this strain of mouse (n=15). Three weeks after the AAV8 injection, mice were then injected with either saline (PBS), 150mg/kg or 300mg/kg paracetamol (n=5 per group) keeping to the methods described in Section 2.4(Figure 4.1). Tissue and blood were collected 6 hours following the paracetamol dosing and measured for mRNA and miRNA expression (as per methods). Tissues were perfused prior to collection with sterile saline.

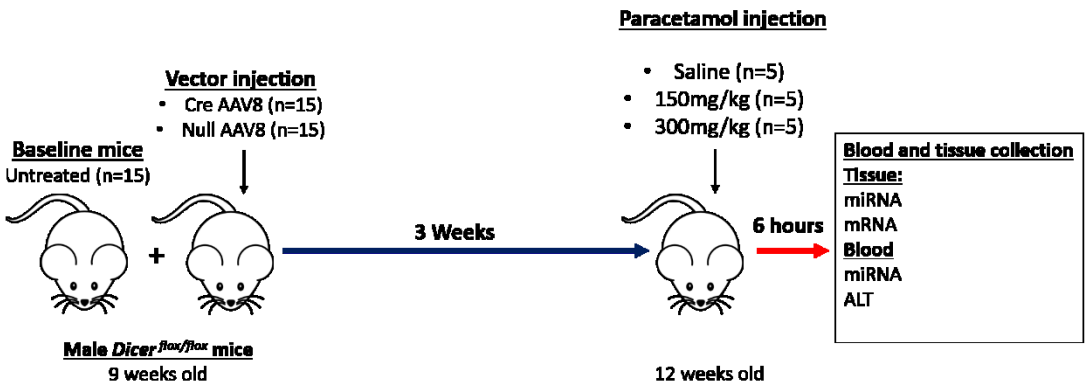

Figure 4.1 Schematic of paracetamol induced liver toxicity model in the *Dicer1* $^{flox/flox}$ mice.

4.2.2 C57BL/6 mice

Carbon tetrachloride (CCl_4.), is an environmental toxin which is widely used in experimental models to induce liver injury. Similar to paracetamol toxicity, CCl_4 is metabolised into a toxic metabolite by the CYP450 enzyme, CYP2E1 [235, 236]. The toxic metabolite, $CCl_3^{\bullet-}$, has been shown to be responsible for hepatotoxicity characterised by lipid peroxidation, depletion of GSH, a rise in ALT and liver fibrosis [235, 237, 238]. Subsequently, in this chapter, CCl_4 was used as a second model of acute liver injury to investigate the transfer of hepatic miR-122 in C57BL/6 mice.

Male C57BL/6J mice (8 weeks old) were fasted for 12 hours overnight prior treatment. After fasting, mice underwent an intraperitoneal injection of 1ml/kg CCl_4 (sterile CCl_4 in a 1:3 ratio with olive oil) or with olive oil (control) at the equivalent volume (n=6 per group). To assess the time course of hepatic miRNA release, blood was collected via tail bleeds at 6 and 12 hour time points. Tissue and blood were harvested 24 hours after treatment. MiRNA known to be expressed in the hepatocytes were measured in the plasma and tissue at each time point using RT-qPCR described in Section 2.7(Figure 4.2).

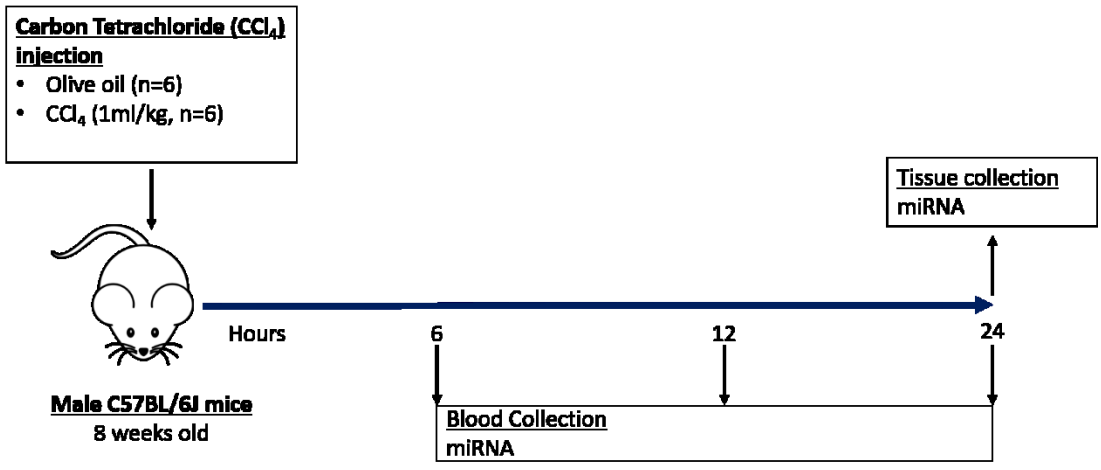

Figure 4.2 Experimental plan of acute liver injury induced by carbon tetrachloride in C57BL/6J mice

4.3 Results

4.3.1 Loss of mature miRNA leads to a significant increase in centrilobular necrosis following paracetamol-induced liver injury

Due to a reduction in the AAV8 dose (compared to Chapter 3, Section 3.3.2), Dicer mRNA expression was first assessed in the liver (Figure 6.5). There was a significant reduction of Dicer mRNA observed in the Cre-AAV8 saline group compared to the Null mice.

The miRNA expression was then assessed following PBS, 150mg/kg and 300mg/kg of paracetamol (Figure 4.3). Regardless of paracetamol dosing, it was observed that the Null-AAV8 did not alter the expression of miRNA in the liver, compared to the baseline mice (ANOVA: baseline vs Null: $p>0.05$) (Figure 4.3A-C). In the baseline and Null-AAV8 treated mice, miR-122 expression remained stable in the liver across all three paracetamol doses (Figure 4.3A). However, miR-192 and miR-151 expression decreased with increasing paracetamol treatment (Figure 4.3B-C).

Following Cre-AAV8 and a PBS injection, all three of the hepatocyte enriched miRNA were significantly reduced in the liver (Figure 4.3A-C). The expression of miR-122 in the Cre-AAV8 treated mice was significantly reduced across all three paracetamol treatments (Figure 4.3A). The significant loss of miR-192 and miR-151 displayed in the Cre-AAV8 group was maintained until 300mg/kg paracetamol dosing. Due to a loss of miR-192 and miR-151 in the baseline and Null-AAV8 mice at the 300mg/kg dose, there was a non-significant difference in expression compared to the Cre-AAV8 group (Figure 4.3B-C).

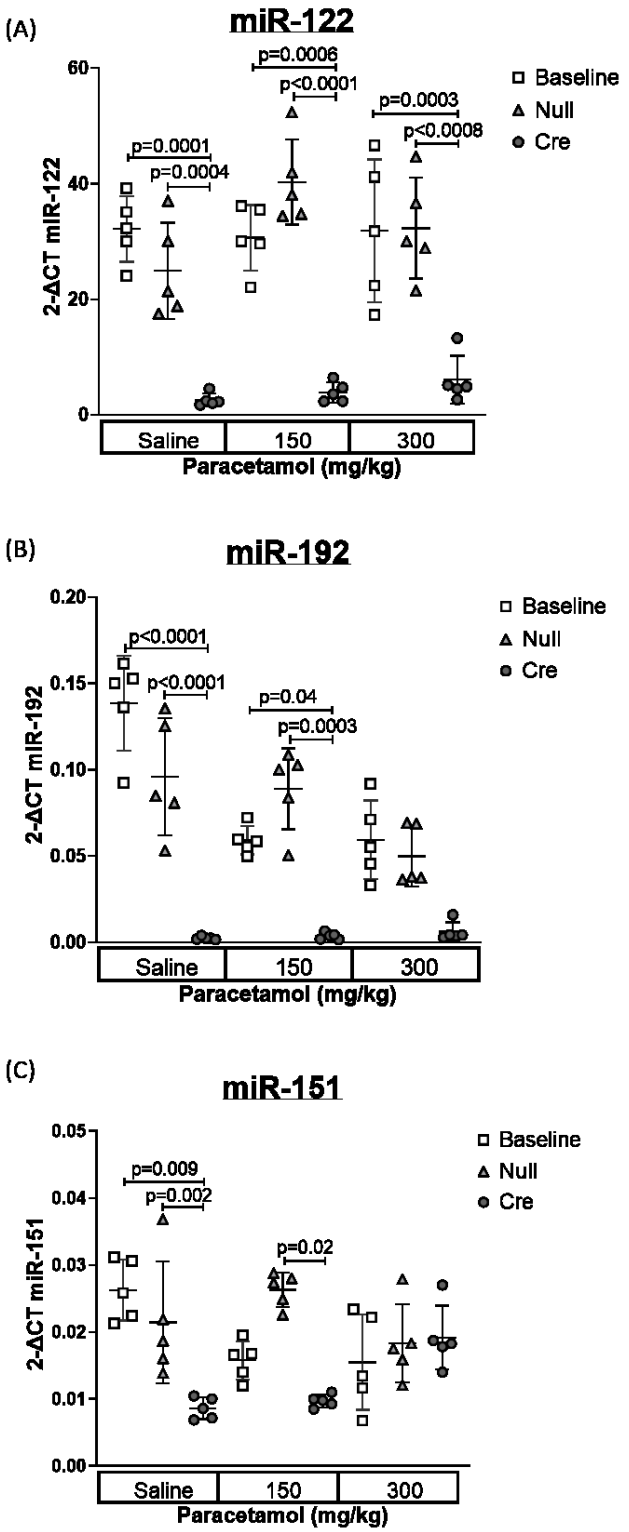

Figure 4.3 The expression of hepatocyte enriched miRNA following Dicer deletion and paracetamol treatment

Hepatocyte enriched (A) miR-122, (B) miR-192 and (C) miR-151 expression were measured in the liver following saline, 150mg/kg paracetamol and 300mg/kg paracetamol in the baseline (untreated, white squares), Null-AAV8 (light grey triangles) and Cre-AAV8 treated Dicer1 $^{flox/flox}$ mice (dark grey circles). MiRNA measurements were taken 3 weeks post AAV8 treatment and 6 hours following paracetamol dosing. Each point was normalised to U6, error bars represent mean ±SD, n=5. A multiple comparison two-way ANOVA was used to determine if expression was significantly different across all 9 treatment groups.

Next, *in situ* hybridisation of miR-122 was carried out to determine its localisation in the livers of the Null-AAV8 and Cre-AAV8 treated mice after a single dose of saline, 150mg/kg and 300mg/kg paracetamol (Figure 4.4). Alongside the miR-122 *in situ* hybridisation, there were 3 controls, no probe (S), scrambled miRNA control (T) and U6 (U) (Figure 4.4).

The Null-AAV8 and saline treated livers had an even dispersal of miR-122 in the cytoplasm of the hepatocytes (Figure 4.4A-C). The Null-AAV8 livers after 150mg/kg paracetamol (Figure 4.4G-I) and 300mg/kg paracetamol (Figure 4.4M-O) displayed a gradient of miR-122 staining (expression), with the greatest staining in the viable hepatocytes closest to the centrilobular necrotic areas. In contrast, the Cre-AAV8 treated mice had minimal to no miR-122 staining which was not altered in the presence of paracetamol (Figure 4.4 saline: D-F, 150mg/kg paracetamol: J-L and 300mg/kg paracetamol: P-R).

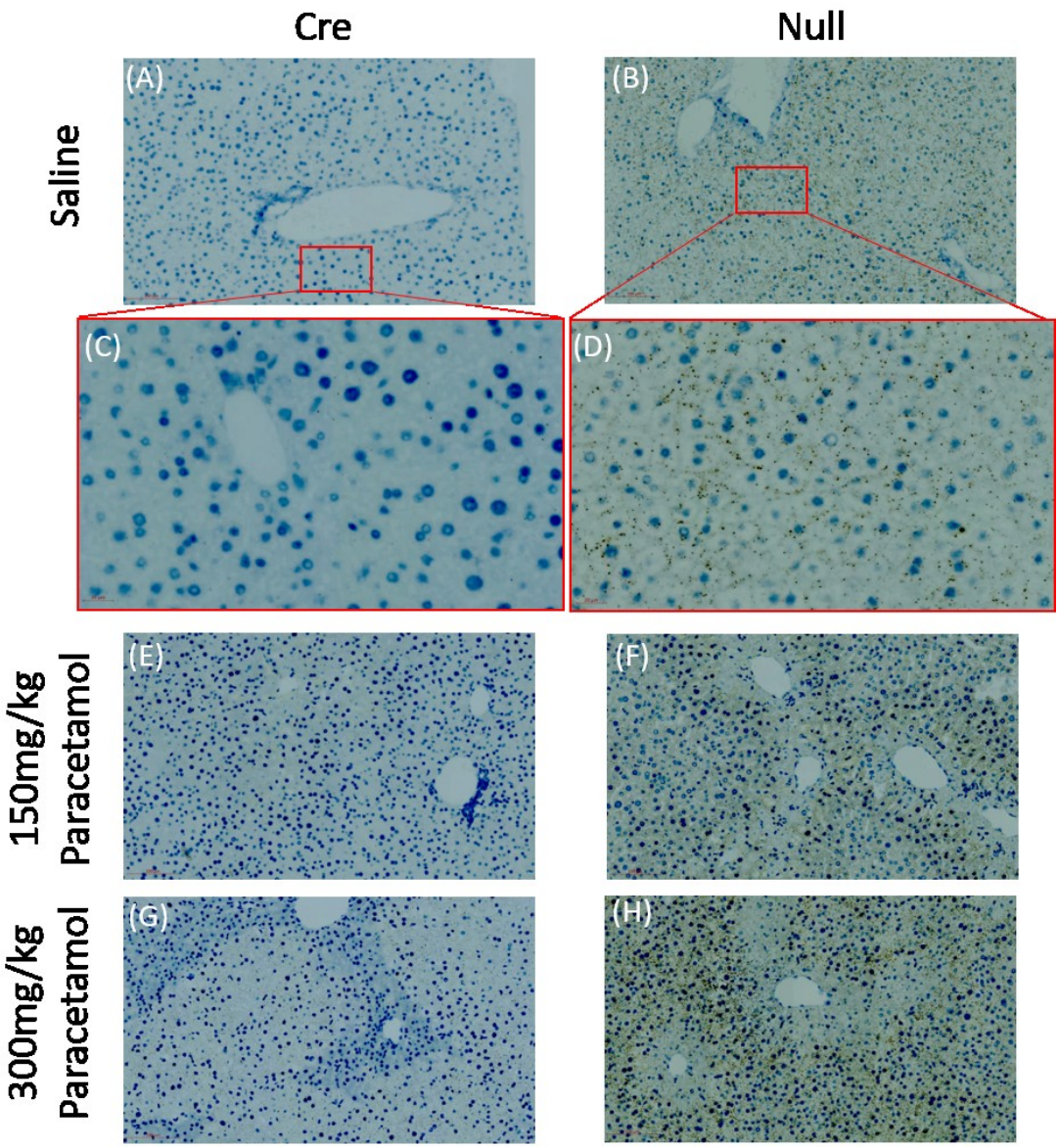

Figure 4.4 *In situ* hybridisation of miR-122 in the Null-AAV8 and Cre-AAV8 liver sections following paracetamol dosing

In situ hybridisation of miR-122 was carried out on the Dicer1 $^{flox/flox}$ liver sections. Images represent miR-122 expression (silver dots) 3 weeks after Null-AAV8 or Cre-AAV8 treatment, followed by 6 hours a single paracetamol dosing of either saline (A-D), 150mg/kg paracetamol (E and F) or 300mg/kg paracetamol (G and H). Controls for staining (I) No probe, (J) Scrambled miRNA and (K) U6 ran alongside the staining and used as comparison for the analysis. Scale bar represents 100µm or 20µm (C and

D), 40x magnification. Each image represents an n=3per AAV8 and paracetamol dosing.

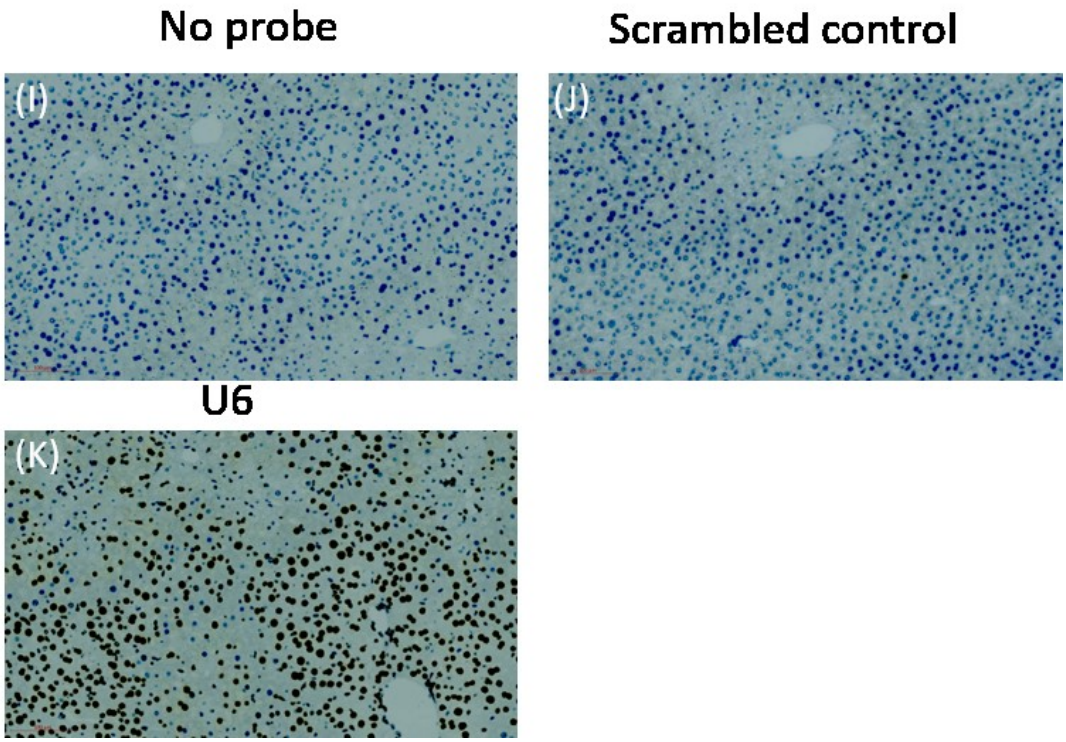

Figure 4.5 C*ontinued*

To assess the influence miRNA knockdown has on liver injury, H&E stained livers were assessed in the saline, 150mg/kg and 300mg/kg paracetamol treated mice (Figure 4.6). As seen in Chapter 3, the saline (PBS, control) treated baseline, Null-AAV8 and Cre-AAV8 mice displayed no signs of liver injury (Figure 4.6A, D, G). For all three groups, increasing levels of centrilobular necrosis were present with increasing doses of paracetamol. It was noted following 300mg/kg paracetamol, that the Cre-AAV8 mice had larger areas of necrosis than the baseline and Null AAV8 mice (Figure 4.6C, F, I). The greater extent of necrosis in the Cre-AAV8 treated mice was significant when the percentage of necrosis was calculated and compared (Figure 4.6J: ANOVA 300mg/kg paracetamol: baseline vs Cre, $p=0.0024$; Null vs Cre, $p=0.007$).

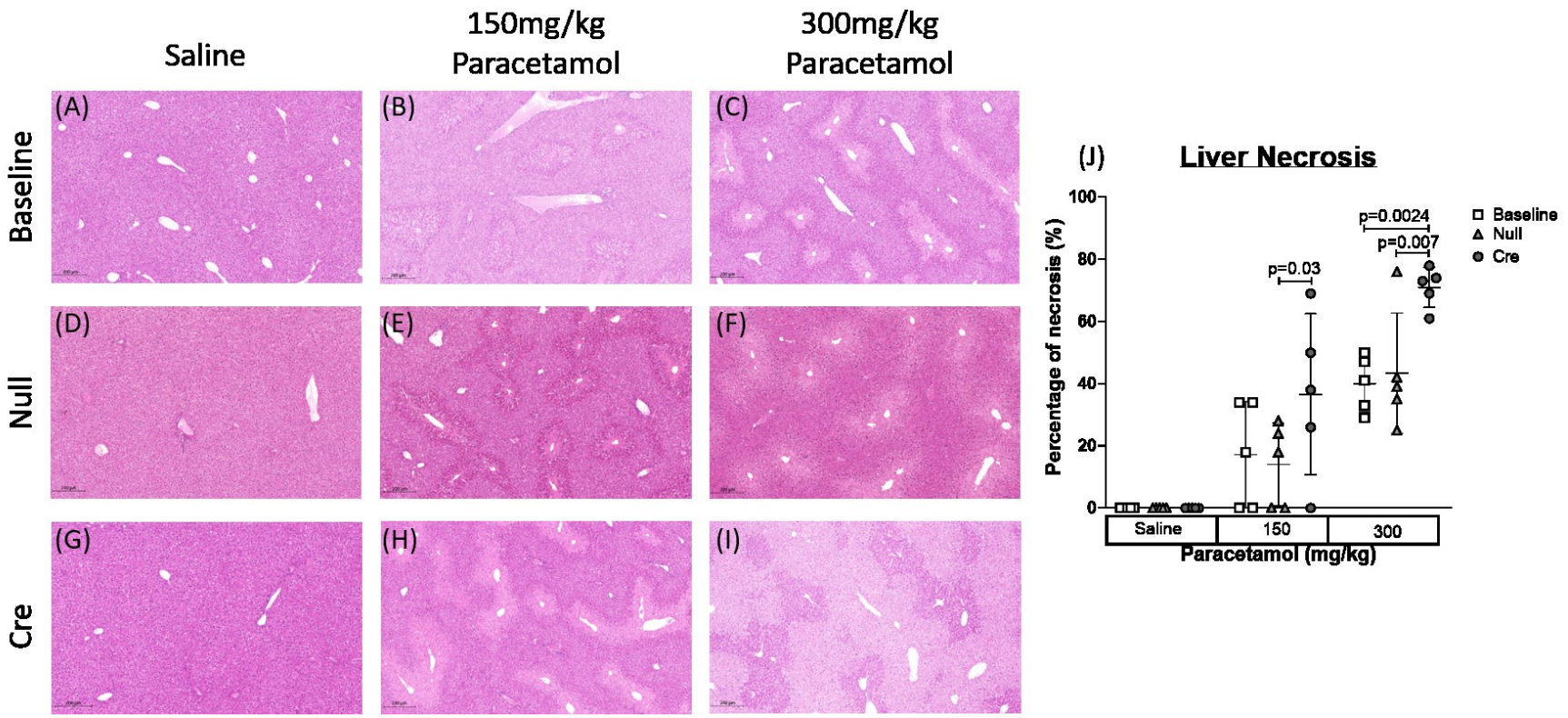

Figure 4.6 H&E staining and percentage of necrosis measurements in the liver

(A-I) H&E stained livers 3 weeks after baseline, Null-AAV8 and Cre-AAV8 treatment and 6 hours following saline, 150mg/kg and 300mg/kg paracetamol. Scale bar represents 200µm, 20x magnification. *Images representative of n=5. (J) In reference to the H&E stained livers, the level of necrosis was calculated as a percentage for each liver section: baseline (untreated, white squares), Null-AAV8 (light grey*

triangles) and Cre-AAV8 treated (dark grey circles) Dicer1 $^{flox/flox}$ mice. Error bars represent mean ±SD, n=5. A multiple comparison two-way ANOVA was used to determine if the percentage of necrosis was significant between treatment groups.

ALT activity was measured in the plasma as another measure of liver injury (Figure 4.7). In the baseline and Cre-AAV8 treated mice, ALT significantly increased following 300mg/kg paracetamol in comparison to their equivalent saline controls (ANOVA: baseline saline vs baseline 300mg/kg $p=0.01$; Cre saline vs Cre 300mg/kg $p<0.0001$). Nevertheless, the mean activity of circulating ALT is greater in the Cre-AAV8 treated mice at the 300mg/kg paracetamol dose in comparison to the baseline and Null-AAV8 treated mice (ANOVA: Null 300mg/kg vs Cre 300mg/kg $p=0.02$). In the Null-AAV8 mice, there was a non-significant increase in circulating ALT at the 150mg/kg and 300mg/kg paracetamol dose.

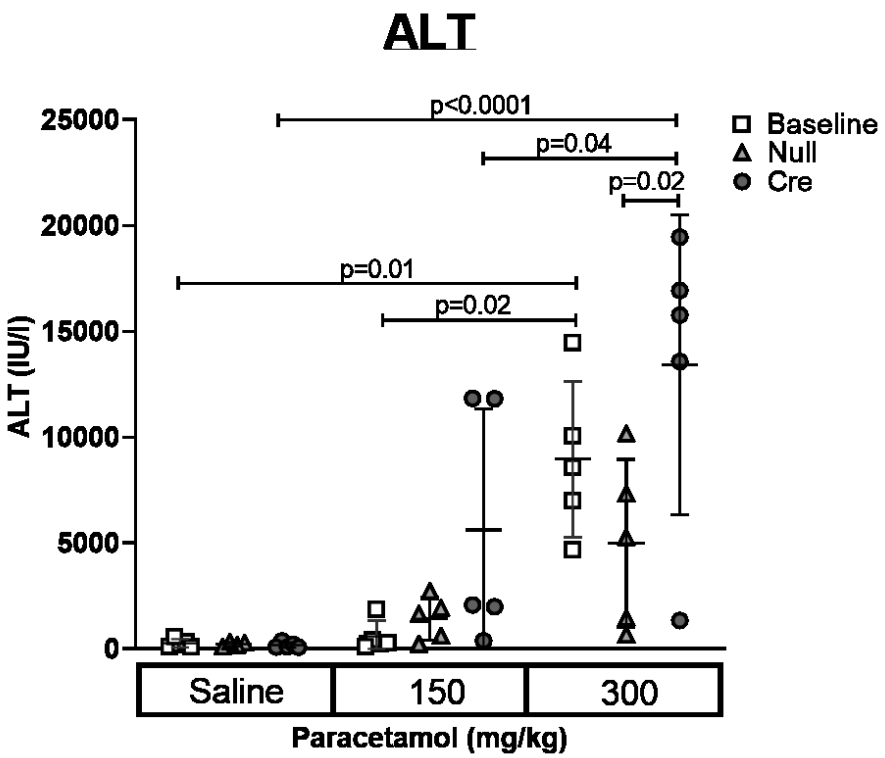

Figure 4.7 Circulating ALT activity following AAV8 and paracetamol treatment

Plasma ALT activity (IU/l) were measured in the baseline (untreated, white squares), Null-AAV8 (light grey triangles) and Cre-AAV8 (dark grey circles) treated mice 6 hours post-saline, 150mg/kg and 300mg/kg paracetamol injection. Bars represent mean ±SD, n=5. A multiple comparison two-way ANOVA was used to determine significance across the 9 treatment groups.

4.3.2 Increase of miR-122 in the spleen during paracetamol toxicity is significantly reduced when miRNA is knocked down in the hepatocytes

First, it was confirmed that Dicer mRNA was not reduced in the spleen following Cre-AAV8 treatment (Figure 6.6). Subsequently, miRNA was measured in the spleen to determine if DILI altered the uptake of miR-122 displayed in Chapter 3. The hepatocyte enriched miR-122 displayed a 25-fold increase in the baseline mice and a 9-fold increase in the Null-AAV8 mice following 300mg/kg paracetamol verses the saline treatment (ANOVA: baseline saline vs 300mg/kg, $p<0.0001$; Null saline vs 300mg/kg, $p=0.002$). In the Cre-AAV8 mice, an increase in miR-122 was not seen following 300mg/kg paracetamol (ANOVA: 300mg/kg paracetamol: baseline vs Cre, $p<0.0001$; Null vs Cre, $p<0.0001$).

The splenocyte enriched miR-146a increased 3.6-fold and 2.6-fold in the 150mg/kg and 300mg/kg paracetamol treated baseline mice respectively, in contrast to the saline control (ANOVA: baseline; saline vs 150mg/kg, $p<0.0001$, saline vs 300mg/kg, $p<0.0001$) (Figure 4.8B). On the other hand, the Null-AAV8 treated mice had a 4-fold greater expression of miR-146 than baseline following saline treatment (ANOVA: baseline saline vs null saline $p<0.0001$), which decreased with increasing paracetamol dosing. Lastly, at the saline dose, Cre-AAV8 mice had comparable expression of miR-146 to the baseline mice (ANOVA: baseline saline vs Cre saline, $p>0.05$). However, this expression was not influenced by paracetamol treatment and remained significantly lower than the baseline mice (ANOVA: baseline 150mg/kg vs Cre 150mg/kg, $p<0.0001$; baseline 300mg/kg vs Cre 300mg/kg, $p<0.0001$) (Figure 4.8B).

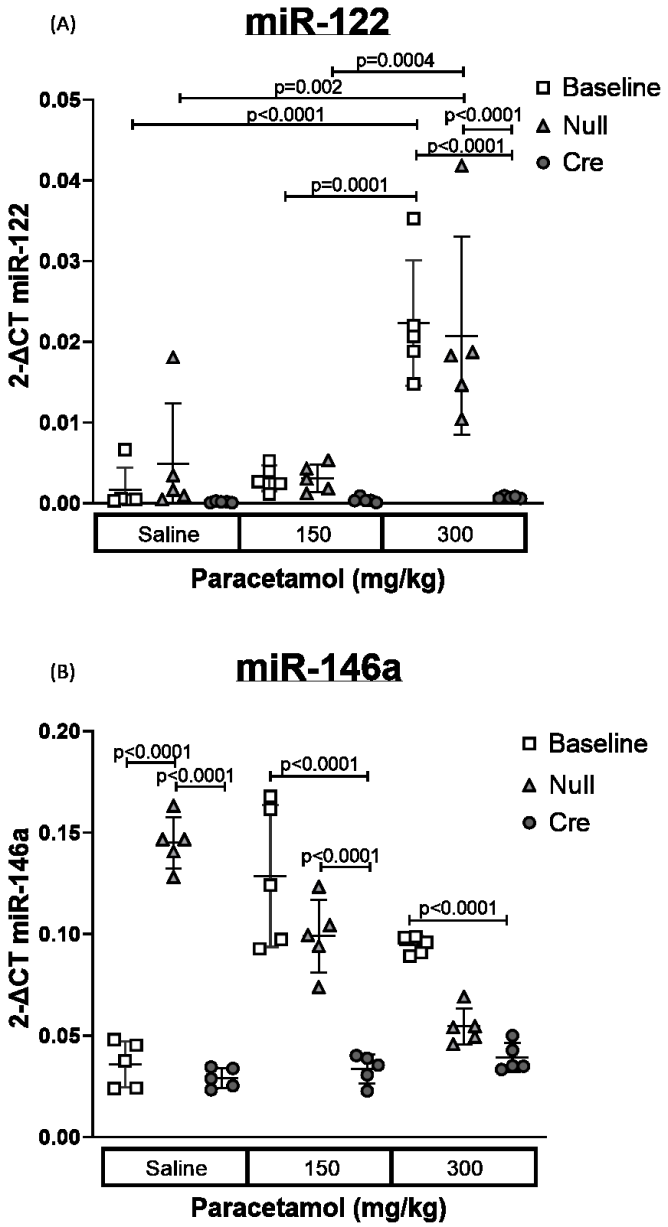

Figure 4.8 miR-122 and tissue enriched miRNA expression in the spleen

MiR-122 (A) and miR-146a (B) were measured in the spleen of the male Dicer1 $^{flox/flox}$ mice. MiRNA measurements were carried out via RT-qPCR 3 weeks following baseline (white squares), Null-AAV8 (light grey triangles) and Cre-AAV8 (dark grey circles) treatment and 6 hours after saline, 150mg/kg and 300mg/kg of paracetamol. Each point was normalised by SNORD95, error bars represent mean ±SD, n=5. A multiple

comparison two-way ANOVA was used to determine if the expression is significantly different between treatment groups.

Next, H&E stained spleens were assessed to see if the loss of miR-122 results in a susceptibility to injury during DILI. Figure 4.9 shows the spleens of the Null-AAV8 and Cre-AAV8 *Dicer1*$^{flox/flox}$ mice following saline, 150mg/kg and 300mg/kg paracetamol. Here, it can be seen that the morphology of the spleens remain unchanged and uninjured with normal red and white pulp following paracetamol dosing.

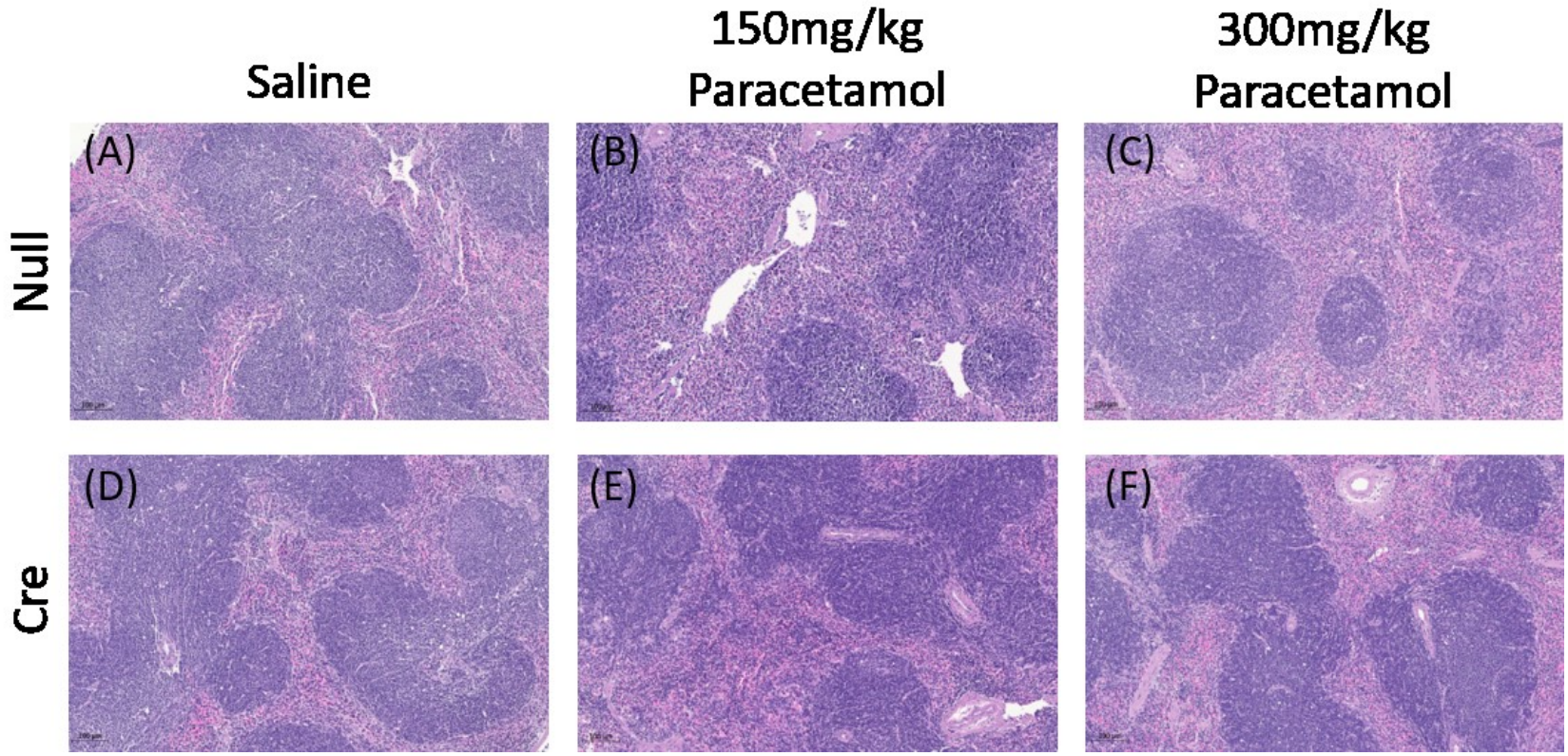

Figure 4.9 H&E stained spleens following AAV8 and paracetamol treatment

H&E staining of whole spleen sections 3 weeks after Null-AAV8 (A-C) and Cre-AAV8 (D-F) treatment and 6 hours following saline (A, D), 150mg/kg paracetamol (B, E) and 300mg/kg paracetamol (C, F). Scale bar represents 200µm, 20x magnification. Images representative of n=5.

4.3.3 When miRNA is diminished in the hepatocytes the transfer of miR-122 to the kidney is lost during paracetamol toxicity

Dicer, miR-122, miR-192 and miR-196 were measured in the kidney cortex (and kidney medulla of the baseline, Null-AAV8 and Cre AAV8 treated mice, after saline, 150mg/kg and 300mg/kg paracetamol (Figure 4.10). In both sections of the kidney, Dicer mRNA expression did not significantly decrease following Cre-AAV8 or paracetamol treatment (Figure 6.6). Moreover, tissue enriched miR-192 and miR-196 did not decrease in the Cre-AAV8 treated mice (Figure 4.10B-C and Figure 4.10B-C).

In the cortex, miR-122 increased 8-fold in the baseline and 7-fold in Null-AAV8 treated mice following 300mg/kg paracetamol, in comparison to the saline group (ANOVA: baseline saline vs 300mg/kg, p=0.003; Null saline vs Null 300mg/kg, p=0.0009). With miR-122 expression decreased in the kidney cortex of the Cre-AAV8 treated mice, this increase in expression following paracetamol-induced liver injury was not observed (ANOVA: baseline 300mg/kg vs Cre 300mg/kg, 18-fold difference p=0.0009; Null 300mg/kg vs Cre 300mg/kg, 19-fold difference, p=0.0002).

A similar trend was exhibited in the medulla, with miR-122 increasing 11-fold in the baseline and 13-fold in the Null-AAV8 mice treated with 300mg/kg paracetamol (ANOVA: baseline saline vs baseline 300mg/kg, p>0.05; Null saline vs Null 300mg/kg, p=0.001). Again, the Cre-AAV8 miR-122 expression remained unchanged and significantly lower following increasing paracetamol doing (ANOVA: Null 300mg/kg vs Cre 300mg/kg, 19 fold difference, p=0.0009).

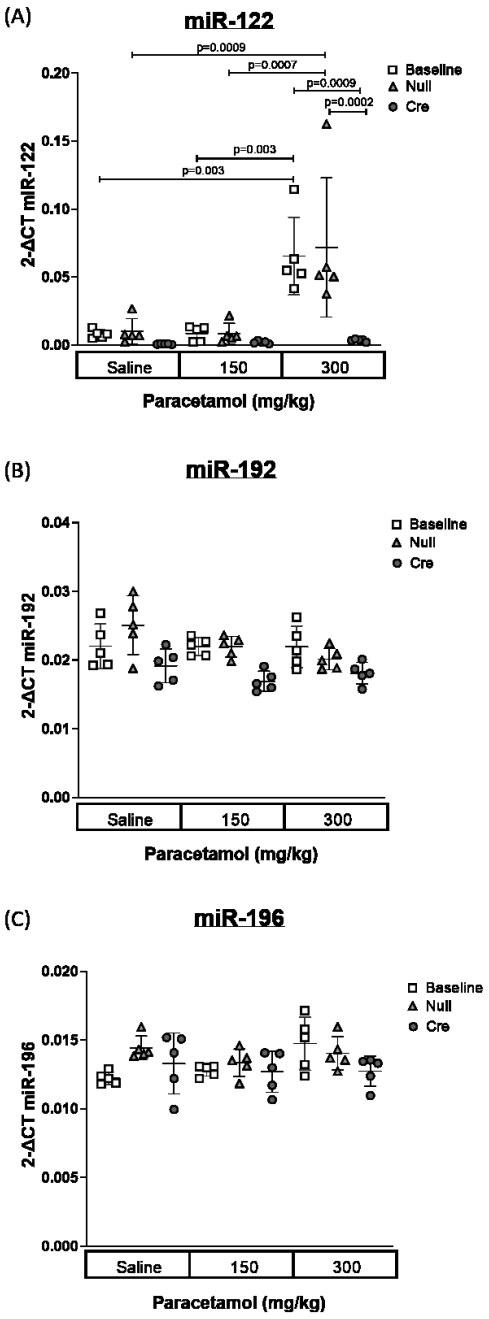

Figure 4.10 MiR-122, miR-192 and miR-196 expression in the kidney cortex after paracetamol-induced liver injury

MiR-122 (A) and miR-192 (B) and miR-196 (C) were measured in the kidney cortex of the male *Dicer1* $^{flox/flox}$ mice. MiRNA measurements were carried out via RT-qPCR 3 weeks following baseline (white squares), Null-AAV8 (light grey triangles) and Cre-AAV8 (dark grey circles) treatment and 6 hours after saline, 150mg/kg and 300mg/kg

of paracetamol. Each point was normalised by SNORD68, error bars represent mean ±SD, n=5. A multiple comparison two-way ANOVA was used to determine if the expression is significantly different between treatment groups.

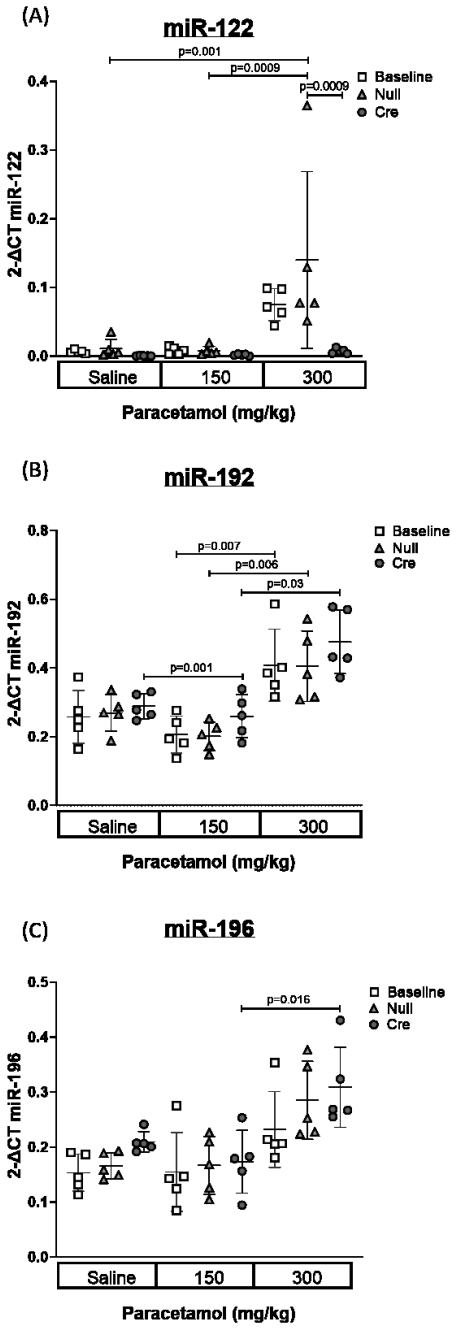

Figure 4.11 miR-122, miR-192 and miR-196 expression in the kidney medulla following paracetamol-induced liver injury

MiR-122 (A), miR-192 (B) and miR-196 (C) were measured in the kidney medulla of the male *Dicer1* $^{flox/flox}$ mice. MiRNA measurements were carried out via RT-qPCR 3 weeks following baseline (white squares), Null-AAV8 (light grey triangles) and Cre-AAV8 (dark grey circles) treatment and 6 hours after saline, 150mg/kg and 300mg/kg

of paracetamol. Data were normalised by U6, error bars represent mean ±SD, n=5. A multiple comparison two-way ANOVA was used to determine if the expression is significantly different between treatment groups.

H&E stains of whole kidney sections were assessed to determine if a loss of miR-122 alters the extent of injury following DILI (Figure 4.12). Assessments were carried out on the Null-AAV8 and Cre-AAV8 treated kidney sections with either saline (A, B), 150mg/kg paracetamol (C, D) or 300mg/kg paracetamol (E, F). For all paracetamol doses, in the Null and Cre-AAV8 treated mice, there were no signs of acute tubular injury associated with paracetamol toxicity (Figure 4.12).

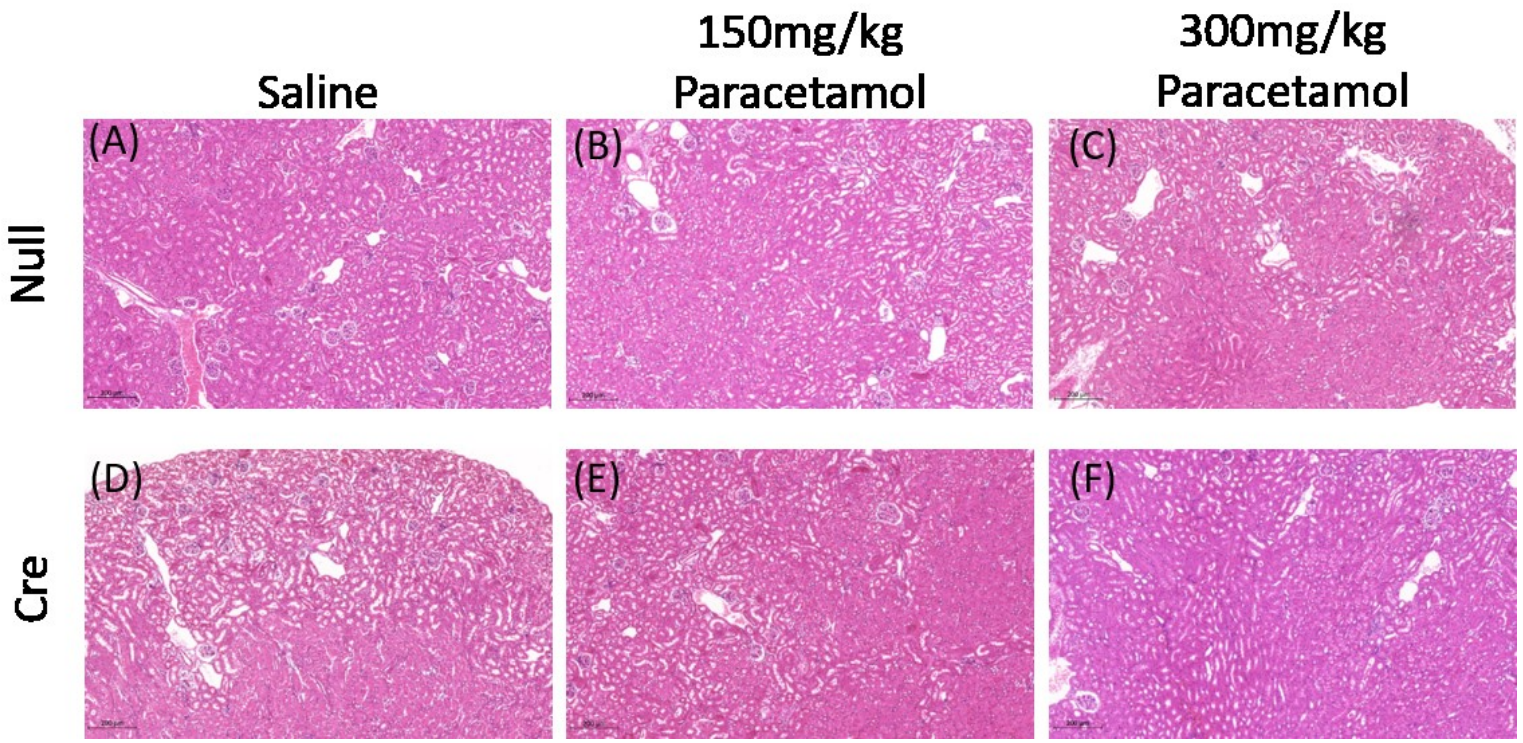

Figure 4.12 H&E staining of the kidney after AAV8 and paracetamol treatment

Assessments were carried out 3 weeks following Null-AAV8 and Cre-AAV8 treated kidney sections and 6 hours after saline (A, B), 150mg/kg paracetamol (C, D) or 300mg/kg paracetamol (E, F). Scale bar represents 200µm, 20x magnification. Images representative of n=5.

4.3.4 Increase of miR-122 during paracetamol DILI is reduced in the heart, lung and brain following Cre-AAV8 injection

As before, Dicer mRNA expression did not decrease in the heart, lung and brain with the exposure of Cre-AAV8 (Figure 6.7).

3.4.4.1. MiR-122 and miR-1 expression in the heart

MiR-122 and miR-1 were measured in the baseline, Null and Cre-AAV8 treated mice 6 hours post paracetamol dosing (Figure 4.13). At the highest dose of paracetamol (300mg/kg), there was a 10-fold and 50-fold increase of miR-122 in comparison to the saline dose in the baseline and Null-AAV8 treated mice respectively (ANOVA: Baseline saline vs 300mg/kg, $p<0.0001$; Null saline vs Null 300mg/kg, $p<0.0001$)(Figure 4.13A). In the Cre-AAV8 treated group, there was no increase in cardiac miR-122 (ANOVA: Baseline 300mg/kg vs Cre 300mg/kg, $p<0.0001$; Null 300mg/kg vs Cre 300mg/kg, $p<0.0001$) (Figure 4.13A).

With increasing doses of paracetamol, it was observed that miR-1 increases in the baseline and Null-AAV8 treated mice (ANOVA: Baseline saline vs 300mg/kg, $p<0.01$; Null saline vs Null 300mg/kg, $p<0.03$). This increase was exhibited in the Cre-AAV8 mice but to a lower extent.

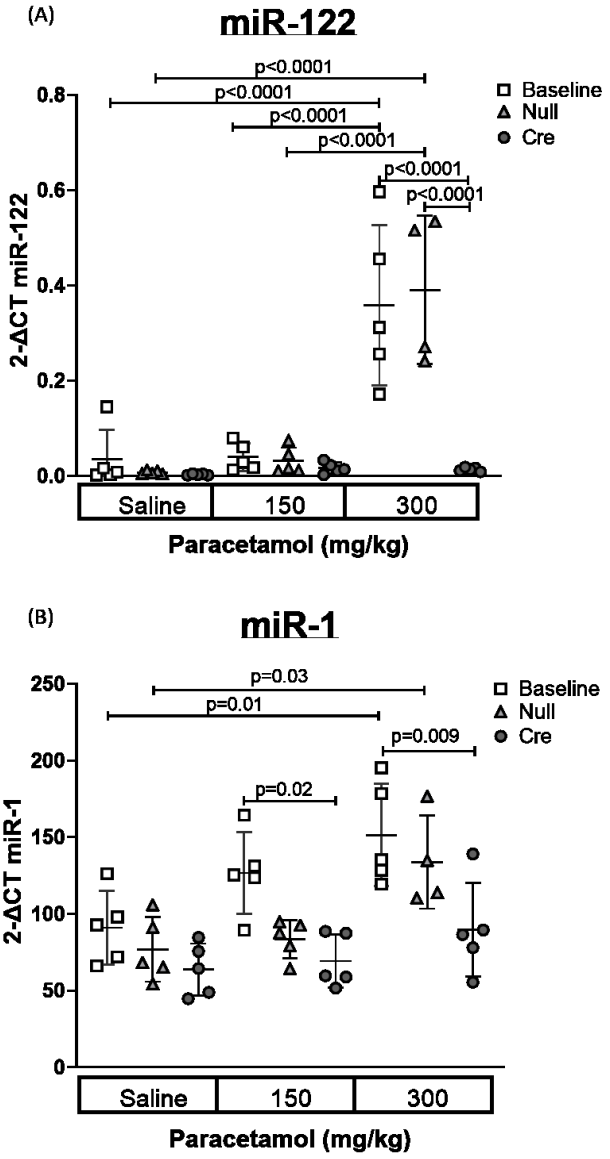

Figure 4.13 miR-122 and miR-1 expression in the heart of the AAV8 and paracetamol treated *Dicer1* $^{flox/flox}$ mice

MiR-122 (A) and miR-1 (B) was measured in the heart of the male Dicer1 $^{flox/flox}$ *mice. MiRNA measurements were carried out via RT-qPCR 3 weeks following baseline (white squares), Null (light grey triangles) and Cre-AAV8 (dark grey circles) treatment and 6 hours after saline, 150mg/kg and 300mg/kg of paracetamol. Each point was normalised by U6. Error bars represent mean ±SD, n=5 (300mg/kg Null-AAV8 mice, n=4). A multiple comparison two-way ANOVA was used to determine if the expression is significantly different between treatment groups.*

3.4.4.2. MiR-122 and miR-195a expression in the lung

MiR-122 and miR-195a expression were measured in the lung of the baseline, Cre-AAV8 and Null-AAV8 treated mice following saline, 150mg/kg and 300mg/kg paracetamol (Figure 4.14). MiRNA expression was investigated to see if paracetamol toxicity influences the uptake of hepatic miRNA into the lung.

In Figure 4.14 A, miR-122 expression of the saline and 300mg/kg of paracetamol treated baseline and Null-AAV8 treated mice was observed to be non-significant. Additionally, miR-122 expression at the 300mg/kg paracetamol dose, compared to the saline treated mice was not significant in the Cre-AAV8 treatment (Figure 4.14A).In Figure 4.14B, a non-significant difference was displayed in the miR-195a expression across all treatment groups (ANOVA: $p>0.05$).

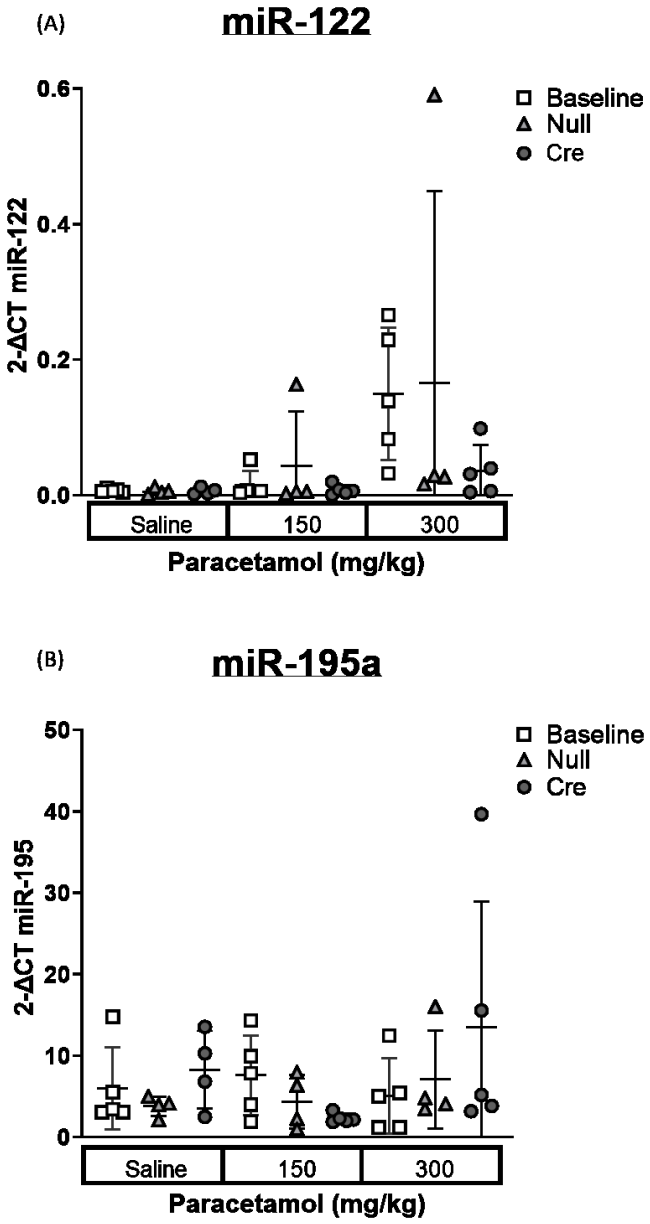

Figure 4.14 miR-122 and miR-195 expression in the lung post-AAV8 and paracetamol related DILI

MiR-122 (A) and miR-195a (B) were measured in the lung of the male Dicer1 $^{flox/flox}$ mice. MiRNA measurements were carried out via RT-qPCR 3 weeks following baseline (white squares), Null (light grey triangles) and Cre-AAV8 (dark grey circles) treatment and 6 hours after saline, 150mg/kg and 300mg/kg of paracetamol. Each point was normalised by U6, error bars represent mean ±SD, n=5 (Null: saline, 150mg/kg and

300mg/kg and Cre: saline, n=4). A multiple comparison two-way ANOVA was used to determine if the expression is significantly different between treatment groups.

3.4.4.3. MiR-122 and miR-124 expression in the brain after paracetamol dosing

A significant increase in miR-122 expression was displayed in the 300mg/kg baseline treated mice, in comparison to its saline control (ANOVA: baseline saline vs baseline 300mg/kg, $p<0.0001$, 5-fold change difference). The increase of miR-122 in the baseline 300mg/kg treated mice was significantly greater than both the Null-AAV8 and Cre-AAV8 treated mice at the equivalent dose (ANOVA: baseline 300mg/kg vs Null 300mg/kg, $p<0.0001$; 6-fold change difference; Baseline 300mg/kg vs Cre 300mg/kg, $p<0.0001$, 12-fold change difference). In contrast, miR-124 expression increases with increasing doses of paracetamol regardless of AAV8 treatment. A significant increase was seen in the Cre-AAV8 300mg/kg treated mice when compared to its saline control (ANOVA: Cre saline vs Cre 300mg/kg, $p=0.014$).

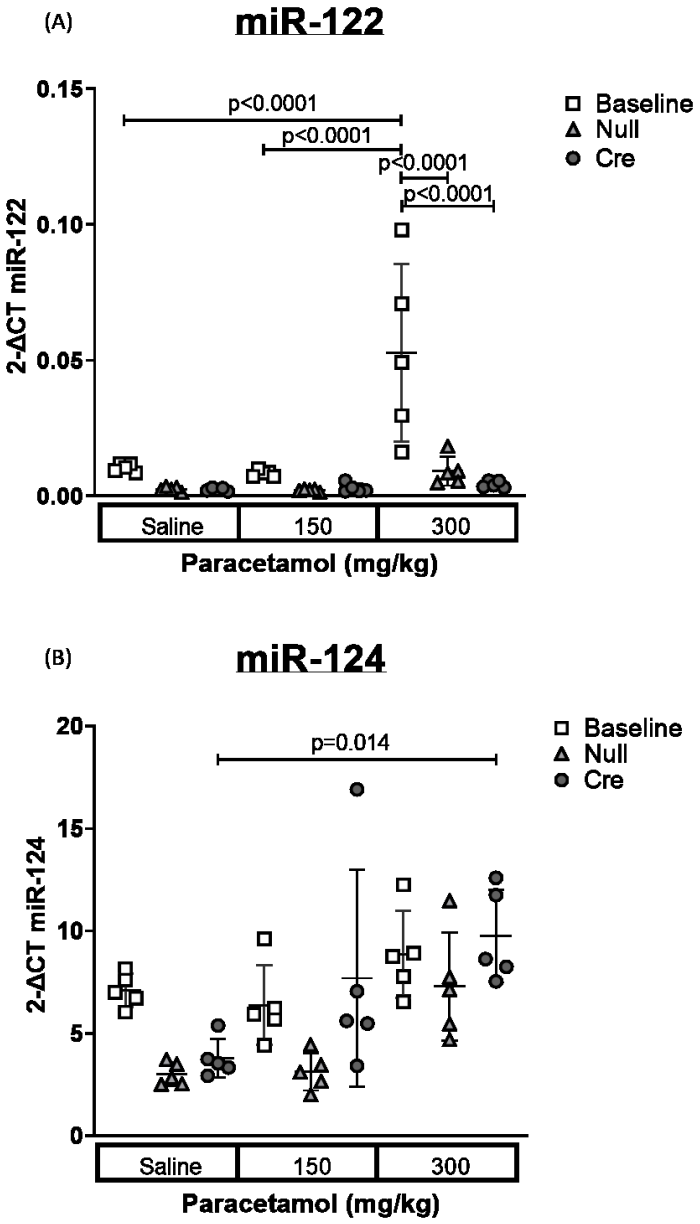

Figure 4.15 miR-122 and miR-124 expression in the brain following AAV8 and paracetamol treatment

MiR-122 (A) and miR-124 (B) were measured in the brain of the male Dicer1 $^{flox/flox}$ mice. MiRNA measurements were carried out via RT-qPCR 3 weeks following baseline (white squares), Null (light grey triangles) and Cre-AAV8 (dark grey circles) treatment and 6 hours after saline, 150mg/kg and 300mg/kg of paracetamol. Data were normalised to U6, error bars represent mean ±SD, n=5. A multiple comparison two-

way ANOVA was used to determine if the expression is significantly different between treatment groups.

4.3.5 Primary transcript of miR-122

Primary transcript of miR-122 (pri-miR-122) was measured in the liver, spleen, kidney cortex and medulla following AAV8 treatment and saline, 150mg/kg and 300mg/kg paracetamol dosing (Figure 4.16). As seen in Chapter 3 (Section 3.4.5), pri-miR-122 was expressed at minimal levels in the spleen, kidney cortex and medulla regardless of AAV8 and paracetamol treatment (Ct ~33-35 in the baseline mice treated with saline). Whereas the liver displayed the greatest level of pri-miR-122 expression in comparison to the spleen, kidney cortex and medulla (Ct~22 in baseline mice treated with saline).

In the liver, at the saline dose, the Cre-AAV8 treated mice had significantly higher levels of pri-miR-122 than the baseline and Null-AAV8 treated mice (ANOVA: baseline saline vs Cre saline $p<0.0001$; Null saline vs Cre saline $p<0.0001$) (Figure 4.16A). However, with increasing doses of paracetamol, pri-miR-122 expression decreases in all three treatment groups and are non-significantly different from each other (ANOVA: $p>0.05$). In the spleen, the Cre-AAV8 mice had higher pri-miR-122 expression than the baseline treated mice (ANOVA: Baseline saline vs Cre saline $p=0.036$) (Figure 4.16B). Again, this significantly greater expression of pri-miR-122 in the Cre-AAV8 mice, compared to the baseline and Null-AAV8 mice, is not observed in the spleen at the 150mg/kg or 300mg/kg paracetamol dose.

In the kidney cortex and medulla, there were no significant differences between the three AAV8 treated mice (Baseline, Null-AAV8 and Cre-AAV8) after saline, 150mg/kg and 300mg/kg paracetamol (Figure 4.16C-D).

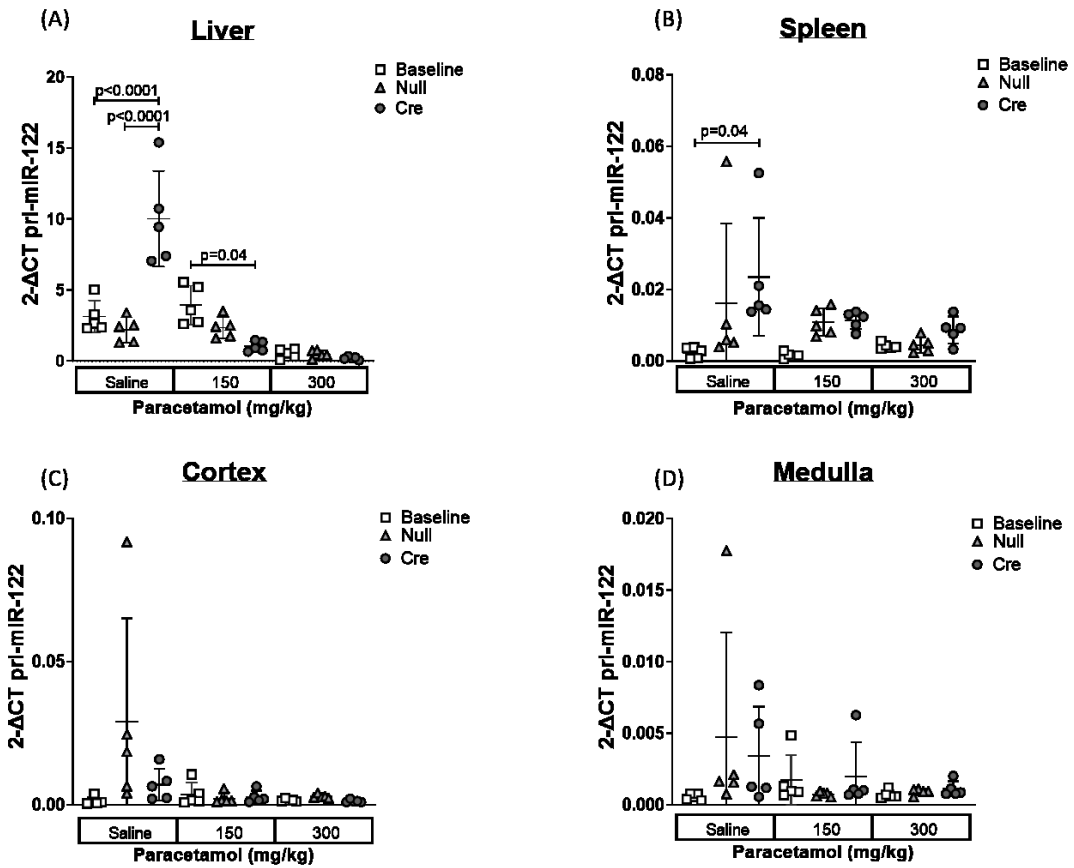

Figure 4.16 Primary transcript of miR-122 measured in the liver, spleen, kidney cortex and medulla following paracetamol induced liver injury

Pri-miR-122 was measured in the liver (A), spleen (B), kidney cortex (C) and medulla (D) of male Dicer1 $^{flox/flox}$ mice. MiRNA measurements were carried out via RT-qPCR 3 weeks following baseline (white squares), Null-AAV8 (light grey triangles) and Cre-AAV8 (dark grey circles) treatment and 6 hours after saline, 150mg/kg and 300mg/kg of paracetamol. In the liver and spleen the data were normalised by GAPDH, in the kidney cortex and medulla data were normalised to Hprt and β-actin respectively. Error bars represent mean ±SD, n=5. Multiple comparison two-way ANOVA was used to determine if the expression was significantly different between treatment groups.

4.3.6 The characteristic increase of circulating hepatic miRNA following paracetamol toxicity is lost with Cre-AAV8 treatment

Assessment of miRNA were carried out in the plasma to determine whether *Dicer1* knockdown in the hepatocytes (via Cre-AAV8 injection) influences the circulating profile of liver toxicity (Figure 4.17).

In the baseline mice, miR-122, miR-192 and miR-151 significantly increased following a single dose of 300mg/kg paracetamol (average copy numbers and ANOVA: baseline saline vs baseline 300mg/kg: miR-122, 6700 vs 310000, $p<0.0001$; miR-192: 0.6 vs 7000 $p=0.003$ and miR-151: 3 vs 54, $p<0.0001$) (Figure 4.17). Circulating miR-122, miR-192 and miR-151 in the 300mg/kg treated Null-AAV8 mice was not significantly different compared to its saline control (average copy number and ANOVA: Null saline vs Null 300mg/kg: miR-122: 4000 vs 120000, $p>0.05$; miR-192: 0.1 vs 2000, $p>0.05$ and miR-151: 2 vs 12, $p>0.05$). In the Cre-AAV8 treated mice, miRNA expression remained unchanged and significantly lower than the baseline mice at 300mg/kg paracetamol (average copy number and ANOVA: baseline 300mg/kg vs Cre 300mg/kg: miR-122: 310000 vs 1600, $p<0.0001$; miR-192: 7000 vs 0.3, $p=0.003$; miR-151: 54 vs 0.03, $p<0.0001$).

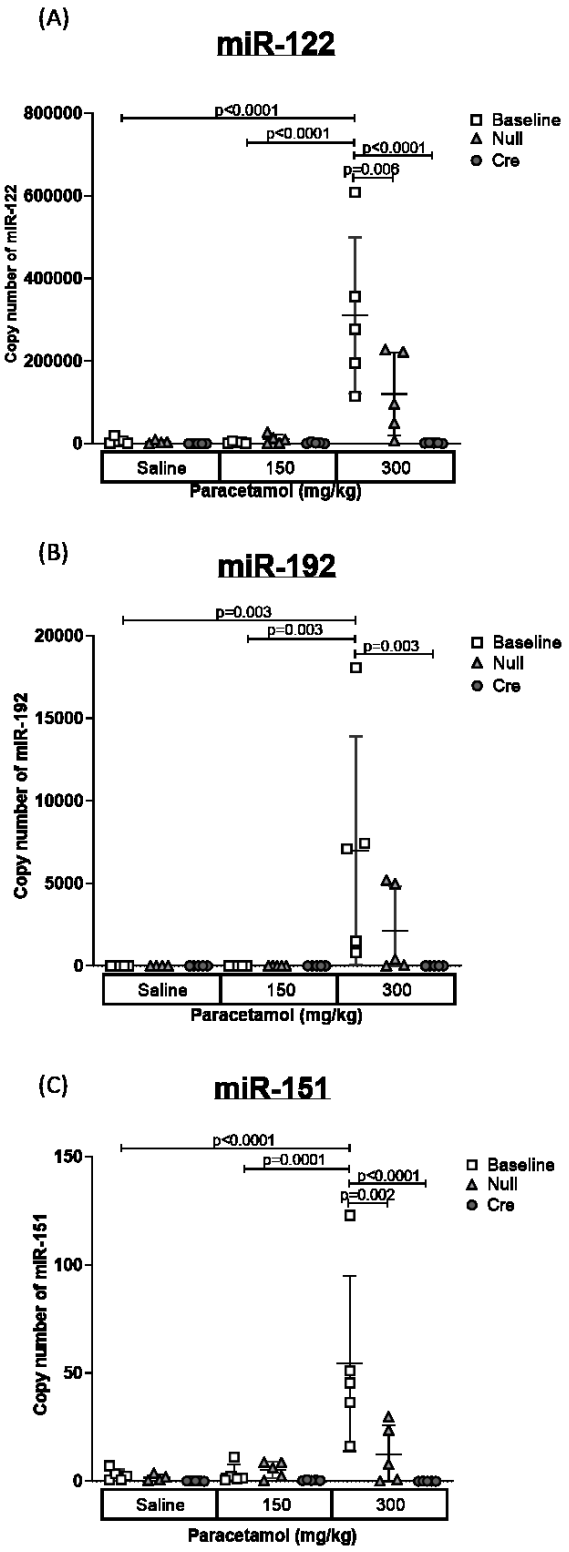

Figure 4.17 Circulating hepatocyte enriched miRNA expression following AAV8 and paracetamol-related DILI

MiR-122 (A), miR-192 (B) and miR-151 (C) were measured in the plasma of the male *Dicer1* $^{flox/flox}$ mice. MiRNA measurements were carried out via RT-qPCR 3 weeks following baseline (white squares), Null (light grey triangles) and Cre-AAV8 (dark grey circles) treatment and 6 hours after saline, 150mg/kg and 300mg/kg of paracetamol. Copy number was determined by absolute quantification, error bars represent mean ±SD (n=5; Null saline n=4). A multiple comparison two-way ANOVA was used to determine if the expression is significantly different between treatment groups

4.3.7 Transfer of miR-122 is not observed following CCl_4-induced liver injury

To investigate the profile of miRNA release from the liver into the circulation, plasma was collected and analysed from C57BL/6 mice, 6 hours, 12 hours and 24 hours following a single injection of CCl_4 (Figure 4.2). Hepatocyte enriched miRNA, miR-122, miR-192 and miR-151 were measured in the plasma (Figure 4.18A-C).

It was observed that miR-122 significantly increased in the plasma 24 hours after CCl_4 treatment, when compared to the 6 hour and 12 hour time points (Average copy number: 6 hours= 110, 12 hours= 820, 24 hours= 16600)(ANOVA: CCl_4 6 vs 24 hours, p=0.01; CCl_4 12 hours vs 24 hours, p=0.015) (Figure 4.18A). This increase was also significant when compared to the control group at 24 hours (olive oil) (ANOVA: 24 hours, olive oil vs CCl_4, p=0.014). At the 6-hour and 12-hour time point, miR-122 expression in the circulation did not significantly differ between the olive oil and CCl_4 treatments (ANOVA: p>0.05) (Figure 4.18A).

MiR-192 and miR-151 expression was at its highest in the circulation 24 hours after a single treatment of CCl_4 (miR-192: average copy number: 6 hours= 0.003, 12 hours= 0.2, 24 hours= 35) (miR-151: average copy number: 6 hours= 3, 12 hours= 4, 24 hours= 21). However, this was not significant in comparison to both the controls and other CCl_4 post-treatment time points (Figure 4.18B-C).

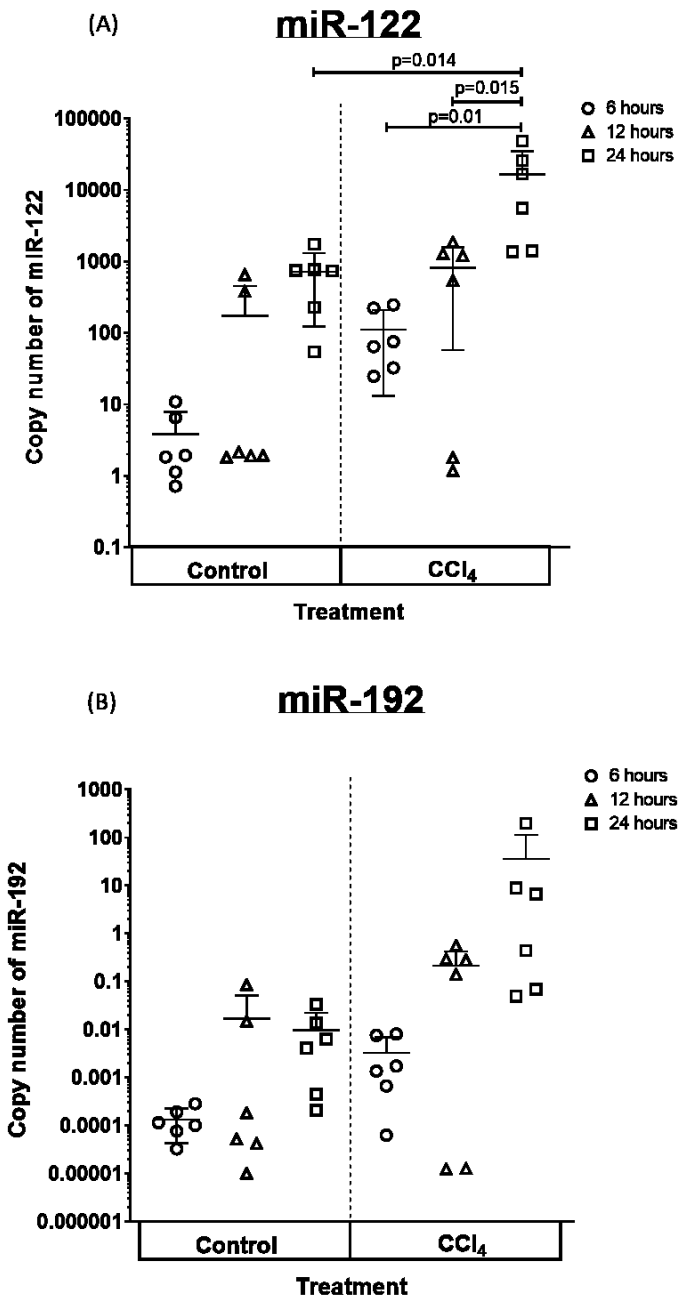

Figure 4.18 Hepatic miRNA measurements in the circulation following CCl_4 treatment

Using RT-qPCR, miRNA were measured in the plasma of the male C57BL/6 mice. Hepatocyte enriched miRNA: (A) miR-122, (B) miR-192 and (C) miR-151 were measured in the plasma 6 (circles), 12 (triangles) and 24 hours (squares) after a single injection of olive oil or CCl_4. Copy number was determined by absolute quantification, error bars represent mean ±SD, n=6. A multiple comparison two-way ANOVA was used to determine if the expression is significantly different between treatment groups.

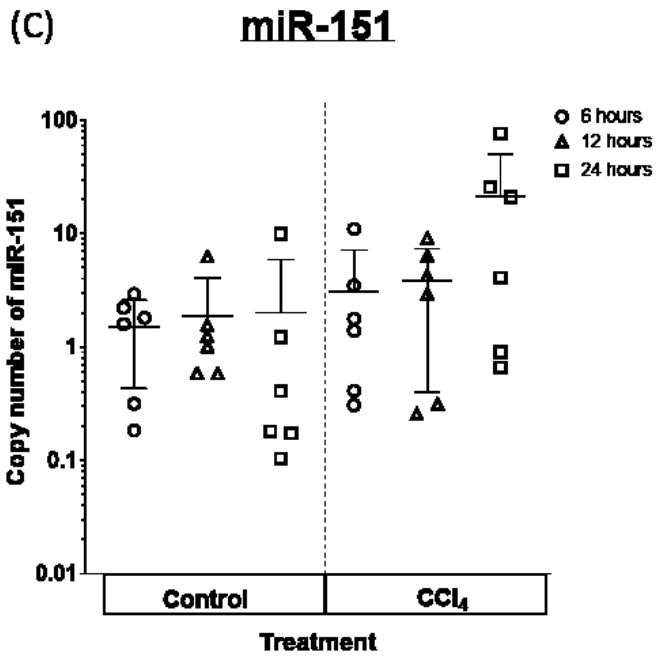

Figure 4.18 ***Continued***

To see whether an increase in circulating hepatocyte enriched miRNA reflected the extent of liver injury, H&E stained livers were investigated at the 24 hours following acute exposure to CCl_4 (Figure 4.19). In the control group (injection of olive oil), there were no signs of injury observed (Figure 4.19A-B). Whereas in the CCl_4 treated mice centrilobular necrosis was present (Figure 4.19C-E).

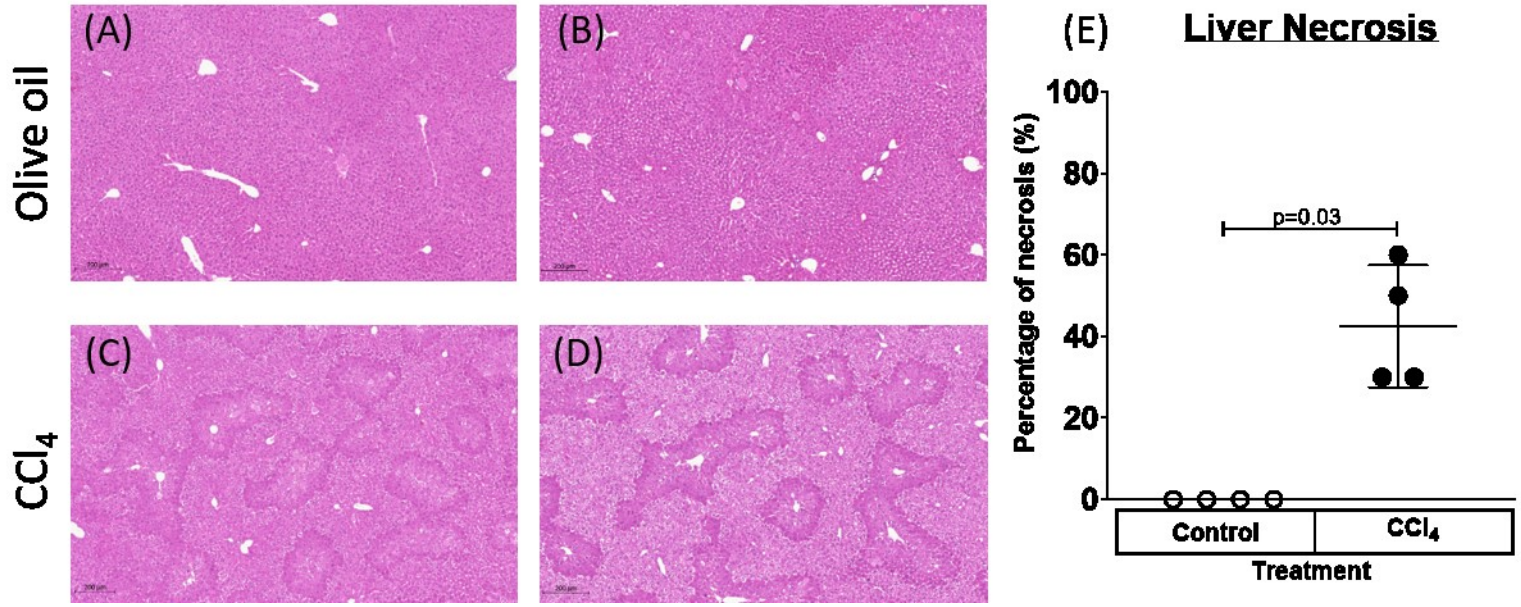

Figure 4.19 H&E staining and measurements of centrilobular in the liver 24 hours after a single CCl_4 injection

H&E staining of whole liver sections 24 hours after a single injection of olive oil (A and B) and CCl_4 (C and D). Scale bar represents 200µm, 20x magnification. Images representative of n=4. (E) In reference to the H&E stained livers, the level of necrosis was calculated as a percentage for each section (as per Section 2.9.4): control (olive oil, white circles) and CCl_4 (Black circles). Error bars represent mean ±SD, n=4. Unpaired t-test was carried out to determine if the percentage of necrosis was significantly different between the control and treated (CCl_4) group.

Next, miRNA were measured in the tissues to investigate whether hepatocyte miRNA is transferred from the liver to other organs during CCl_4-induced liver injury. Hence, miR-122, miR-192 and miR-151 were measured in the liver, kidney cortex, kidney medulla, spleen, heart, lung and brain (Figure 4.20A-C).

In the liver, miR-122 and miR-192 expression were significantly reduced in the CCl_4 treated mice, in contrast to the olive oil control (Unpaired t-test: miR-122, p=0.05; miR-192, p=0.02) (Figure 4.20A, B). However, a loss of miR-151 was not observed in the liver following CCl_4 (Figure 4.20C). Across the six non-hepatic tissues (spleen, kidney cortex and medulla, heart, brain and lung), miRNA-122, miR-192 and miR-151 expression remained unchanged after CCl_4 treatment, compared to the control mice (Figure 4.20A-C).

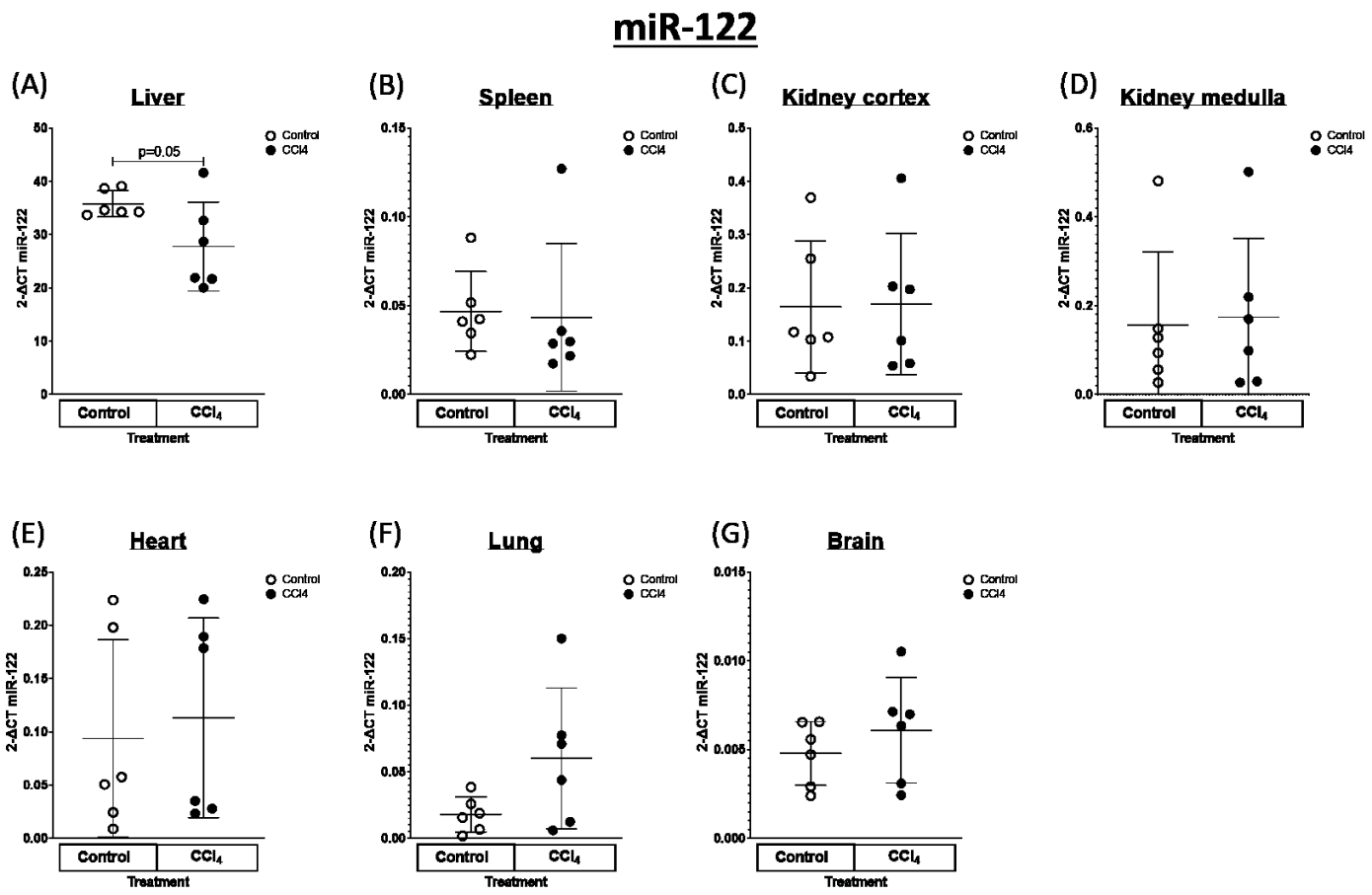

Figure 4.20 miRNA expression in the liver and 6 non-hepatic tissues following CCl_4 related liver injury

Using RT-qPCR, miRNA were measured in 7 tissues from male C57BL/6 mice treated with either olive oil (control white) or CCl_4 (black). Hepatocyte enriched miRNA: miR-122(A-G), miR-192 (H-N) and miR-151 (O-U) were measured in the liver (A, H, O), spleen (B, I, P), kidney cortex (C, J, Q) and medulla (D, K, R), heart (E, L, S), lung (F, L, T) and brain (G, N, U). Data were normalised to U6, error bars represent mean ±SD, n=6. In each tissue, an unpaired t-test was used to determine whether the expression significantly differed between the control and CCl_4 treated mice.

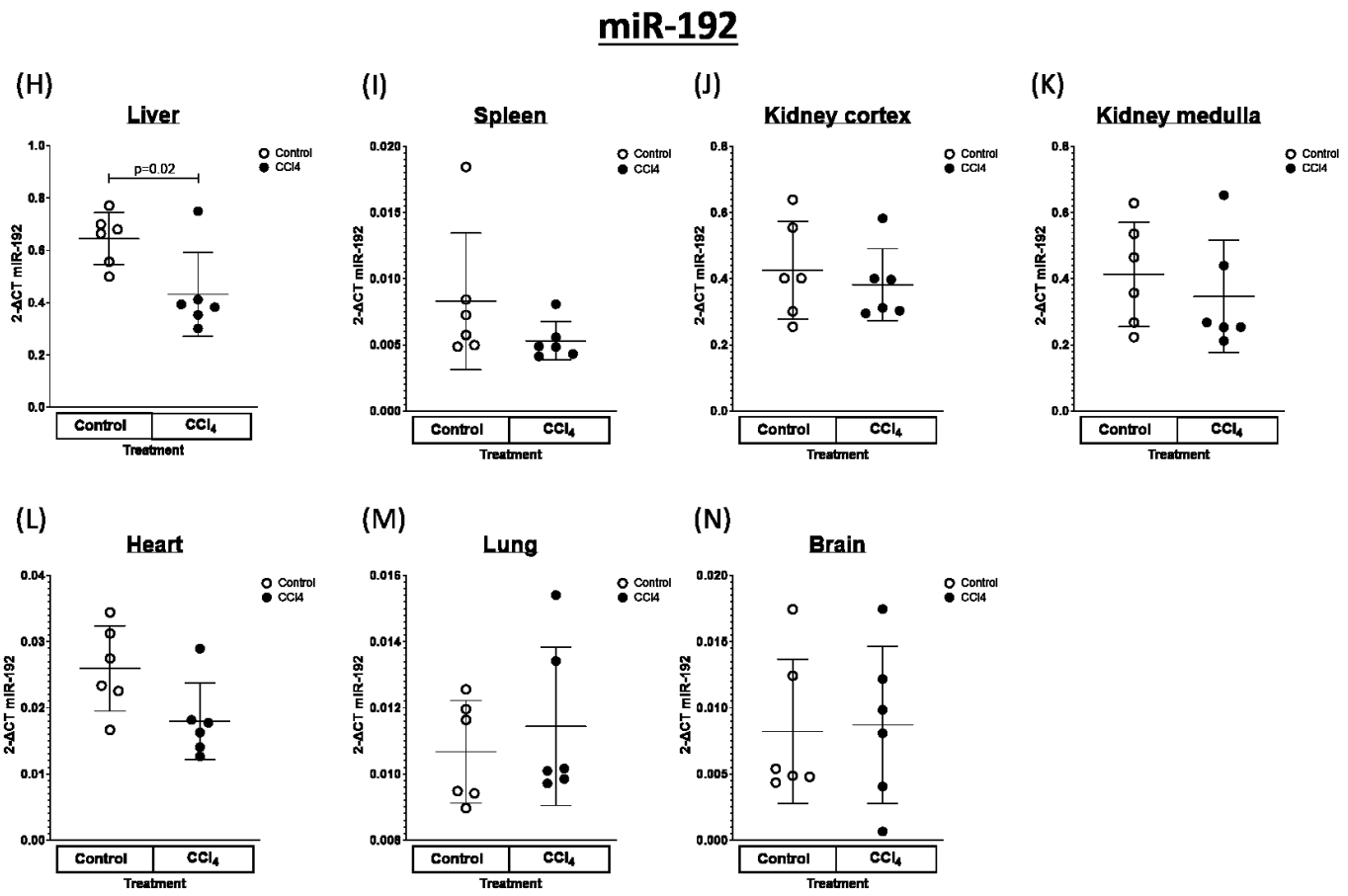

Figure 4.20 ***Continued***

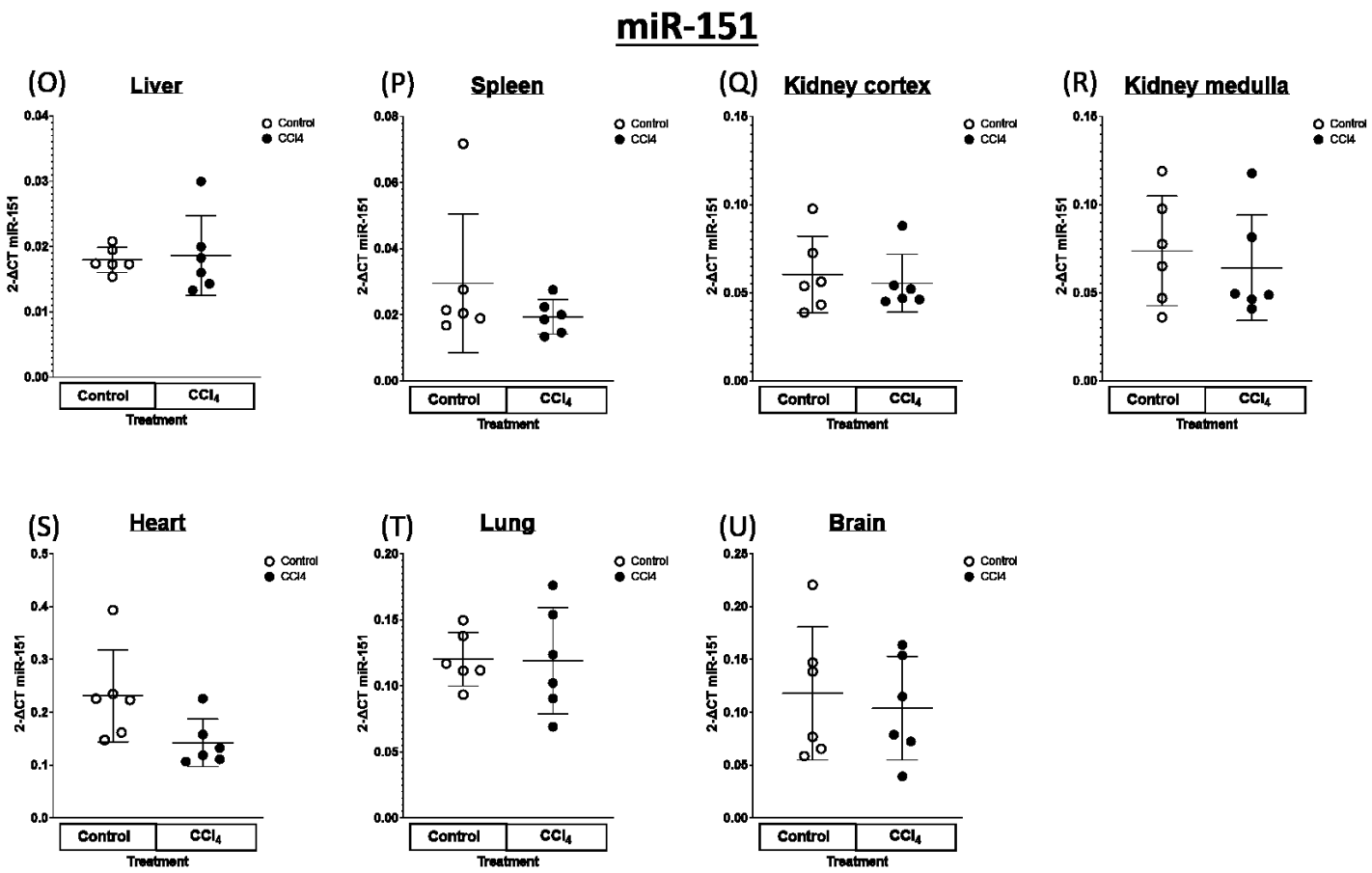

Figure 4.20 ***Continued***

4.3.8 Main findings

- Successful *Dicer1* and miRNA knockdown was observed in the livers of the *Dicer1* $^{flox/flox}$ mice following a lower dose of Cre-AAV8.
- A loss of hepatic miRNA resulted in an increased susceptibility of paracetamol toxicity in the liver.
- The characteristic increase of circulating miR-122 and miR-192 during paracetamol toxicity was lost following Cre-AAV8 injection.
- The significant uptake of miR-122 in the spleen, kidney (cortex and medulla) and heart during paracetamol injured liver injury was diminished in the Cre-AAV8 mice.
- Transfer of miR-122 from the liver to other tissues was not observed following CCl_4 toxicity.

4.4 Discussion

MiR-122 has been extensively researched for its application as a biomarker of liver injury in a clinical setting. However, there have been few studies focussing on the destination of miR-122 following its release during DILI. Hence, this chapter focussed on identifying the organs involved in the uptake and clearance of miR-122 when it is abundant in the circulation. To achieve this, two models of toxicity were investigated: paracetamol toxicity in the *Dicer1* $^{flox/flox}$ mice and acute CCl_4 toxicity in C57BL/6 mice.

Figure 4.3 confirmed that the lower Cre-AAV8 dose (Victoria Gadd, CRM; $6.25x10^{10}$ viral genomes/dose) caused a significant loss of Dicer mRNA expression in the saline Cre-AAV8 treated *Dicer1* $^{flox/flox}$ mice, compared to the baseline and Null-AAV8 treated mice. Moreover, as seen in Chapter Chapter 3 and previous reports [227], the induction of *Dicer1* knockdown resulted in the significant loss of mature hepatic enriched miRNA in the liver. The loss of miR-122 and miR-192 was maintained in the liver of the Cre-AAV8 mice regardless of paracetamol dosing. Nevertheless, mirroring earlier findings [123], the baseline and Null-AAV8 (negative control) livers displayed a loss of miR-192 and miR-151 with increasing doses of paracetamol. Compared to the baseline and Null-AAV8 treated mice, the Cre-AAV8 mice had equal or greater expression of pri-miR-122. This implies that the loss of mature miR-122 observed was due to *Dicer1* knockdown, rather than an alteration in the components upstream the *de novo* synthesis.

A loss of hepatic miRNA in the Cre-AAV8 mice was mirrored in the plasma. However, as previously described, the baseline and Null-AAV8 control mice displayed a significant increase of miR-122, miR-192 and miR-151 in the circulation following paracetamol toxicity [82, 86, 87, 123, 239]. As before, Dicer mRNA expression did not decrease after Cre-AAV8 treatment in the spleen, kidney cortex and medulla, heart, lung and brain (Appendix). Additionally, the stable expression of the tissue enriched miRNA at the saline dose: miR-146a (spleen), miR-192 and miR-196 (kidney cortex

and medulla), miR-1 (heart), miR-195a (lung) and miR-124 (brain), reinforced the hepatocyte specificity of the Cre-AAV8.

MiRNA are regularly described as regulators of gene function and consequently biological responses [172, 240]. Unsurprisingly, multiple studies have indicated a dysregulation of various miRNAs can influence the progression of cell injury and death during acute liver injury [172, 241, 242]. Additionally, they have been extensively described to modulate drug metabolism by negatively regulating the translation of the cytochrome P450 enzymes (CYP450) [203, 243-247]. As the reactive metabolite of paracetamol metabolism (N-acetyl-p-benzoquinone imine, NAPQI) is a product of CYP450 mediated oxidation [37, 46, 248], the *Dicer1*$^{floxed/flox}$ livers were assessed to determine if a loss of hepatic miRNA alters its response and survival during paracetamol toxicity.

The mechanism of paracetamol-induced liver injury is a defined by the accumulation of NAPQI through CYP450 mediated oxidation, depletion of glutathione (GSH) and in turn hepatotoxicity and centrilobular hepatic necrosis [247, 249]. As proposed by other studies, an increase in circulating ALT [82, 250] and hepatic miRNA [82, 86, 123] after paracetamol dosing accurately reflected the level of hepatocyte death and injury displayed in the liver sections. In the baseline, Null-AAV8 and Cre-AAV8, increasing doses of paracetamol increased the percentage of necrosis, circulating ALT and miRNA. Furthermore, as observed in Chapter 3 and previous studies, miR-122 in the circulation had a significant positive correlation with ALT in the absence and presence of liver injury (Section 3.4.2)[86]. However, assessment of all three measures indicated that the loss of total hepatic miRNA increased the extent of centrilobular necrosis and injury induced by paracetamol toxicity. In the next chapter, I will explore the activity of CYP450 enzymes following miRNA depletion.

Gender has shown to impact the pharmacokinetics and pharmacodynamics of a drug [251]. Furthermore, extensive research has discovered that male mice have a greater susceptibility to paracetamol-induced acute liver injury, in comparison to female mice [252-254]. In this chapter, like many studies of paracetamol-induced liver injury, only male mice were used. Consequently, a limitation of this study was that female

mice were not examined. Although, due to time constraints it was not feasible to analyse both sexes, it would be interesting to see if the total loss of miRNA in female livers caused a comparable increase in injury seen in the male mice. I suspect there would be a greater extent of injury in the female mice with the loss of miRNA but perhaps not to the same degree as their male counterparts.

Previously miR-122 has been described, via *in situ* hybridisation, to have a strong even expression across healthy hepatocytes [177]. In the presence of paracetamol-induced liver injury, miR-122 expression is lost from the necrotic cells around the central vein and in turn released into the circulation [87]. Matching previous findings, there was a uniform dispersal of miR-122 in the hepatocytes of the saline treated Null-AAV8 mice. Increased dosing of paracetamol in the Null-AAV8 mice caused a loss of miR-122 expression in the necrotic areas and an upregulation of miR-122 expression in the healthy hepatocytes surrounding the centrilobular necrotic areas. This loss was not reflected in the RT-qPCR results, with the upregulation in the healthy cells counteracting the loss of miR-122 from the necrotic.

Interestingly, this non-significant change in miR-122 expression in the baseline and Null-AAV8 treated mice did not mirror previous findings [123]. Instead, following 300mg/kg paracetamol, a significant loss of miR-122 in the liver was previously observed [123]. In their study, miR-122 was measured in the liver 24 hours after dosing. Whereas, in this chapter, following previous reports [203, 207], miR-122 investigations were carried out 6 hours after dosing. Furthermore, centrilobular necrosis and circulating ALT has been observed to be greater at 24 hours compared to 6 hours [204, 207, 255]. However, miR-122 peaks in the circulation at 6 hours post-treatment [207]. Indicating, the differences seen in this chapter could be due to differing levels of paracetamol metabolism, necrosis, inflammation and immune related responses at each time point [204]. In future studies, it would be interesting to investigate miR-122 expression and localisation past the 6 hour time point. Perhaps 24 hours after dosing, the loss of miR-122 in the liver Wang *et al.* observed would be replicated.

As seen in the RT-qPCR data, a loss of miR-122 was visualised in both the healthy and necrotic hepatocytes of the Cre-AAV8 mice across all three paracetamol doses. This,

along with the increased levels of injury and necrosis in the Cre-AAV8 treated mice suggests the increase of miR-122 in the healthy cells (surrounding the necrotic areas) in the Null-AAV8 may be protective against further injury. The potential mechanism of protection could be linked to its known repression of the CYP enzymes. An increased concentration of miR-122 in these areas would reduce the activity of the CYP enzymes and hence production of NAPQI.

In Chapter 3, it was discovered that the spleen and kidney (cortex and medulla) were involved in the clearance of miR-122 from the circulation in a healthy mouse. In this chapter, it was found that during paracetamol-induced liver injury (300mg/kg), the release of miR-122 into the plasma of baseline and Null-AAV8 mice resulted in a significant increase of miR-122 in the spleen and kidney cortex and medulla. This increase in miR-122 expression was not observed following hepatocyte Dicer and miRNA knockdown in the liver. Moreover, the expression of miR-122 in the kidney cortex, kidney medulla and the spleen had a significant positive correlation when plotted against plasma miR-122 in the presence of paracetamol-induced liver injury. Therefore, as discussed in Chapter 3, these results support previous findings indicating miR-122 is transferred from the liver to the spleen and kidney via the portal and systemic circulation [122, 193].

Surprisingly, despite no transfer observed in a healthy mouse, miR-122 was also observed to be significantly greater in the heart of the baseline and Null-AAV8, 300mg/kg paracetamol, treated mice. The Cre-AAV8 treated mice had a significantly reduced level of miR-122 expression at the 300mg/kg paracetamol dose, suggesting the dependency of miR-122 transfer from an injured liver to produce this upregulation.

Multiple studies have shown that through a negative feedback loop, miR-146a mediates the innate inflammatory response by controlling cytokine and toll-like receptor (TLR) signalling As seen in Chapter Chapter 3, miR-146a expression was unchanged in the spleen following Cre-AAV8 and saline treatment, compared to the baseline mice. During paracetamol toxicity, it has been demonstrated that there is a modest but significant increase in circulating miR-146a [172]. In this study, Bala *et al.*

indicated that the increase of miR-146a in the circulation was a result of hepatocyte and immune cell death in the liver, rather than an increase in the inflammatory response [172].

In this chapter, there was a significant increase in miR-146a expression in the spleen of the paracetamol treated baseline mice. In turn, the loss of hepatic *Dicer1* and miRNA inhibited the increase of miR-146a in the spleen of the Cre-AAV8 treated mice. Hence, it is possible that like miR-122, miR-146a is transferred from the liver to spleen during paracetamol DILI. Indeed, the innate immune response has been described to be mainly beneficial during paracetamol toxicity, contributing to tissue repair [256]. Therefore, the loss of miR-146a may be a contributor to the increased susceptibility to injury seen in the Cre-AAV8 mice. Nevertheless, further investigations into the circulating profile of miR-146a, its interaction and *de novo* synthesis in other tissues and potential targets once entering the spleen is required for confirmation of hepatic transfer and function. Interestingly, in the brain, it was found that miR-122 increased significantly in the baseline mice following 300mg/kg paracetamol, in comparison to the saline and 150mg/kg paracetamol treated mice. This suggests that miR-122 is transferred from the liver to the brain during paracetamol toxicity. However, a notable finding was that the empty AAV8 control, Null-AAV8, did not display the same pattern of expression. It was observed that the Null-AAV8 had a reduced increase of miR-122 after 300mg/kg paracetamol, comparable to the Cre-AAV8 mice. Studies have shown that although inefficient, AAV8's can enter and transduce cells in the brain [228, 257]. Yet, Dicer mRNA and its tissue enriched miR-124 expression was unchanged, indicating that the lack miR-122 increase in the brain could be due to a response to an AAV8 infection rather than the occurrence off-target *Dicer1* deletion.

Recently it was demonstrated that the lung had significantly increased levels of miR-122, 6 hours following Concanavalin (ConA)-induced liver injury [122]. Here, Wang *et al.* highlighted that during DILI, the lung contained the highest level of miR-122 in comparison to the heart, spleen, lung, kidney and colon [122]. Nevertheless, in this chapter, miR-122expression in the lungs of the 300mg/kg paracetamol treated baseline and Null-AAV8 mice were not significantly different from the saline controls.

Although the outcome of paracetamol and Con-A-induced liver injury is similar, both leading to inflammation, cell death and an increase in circulating biomarkers such as ALT, there are fundamental differences in the cause and progression of injury [258]. In paracetamol toxicity, the formation of NAPQI drives hepatocyte necrosis [37]. Whereas, in Con-A-induced liver injury, the recruitment and activation of T-cells and natural killer cells initiates apoptotic cell death in the hepatocytes and liver sinusoidal endothelial cells [258-261]. Perhaps, the different mechanism of cell death and in turn release of miR-122 explains the inconsistency of miR-122 uptake between the two models of liver toxicity.

In the early stages of CCl_4-induced liver injury, miRNA, including known hepatotoxicity markers, miR-122 and miR-192, have been described to significantly increase in the circulation [262-264]. 24 hours after CCl_4 dosing, a significant loss of miR-122 in the liver was paired with a significant increase in the circulation. Furthermore, the increase of miR-192 and miR-151 observed 24 hours after CCl_4 dosing were non-significant. Nonetheless, as seen in paracetamol toxicity, the increase in circulating hepatic miRNA reflected the presence of centrilobular necrosis in the liver [262-264].

In comparison to the 150mg/kg and 300mg/kg paracetamol treated mice, the CCl_4 mice had around a 5-fold greater and a 19-fold lower concentration of circulating miR-122 respectively. Moreover, unlike 300mg/kg paracetamol toxicity, the increase in circulating miR-122 did not result in its significant uptake in the spleen, kidney, heart, lung and brain. These findings suggest that like 150mg/kg paracetamol, the increase in circulating miR-122 produced after 0.25ml/kg CCl_4 treatment was not sufficient enough to produce a significant uptake elsewhere. Perhaps a greater dose of CCl_4, and in turn greater extent of hepatocyte injury, is required to observe a significant transfer and uptake of miR-122 to other organs. Thus, for future study, it would be interesting to investigate whether an increase in CCl_4 dosage induces a selective and significant uptake of hepatic miRNA in other organs. Alternatively, the different nature of acute hepatocyte injury, and subsequent mechanism of miRNA

release from the CCl_4 injured liver could influence the expression profile of circulating miRNA.

Previous studies have shown that the profile of circulating miRNA following CCl_4 toxicity differs from paracetamol, with miRNA such as miR-802-5p and miR-34a-5p described to increase significantly in the bloodstream during CCl_4 toxicity but not during paracetamol-induced liver injury [87, 263, 264]. Consequently, it would be interesting to expand the range of miRNA investigated in the bloodstream and organs following both CCl_4 and paracetamol toxicity. This would enable us to observe if other miRNA are taken up by other organs during paracetamol-related DILI. I suspect there would be a large overlap of miRNA transfer between the two models of hepatotoxicity, however, like miR-122, some of the miRNA transferred will be specific to the injury model investigated.

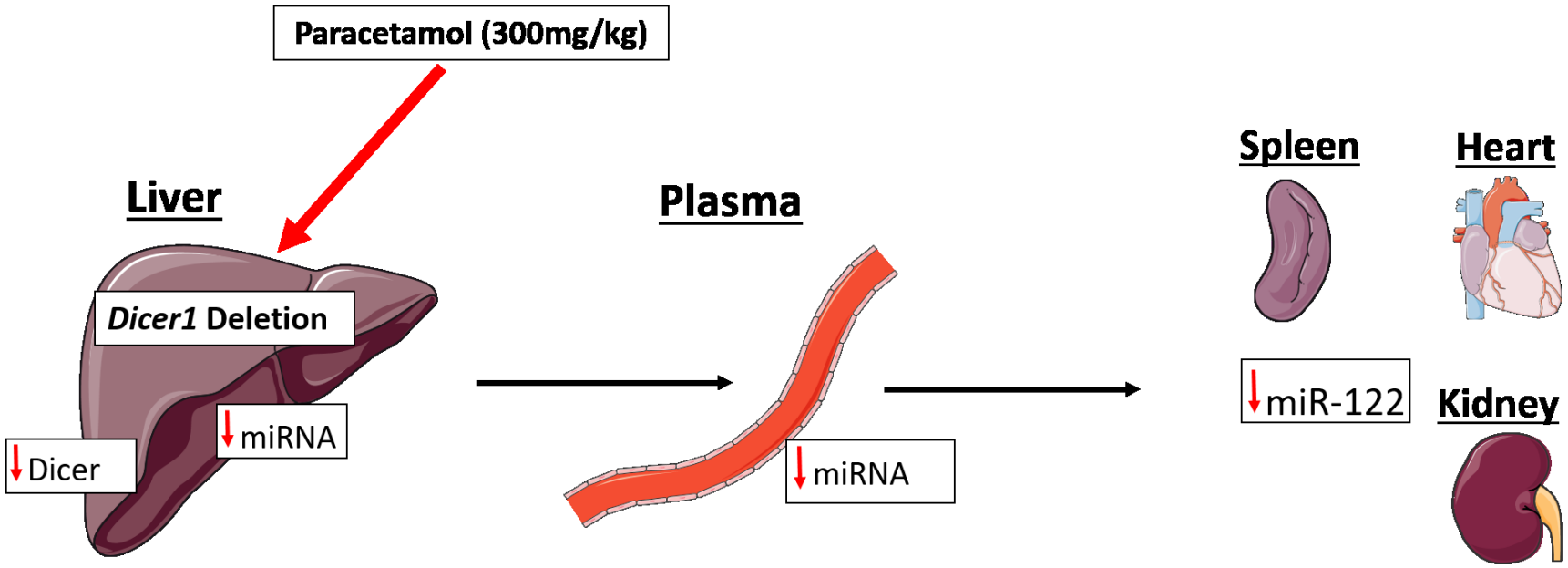

Figure 4.21 Diagram of Chapter 4's key findings

Hepatocyte specific Dicer1 knockdown resulted in the total loss of mature miRNA in the hepatocytes. This in turn lead to the loss of circulating miRNA, such as miR-122 and miR-192 following paracetamol toxicity. Interestingly, a loss of circulating miR-122 lead to the loss of miR-122 transferred from the liver to the spleen, kidney (cortex and medulla) and heart. Indicating, during paracetamol toxicity, these tissues are responsible for the uptake and clearance of miR-122. Figure created using Servier Medical Art, Les Laboratoires Servier.

Chapter 5 The functional impact of miR-122 transfer from the liver to the kidney

5.1 Introduction

5.1.1 Background

Cytochrome P450 (CYP450) enzymes are a superfamily of haem-containing enzymes involved in the oxidation of endogenous and exogenous compounds [48]. Approximately 75% of all known drugs are metabolised via CYP450 mediated oxidation, including paracetamol [265]. In humans, the CYP450 enzymes involved in the oxidation of paracetamol into its highly reactive metabolite, NAPQI, are: CYP1A2, CYP2E1 and CYP3A4 [38, 70, 248]. Following a comparison study with humans, mice were found to lack the cyp3a4 enzyme, but express fully functional cyp1a2 and cyp2e1 enzymes[266]. The CYP2E1 enzyme is deemed the most prominent contributor in paracetamol bioactivation [70, 203]. CYP2E1, like others in its superfamily, is predominately found in the liver [215, 267-270]. Nevertheless, studies have shown that CYP2E1 is found in other organs including the kidney and lung [49-51].

It has been well described that miRNA plays an important role in the regulation of the CYP450 enzymes expression and activity [243, 244, 271, 272]. Recently, miR-122 has been described to negatively regulate multiple CYP450 enzymes, including CYP2E1 [203, 246]. In both reports, it was noted that a loss of miR-122 resulted in an increased expression of CYP2E1 and CYP1A2, increased production of NAPQI and hence toxicity in the liver following paracetamol overdose [203, 246]. Due to these findings and an observed significant loss of miR-122 in the kidney in Chapter 3 and 4, the aim of the studies in this chapter was to investigate whether the loss of miR-122 transfer during paracetamol-induced liver injury has an impact on CYP2E1 expression and activity in the kidney. To investigate this, liver and kidney samples collected from the healthy and paracetamol treated *Dicer1* $^{flox/flox}$ mice from Chapter 3 and 4 were assessed.

5.2 Experimental animals

5.2.1 *Dicer1* $^{flox/flox}$ mice

Tissue harvested from healthy and DILI *Dicer1* $^{flox/flox}$ mice described in Chapter 3 (Section 3.3.2) and Chapter 4 (Section 4.2.1) were investigated in this chapter.

Chapter 3 described male and female *Dicer1*$^{flox/flox}$ mice treated with the hepatocyte-specific Null-AAV8 and Cre-AAV8 ($2.5x10^{11}$ viral genomes/100µL dose). Following the AAV8 injection, tissue was collected weekly for up to 4 weeks. Untreated *Dicer1*$^{flox/flox}$ mice were used as a control (baseline mice, week 0). This was done to investigate hepatic miRNA transfer during health. In this chapter, mRNA and protein expression were investigated in the liver and kidney by RT-qPCR and western blotting described in Chapter 2.

Male *Dicer1*$^{flox/flox}$ mice described in Chapter 4, were injected with either a Null-AAV8 or Cre-AAV8 ($6.25x10^{10}$ viral genomes/100µL dose). Again, untreated *Dicer1*$^{flox/flox}$ mice (baseline) were ran alongside the experiment as a control. Three weeks after the injection, DILI was induced via saline (control), 150mg/kg paracetamol or 300mg/kg paracetamol. Six hours later, tissue was harvested. In this chapter, results of mRNA and protein expression measurements are described. Additionally, immunohistochemistry and CYP450 enzyme activity were measured in the Null-AAV8 and Cre-AAV8 mice (as per methods).

5.3 Results

5.3.1 Expression of multiple miR-122 mRNA targets significantly increase in the liver of the healthy *Dicer1* $^{flox/flox}$ mice, following a single Cre-AAV8 injection

First, RT-qPCR was carried out to explore whether the time dependent loss of hepatic miRNA (observed in Chapter 3, Section 3.4.1), resulted in a change of mRNA expression in the liver. Due to the high abundance of miR-122 in healthy hepatocytes and its observed loss in the hepatocytes of the Cre-AAV8 treated mice (Figure 3.4), known miR-122 targets were measured in the liver: Aldoa, Ndrg3 and Tmed3 [174, 227, 273-275].

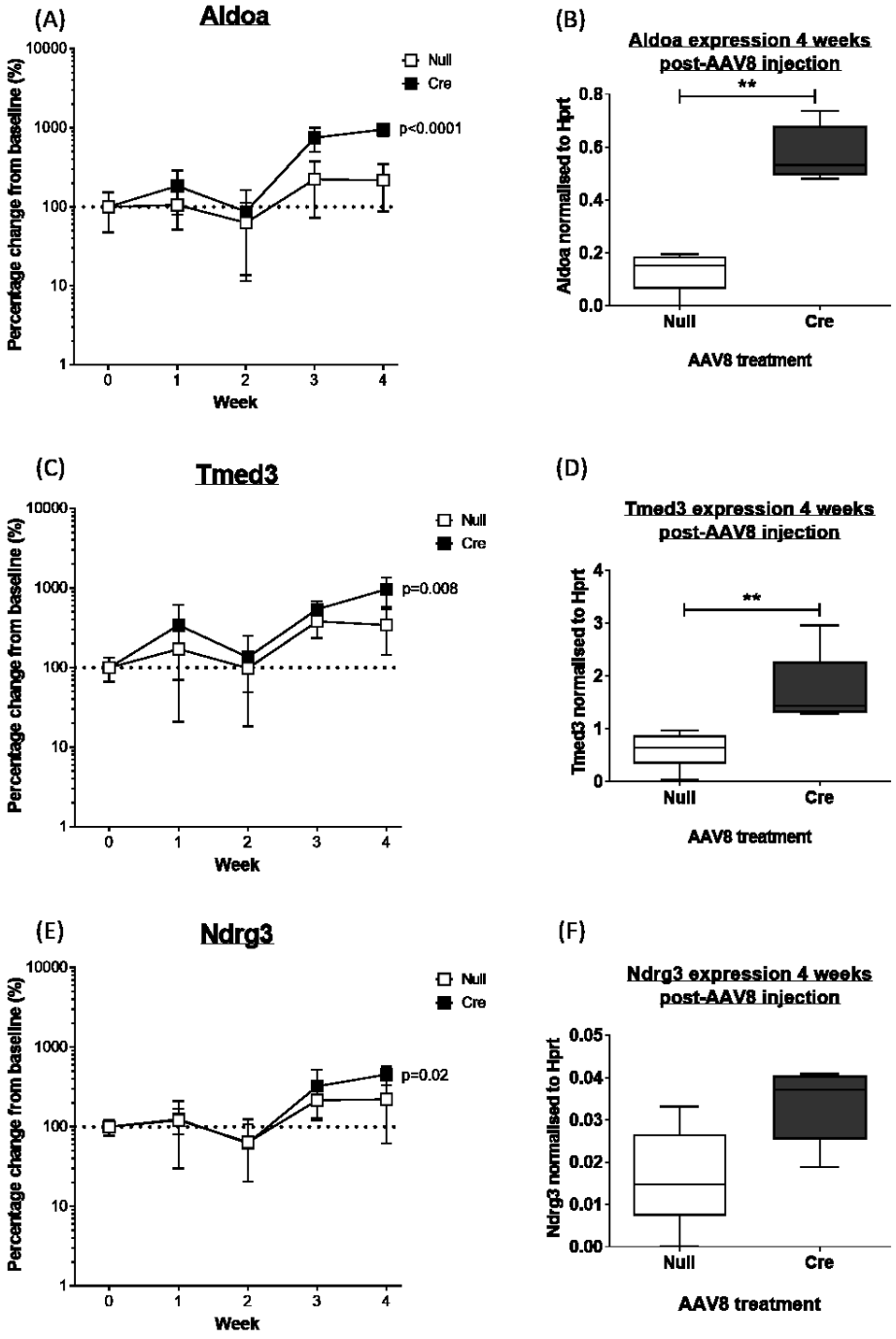

In

Figure **5.1**, it was observed that the mRNA expression of Aldoa, Ndrg3 and Tmed3 were significantly greater in the Cre-AAV8 treated mice, compared to the Null-AAV8 mice (Linear Regression, Aldoa: Cre slope=235 week^{-1}, Cre slope vs zero p<0.0001, Null vs Cre p=0<0.0001; Tmed3: Cre slope=200 week^{-1}, Cre slope vs zero p<0.0001, Null vs Cre p=0.008; Ndrg3: Cre slope=94 week^{-1}, Cre slope vs zero p=0.0001, Null vs

Cre p=0.02). Comparisons at week 4 only, highlighted there was a significant difference in Aldoa and Tmed3 expression between the Null-AAV8 and the Cre-AAV8 treated mice (Mann Whitney U test, Null vs Cre: Aldoa, p=0.008; Tmed3, p=0.008). Whereas, at week 4, there was no significant difference in Ndrg3 expression between the Null-AAV8 and Cre-AAV8 treated mice (Mann Whitney U test Null vs Cre, p=0.056).

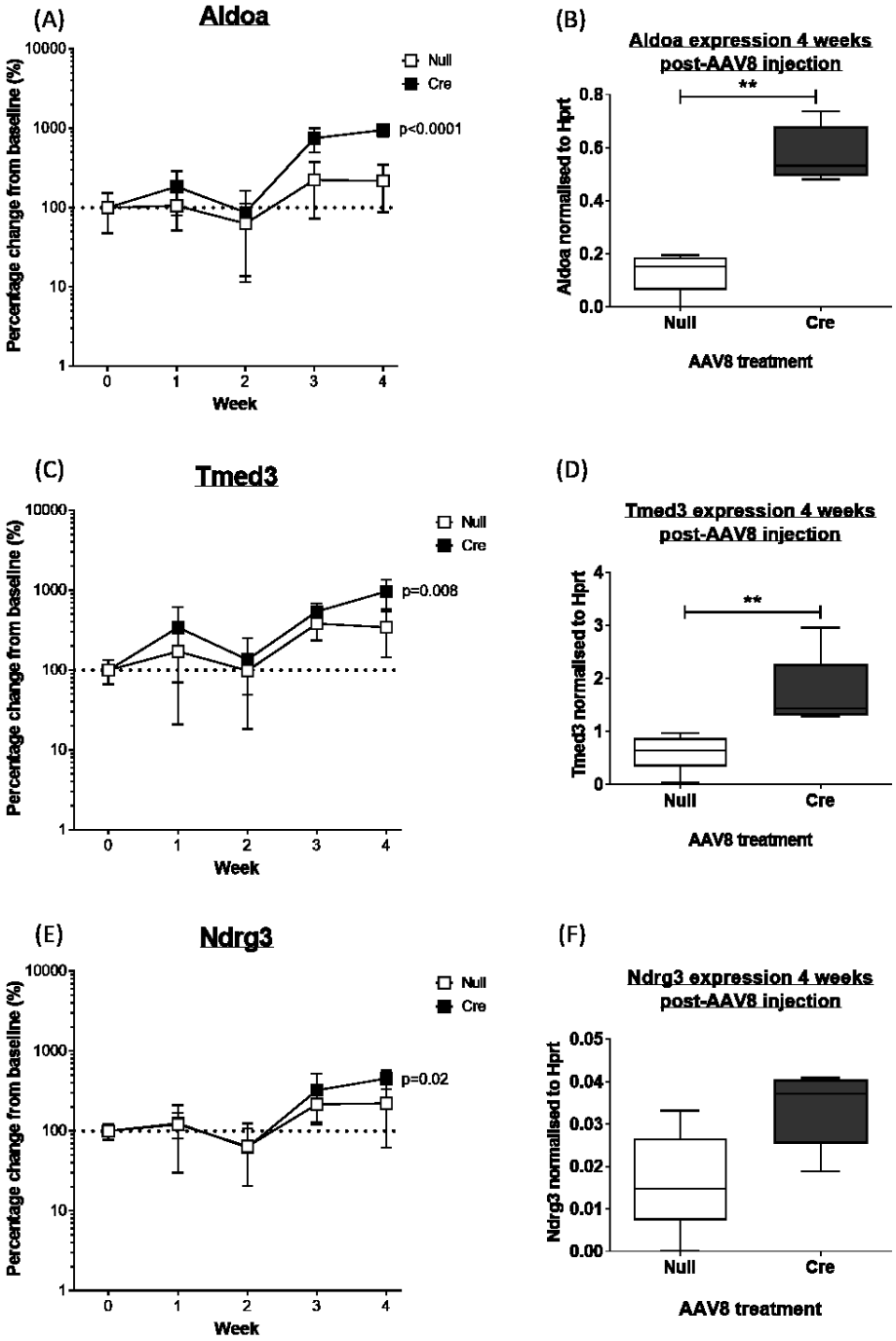

Figure 5.1 Expression of miR-122 mRNA targets in the liver of the *Dicer1*$^{flox/flox}$ mice following the loss of total hepatic miRNA

Known mRNA targets of miR-122 were measured in the liver by RT-qPCR. (A and B) Aldoa, (C and D) Tmed3 and (E and F) Ndrg3 in the liver of the Null-AAV8 (white) and Cre-AAV8 (black) treated mice (male and female). (A, C and E) data were first

*normalised to Hprt, and then converted as a percentage to the baseline mice (untreated, week 0, dotted line). (B, D and F) data from week 4 post-Null-AAV8 (white) and Cre-AAV8 (dark grey) injection were normalised by Hrpt. Data represented as mean ±SD n=5. (A, C and E) P values were calculated by linear regression, comparing the slopes of the Null-AAV8 and Cre-AAV8 treated Dicer1 $^{flox/flox}$ mice. (B, D and F) P values were calculated by Mann Whitney U test. *p≤0.05, **p≤0.01.*

Furthermore, additional targets of miR-122, cyp1a2 and cyp2e1 were measured in the liver of the healthy AAV8 treated *Dicer1* $^{flox/flox}$ mice (Figure 5.2). The mRNA expression of cyp1a2 was significantly higher in the Cre-AAV8 treated mice, in comparison to the Null-AAV8 mice (Linear Regression: Cre slope=230 week^{-1}, Cre slope vs zero p<0.0001, Null vs Cre p=0.0001). However, cyp2e1 mRNA expression did not differ between the Cre-AAV8 and Null-AAV8 mice (Linear Regression: Cre slope=73 week^{-1}, Cre slope vs zero p=0.008, Null vs Cre p=0.3).Comparisons at week 4 only, highlighted there was a significant difference in cyp1a2 expression between the Null-AAV8 and the Cre-AAV8 treated mice (Mann Whitney U test, Null vs Cre: p=0.02). Whereas, at week 4, cyp2e1 expression was not significantly different between the Null-AAV8 and Cre-AAV8 treated mice (Mann Whitney U test Null vs Cre, p>0.05).

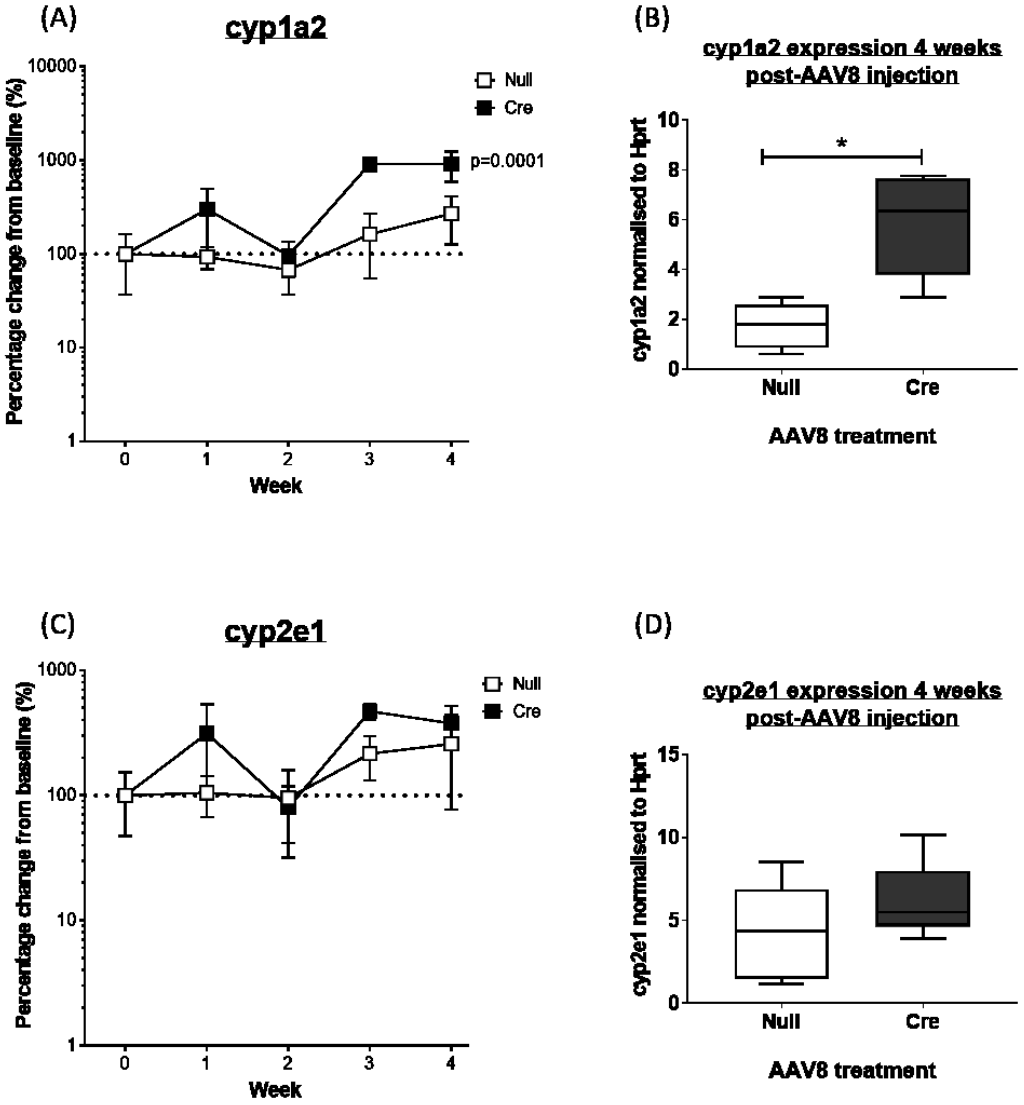

Figure 5.2 mRNA of cyp1a2 and cyp2e1 in the liver of the *Dicer1*$^{flox/flox}$ mice following a single treatment of AAV8

Known mRNA targets of miR-122 were measured in the liver by RT-qPCR. (A and B) cyp1a2 and (C and D) cyp2e1 in the liver of the Null-AAV8 (white) and Cre-AAV8 (black) treated mice (male and female). (A and C) data were first normalised to Hprt, and then converted as a percentage to the baseline mice (untreated, week 0, dotted line). (B and D) data from week 4 post-Null-AAV8 (white) and Cre-AAV8 (dark grey) injection were normalised by Hrpt. Data represented as mean ±SD n=5. (A and C) P values were calculated by linear regression, comparing the slopes of the Null-AAV8

*and Cre-AAV8 treated Dicer1 $^{flox/flox}$ mice. (B and D) P values were calculated by Mann Whitney U test. *p≤0.05.*

In addition to measuring mRNA expression, protein expression of cyp2e1 was measured in the liver of the baseline, Null-AAV8 and Cre-AAV8 treated mice, from week 1-4 post injection (Figure 5.3). Mirroring the mRNA measurements, cyp2e1 protein (~55kDa) did not differ across the 3 treatment groups regardless of time (Figure 5.3A and B). For both western blots, the loading control, β-actin (~42kDa), remains stable across each well (Figure 3.8A and B). The relative density analysis of each band (Figure 5.3C and D), supported these findings further.

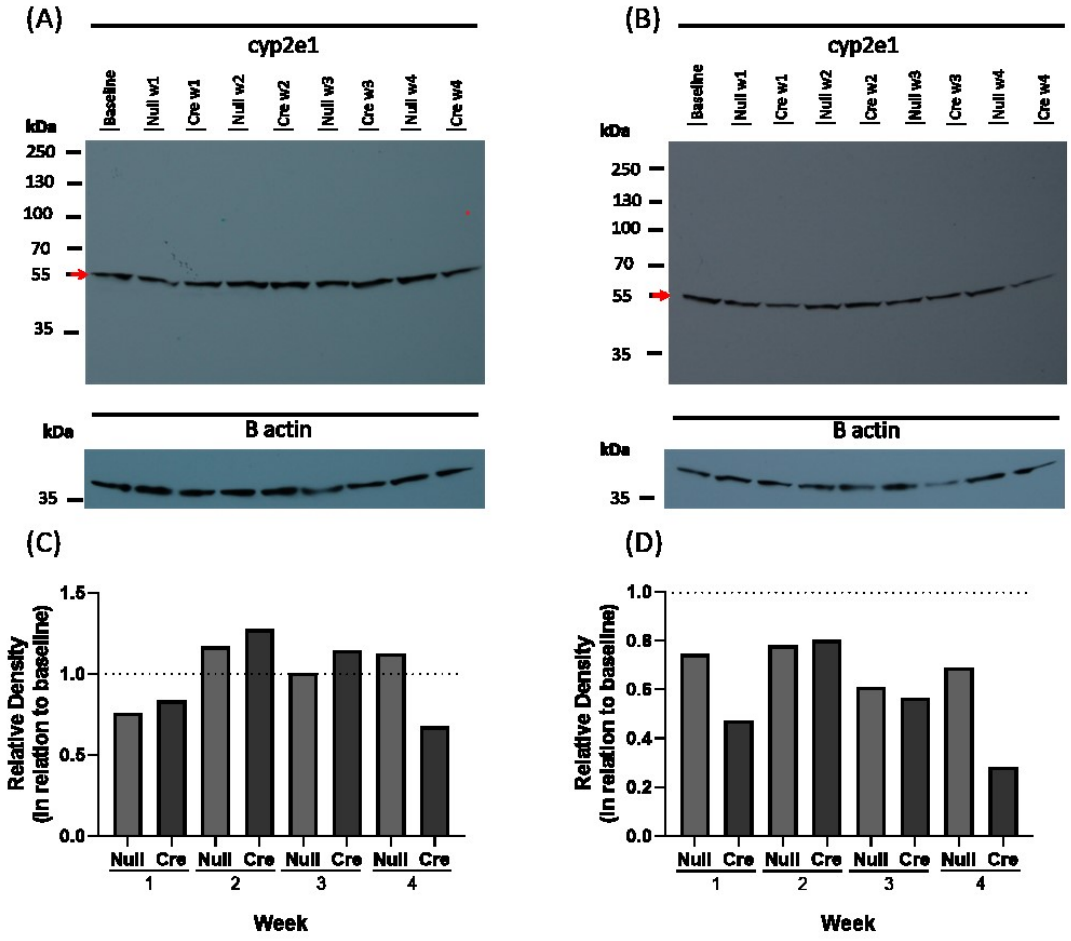

Figure 5.3 Protein expression of cyp2e1 in the liver of the *Dicer1* $^{flox/flox}$ mice following Cre-AAV8 treatment

(A and B) Protein expression of cyp2e1 (~55kDa, indicated by the red arrows) in the liver of the baseline (untreated) and week 1 to 4 of the Null-AAV8 and Cre-AAV8

treated mice (male and female), was determined by western blotting. For each western blot, β-actin (~42kDa) was used as a loading control. (C, D)To quantify cyp2e1 protein expression, relative density of the ~55kDa band was calculated in the Null-AAV8 (light grey) and Cre-AAV8 (dark grey) treated mice (week 1 to 4, post injection), normalised to the baseline control cyp2e1 band (dotted line). Each western blot represents an n=1 from each treatment group

5.3.2 Expression of cyp2e1 decreases in the liver following paracetamol treatment

After measuring mRNA targets of miR-122 in the liver in the absence of paracetamol DILI, investigations were then carried out in the paracetamol treated *Dicer1* $^{flox/flox}$ mice. In Chapter 4, it was discovered that the significant reduction in hepatic miRNA following Cre-AAV8 treatment was maintained following paracetamol dosing (Figure 4.3). First, mRNA expression of the two CYP450 enzymes, cyp1a2 and cyp2e1, were assessed in the liver via RT-qPCR, 3 weeks following baseline, Null-AAV8 and Cre-AAV8 treatment and then 6 hours after saline, 150mg/kg and 300mg/kg paracetamol.

At the saline dose, cyp1a2 mRNA expression was 2-fold and 1.7-fold greater in the Null-AAV8 and Cre-AAV8 mice respectively, in contrast to the baseline mice mean expression (ANOVA saline baseline vs Null, p=0.02). With increasing doses of paracetamol, expression of cyp1a2 mRNA in the liver was significantly reduced in the baseline, Null-AAV8 and Cre-AAV8 groups (ANOVA: Null: saline vs 150mg/kg, p=0.0001, saline vs 300mg/kg, p<0.0001; Cre: saline vs 150mg/kg, p=0.007, saline vs 300mg/kg, p=0.04). At 300mg/kg paracetamol, the Cre-AAV8 the expression of cyp1a2 was not significantly different, compared to the baseline and Null-AAV8 mice at the equivalent dose (ANOVA: p>0.05, baseline vs Cre 1.75-fold difference; Null vs Cre 3.8-fold difference).

Similarly, at the saline dose, cyp2e1 mRNA expression in the liver was non-significantly greater following Null-AAV8 and Cre-AAV8 treatment, compared to the baseline mice (ANOVA p>0.05; baseline vs Null fold difference of 2; baseline vs Cre fold difference 1.3). Nevertheless, the expression of cyp2e1 in the Null-AAV8 mice decreases significantly with increasing doses of paracetamol (ANOVA: Null: saline vs

150mg/kg, p=0.009, saline vs 300mg/kg, p=0.0005). This is not observed in the baseline and Cre-AAV8 treated mice, were expression remains unchanged (ANOVA: p>0.05).

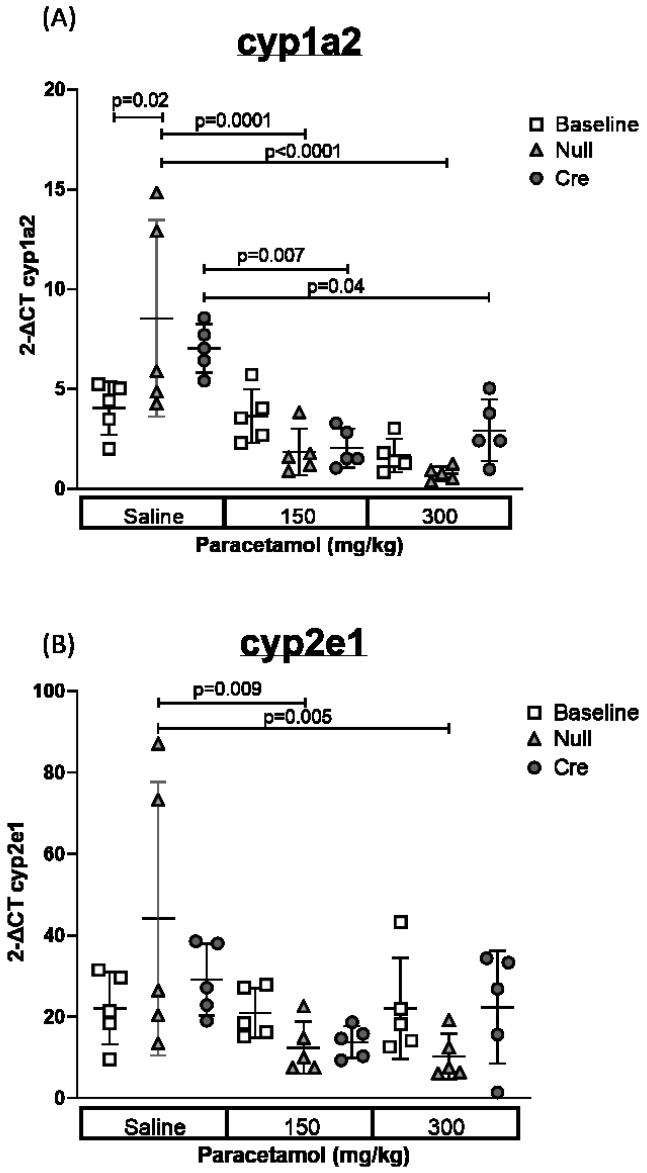

Figure 5.4 cyp1a2 and cyp2e1 expression in the liver of *Dicer1 flox/flox* mice following paracetamol dosing

mRNA expression of the CYP450 enzymes (A) cyp1a2 and (B) cyp2e1 were measured in the liver following saline, 150mg/kg paracetamol and 300mg/kg paracetamol in the baseline (untreated, white squares), Null-AAV8 (light grey triangles) and Cre-AAV8 treated male Dicer1 flox/flox mice (dark grey circles). mRNA measurements were taken 3 weeks post AAV8 treatment and 6 hours following paracetamol dosing. Each point

was normalised to β-actin, error bars represent mean ±SD, n=5. A multiple comparison two-way ANOVA was used to determine if expression was significantly different across all 9 treatment groups.

Subsequently, cyp2e1 expression was further evaluated in the paracetamol treated livers via western blotting. In Figure 5.5, cyp2e1 protein (~55kDa) was measured in the baseline, Null-AAV8 and Cre-AAV8 mice 6 hours following saline, 150mg/kg and 300mg/kg paracetamol. As observed with the PCR data, cyp2e1 protein expression was greater in the saline treated mice, in comparison to the 150mg/kg and 300mg/kg paracetamol treated mice (Figure 5.5A and C).

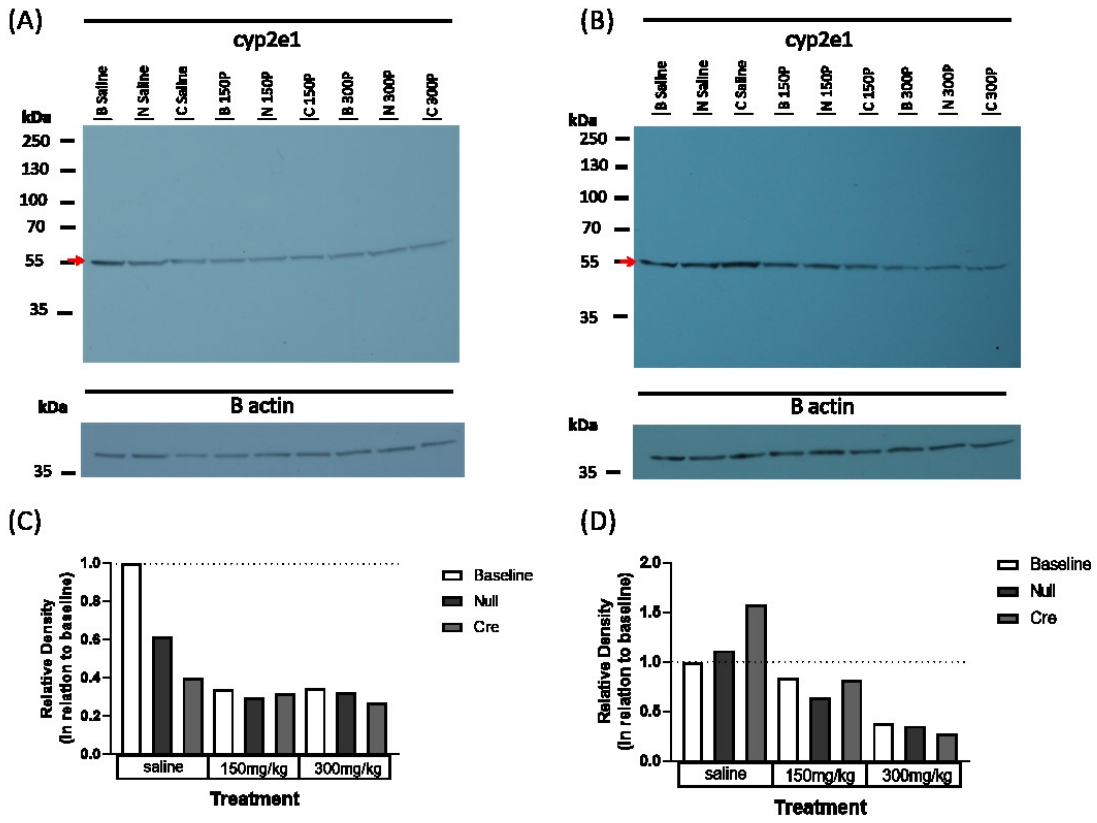

Figure 5.5 cyp2e1 protein expression in the liver following a single dose of paracetamol

(A and B) Protein expression of cyp2e1 (~55kDa, indicated by the red arrows) in the liver of the baseline (B, untreated), Null-AAV8 (N) and Cre-AAV8 (C) male Dicer1$^{flox/flox}$ mice treated with either saline, 150mg/kg paracetamol or 300mg/kg paracetamol, was determined by western blotting. For each western blot, β-actin (~42kDa) was used as a loading control. (C and D) To quantify cyp2e1 protein expression, relative density of the ~55kDa band was calculated in the baseline (white), Null-AAV8 (light grey) and Cre-AAV8 (dark grey) treated mice (following saline, 150mg/kg and 300mg/kg paracetamol), normalised to the baseline saline cyp2e1 band (dotted line). Each western blot represents an n=1 from each treatment group.

Immunohistochemistry of cyp2e1 was carried out to determine if the loss of miRNA in the hepatocytes lead to changes in cyp2e1 expression and localisation. Figure 5.6

visualises the expression of cyp2e1 in the liver of the Null-AAV8 and Cre-AAV8 mice treated with either saline, 150mg/kg and 300mg/kg paracetamol. In addition, positive and negative control liver sections from healthy C57BL/6 mice were ran alongside the treatment groups (S and T). From the images and supporting percentage of cyp2e1 staining calculated (Figure 5.6U), there was no significant difference between the Cre-AAV8 and Null-AAV8 treated mice.

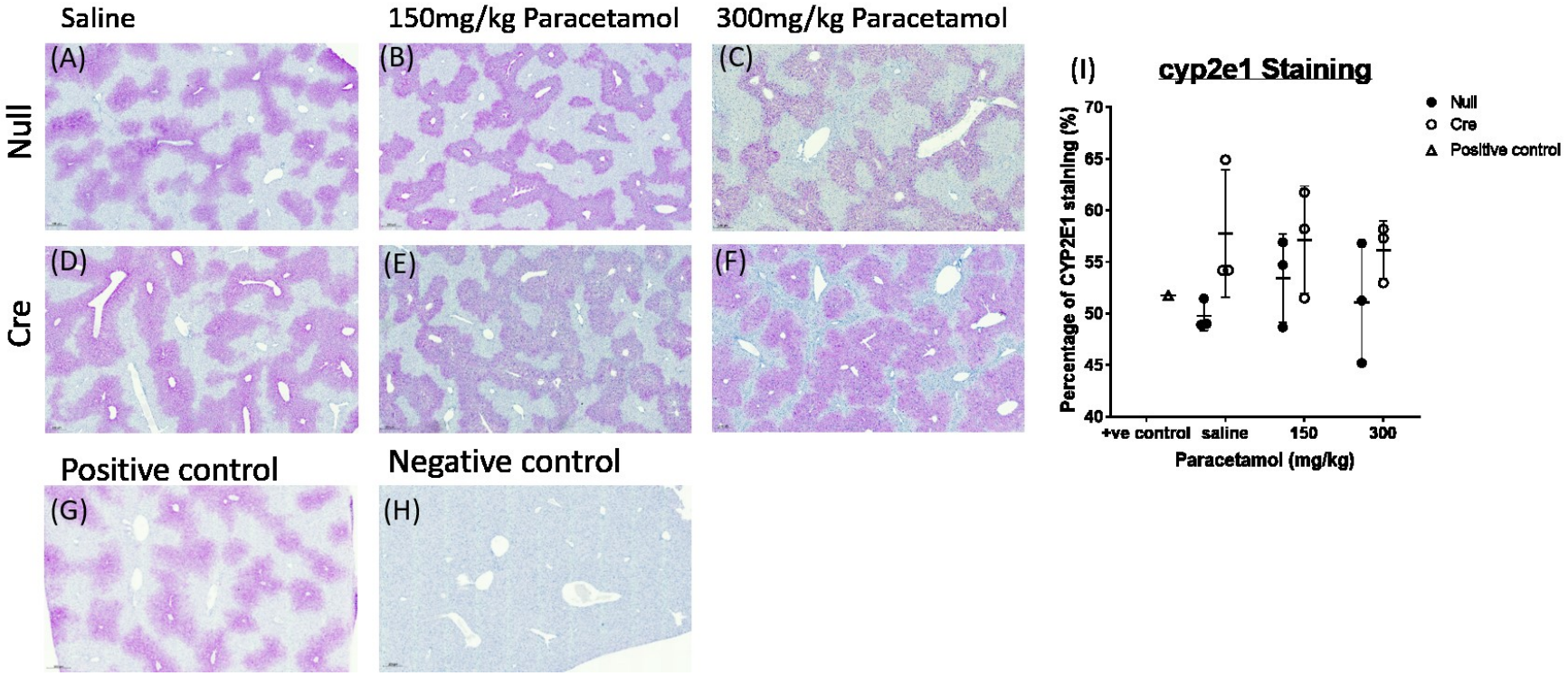

Figure 5.6 Immunohistochemistry of cyp2e1 in the liver of the paracetamol treated Null-AAV8 and Cre-AAV8 *Dicer1* $^{flox/flox}$ mice

Immunohistochemistry of cyp2e1 was carried out on the male Dicer1 $^{flox/flox}$ *liver sections. Images represent cyp2e1 expression (purple staining) 3 weeks after Null-AAV8 or Cre-AAV8 treatment, followed by 6 hours a single paracetamol dosing of either saline (A and D), 150mg/kg paracetamol (B and E) or 300mg/kg paracetamol (C and F). Liver sections from C57BL/6 mice were used as a positive (G) and negative control (no antibody, H) ran alongside the staining and used as comparison for the analysis. (I) Analysis was carried out following*

methods described in Section 2.9.4. Scale bar represents 200µm, 20x magnification. *Each image represents an n=3 per AAV8 and paracetamol dosing.*

To explore whether the loss of hepatic miRNA alters the CYP450 enzymatic activity in the liver, the relative levels of phenacetin (cyp1a2), bupropion, amodiaquine, diclofenac , bufuralol, midazolam and chlorzoxazone (cyp2e1) hydroxylase activities were determined in the saline treated Null-AAV8 and Cre-AAV8 *Dicer1* $^{flox/flox}$ mice (Figure 5.7). It was found that the loss of hepatic miRNA had nosignificant impact on midazolam, diclofenac and bufuralol hydroxylase activity in the liver, in comparison to the Null-AAV8 controls (Mann Whitney U; Null vs Cre $p>0.05$, Figure 5.7). However, it was found that there was a significant increase in phenacetin (cyp1a2), bupropion. amodiaquine, and chlorzoxazone (cyp2e1) hydoxylase activity in the Cre-AAV8 mice compared to the Null-AAV8 mice (Mann Whitney U, Null vs Cre: phenacetin hydroxylase (cyp1a2) p=0.01; bupropion hydroxylase p=0.02; amodiaquine hydroxylase p=0.01; chlorzoxaxzone hydroxylase (cyp2e1) p=0.01).

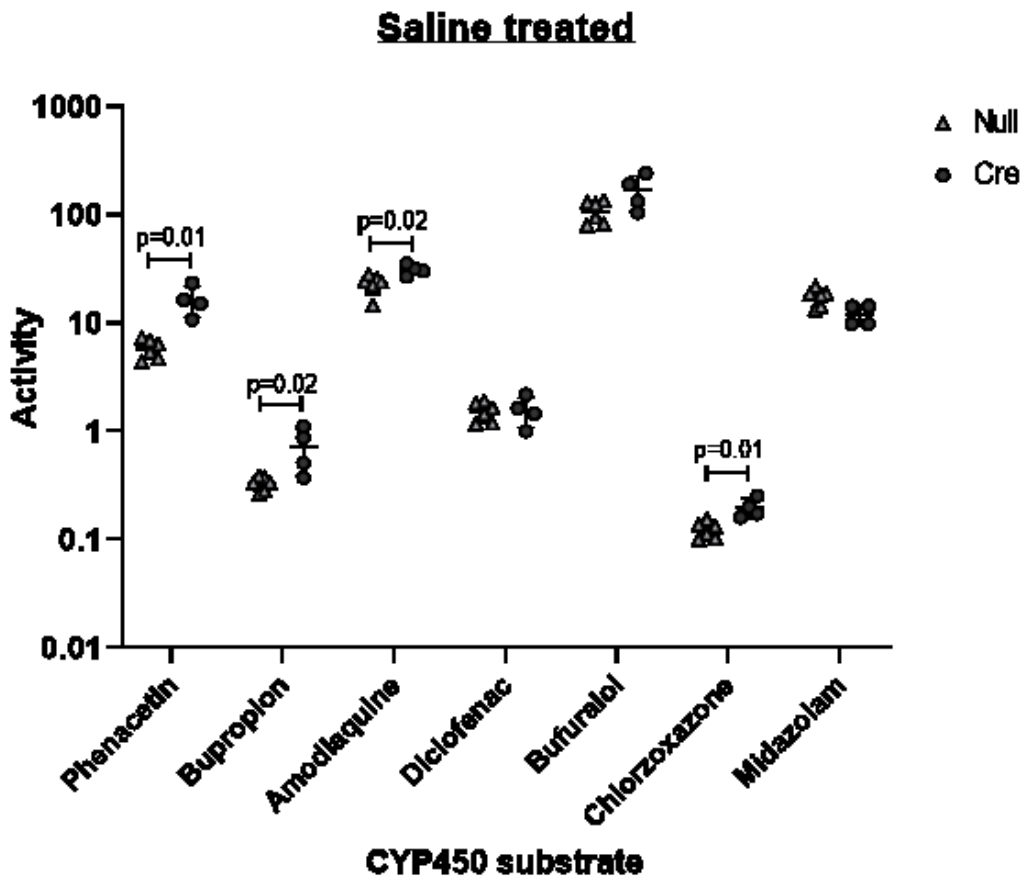

Figure 5.7 CYP450 activity was measured in the liver of the saline treated AAV8 mice

CYP450 activity was calculated in the liver following the methods described in Section 2.12. Measurements were taken in the Null-AAV8 and Cre-AAV8 treated male Dicer1 $^{flox/flox}$ mice 3 weeks following AAV8 injection and 6 hours following a single injection of saline. The CYP450 enzymatic activity was determined via measurements of phenacetin (cyp1a2), bupropion, amodiaquine, diclofenac , bufuralol, midazolam and chlorzoxazone (cyp2e1) hydroxylase activity. . Data are represented as mean ±SD, Null-AAV8 n=3, Cre-AAV8 n=2 (in duplicate). A Mann Whitney U test was used to determine whether the activity of each CYP450 activity was significantly different between the Null-AAV8 and Cre-AAV8 mice.

5.3.3 cyp1a2 and cyp2e1 expression remains unchanged in the kidney cortex and medulla of *Dicer1* $^{flox/flox}$ mice, following the loss of hepatic miRNA

A significant loss of miR-122 is observed in the kidney cortex and medulla of the non-DILI *Dicer1* $^{flox/flox}$ mice treated with the Cre-AAV8 (Chapter 3, Section 3.4.3). Hence, mRNA expression of the known miR-122 targets, cyp2e1 and cyp1a2 were measured in the kidney cortex and medulla (Figure 5.8 and Figure 5.9). First, it was noted that compared to the liver (average Ct values of cyp1a2 and cyp2e1=20), the mRNA expression of cyp1a2 and cyp2e1 were lower in both sections of the kidney (average Ct values: cyp1a2: cortex=34, medulla=32; cyp2e1: cortex=21, medulla=23) (Table 6.12 and Table 6.13).

In the kidney cortex, the mRNA expression of cyp1a2 and cyp2e1 were unchanged following the loss of hepatic miRNA, including miR-122, in contrast to the Null-AAV8 treated mice (Linear Regression cyp1a2: Cre slope=-8.4 week^{-1}, Cre slope vs zero p=0.45, Null vs Cre p=0.7; cyp2e1: Cre slope=-8.2 week^{-1}, Cre slope vs zero p=0.21, Null vs Cre p=0.15).

Similarly, the kidney medulla displayed no significant change in cyp1a2 and cyp2e1 expression in the Cre-AAV8 treated mice, compared to the Null-AAV8 mice (Linear Regression cyp1a2: Cre slope=4 week^{-1}, Cre slope vs zero p=0.67, Null vs Cre p=0.8; cyp2e1: Cre slope=-8.2 week^{-1}, Cre slope vs zero p=0.14, Null vs Cre p=0.3).

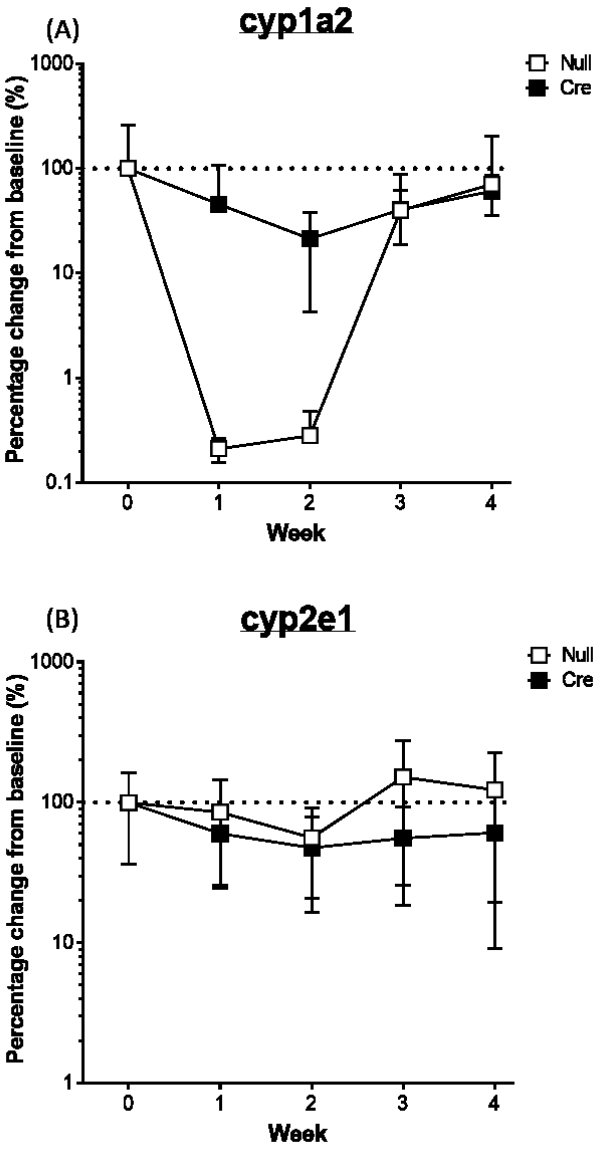

Figure 5.8 mRNA expression of cyp1a2 and cyp2e1 in the kidney cortex of the *Dicer1 $^{flox/flox}$* mice

Known mRNA targets of miR-122 were measured in the kidney cortex by RT-qPCR. (A) CYP1A2 and (B) CYP2E1 in the kidney cortex of male and female Null-AAV8 (white) and Cre-AAV8 (black) treated mice, first normalised to β-actin, and then converted as a percentage to the baseline mice (untreated, week 0, dotted line). Data represented as mean ±SD n=5. P values were calculated by linear regression, comparing the slopes of the Null-AAV8 and Cre-AAV8 treated Dicer1 $^{flox/flox}$ mice.

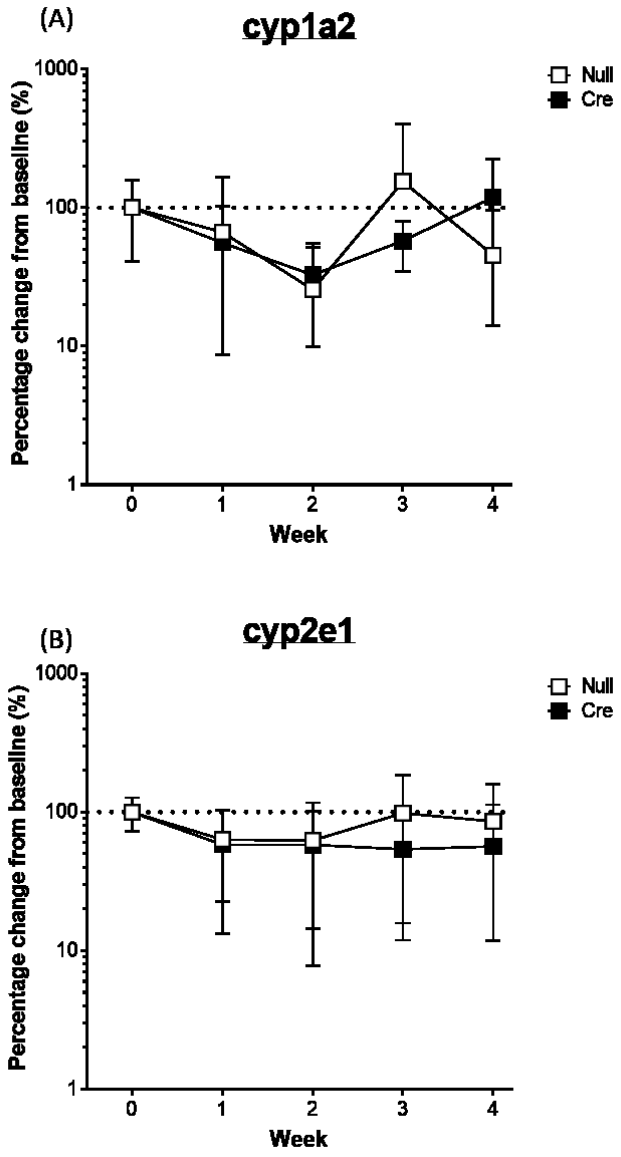

Figure 5.9 mRNA expression of cyp1a2 and cyp2e1 in the kidney medulla of the *Dicer1*$^{flox/flox}$ mice

Known mRNA targets of miR-122 were measured in the kidney medulla by RT-qPCR. (A) cyp1a2 and (B) cyp2e1 in the kidney medulla of male and female Null-AAV8 (white) and Cre-AAV8 (black) treated mice, first normalised to β-actin, and then converted as a percentage to the baseline mice (untreated, week 0, dotted line). Data represented as mean ±SD n=5. P values were calculated by linear regression, comparing the slopes of the Null-AAV8 and Cre-AAV8 treated Dicer1 $^{flox/flox}$ *mice.*

5.3.4 Expression and activity of cyp2e1 were significantly upregulated in the *Dicer1* $^{flox/flox}$ kidney following Cre-AAV8 and 300mg/kg paracetamol treatments.

As in the liver, the mRNA, location and response of the CYP450 enzymes were measured in the kidney cortex and medulla following paracetamol dosing. Replicating the methods in the liver, cyp1a2 and cyp2e1 were measured in the 2 sections of the kidney (cortex and medulla, Figure 5.10 and Figure 5.11). The kidney cortex and medulla, displayed minimal levels of cyp1a2 mRNA expression (average Ct values: cortex and medulla=34). However, for both kidney sections, the saline treated mice (baseline, Null-AAV8 and Cre-AAV8) cyp1a2 expression was not significantly different compared to the 150mg/kg and 300mg/kg treated mice (Figure 5.10 and Figure 5.11).

MRNA of cyp2e1 was greater in the kidney cortex and medulla, in contrast to cyp1a2 mRNA expression (average Ct values: cortex=20 and medulla=21). Furthermore, the kidney cortex exhibited a higher concentration of cyp2e1 mRNA compared to the medulla. In the kidney cortex, cyp2e1 was significantly higher in the saline treated baseline mice in contrast to the Null-AAV8 and Cre-AAV8 mice at the equivalent dose (Figure 5.10, ANOVA: saline: baseline vs Null $p<0.0001$; baseline vs Cre $p=0.0002$).

However, with increasing doses of paracetamol, cyp2e1 mRNA decreases significantly in the baseline mice (ANOVA: saline vs 150mg/kg $p<0.0001$; saline vs 300mg/kg $p=0.01$). MRNA expression of cyp2e1 is unaltered in the Null-AAV8 mice regardless of paracetamol. Whereas, cyp2e1 mRNA in the Cre-AAV8 mice increased significantly at the 300mg/kg paracetamol dose (ANOVA: saline vs 300mg/kg $p=0.0006$; 150mg/kg vs 300mg/kg $p=0.0005$). Moreover, the cyp2e1 expression in the 300mg/kg paracetamol treated Cre-AAV8 mice was significantly higher than the baseline and Null-AAV8 mice (ANOVA: baseline vs Cre $p=0.03$; Null vs Cre $p=0.004$).

In the medulla, cyp2e1 mRNA expression is not significantly different across the baseline, Null-AAV8 and Cre-AAV8 mice. At the saline and 150mg/kg paracetamol dose, cyp2e1 expression was not significantly different (Figure 5.11, ANOVA: $p>0.05$). However at the 300mg/kg dose, cyp2e1 expression increases in all three groups, with

a significant increase observed in the Cre-AAV8 mice (ANOVA: saline vs 300mg/kg p=0.03, 150mg/kg p=0.003).

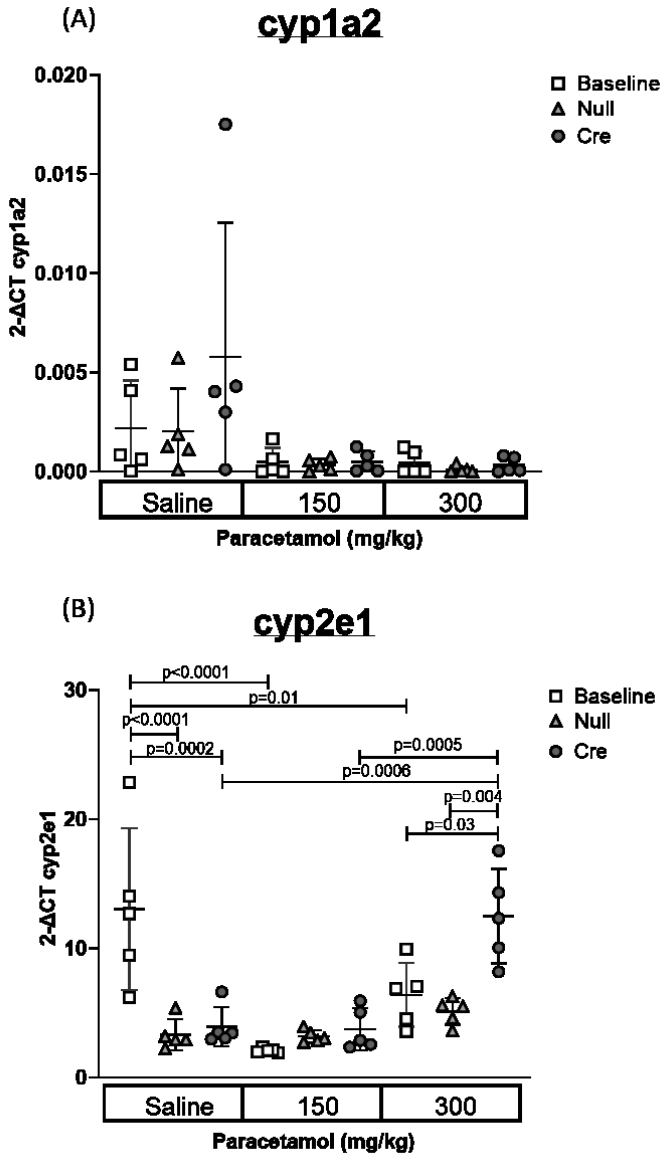

Figure 5.10 cyp1a2 and cyp2e1 mRNA in the kidney cortex of the AAV8 and paracetamol treated mice

mRNA expression of the CYP450 enzymes (A) cyp1a2 and (B) cyp2e1 were measured in the kidney cortex following saline, 150mg/kg paracetamol and 300mg/kg paracetamol in the baseline (untreated, white squares), Null-AAV8 (light grey

triangles) and Cre-AAV8 treated male Dicer1 $^{flox/flox}$ mice (dark grey circles). MRNA measurements were taken 3 weeks post AAV8 treatment and 6 hours following paracetamol dosing. Each point was normalised to β-actin, error bars represent mean ±SD, n=5. A multiple comparison two-way ANOVA was used to determine if expression was significantly different across all 9 treatment groups.

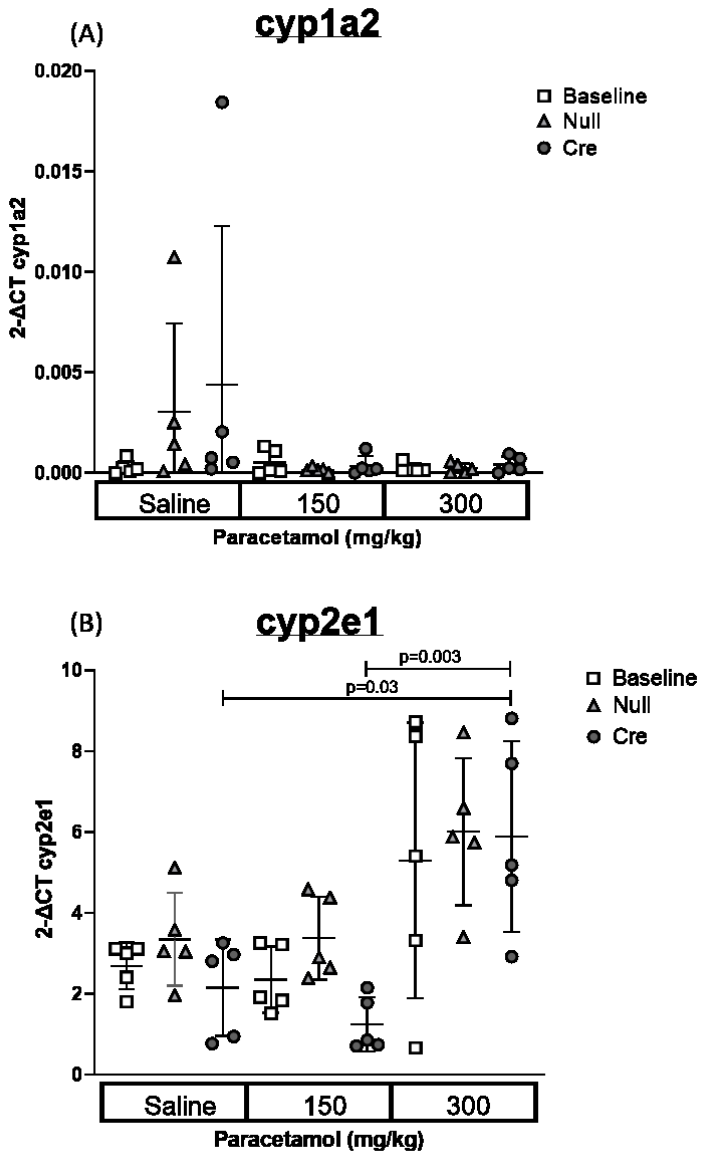

Figure 5.11 cyp1a2 and cyp2e1 expression in the kidney medulla of the baseline, Null-AAV8 and Cre-AAV8 mice

MRNA expression of the CYP450 enzymes (A) cyp1a2 and (B) cyp2e1 were measured in the kidney medulla following saline, 150mg/kg paracetamol and 300mg/kg paracetamol in the baseline (untreated, white squares), Null-AAV8 (light grey triangles) and Cre-AAV8 treated male Dicer1 $^{flox/flox}$ mice (dark grey circles). MRNA measurements were taken 3 weeks post AAV8 treatment and 6 hours following paracetamol dosing. Each point was normalised to β-actin, error bars represent mean ±SD, n=5. A multiple comparison two-way ANOVA was used to determine if expression was significantly different across all 9 treatment groups.

As cyp2e1 displayed minimal expression in the kidney medulla (**Figure 5.11**), further assessments into CYP2E1 mRNA expression was assessed in the kidney cortex only. To determine if there was a correlation between CYP2E1 mRNA and miR-122 expression in the kidney cortex, a Pearson's correlation coefficient test was carried out. As there was an observed significant increase of CYP2E1 in the 300mg/kg treated Cre-AAV8 mice, compared to controls (baseline and Null-AAV8 mice), correlation analysis was carried out at this dose only alongside the paracetamol treatments combined (saline, 150mg/kg and 300mg/kg paracetamol). In Figure 5.12A, there was no-correlation between CYP2E1 and miR-122 expression in the kidney cortex of the saline, 150mg/kg and 300mg/kg treated mice (Pearson's correlation: r=-0.05, p=0.8). However, a significant negative correlation was observed between miR-122 and CYP2E1 expression in the kidney cortex of the 300mg/kg paracetamol treated mice only (Pearson's correlation: r=-0.6, p=0.002) (Figure 5.12B).

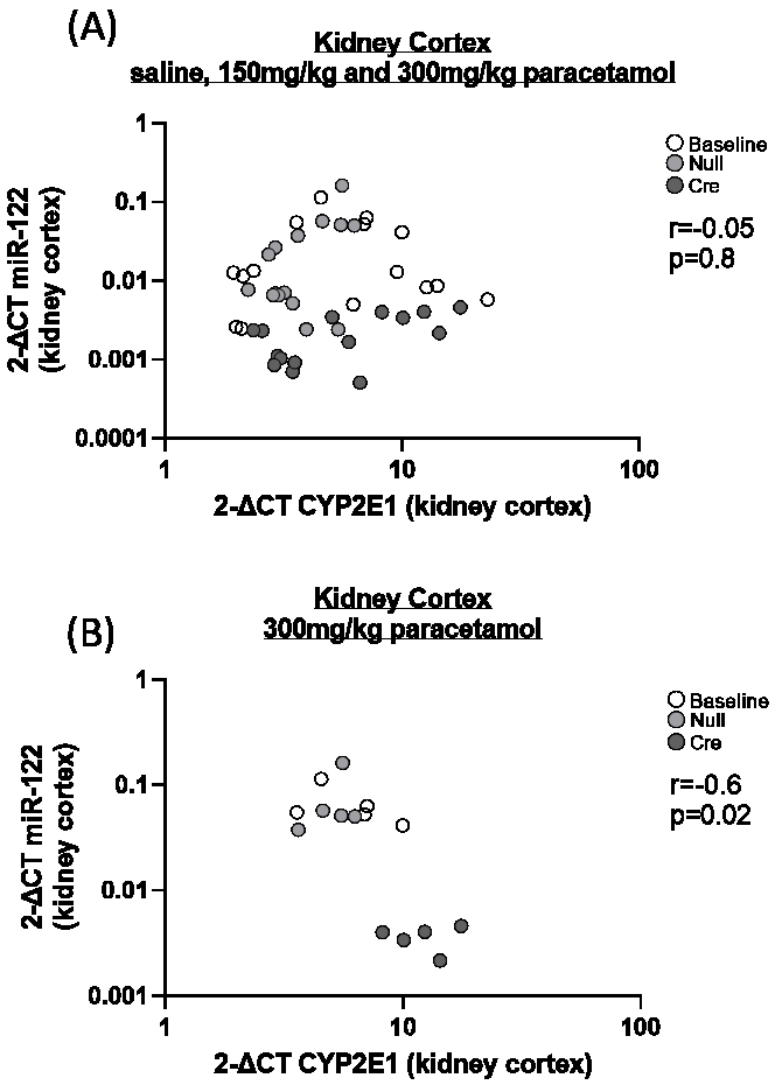

Figure 5.12 cyp2e1 mRNA expression correlated with miR-122 expression in the kidney cortex

Pearson's correlation was calculated to determine if there was a correlation between cyp2e1 mRNA and miR-122 expression in the kidney cortex of (A) all paracetamol groups (saline, 150mg/kg and 300mg/kg paracetamol) and (B) in the 300mg/kg paracetamol treated mice only. Both assessments were carried out in the untreated AAV8 (baseline, white), Null-AAV8 (light grey) and Cre-AAV8 (dark grey) Dicer1$^{flox/flox}$ mice. For each data set, correlation coefficient, r, was used to interpret the strength and nature of the correlation. Correlation was deemed significant if p≤ 0.05.

As mRNA expression displayed minimal levels of cyp1a2 expression, cyp1a2 protein was not measured in these tissues. Nevertheless, western blotting of cyp2e1 was carried out in the whole kidney of the baseline, Null-AAV8 and Cre-AAV8 *Dicer1* $^{flox/flox}$ mice, 1 to 4 weeks following the AAV8 injection. The protein bands were analysed to determine whether the stable mRNA expression of cyp2e1 was exhibited at the protein level.

In Figure 5.13A, it was observed that the protein expression of CYP2E1 remained unchanged in the *Dicer1* $^{flox/flox}$ mice presence of AAV8 treatment. Relative density analysis of each CYP2E1 band (Figure 5.13B) supported these findings further.In Figure 5.13 the loading control, β-actin (~42kDa), remains consistent across each well.

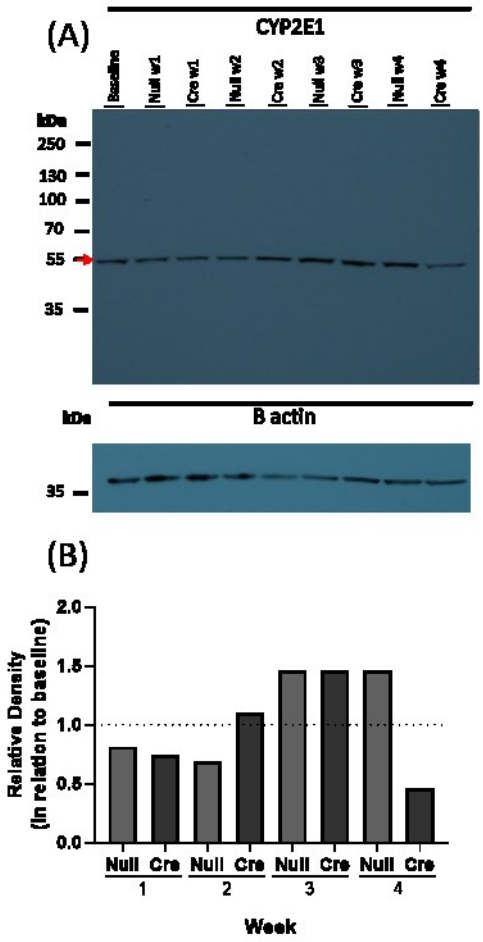

Figure 5.13 Kidney CYP2E1 protein expression in the AAV8 treated mice

(A)Protein expression of cyp2e1 (~55kDa, indicated by the red arrows) in the whole kidney of baseline (untreated) and week 1 to 4 of the Null-AAV8 and Cre-AAV8 treated mice, was determined by western blottingβ-actin (~42kDa) was used as a loading control. (B) To quantify cyp2e1 protein expression, relative density of the ~55kDa band was calculated in the Null (light grey) and Cre-AAV8 (dark grey) treated mice (week 1 to 4, post injection), normalised to the baseline control cyp2e1 band (dotted line). Each western blot represents an n=1 from each treatment group.

Subsequently, the localisation and distribution of cyp2e1 were assessed in the whole kidney by immunohistochemistry (Figure 5.14 and Figure 5.15). In the kidney cortex, shown in Figure 5.14, the expression of cyp2e1 (purple staining) was localised to the tubules. With increasing doses of paracetamol, there was no observed increase in cyp2e1 expression in the kidney cortex of the Null-AAV8 or Cre-AAV8 mice (Figure 5.14). Whereas, in the medulla (Figure 5.15), there was no visible staining of cyp2e1.

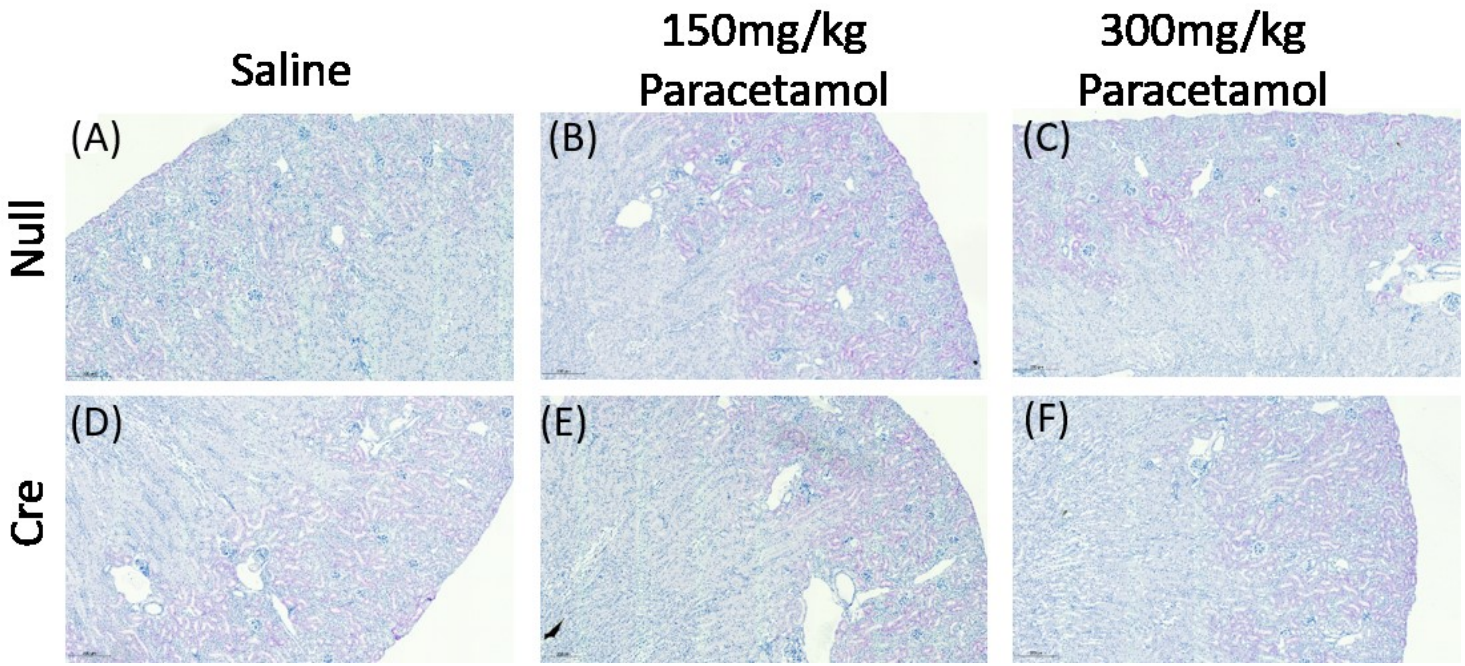

Figure 5.14 CYP2E1 staining in the kidney cortex

Immunohistochemistry of cyp2e1 was carried out on the Dicer1 $^{flox/flox}$ kidney sections. Images represent cyp2e1 expression in the kidney cortex (purple staining) 3 weeks after Null-AAV8 or Cre-AAV8 treatment, followed by 6 hours a single paracetamol dosing of either saline (A and D), 150mg/kg paracetamol (B and E) or 300mg/kg paracetamol (C and F). Liver sections from C57BL/6 mice were used as a positive (G) and negative control (no antibody, H) ran alongside the staining (Figure 5.6). Scale bar represents 200µm, 20x magnification. Each image represents an n=3per AAV8 and paracetamol dosing.

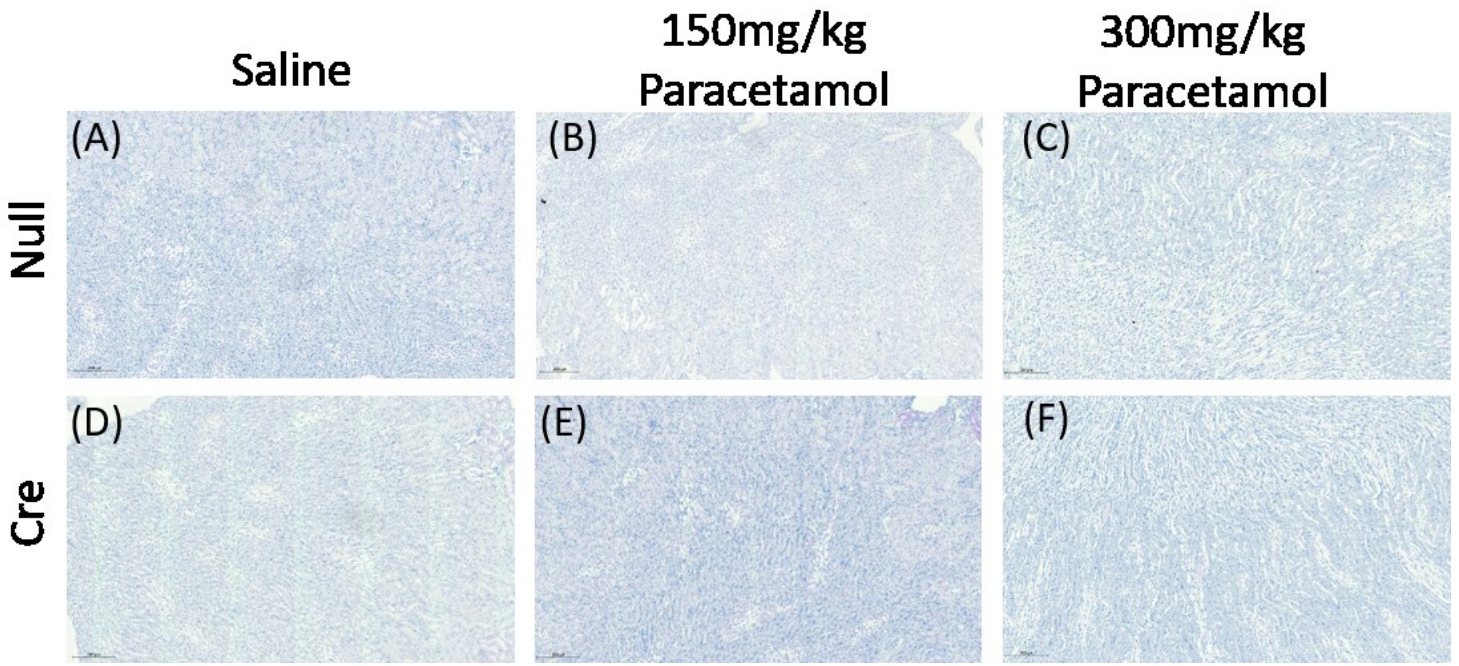

Figure 5.15 CYP2E1 staining in the kidney medulla

Immunohistochemistry of CYP2E1 was carried out on the Dicer1 $^{flox/flox}$ kidney sections. Images represent CYP2E1 expression in the kidney medulla (purple staining) 3 weeks after Null-AAV8 or Cre-AAV8 treatment, followed by 6 hours a single paracetamol dosing of either saline (A and D), 150mg/kg paracetamol (B and E) or 300mg/kg paracetamol (C and F). Liver sections from C57BL/6 mice were used as a positive (G) and negative control (no antibody, H) ran alongside the staining (Figure 5.6). Scale bar represents 200µm, 20x magnification. Each image represents an n=3 per AAV8 and paracetamol dosing.

CYP450 enzymatic activity was then measured in the whole kidney. This was carried out to investigate whether the loss of hepatic miR-122 transfer resulted loss of CYP450 downregulation in the kidney.

In the saline treated mice, it was observed that the activities of midazolam, bupropion, diclofenac and bufuralol hydroxylase were lower in the Cre-AAV8 mice, in comparison to the Null-AAV8 treated mice (Figure 5.16). At the saline and 300mg/kg dose, chlorzoxazone hydroxylase (cyp2e1) activity was greater in the Cre-AAV8 mice compared to the Null-AAV8 mice.

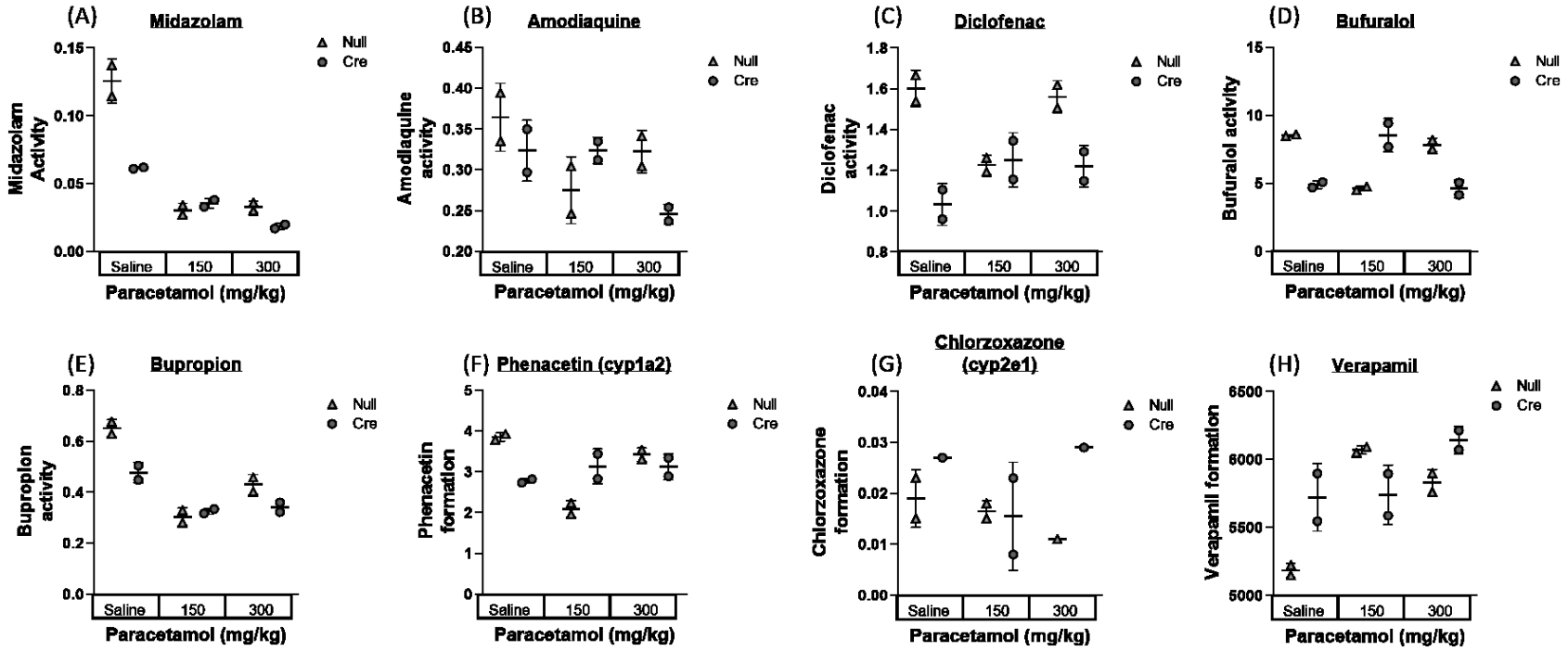

Figure 5.16 CYP450 enzyme activities in the Null-AAV8 and Cre-AAV8 mice treated with paracetamol

CYP450 enzymatic activity was calculated in the kidney following the methods described in Section 2.12.2. Measurements were taken in the Null-AAV8 and Cre-AAV8 treated Dicer1 $^{flox/flox}$ mice, 3 weeks following AAV8 injection and 6 hours following a single injection of saline. The CYP450 enzymatic activity was measured by was determined via measurements of (A) *midazolam, (B) amodiaquine, (C)*

diclofenac, (D) bufuralol, (E) bupropion, (F) phenacetin (cyp1a2) and (G) chlorzoxazone (cyp2e1) hydroxylase activity. (H) Verapamil was used as a control. Data are represented as mean ±SD, n=1 (5 individual samples pooled, in duplicate).

5.3.5 KIM-1 mRNA expression was unchanged following AVV8 and paracetamol treatment

KIM-1 is primarily found in the proximal tubule cells of the kidney cortex [276] . Due to this, assessments into its expression were explored in the kidney cortex only. First, KIM-1 mRNA expression was measured in the baseline, 150mg/kg and 300mg/kg paracetamol treated baseline, Null-AAV8 and Cre-AAV8 mice via RT-qPCR. In **Figure 5.17**, the expression of KIM-1 did not increase in the kidney cortex, with increasing doses of paracetamol. Interestingly, there was a significant increase in the 150mg/kg paracetamol Null-AAV8 treated mice, however, this was not maintained at the 300mg/kg paracetamol dose (ANOVA: 150mg/kg: baseline vs Null, p<0.0001; Null vs Cre, p<0.0001).

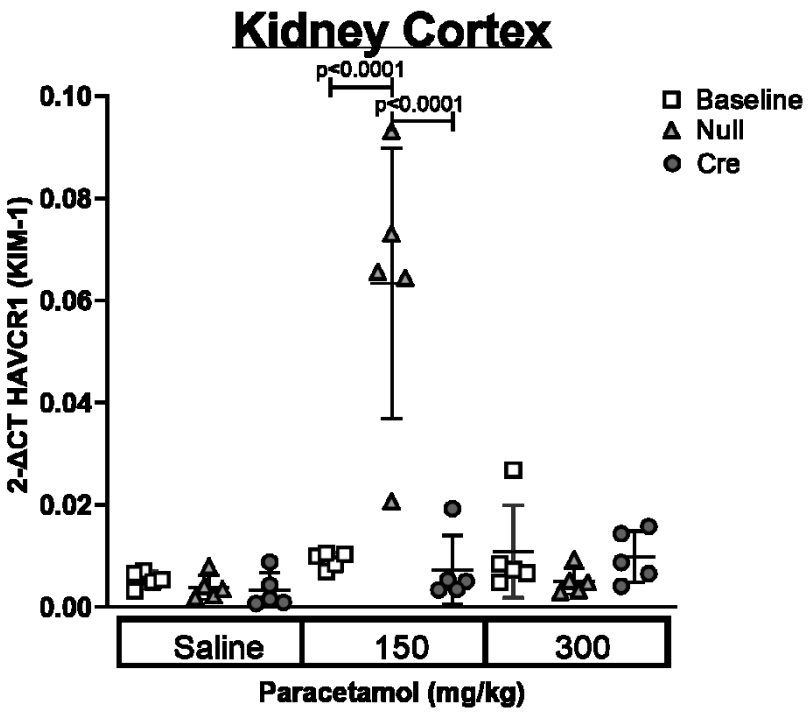

Figure 5.17 KIM-1 expression does not significantly increase with increasing paracetamol doses

KIM-1 mRNA expression was measured in the kidney cortex of the male *Dicer1* $^{flox/flox}$ mice. MRNA measurements were carried out via RT-qPCR 3 weeks following baseline

(white squares), Null (light grey triangles) and Cre-AAV8 (dark grey circles) treatment and 6 hours after saline, 150mg/kg and 300mg/kg of paracetamol. Each point was normalised by β-actin. Error bars represent mean ±SD, n=5. A multiple comparison two-way ANOVA was used to determine if the expression is significantly different between treatment groups.

5.3.6 Main findings

- Total loss of hepatic miRNA alters mRNA targets of miR-122 in the liver.
- Response of multiple CYP450 enzymes significantly increase in the liver of the saline treated Cre-AAV8 mice.
- In the absence of hepatic miRNA and 300mg/kg paracetamol, CYP2E1 significantly increases in expression and response in the kidney cortex.

5.4 Discussion

In the two previous chapters, the loss of hepatic miRNA resulted in the significant loss of miR-122 in the kidney in the absence of DILI (Chapter 3) and paracetamol-related DILI (Chapter 4, paracetamol toxicity). Hence, in this chapter, the functional role of hepatic miR-122 transferred from liver to kidney was investigated following in the AAV8 treated *Dicer1* $^{flox/flox}$ mice.

In Chapter 3, a time dependent loss of hepatic miRNA was observed following the conditional knockdown of Dicer in the *Dicer1* $^{flox/flox}$ mice. Thus, the studies in this chapter aimed to determine if there was a change in gene expression as a consequence of hepatic miRNA loss. Induction of Aldoa, Tmed3 and Ndgr3 following the loss of miR-122 has frequently been observed in the liver [174, 274, 277]. Additionally, previous reports found a slow increase of these genes following the conditional knockdown of Dicer and total miRNA in the liver [227]. Mirroring previous reports, the mRNA expression of these three genes were significantly higher in the Cre-AAV8 mice, compared to the Null-AAV8 treated mice. Highlighting that the knockdown of Dicer and loss of hepatic miRNA results in the derepression of miR-122 targets in the liver.

Recently, miRNA, including miR-122 have been shown to negatively regulate cyp1a2 and cyp2e1 expression in the liver [203, 246]. For both CYP450 enzymes, the suggested mechanism of miR-122 mediated downregulation is believed to be indirect. For cyp1a2, miR-122 targets and repress well described transcription factors of cyp1a2: Ahr (Aryl hydrocarbon receptor), Med1 (Mediator 1) and Ctcf [187, 203, 278, 279], which consequently contributes to the loss of cyp1a2 expression. Whereas, following liver specific miR-122 knockdown, the mechanism of miR-122 mediated cyp2e1 suppression is unknown, with an upregulation of the enzyme observed at the protein level only [203]. However, previous results suggest it is due to enhanced translation, rather than alterations in protein turnover or stability [203, 246]. Hence, the localisation, mRNA and protein expression of cyp1a2 and cyp2e1 was investigated in healthy and DILI livers.

cyp1a2 and cyp2e1 accounts for around 12% and 20% of the total hepatic CYP450 enzyme expression respectively [280]. Through immunohistochemistry, expression of cyp1a2 and CYP2E1 have been described to be localised around the central vein (centrilobular zone) of the liver [44, 281, 282]. cyp2e1 localisation via immunohistochemistry further confirmed these findings with the treated Cre-AAV8 mice having a non-significantly greater area of staining compared to the Null-AAV8 mice.

In the absence of paracetamol-induced liver injury, cyp1a2 mRNA was significantly greater in the Cre-AAV8 treated livers in comparison to the Null-AAV8 treated mice. As seen before, cyp2e1 mRNA expression was non-significantly different following the loss of miR-122 [203]. Unlike other reports, the protein expression of cyp2e1 did not significantly increase following the loss of miR-122 [203, 246]. Nevertheless, in the studies described in this chapter, total hepatic miRNA was significantly reduced in the liver, rather than miR-122 alone. Subsequently, previously described miRNA, such as miR-378 [244, 246, 271], involved in the regulation of cyp2e1 have been altered too. This could explain the lack of cyp2e1 protein upregulation in the liver following the loss of miR-122 in the Cre-AAV8 treated *Dicer1* $^{flox/flox}$ mice.

As seen in earlier studies, a loss of cyp1a2 and cyp2e1 mRNA and protein expression was observed with paracetamol treatment in all three AAV8 treatment groups [246]. Furthermore, enzymatic activity of cyp1a2 and cyp2e1 were significantly higher in the saline treated Cre-AAV8 mice, compared to the Null-AAV8 mice. However, in both AAV8 treatment groups, the activity of the two CYP450 enzymes decrease considerably following paracetamol dosing (data not shown). A reduction in cyp2e1 mediated paracetamol oxidation would reduce the accumulation of the reactive metabolite, NAPQI, during a paracetamol overdose [38, 248]. Thus, repressing cyp2e1 expression in the liver in response to paracetamol dosing reveals a potential protective mechanism to injury. However, it was noted that there were no significant differences in expression between the Null-AAV8 and Cre-AAV8 mice. Highlighting, the total loss of hepatic miRNA does not significantly influence the mechanism of cyp2e1 and cyp1a2 repression following paracetamol exposure.

cyp2e1Although cyp2e1 is highly enriched in the liver, its expression and activity has also been noted in the kidney [49-51, 283]. For example, the knockdown of cyp2e1 in the kidney prevents reactive metabolite production and nephrotoxicity following cisplatin treatment [49]. Mirroring previous findings, mRNA expression was lower in kidney in comparison to the liver before and after paracetamol-related DILI in the *Dicer1* $^{flox/flox}$ mice [283, 284]. Furthermore, it was noted that mRNA expression of cyp2e1 was present primarily in the kidney cortex with minimal expression in the kidney medulla. Localisation of cyp2e1 via immunohistochemistry supported these findings further as staining was present in the kidney cortex tubules and absent in the medulla [49, 285].

Prior to paracetamol-related DILI, a non-significant difference of cyp1a2 and cyp2e1 mRNA expression was observed in the kidney cortex and medulla following the loss of hepatic miRNA. Protein expression also determined that, overall, there were no-significant differences in cyp2e1 across all three treatment groups.

In the studies described in Chapter 4, there was an increase in paracetamol-induced liver injury in the Cre-AAV8 treated mice, compared to the baseline and Null-AAV8 mice. However, there were no signs of kidney injury across the AAV8 and paracetamol treatment groups (Chapter Chapter 4). It was discovered that the distribution and intensity of cyp2e1 staining in the kidney did not differ between the Cre-AAV8 and Null-AAV8 treated mice, or in the presence of paracetamol treatment. Nonetheless, mRNA expression of cyp2e1 was observed to increase in the kidney cortex of all three AAV8 treatment groups at the 300mg/kg paracetamol dose. The Cre-AAV8 mice had significantly greater cyp2e1 expression compared to the baseline and Null-AAV8 mice treated at the 300mg/kg paracetamol dose. Therefore, this suggests that paracetamol toxicity alone increases cyp2e1 expression in the kidney cortex and the loss of hepatic miRNA heightens this increase further.

Alternatively, the marked increase in cyp2e1 in the kidney cortex of the 300mg/kg paracetamol treated Cre-AAV8 mice could be related to the increase in liver toxicity, rather than a loss of hepatic miRNA transfer. Due to this, a future study matching the level of toxicity rather than the dose of paracetamol may be a better comparison

between the Cre AAV8 mice and Null-AAV8 mice. Additionally, an increase in cyp2e1 mediated metabolism of chlorzoxazone was calculated to have a greater response in the kidney of the Cre-AAV8 mice, in contrast to the Null-AAV8 mice ([286], Section 2.12).Therefore, it was identified that hepatic miRNA, including miR-122, transferred from the liver to the kidney, during DILI, alters the expression and activity of cyp2e1 in the kidney cortex.

It could be proposed that an upregulation of miR-122 and resultant decrease of cyp2e1 activity in the kidney, during DILI, reduces the extent of drug metabolism and toxicity in the kidney. Consistent with this theory of miR-122 mediated protection, non-recovering patients of ALF have shown to exhibit lower levels of circulating miR-122, than patients that recover from ALF [287]. However, the loss of miR-122, and in turn, an increase of cyp2e1 in the kidney of the Cre-AAV8 mice did not induce an increase in KIM-1 expression in the kidney cortex or visible injury following histological analysis, compared to the baseline and Null-AAV8 treated mice. In paracetamol toxicity, kidney injury is a rare event and is not consistently observed in pre-clinical models or humans [288]. Hence, to explore the influence hepatic miRNA has during kidney injury, I would suggest using a known nephrotoxic agent such as cisplatin, rather than paracetamol, in the Cre-AAV8 *Dicer1* $^{flox/flox}$ mice. Nevertheless, the results in this chapter has uncovered a potential new avenue in the understanding of renal drug metabolism and nephrotoxicity.

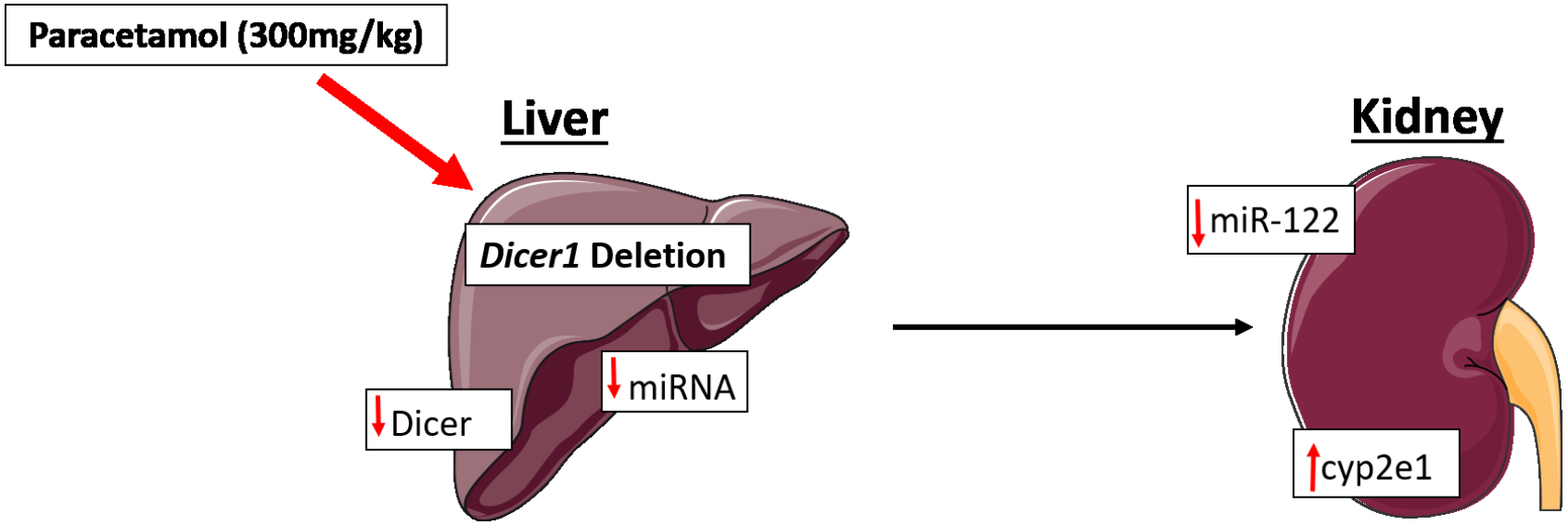

Figure 5.18 The loss of hepatic miRNA transferred from the liver to the kidney during 300mg/kg paracetamol dosing results in the derepression of cyp2e1 in the kidney

Hepatocyte specific Dicer1 knockdown resulted in the total loss of mature miRNA in the hepatocytes. Consequently, the loss of hepatic miRNA lead to the significant reduction of miR-122 transferred from the liver to the kidney during health and paracetamol toxicity. Following 300mg/kg paracetamol dosing, there was an increase of cyp2e1 expression and activity in the kidney cortex following the loss of miR-122 transfer. Indicating, an upregulation of miR-122 in the circulation and kidney, and resultant decrease of cyp2e1 activity during DILI reduces the extent of drug toxicity in the kidney. Figure created using Servier Medical Art, Les Laboratoires Servier.

Chapter 6 Conclusions

ALF is a sudden and severe clinical disease which is often accompanied by acute kidney injury (AKI) [289]. Therefore, investigations aimed to better understand the mechanism of hepatocyte to renal signalling are of clinical importance. MiR-122's enrichment in the hepatocytes of the liver and little-to-no expression elsewhere [164], enabled us to confidently identify the origin of transfer. Furthermore, miRNA, including miR-122, have been demonstrated to mediate cellular signalling and alter cellular activity in both neighbouring and distant cells [138-140, 190]. Thus, the work in this thesis aimed to better understand the role of hepatocyte enriched miR-122, following its release from the liver.

6.1 Summary of key findings

The hypothesis of the work carried out in this thesis proposed that the large release of miR-122 from the liver to the circulation during DILI results in miR-122 entering the kidney and inducing resistance to subsequent injury. Therefore, the key research aims chosen to address the hypothesis included: characterise an inducible model of liver-specific Dicer deletion, investigate which organs are responsible for the uptake of circulating microRNA-122 during DILI and, lastly, investigate if the loss of miRNA-122 signalling from the liver to the kidney has a functional effect. Consequently, it was discovered that the spleen and kidney are involved in the uptake of circulating hepatocyte-derived miR-122, during health and liver injury. Following its uptake, it was revealed that hepatocyte derived miRNA may play a role in regulating the transcriptome in the kidney.

6.1.1 MiR-122 is transferred from the liver to the spleen and kidney *in vivo* during health

The studies described in Chapter 3 aimed to characterise an inducible model of hepatocyte-specific Dicer and mature miRNA knockdown in *Dicer1*$^{flox/flox}$ mice. After a single injection of a hepatocyte specific Cre-AAV8, we were able to demonstrate successful knockdown of Dicer and total hepatic miRNA in the liver of the *Dicer1*$^{flox/flox}$ mice. Alongside the Cre-AAV8 treatment, untreated AAV8 (baseline) mice and mice that were treated with an empty AAV8, Null-AAV8, were observed to have stable expression of hepatic Dicer and miRNA.

Matching previous studies, the loss of hepatic Dicer was observed one week following Cre-AAV8 injection and a significant reduction in miRNA was demonstrated a week later [227]. The hepatocyte specificity of the AAV8 was confirmed via the unchanged expression of Dicer and tissue enriched miRNA in the spleen, kidney (cortex and medulla), heart, lung and brain. Furthermore, there was no histological evidence of injury in the liver, spleen and kidney, following Null-AAV8 or Cre-AAV8 treatment. Nevertheless, it was identified that the total loss of hepatic miRNA led to the significant reduction of miR-122 expression in the spleen and kidney cortex and medulla. This highlights that in a healthy mouse, the spleen and kidney are involved in the uptake and clearance of circulating miR-122 released from the liver. Additionally, it indicates that miR-122 is involved in inter-organ signalling proposed in the hypothesis.

It is often difficult to define the origin of miRNA that are ubiquitous in expression [239]. This was seen with miR-192, a miRNA described to be enriched in both the hepatocytes [86, 123] and the kidney [158, 290]. In the liver, miR-192 was significantly lost, however, unlike miR-122, its expression remained unchanged in the kidney. Potentially, the loss of hepatic miR-192 transfer was concealed due to its local synthesis in the kidney. Nevertheless, it is likely that multiple miRNA species are transferred from the liver to other organs. In order to investigate this further, the consequence the total loss of hepatic miRNA transfer should be conducted through the analysis of miRNA and mRNA in each tissue.

6.1.2 MiR-122 transfer increases during liver injury

As Chapter 3 investigated the transfer of hepatocellular miRNA during health, Chapter 4 aimed to underpin the impact DILI has on the transfer of hepatocyte enriched miRNA to other tissues. The well described increase of circulating miR-122 and miR-192 during paracetamol toxicity (300mg/kg) was observed in the untreated AAV8 (baseline) and Null-AAV8 treated mice. Subsequently, as suggested in the hypothesis, the uptake of miR-122 in the spleen and kidney was significantly upregulated, compared to the saline treated mice. Furthermore, miR-122 was observed to increase significantly in the heart which was not observed in Chapter 3,

during health. The increase of miR-122 in the circulation and consequently in the spleen, kidney and heart following paracetamol toxicity was diminished in the Cre-AAV8 mice. Moreover, the loss of mature miRNA in the hepatocytes resulted in a significant increase of cellular death in the livers of the Cre-AAV8 treated mice. In the kidney and spleen, injury was not observed across all AAV8 and paracetamol treatment groups.

6.1.3 During paracetamol toxicity, hepatic miRNA transfer represses cyp2e1 activity and expression in the kidney

Lastly, Chapter 5 investigated whether the loss of hepatic miRNA, including miR-122, transferred from the liver to the kidney had an impact on renal CYP450 expression during health and DILI. During physiological conditions, the loss of hepatic miRNA resulted in the increase of known miR-122 mRNA targets including: Aldoa, Ndrg3, Tmed3 and cyp1a2 targets in the liver. Nevertheless, cyp2e1, another CYP450 enzyme believed to be targeted by miR-122, did not alter at the mRNA or protein level. In the kidney, there was also a non-significant change in cyp2e1 expression following the loss of hepatic miRNA transfer.

Following a single dose of 300mg/kg paracetamol, it was observed that the cyp2e1 increases in the kidney in all AAV8 treatment groups. However, the absence of hepatic miRNA transfer to the kidney and in turn a loss of miR-122 mediated repression, the increase in cyp2e1 mRNA expression and activity was significantly greater in the Cre-AAV8 mice. Correlation analysis supported these findings further with an observed negative correlation between miR-122 and cyp2e1 expression in the cortex following a single dose of 300mg/kg paracetamol in all three groups. The loss of miR-122 and in turn, an increase of cyp2e1 in the kidneys of the Cre-AAV8 mice did not induce an increase in KIM-1 expression or visible injury following histological analysis, compared to the baseline and Null-AAV8 treated mice. Nonetheless, in line with Rivkin *et al.*, these findings indicate that hepatocyte derived miR-122 influences mRNA expression and cellular activity in the kidney [193]. Furthermore, the alteration of the kidneys ability to perform cyp2e1 oxidation

suggests miR-122 has the ability to modify kidney mediated drug metabolism and the formation of toxic metabolites.

6.1.4 Limitations

Due to time and resources, the studies in this thesis were restricted to 5 mice per treatment group and time point. Due to this, a limitation of the studies described throughout this thesis are the low n numbers providing a greater chance of type I and type II error. Furthermore, using the data collected in Chapter 3: mean miR-122 expression in the kidney of the Null-AAV8 (0.14, SD=0.13) and Cre-AAV8 mice (0.007, SD=0.004), a sample size of 8 mice per group would provide 80% power (α=0.05). Thus, it would be recommended to use an n=8, rather than an n=5, for future studies in this mouse model.

The low numbers of mice per group also meant that kidney samples used for the investigation of CYP450 activity were measured as an n=1 for each group (5 kidneys from 5 mice, pooled, in duplicate). This was carried out as CYP450 expression is much lower in the kidney, in comparison to the liver [215]. Thus, a limitation of the results presented in Figure 5.16 was that statistical analysis could not be performed to produce a reliable p value. Therefore, with greater time and resources, it would be necessary to repeat these measures in a greater number of mice to determine if the results seen in Figure 5.16 are not influenced by chance.

In addition, due to limited tissue collected, protein expression of CYP2E1 was not investigated in the kidney of the *Dicer1* $^{flox/flox}$ mice treated with paracetamol. In future investigations, it would be interesting to measure the protein expression of CYP2E1 in the kidney to see whether the observed changes in mRNA expression and activity following Cre-AAV8 and 300mg/kg paracetamol is linked to increased protein expression.

6.2 Future work

The results in this thesis highlight that hepatic derived miR-122 released from the liver is taken up by the spleen and kidney during health and paracetamol induced liver injury. Furthermore, it was identified that the loss of hepatic miRNA transferred from the liver to the kidney significantly altered the expression and activity of previously identified miR-122 mRNA targets. However, as this phenotype was observed following the loss of total hepatic miRNA, it raises the question of whether hepatocyte-derived miR-122 alone acts as a regulator of kidney function and immune response during DILI. To clarify this, homozygous miR-122$^{flox/flox}$ mice [165, 291], could undergo Cre-AAV8 and Null-AAV8 (negative control) treatment described in this thesis. The treatment with Cre-AAV8 would lead to hepatocyte-specific miR-122 knockdown only, rather than the total hepatocyte miRNA knockdown observed in this thesis. In this mouse model, the production and expression of miR-122 would cease in the liver only, with miR-122 biogenesis and expression unaffected elsewhere in the body.

6.2.1 Characterise the effect hepatocyte-derived miR-122 has on renal physiology and its response to injury

Alongside liver injury biomarkers, markers of kidney function such as serum creatinine and KIM-1 are important factors used to determine patient prognosis and stratification for liver transplantation during ALI and ALF [91, 92]. Rivkin *et al*. published evidence that kidney miR-122 expression is reliant on its transfer from the liver. Additionally, they discovered that an increase of miR-122 transfer following liver inflammation resulted in the repression of the miR-122 mRNA target Epo [193]. Furthermore, data collected in this thesis indicates hepatic miRNA, including miR-122 plays a role in regulating cyp2e1 expression and activity in the kidney.

To understand whether hepatic derived miR-122 is a protective mediator of kidney injury (AKI), we could use the miR-122$^{flox/flox}$ mouse model mentioned above alongside established model of renal injury. Following liver specific miR-122 knockdown, we could investigate miR-122's role during acute kidney injury by nephrotoxicity or ischemia-reperfusion. It would be particularly interesting to see its

role during cisplatin nephrotoxicity, as miR-122 has been described to decrease cisplatin-induced apoptosis and repress gene expression of the key enzyme involved in its oxidation, cyp2e1 [200, 203, 246]. If following the loss of miR-122 in the liver and in turn a loss of renal miR-122 expression leads to an increase in kidney injury, it would confirm that miR-122 transferred from the liver to the kidney is protective.

AKI is characterised by the sudden loss of kidney excretory function [292]. The rapid decline of glomerular filtration rate (GFR) during AKI is usually associated with a reduction in renal blood flow [292]. The diagnosis of AKI is determined by the accumulation of the by-products of nitrogen metabolism, biomarkers of kidney injury and decreased urine output [292, 293]. Therefore, to evaluate the extent of kidney injury, multiple assessments would be measured in the miR-122$^{flox/flox}$ mice. To assess the haemodynamic and excretory response to AKI, biomarkers reflecting GFR, such as blood urea nitrogen and serum creatinine, and markers of kidney damage including KIM-1 could be measured. In addition, kidney histology could be investigated to assess the extent of injury and fibrosis. Immune cells have been described to mediate kidney injury and repair. Furthermore, hepatic derived miR-122 has been previously described to be taken up by macrophages initiating an immune response [122]. Thus, staining for neutrophils, T-cell and macrophages could also be carried out to determine if the loss of miR-122 influences the immune response to kidney injury.

6.2.2 Investigate the effect hepatocyte-derived miR-122 has on leukocyte response during acute liver injury

Hyper-stimulation and over-activation of inflammatory signalling can provoke further injury during ALI [294]. Nonetheless, inflammatory signalling is also required for the regeneration and repair of the liver via the shift of pro-inflammatory monocytes to pro-reparative monocytes [294, 295]. Patients displaying low levels of blood monocytes, lymphocytes and NK cells during ALI, have been described to have poor clinical outcomes [296]. Therefore, sterile inflammation is a key feature of ALI and monocytes are measured in the blood to help determine clinical outcome in ALI patients. Hence,

understanding the role of the immune response and its mediators is important for developing therapeutics and improving patient care during ALI.

During ALI, miR-122 has been described to activate alveolar macrophages and inflammation in the lung [122]. Thus, it would be interesting to explore the influence miR-122 has on the dynamic leucocyte response to acute liver injury and regeneration. To investigate this, I would propose using the miR-122 model described above (Section6.2). As the Dicer and hepatic miRNA knockout mice had greater levels of liver necrosis, compared to the Null-AAV8 mice (Chapter 4), I would first carry out a dose comparison study between the Cre-AAV8 and Null-AAV8 treated miR-122$^{flox/flox}$ mice. From this experiment, a dose providing comparable levels of injury will be determined and used for both AAV8 treatment groups.

Subsequently, the effect of miR-122 depletion on leucocyte expression and response could be explored. A paracetamol overdose (300mg/kg) has been described to induce a distinct phase of injury (0-24 hours) and a period of injury resolution (24-72 hours) in C57/BL6 mice [297]. Thus, to investigate miR-122's role in paracetamol injury and liver regeneration, tissue and blood could be collected after a single injection of 300mg/kg paracetamol, at various time points across the injury and resolution phases. The extent of injury could be assessed at each time point by histology and measurements of circulating biomarkers such as ALT, AST and GLDH. In the liver, dynamic changes of macrophages, kupffer cells and the proportion of Ly6C^{Hi} and Ly6C^{Lo} monocytes could be assessed and quantified by flow cytometry.

6.2.3 Identify which leukocytes and renal cell populations are regulated by hepatocyte-derived miR-122

MiR-122 has been described to mediate various pathways following its release from the liver. In the lung, hepatic miR-122 has also been suggested to play a role in the activation of alveolar macrophages in the lung and initiate pulmonary inflammation [122]. Moreover, unpublished data has (John Tranter and Wilna Oosthuyzen) identified that the CD11b+ macrophages in the spleen and the LTL+ tubular cells of the kidney are involved in the uptake of miR-122 following paracetamol-induced liver injury.

Therefore, it would be interesting to explore which cell subpopulations of the kidney and leucocytes are involved in the uptake of miR-122, and whether this impacts gene expression.

I would suggest carrying out single cell RNA-seq to assess the similarities and differences in transcriptome within a cell population. To achieve this, single cell RNA seq could be performed on the miR-122$^{flox/flox}$ mice at the early and later stages of miR-122 knockdown induced by the Cre-AAV8 treatment. In addition to investigating changes in the transcriptome of kidney cells and leucocytes during health, the mice could also be assessed after ALI (paracetamol-induced, Section 6.2.1) or AKI (nephrotoxicity or ischemia-reperfusion, Section 6.2.2

6.3 Final conclusions

The studies in this thesis aimed to better understand the role of hepatocyte enriched miR-122, following its release from the liver. Hepatic miR-122 was shown to be transferred from the liver to the kidney and spleen, before and after liver injury *in vivo*. Furthermore, liver derived miRNA was observed to negatively regulate the expression and activity of the miR-122 mRNA target, cyp2e1, in the kidney during paracetamol DILI. If translated into an *in vivo* model of hepatic miR-122 knockdown, this could represent a novel signalling mechanism available for therapeutic intervention to protect against kidney injury during ALF.

[1] Anderson SI, Anderson PG, Lowe JS. Stevens & Lowe's Human Histology. Philadephia, PA: Elsevier, 2018.
[2] Heinz S, Braspenning J. Measurement of Blood Coagulation Factor Synthesis in Cultures of Human Hepatocytes. Methods Mol Biol 2015; 1250: 309-316.
[3] Costanzo LS. Physiology. Sixth edition.. ed. Philadelphia, PA: Philadelphia, PA : Elsevier, 2018.
[4] Stravitz RT, Lee WM. Acute liver failure. The Lancet 2019; 394(10201): 869-881.
[5] Bower WA, Johns M, Margolis HS, Williams IT, Bell BP. Population-based surveillance for acute liver failure. Am J Gastroenterol 2007; 102(11): 2459-2463.
[6] Escorsell À, Mas A, De La Mata M. Acute liver failure in Spain: Analysis of 267 cases. Liver Transplantation 2007; 13(10): 1389-1395.
[7] Ostapowicz G, Fontana RJ, Schiødt FV, Larson A, Davern TJ, Han SH, McCashland TM, Shakil AO, Hay JE, Hynan L, Crippin JS, Blei AT, Samuel G, Reisch J, Lee WM. Results of a prospective study of acute liver failure at 17 tertiary care centers in the United States. Ann Intern Med 2002; 137(12): 947-954.
[8] Bernal W, Auzinger G, Dhawan A, Wendon J. Acute liver failure. The Lancet 2010; 376(9736): 190-201.
[9] Williams R, Schalm SW, O'Grady JG. Acute liver failure: redefining the syndromes. The Lancet 1993; 342(8866): 273-275.
[10] O'Grady JG, Alexander GJM, Hayllar KM, Williams R. Early indicators of prognosis in fulminant hepatic failure. Gastroenterology 1989; 97(2): 439-445.
[11] Castaldo ET, Chari RS. Liver transplantation for acute hepatic failure. HPB (Oxford) 2006; 8(1): 29-34.
[12] Björnsson ES. Epidemiology, Predisposing Factors, and Outcomes of Drug-Induced Liver Injury. Clin Liver Dis 2020; 24(1): 1-10.
[13] NHS. Management of Acute Liver Failure. Adult Therapeutics Handbook 2019; 2021(6th January).
[14] Leise MD, Poterucha JJ, Talwalkar JA. Drug-induced liver injury. Mayo Clin Proc 2014; 89(1): 95-106.
[15] Bleibel W, Kim S, D'Silva K, Lemmer ER. Drug-induced liver injury: review article. Digestive diseases and sciences 2007; 52(10): 2463-2471.
[16] Andrade RJ, Chalasani N, Björnsson ES, Suzuki A, Kullak-Ublick GA, Watkins PB, Devarbhavi H, Merz M, Lucena MI, Kaplowitz N, Aithal GP. Drug-induced liver injury. Nature Reviews Disease Primers 2019; 5(1).
[17] Kleiner DE, Chalasani NP, Lee WM, Fontana RJ, Bonkovsky HL, Watkins PB, Hayashi PH, Davern TJ, Navarro V, Reddy R, Talwalkar JA, Stolz A, Gu J, Barnhart H, Hoofnagle JH. Hepatic histological findings in suspected drug-induced liver injury: Systematic evaluation and clinical associations. Hepatology 2014; 59(2): 661-670.
[18] García-Cortés M, Ortega-Alonso A, Lucena MI, Andrade RJ. Drug-induced liver injury: a safety review. Expert Opin Drug Saf 2018; 17(8): 795-804.
[19] Amacher DE, Schomaker SJ, Aubrecht J. Development of blood biomarkers for drug-induced liver injury: an evaluation of their potential for risk assessment and diagnostics. Molecular diagnosis & therapy 2013; 17(6): 343.
[20] Kaplowitz N. Idiosyncratic drug hepatotoxicity. Nature Reviews Drug Discovery 2005; 4(6): 489-499.

[21] De Abajo FJ, Montero D, Madurga M, Rodriguez LAG. Acute and clinically relevant drug-induced liver injury: a population based case-control study. British Journal of Clinical Pharmacology 2004; 58(1): 71-80.
[22] Björnsson ES, Bergmann OM, Björnsson HK, Kvaran RB, Olafsson S. Incidence, Presentation, and Outcomes in Patients With Drug-Induced Liver Injury in the General Population of Iceland. Gastroenterology 2013; 144(7): 1419-1425.e1413.
[23] Sgro C. Incidence of drug-induced hepatic injuries: A French population-based study. Hepatology 2002; 36(2): 451-455.
[24] Hoofnagle JH, Björnsson ES. Drug-Induced Liver Injury — Types and Phenotypes. New England Journal of Medicine 2019; 381(3): 264-273.
[25] Chen M, Bisgin H, Tong L, Hong H, Fang H, Borlak J, Tong W. Toward predictive models for drug-induced liver injury in humans: are we there yet? Biomarkers 2014; 8(2): 201-213.
[26] Temple RJ, Himmel MH. Safety of newly approved drugs: implications for prescribing. Jama 2002; 287(17): 2273-2275.
[27] Mosedale M, Watkins P. Drug-induced liver injury: Advances in mechanistic understanding that will inform risk management. Clinical Pharmacology & Therapeutics 2017; 101(4): 469-480.
[28] Khan LR, Oniscu GC, Powell JJ. Long-term outcome following liver transplantation for paracetamol overdose. Transpl Int 2010; 23(5): 524-529.
[29] Larson AM, Polson J, Fontana RJ, Davern TJ, Lalani E, Hynan LS, Reisch JS, Schiødt FV, Ostapowicz G, Shakil AO, Lee WM. Acetaminophen-induced acute liver failure: results of a United States multicenter, prospective study. Hepatology 2005; 42(6): 1364-1372.
[30] Heard KJ. Acetylcysteine for acetaminophen poisoning. N Engl J Med 2008; 359(3): 285-292.
[31] Lee WM. Drug-induced acute liver failure. Clinics in liver disease 2013; 17(4): 575-586.
[32] Vrbova M, Rousarova E, Bruckova L, Cesla P, Rousar T. Characterization of acetaminophen toxicity in human kidney HK-2 cells. Physiological research 2016; 65(4): 627.
[33] Budnitz DS, Lovegrove MC, Crosby AE. Emergency Department Visits for Overdoses of Acetaminophen-Containing Products. Am J Prev Med 2011; 40(6): 585-592.
[34] Clements JA, Heading RC, Nimmo WS, Prescott LF. Kinetics of acetaminophen absorption and gastric emptying in man. Clinical Pharmacology & Therapeutics 1978; 24(4): 420-431.
[35] McPhail ME, Knowles RG, Salter M, Dawson J, Burchell B, Pooson CI. Uptake of acetaminophen (paracetamol) by isolated rat liver cells. Biochemical pharmacology 1993; 45(8): 1599-1604.
[36] Davis M, Labadarios D, Williams RS. Metabolism of paracetamol after therapeutic and hepatotoxic doses in man. J Int Med Res 1976; 4(4 Suppl): 40-45.
[37] Ferner RE, Dear JW, Bateman DN. Management of paracetamol poisoning. Bmj 2011; 342(9): d2218.

[38] Zaher H, Buters JT, Ward JM, Bruno MK, Lucas AM, Stern ST, Cohen SD, Gonzalez FJ. Protection against acetaminophen toxicity in CYP1A2 and CYP2E1 double-null mice. Toxicology applied pharmacology 1998; 152(1): 193-199.
[39] Raucy JL, Lasker JM, Lieber CS, Black M. Acetaminophen activation by human liver cytochromes P450IIE1 and P450IA2. Arch Biochem Biophys 1989; 271(2): 270-283.
[40] Ghanem CI, Pérez MJ, Manautou JE, Mottino AD. Acetaminophen from liver to brain: New insights into drug pharmacological action and toxicity. Pharmacological Research 2016; 109: 119-131.
[41] Ramsay RR, Rashed MS, Nelson SD. In vitro effects of acetaminophen metabolites and analogs on the respiration of mouse liver mitochondria. Arch Biochem Biophys 1989; 273(2): 449-457.
[42] Burcham PC, Harman AW. Acetaminophen toxicity results in site-specific mitochondrial damage in isolated mouse hepatocytes. J Biol Chem 1991; 266(8): 5049-5054.
[43] Mazer M, Perrone J. Acetaminophen-induced nephrotoxicity: pathophysiology, clinical manifestations, and management. Journal of Medical Toxicology 2008; 4(1): 2-6.
[44] Sekine S, Ogawa R, McManus MT, Kanai Y, Hebrok M. Dicer is required for proper liver zonation. J Pathol 2009; 219(3): 365-372.
[45] Smilkstein MJ, Knapp GL, Kulig KW, Rumack BH. Efficacy of Oral N-Acetylcysteine in the Treatment of Acetaminophen Overdose. New England Journal of Medicine 1988; 319(24): 1557-1562.
[46] Vliegenthart A, Antoine DJ, Dear JW. Target biomarker profile for the clinical management of paracetamol overdose. British journal of clinical pharmacology 2015; 80(3): 351-362.
[47] McDonnell AM, Dang CH. Basic review of the cytochrome p450 system. Journal of the advanced practitioner in oncology 2013; 4(4): 263-268.
[48] Gonzalez FJ. The molecular biology of cytochrome P450s. 1988; 40(4): 243-288.
[49] Liu H, Baliga R. Cytochrome P450 2E1 null mice provide novel protection against cisplatin-induced nephrotoxicity and apoptosis. Kidney international 2003; 63(5): 1687-1696.
[50] Forkert PG. CYP2E1 is preferentially expressed in Clara cells of murine lung: localization by in situ hybridization and immunohistochemical methods. Am J Respir Cell Mol Biol 1995; 12(6): 589-596.
[51] Luo Y-S, Furuya S, Soldatov VY, Kosyk O, Yoo HS, Fukushima H, Lewis L, Iwata Y, Rusyn I. Metabolism and Toxicity of Trichloroethylene and Tetrachloroethylene in Cytochrome P450 2E1 Knockout and Humanized Transgenic Mice. Toxicological Sciences 2018; 164(2): 489-500.
[52] Ding X, Kaminsky LS. HUMAN EXTRAHEPATIC CYTOCHROMES P450: Function in Xenobiotic Metabolism and Tissue-Selective Chemical Toxicity in the Respiratory and Gastrointestinal Tracts. Annual Review of Pharmacology and Toxicology 2003; 43(1): 149-173.
[53] Nelson DR, Koymans L, Kamataki T, Stegeman JJ, Feyereisen R, Waxman DJ, Waterman MR, Gotoh O, Coon MJ, Estabrook RW, Gunsalus IC, Nebert DW. P450

superfamily: update on new sequences, gene mapping, accession numbers and nomenclature. Pharmacogenetics (London) 1996; 6(1): 1-42.
[54] Rang HP, Ritter JM, Flower RJ, Henderson G. Rang & Dale's Pharmacology E-Book: with STUDENT CONSULT Online Access. London: London: Elsevier, 2015.
[55] Zanger UM, Schwab M. Cytochrome P450 enzymes in drug metabolism: Regulation of gene expression, enzyme activities, and impact of genetic variation. Pharmacology & Therapeutics 2013; 138(1): 103-141.
[56] Tolson AH, Wang H. Regulation of drug-metabolizing enzymes by xenobiotic receptors: PXR and CAR. Advanced drug delivery reviews 2010; 62(13): 1238-1249.
[57] Trombino AF, Near RI, Matulka RA, Yang S, Hafer LJ, Toselli PA, Kim DW, Rogers AE, Sonenshein GE, Sherr DH. Expression of the aryl hydrocarbon receptor/transcription factor (AhR) and AhR-regulated CYP1. Breast Cancer Research and Treatment 2000; 63(2): 117-131.
[58] Nebert DW, Karp CL. Endogenous functions of the aryl hydrocarbon receptor (AHR): intersection of cytochrome P450 1 (CYP1)-metabolized eicosanoids and AHR biology. J Biol Chem 2008; 283(52): 36061-36065.
[59] Martínez-Jiménez CP, Jover R, Donato MT, Castell JV, Gómez-Lechón MJ. Transcriptional regulation and expression of CYP3A4 in hepatocytes. Curr Drug Metab 2007; 8(2): 185-194.
[60] Kohalmy K, Tamási V, Kóbori L, Sárváry E, Pascussi JM, Porrogi P, Rozman D, Prough RA, Meyer UA, Monostory K. Dehydroepiandrosterone induces human CYP2B6 through the constitutive androstane receptor. Drug Metab Dispos 2007; 35(9): 1495-1501.
[61] Michaut A, Le Guillou D, Moreau C, Bucher S, McGill MR, Martinais S, Gicquel T, Morel I, Robin MA, Jaeschke H, Fromenty B. A cellular model to study drug-induced liver injury in nonalcoholic fatty liver disease: Application to acetaminophen. Toxicol Appl Pharmacol 2016; 292: 40-55.
[62] Chen W, Koenigs LL, Thompson SJ, Peter RM, Rettie AE, Trager WF, Nelson SD. Oxidation of acetaminophen to its toxic quinone imine and nontoxic catechol metabolites by baculovirus-expressed and purified human cytochromes P450 2E1 and 2A6. Chem Res Toxicol 1998; 11(4): 295-301.
[63] Ko JW, Shin JY, Kim JW, Park SH, Shin NR, Lee IC, Shin IS, Moon C, Kim SH, Kim SH. Protective effects of diallyl disulfide against acetaminophen-induced nephrotoxicity: A possible role of CYP2E1 and NF-κB. Food Chemical Toxicology 2017; 102: 156-165.
[64] Das J, Ghosh J, Manna P, Sil PCJT. Taurine protects acetaminophen-induced oxidative damage in mice kidney through APAP urinary excretion and CYP2E1 inactivation. 2010; 269(1): 24-34.
[65] Gonzalez FJ. The use of gene knockout mice to unravel the mechanisms of toxicity and chemical carcinogenesis. Toxicology Letters 2001; 120(1-3): 199-208.
[66] Lee SS, Buters JT, Pineau T, Fernandez-Salguero P, Gonzalez FJ. Role of CYP2E1 in the hepatotoxicity of acetaminophen. J Biol Chem 1996; 271(20): 12063-12067.
[67] Akakpo J, Ramachandran A, Kandel S, Ni H, Kumer S, Rumack B, Jaeschke H. 4-Methylpyrazole protects against acetaminophen hepatotoxicity in mice and in

primary human hepatocytes. Human & Experimental Toxicology 2018; 37(12): 1310-1322.
[68] Kang AM, Padilla-Jones A, Fisher ES, Akakpo JY, Jaeschke H, Rumack BH, Gerkin RD, Curry SC. The Effect of 4-Methylpyrazole on Oxidative Metabolism of Acetaminophen in Human Volunteers. Journal of Medical Toxicology 2020; 16(2): 169-176.
[69] Wolf KK, Wood SG, Allard JL, Hunt JA, Gorman N, Walton-Strong BW, Szakacs JG, Duan SX, Hao Q, Court MH, von Moltke LL, Greenblatt DJ, Kostrubsky V, Jeffery EH, Wrighton SA, Gonzalez FJ, Sinclair PR, Sinclair JF. Role of CYP3A and CYP2E1 in Alcohol-Mediated Increases in Acetaminophen Hepatotoxicity: Comparison of Wild-Type and Cyp2e1 (–/–) Mice. Drug Metab Dispos 2007; 35(7): 1223-1231.
[70] Chen C, Krausz KW, Idle JR, Gonzalez FJ. Identification of Novel Toxicity-associated Metabolites by Metabolomics and Mass Isotopomer Analysis of Acetaminophen Metabolism in Wild-type and Cyp2e1-null Mice. J Biol Chem 2008; 283(8): 4543-4559.
[71] James LP, McGill MR, Roberts DW, Hinson JA, Lee WM. Chapter Two- Advances in biomarker development in acetaminophen toxicity. Advances in Clinical Chemistry 2020; 98: 35-50.
[72] McGill MR. The past and present of serum aminotransferases and the future of liver injury biomarkers. Excli j 2016; 15: 817-828.
[73] Fu S, Wu D, Jiang W, Li J, Long J, Jia C, Zhou T. Molecular Biomarkers in Drug-Induced Liver Injury: Challenges and Future Perspectives. Frontiers in Pharmacology 2019; 10: 1667.
[74] Dear JW, Antoine DJ. Stratification of paracetamol overdose patients using new toxicity biomarkers: current candidates and future challenges. Expert review of clinical pharmacology 2014; 7(2): 181-189.
[75] Senior JR. Alanine Aminotransferase: A Clinical and Regulatory Tool for Detecting Liver Injury–Past, Present, and Future. Clinical Pharmacology & Therapeutics 2012; 92(3): 332-339.
[76] Prescott K, Stratton R, Freyer A, Hall I, Le Jeune I. Detailed analyses of self-poisoning episodes presenting to a large regional teaching hospital in the UK. Br J Clin Pharmacol 2009; 68(2): 260-268.
[77] Green TJ, Sivilotti MLA, Langmann C, Yarema M, Juurlink D, Burns MJ, Johnson DW. When do the aminotransferases rise after acute acetaminophen overdose? Clinical Toxicology 2010; 48(8): 787-792.
[78] Al-Hourani K, Mansi R, Pettie J, Dow M, Bateman D, Dear J. The predictive value of hospital admission serum alanine transaminase activity in patients treated for paracetamol overdose. An International Journal of Medicine 2013; 106(6): 541-546.
[79] Giboney PT. Mildly elevated liver transaminase levels in the asymptomatic patient. Am Fam Physician 2005; 71(6): 1105-1110.
[80] Yang S-S, Cheng K-S, Lai Y-C, Wu C-H, Chen T-K, Lee C-L, Chen D-S. Decreasing serum alpha-fetoprotein levels in predicting poor prognosis of acute hepatic failure in patients with chronic hepatitis B. J Gastroenterol 2002; 37(8): 626-632.

[81] Schiødt FV, Ostapowicz G, Murray N, Satyanarana R, Zaman A, Munoz S, Lee WM. Alpha-fetoprotein and prognosis in acute liver failure. Liver Transplantation 2006; 12(12): 1776-1781.
[82] Antoine DJ, Dear JW, Lewis PS, Platt V, Coyle J, Masson M, Thanacoody RH, Gray AJ, Webb DJ, Moggs JG. Mechanistic biomarkers provide early and sensitive detection of acetaminophen-induced acute liver injury at first presentation to hospital. Hepatology 2013; 58(2): 777-787.
[83] Antoine DJ, Williams DP, Kipar A, Jenkins RE, Regan SL, Sathish JG, Kitteringham NR, Park BK. High-Mobility Group Box-1 Protein and Keratin-18, Circulating Serum Proteins Informative of Acetaminophen-Induced Necrosis and Apoptosis In Vivo. Toxicological Sciences 2009; 112(2): 521-531.
[84] McGill MR, Staggs VS, Sharpe MR, Lee WM, Jaeschke H. Serum mitochondrial biomarkers and damage-associated molecular patterns are higher in acetaminophen overdose patients with poor outcome. Hepatology 2014; 60(4): 1336-1345.
[85] Wang X, Sun R, Wei H, Tian Z. High-mobility group box 1 (HMGB1)-toll-like receptor (TLR)4-interleukin (IL)-23-IL-17A axis in drug-induced damage-associated lethal hepatitis: Interaction of γδ T cells with macrophages. Hepatology 2013; 57(1): 373-384.
[86] Starkey Lewis PJ, Dear J, Platt V, Simpson KJ, Craig DG, Antoine DJ, French NS, Dhaun N, Webb DJ, Costello EM. Circulating microRNAs as potential markers of human drug-induced liver injury. Hepatology 2011; 54(5): 1767-1776.
[87] Vliegenthart A, Shaffer J, Clarke J, Peeters L, Caporali A, Bateman D, Wood D, Dargan P, Craig D, Moore J. Comprehensive microRNA profiling in acetaminophen toxicity identifies novel circulating biomarkers for human liver and kidney injury. Scientific reports 2015; 5: 15501.
[88] He CY, Liang BB, Fan XY, Cao L, Chen R, Guo YJ, Zhao J. The dual role of osteopontin in acetaminophen hepatotoxicity. Acta Pharmacol Sin 2012; 33(8): 1004-1012.
[89] Manautou JE, Hart SGE, Khairallah EA, Cohen SD. Protection against Acetaminophen Hepatotoxicity by a Single Dose of Clofibrate: Effects on Selective Protein Arylation and Glutathione Depletion. Fundam Appl Toxicol 1996; 29(2): 229-237.
[90] Uchino S, Kellum JA, Bellomo R, Doig GS, Morimatsu H, Morgera S, Schetz M, Tan I, Bouman C, Macedo E. Acute renal failure in critically ill patients: a multinational, multicenter study. Jama 2005; 294(7): 813-818.
[91] O'Grady JG, Alexander GJ, Hayllar KM, Williams R. Early indicators of prognosis in fulminant hepatic failure. Gastroenterology 1989; 97(2): 439-445.
[92] Antoine DJ, Sabbisetti VS, Francis B, Jorgensen AL, Craig DG, Simpson KJ, Bonventre JV, Park BK, Dear JW. Circulating Kidney Injury Molecule 1 Predicts Prognosis and Poor Outcome in Patients With Acetaminophen-Induced Liver Injury. Hepatology 2015; 62(2): 591-599.
[93] Bartel DP. MicroRNAs. Cell 2004; 116(2): 281-297.
[94] Winter J, Jung S, Keller S, Gregory RI, Diederichs S. Many roads to maturity: microRNA biogenesis pathways and their regulation. Nature cell biology 2009; 11(3): 228-234.

[95] Finnegan EF, Pasquinelli AE. MicroRNA biogenesis: regulating the regulators. Critical reviews in biochemistry

molecular biology 2013; 48(1): 51-68.
[96] Friedman RC, Farh KKH, Burge CB, Bartel DP. Most mammalian mRNAs are conserved targets of microRNAs. Genome Research 2008; 19(1): 92-105.
[97] Ha M, Kim VN. Regulation of microRNA biogenesis. Nature Reviews Molecular Cell Biology 2014; 15(8): 509-524.
[98] De Rie D, Abugessaisa I, Alam T, Arner E, Arner P, Ashoor H, Åström G, Babina M, Bertin N, Burroughs AM, Carlisle AJ, Daub CO, Detmar M, Deviatiiarov R, Fort A, Gebhard C, Goldowitz D, Guhl S, Ha TJ, Harshbarger J, Hasegawa A, Hashimoto K, Herlyn M, Heutink P, Hitchens KJ, Hon CC, Huang E, Ishizu Y, Kai C, Kasukawa T, Klinken P, Lassmann T, Lecellier C-H, Lee W, Lizio M, Makeev V, Mathelier A, Medvedeva YA, Mejhert N, Mungall CJ, Noma S, Ohshima M, Okada-Hatakeyama M, Persson H, Rizzu P, Roudnicky F, Sætrom P, Sato H, Severin J, Shin JW, Swoboda RK, Tarui H, Toyoda H, Vitting-Seerup K, Winteringham L, Yamaguchi Y, Yasuzawa K, Yoneda M, Yumoto N, Zabierowski S, Zhang PG, Wells CA, Summers KM, Kawaji H, Sandelin A, Rehli M, Hayashizaki Y, Carninci P, Forrest ARR, De Hoon MJL. An integrated expression atlas of miRNAs and their promoters in human and mouse. Nature Biotechnology 2017; 35(9): 872-878.
[99] Brueckner B, Stresemann C, Kuner R, Mund C, Musch T, Meister M, Sultmann H, Lyko F. The Human let-7a-3 Locus Contains an Epigenetically Regulated MicroRNA Gene with Oncogenic Function. Cancer Research 2007; 67(4): 1419-1423.
[100] O'Brien J, Hayder H, Zayed Y, Peng C. Overview of MicroRNA Biogenesis, Mechanisms of Actions, and Circulation. Front. Endocrinol. 2018; 9(402).
[101] Rahmani A, Saleki K, Javanmehr N, Khodaparast J, Saadat P, Nouri HR. Mesenchymal stem cell-derived extracellular vesicle-based therapies protect against coupled degeneration of the central nervous and vascular systems in stroke. Ageing Research Reviews 2020; 62: 101106.
[102] Borchert GM, Lanier W, Davidson BL. RNA polymerase III transcribes human microRNAs. Nature Structural & Molecular Biology 2006; 13(12): 1097-1101.
[103] Alarcón CR, Lee H, Goodarzi H, Halberg N, Tavazoie SF. N6-methyladenosine marks primary microRNAs for processing. Nature 2015; 519(7544): 482-485.
[104] Ghai V, Wang K. Recent progress toward the use of circulating microRNAs as clinical biomarkers. Archives of toxicology 2016; 90(12): 2959-2978.
[105] Gasser SM, Li E. Epigenetics and disease: pharmaceutical opportunities. Springer Science & Business Media, 2010.
[106] Zhang H, Kolb FA, Jaskiewicz L, Westhof E, Filipowicz W. Single Processing Center Models for Human Dicer and Bacterial RNase III. Cell 2004; 118(1): 57-68.
[107] Meister G, Landthaler M, Patkaniowska A, Dorsett Y, Teng G, Tuschl T. Human Argonaute2 Mediates RNA Cleavage Targeted by miRNAs and siRNAs. Molecular Cell 2004; 15(2): 185-197.
[108] Hedda, Ewan, Bushell M. Regulation of miRNA strand selection: follow the leader? Biochemical Society Transactions 2014; 42(4): 1135-1140.

[109] Jing Q, Huang S, Guth S, Zarubin T, Motoyama A, Chen J, Di Padova F, Lin S-C, Gram H, Han J. Involvement of MicroRNA in AU-Rich Element-Mediated mRNA Instability. Cell 2005; 120(5): 623-634.
[110] Felekkis K, Touvana E, Stefanou C, Deltas C. microRNAs: a newly described class of encoded molecules that play a role in health and disease. Hippokratia 2010; 14(4): 236-240.
[111] Mehta A, Baltimore D. MicroRNAs as regulatory elements in immune system logic. Nature Reviews Immunology 2016; 16(5): 279-294.
[112] Vasudevan S. Posttranscriptional Upregulation by MicroRNAs. Wiley Interdisciplinary Reviews: RNA 2012; 3(3): 311-330.
[113] Lewis BP, Burge CB, Bartel DP. Conserved Seed Pairing, Often Flanked by Adenosines, Indicates that Thousands of Human Genes are MicroRNA Targets. Cell 2005; 120(1): 15-20.
[114] Piletič K, Kunej T. MicroRNA epigenetic signatures in human disease. Archives of Toxicology 2016; 90(10): 2405-2419.
[115] Ali Syeda Z, Langden SSS, Munkhzul C, Lee M, Song SJ. Regulatory Mechanism of MicroRNA Expression in Cancer. Int J Mol Sci 2020; 21(5).
[116] Weber JA, Baxter DH, Zhang S, Huang DY, How Huang K, Jen Lee M, Galas DJ, Wang K. The microRNA spectrum in 12 body fluids. Clinical chemistry 2010; 56(11): 1733-1741.
[117] Arroyo JD, Chevillet JR, Kroh EM, Ruf IK, Pritchard CC, Gibson DF, Mitchell PS, Bennett CF, Pogosova-Agadjanyan EL, Stirewalt DL. Argonaute2 complexes carry a population of circulating microRNAs independent of vesicles in human plasma. Proceedings of the National Academy of Sciences 2011; 108(12): 5003-5008.
[118] Mitchell PS, Parkin RK, Kroh EM, Fritz BR, Wyman SK, Pogosova-Agadjanyan EL, Peterson A, Noteboom J, O'Briant KC, Allen A. Circulating microRNAs as stable blood-based markers for cancer detection. Proceedings of the National Academy of Sciences 2008; 105(30): 10513-10518.
[119] Vickers KC, Palmisano BT, Shoucri BM, Shamburek RD, Remaley AT. MicroRNAs are transported in plasma and delivered to recipient cells by high-density lipoproteins. Nature Cell Biology 2011; 13(4): 423-433.
[120] Turchinovich A, Weiz L, Langheinz A, Burwinkel B. Characterization of extracellular circulating microRNA. Nucleic Acids Research 2011; 39(16): 7223-7233.
[121] Wang K, Zhang S, Weber J, Baxter D, Galas DJ. Export of microRNAs and microRNA-protective protein by mammalian cells. Nucleic acids research 2010: gkq601.
[122] Wang Y, Liang H, Jin F, Yan X, Xu G, Hu H, Liang G, Zhan S, Hu X, Zhao Q. Injured liver-released miRNA-122 elicits acute pulmonary inflammation via activating alveolar macrophage TLR7 signaling pathway. Proceedings of the National Academy of Sciences 2019; 116(13): 6162-6171.
[123] Wang K, Zhang S, Marzolf B, Troisch P, Brightman A, Hu Z, Hood LE, Galas D. Circulating microRNAs, potential biomarkers for drug-induced liver injury. Proceedings of the National Academy of Sciences 2009; 106(11): 4402-4407.
[124] Kinoshita T, Yip KW, Spence T, Liu F-F. MicroRNAs in extracellular vesicles: potential cancer biomarkers. Journal of Human Genetics 2017; 62(1): 67-74.

[125] Pisitkun T, Shen R-F, Knepper MA. Identification and proteomic profiling of exosomes in human urine. Proceedings of the national academy of sciences of the United States of America 2004; 101(36): 13368-13373.
[126] Caby M-P, Lankar D, Vincendeau-Scherrer C, Raposo G, Bonnerot C. Exosomal-like vesicles are present in human blood plasma. International immunology 2005; 17(7): 879-887.
[127] Colombo M, Raposo G, Théry C. Biogenesis, Secretion, and Intercellular Interactions of Exosomes and Other Extracellular Vesicles. Annual Review of Cell and Developmental Biology 2014; 30(1): 255-289.
[128] Lee H, Zhang D, Zhu Z, Cruz CSD, Jin Y. Epithelial cell-derived microvesicles activate macrophages and promote inflammation via microvesicle-containing microRNAs. Scientific reports 2016; 6.
[129] Morrison E, Bailey M, Dear J. Renal extracellular vesicles: from physiology to clinical application. The Journal of physiology 2016; 594(20): 5735-5748.
[130] El Andaloussi S, Mäger I, Breakefield XO, Wood MJA. Extracellular vesicles: biology and emerging therapeutic opportunities. Nature Reviews Drug Discovery 2013; 12(5): 347-357.
[131] Braicu C, Tomuleasa C, Monroig P, Cucuianu A, Berindan-Neagoe I, Calin GA. Exosomes as divine messengers: are they the Hermes of modern molecular oncology? Cell Death Differ 2015; 22(1): 34-45.
[132] Liu T, Zhang Q, Zhang J, Li C, Miao Y-R, Lei Q, Li Q, Guo A-Y. EVmiRNA: a database of miRNA profiling in extracellular vesicles. Nucleic Acids Research 2019; 47(D1): D89-D93.
[133] Tkach M, Théry C. Communication by Extracellular Vesicles: Where We Are and Where We Need to Go. Cell 2016; 164(6): 1226-1232.
[134] Valadi H, Ekström K, Bossios A, Sjöstrand M, Lee JJ, Lötvall JO. Exosome-mediated transfer of mRNAs and microRNAs is a novel mechanism of genetic exchange between cells. Nature cell biology 2007; 9(6): 654-659.
[135] Nolte-'T Hoen ENM, Buermans HPJ, Waasdorp M, Stoorvogel W, Wauben MHM, 'T Hoen PAC. Deep sequencing of RNA from immune cell-derived vesicles uncovers the selective incorporation of small non-coding RNA biotypes with potential regulatory functions. Nucleic Acids Research 2012; 40(18): 9272-9285.
[136] Wang X, Gu H, Qin D, Yang L, Huang W, Essandoh K, Wang Y, Caldwell CC, Peng T, Zingarelli B. Exosomal miR-223 contributes to mesenchymal stem cell-elicited cardioprotection in polymicrobial sepsis. Scientific reports 2015; 5.
[137] Fong MY, Zhou W, Liu L, Alontaga AY, Chandra M, Ashby J, Chow A, O'Connor STF, Li S, Chin AR. Breast-cancer-secreted miR-122 reprograms glucose metabolism in premetastatic niche to promote metastasis. Nature cell biology 2015; 17(2): 183-194.
[138] Zhang Y, Liu D, Chen X, Li J, Li L, Bian Z, Sun F, Lu J, Yin Y, Cai X, Sun Q, Wang K, Ba Y, Wang Q, Wang D, Yang J, Liu P, Xu T, Yan Q, Zhang J, Zen K, Zhang CY. Secreted monocytic miR-150 enhances targeted endothelial cell migration. Mol Cell 2010; 39(1): 133-144.
[139] Ying W, Riopel M, Bandyopadhyay G, Dong Y, Birmingham A, Seo JB, Ofrecio JM, Wollam J, Hernandez-Carretero A, Fu W. Adipose tissue macrophage-derived

exosomal miRNAs can modulate in vivo and in vitro insulin sensitivity. Cell 2017; 171(2): 372-384. e312.
[140] Yin Y, Cai X, Chen X, Liang H, Zhang Y, Li J, Wang Z, Chen X, Zhang W, Yokoyama S, Wang C, Li L, Li L, Hou D, Dong L, Xu T, Hiroi T, Yang F, Ji H, Zhang J, Zen K, Zhang CY. Tumor-secreted miR-214 induces regulatory T cells: a major link between immune evasion and tumor growth. Cell Res 2014; 24(10): 1164-1180.
[141] Kosaka N, Iguchi H, Yoshioka Y, Takeshita F, Matsuki Y, Ochiya TJJoBC. Secretory mechanisms and intercellular transfer of microRNAs in living cells. 2010; 285(23): 17442-17452.
[142] Kogure T, Lin W-L, Yan IK, Braconi C, Patel T. Intercellular nanovesicle-mediated microRNA transfer: A mechanism of environmental modulation of hepatocellular cancer cell growth. Hepatology 2011; 54(4): 1237-1248.
[143] Oosthuyzen W, Scullion KM, Ivy JR, Morrison EE, Hunter RW, Lewis PJS, O'Duibhir E, Street JM, Caporali A, Gregory CD. Vasopressin regulates extracellular vesicle uptake by kidney collecting duct cells. Journal of the American Society of Nephrology 2016: ASN. 2015050568.
[144] Vickers KC, Palmisano BT, Shoucri BM, Shamburek RD, Remaley AT. MicroRNAs are transported in plasma and delivered to recipient cells by high-density lipoproteins. Nat Cell Biol 2011; 13(4): 423-433.
[145] Tabet F, Vickers KC, Cuesta Torres LF, Wiese CB, Shoucri BM, Lambert G, Catherinet C, Prado-Lourenco L, Levin MG, Thacker S, Sethupathy P, Barter PJ, Remaley AT, Rye K-A. HDL-transferred microRNA-223 regulates ICAM-1 expression in endothelial cells. Nature Communications 2014; 5(1).
[146] Wagner J, Riwanto M, Besler C, Knau A, Fichtlscherer S, Röxe T, Zeiher AM, Landmesser U, Dimmeler S. Characterization of Levels and Cellular Transfer of Circulating Lipoprotein-Bound MicroRNAs. Arteriosclerosis, Thrombosis, and Vascular Biology 2013; 33(6): 1392-1400.
[147] Thomou T, Mori MA, Dreyfuss JM, Konishi M, Sakaguchi M, Wolfrum C, Rao TN, Winnay JN, Garcia-Martin R, Grinspoon SK. Adipose-derived circulating miRNAs regulate gene expression in other tissues. Nature 2017; 542(7642): 450-455.
[148] Vu LT, Peng B, Zhang DX, Ma V, Mathey-Andrews CA, Lam CK, Kiomourtzis T, Jin J, McReynolds L, Huang L, Grimson A, Cho WC, Lieberman J, Le MT. Tumor-secreted extracellular vesicles promote the activation of cancer-associated fibroblasts via the transfer of microRNA-125b. Journal of Extracellular Vesicles 2019; 8(1): 1599680.
[149] Tian C, Gao L, Zimmerman MC, Zucker IH. Myocardial infarction-induced microRNA-enriched exosomes contribute to cardiac Nrf2 dysregulation in chronic heart failure. Am J Physiol Heart Circ Physiol 2018; 314(5): H928-h939.
[150] Xu B, Zhang Y, Du X-F, Li J, Zi H-X, Bu J-W, Yan Y, Han H, Du J-L. Neurons secrete miR-132-containing exosomes to regulate brain vascular integrity. Cell Research 2017; 27(7): 882-897.
[151] Zheng P, Chen L, Yuan X, Luo Q, Liu Y, Xie G, Ma Y, Shen L. Exosomal transfer of tumor-associated macrophage-derived miR-21 confers cisplatin resistance in gastric cancer cells. J Exp Clin Cancer Res 2017; 36(1): 53.

[152] De Gasperi R, Hamidi S, Harlow LM, Ksiezak-Reding H, Bauman WA, Cardozo CP. Denervation-related alterations and biological activity of miRNAs contained in exosomes released by skeletal muscle fibers. Scientific Reports 2017; 7(1): 12888.
[153] Viñas JL, Burger D, Zimpelmann J, Haneef R, Knoll W, Campbell P, Gutsol A, Carter A, Allan DS, Burns KD. Transfer of microRNA-486-5p from human endothelial colony forming cell–derived exosomes reduces ischemic kidney injury. Kidney International 2016; 90(6): 1238-1250.
[154] Zhang Z, Xu J, Chen Z, Wang H, Xue H, Yang C, Guo Q, Qi Y, Guo X, Qian M, Wang S, Qiu W, Gao X, Zhao R, Guo X, Li G. Transfer of microRNA via Macrophage-Derived Extracellular Vesicles Promotes Proneural-to-Mesenchymal Transition in Glioma Stem Cells. 2020: canimm.0759.2019.
[155] Fujita Y, Araya J, Ito S, Kobayashi K, Kosaka N, Yoshioka Y, Kadota T, Hara H, Kuwano K, Ochiya T. Suppression of autophagy by extracellular vesicles promotes myofibroblast differentiation in COPD pathogenesis. J Extracell Vesicles 2015; 4: 28388.
[156] Bronisz A, Wang Y, Nowicki MO, Peruzzi P, Ansari K, Ogawa D, Balaj L, De Rienzo G, Mineo M, Nakano I, Ostrowski MC, Hochberg F, Weissleder R, Lawler SE, Chiocca EA, Godlewski J. Extracellular vesicles modulate the glioblastoma microenvironment via a tumor suppression signaling network directed by miR-1. Cancer Res 2014; 74(3): 738-750.
[157] Wang J, Chen J, Sen S. MicroRNA as Biomarkers and Diagnostics. Journal of Cellular Physiology 2016; 231(1): 25-30.
[158] Ludwig N, Leidinger P, Becker K, Backes C, Fehlmann T, Pallasch C, Rheinheimer S, Meder B, Stähler C, Meese E. Distribution of miRNA expression across human tissues. Nucleic acids research 2016; 44(8): 3865-3877.
[159] Lawrie CH, Gal S, Dunlop HM, Pushkaran B, Liggins AP, Pulford K, Banham AH, Pezzella F, Boultwood J, Wainscoat JS, Hatton CSR, Harris AL. Detection of elevated levels of tumour-associated microRNAs in serum of patients with diffuse large B-cell lymphoma. British Journal of Haematology 2008; 141(5): 672-675.
[160] Liang Y, Ridzon D, Wong L, Chen C. Characterization of microRNA expression profiles in normal human tissues. BMC genomics 2007; 8(1): 166.
[161] Jopling C. Liver-specific microRNA-122: Biogenesis and function. J RNA biology 2012; 9(2): 137-142.
[162] Lagos-Quintana M, Rauhut R, Yalcin A, Meyer J, Lendeckel W, Tuschl T. Identification of tissue-specific microRNAs from mouse. J Current biology 2002; 12(9): 735-739.
[163] Thulin P, Nordahl G, Gry M, Yimer G, Aklillu E, Makonnen E, Aderaye G, Lindquist L, Mattsson CM, Ekblom B, Antoine DJ, Park BK, Linder S, Harrill AH, Watkins PB, Glinghammar B, Schuppe-Koistinen I. Keratin-18 and microRNA-122 complement alanine aminotransferase as novel safety biomarkers for drug-induced liver injury in two human cohorts. Liver International 2014; 34(3): 367-378.
[164] Chang J, Nicolas E, Marks D, Sander C, Lerro A, Buendia MA, Xu C, Mason WS, Moloshok T, Bort R. miR-122, a mammalian liver-specific microRNA, is processed from hcr mRNA and maydownregulate the high affinity cationic amino acid transporter CAT-1. RNA biology 2004; 1(2): 106-113.

[165] Hsu S-h, Wang B, Kota J, Yu J, Costinean S, Kutay H, Yu L, Bai S, La Perle K, Chivukula RR. Essential metabolic, anti-inflammatory, and anti-tumorigenic functions of miR-122 in liver. The Journal of clinical investigation 2012; 122(8): 2871-2883.
[166] Vliegenthart AD, Starkey Lewis P, Tucker CS, Del Pozo J, Rider S, Antoine DJ, Dubost V, Westphal M, Moulin P, Bailey MA. Retro-orbital blood acquisition facilitates circulating microRNA measurement in zebrafish with paracetamol hepatotoxicity. Zebrafish 2014; 11(3): 219-226.
[167] Tamai S, Iguchi T, Niino N, Mikamoto K, Sakurai K, Sayama A, Shimoda H, Takasaki W, Mori K. A monkey model of acetaminophen-induced hepatotoxicity; phenotypic similarity to human. The Journal of Toxicological Sciences 2017; 42(1): 73-84.
[168] Su Y-W, Chen X, Jiang Z-Z, Wang T, Wang C, Zhang Y, Wen J, Xue M, Zhu D, Zhang Y, Su Y-J, Xing T-Y, Zhang C-Y, Zhang L-Y. A panel of serum microRNAs as specific biomarkers for diagnosis of compound- and herb-induced liver injury in rats. PloS one 2012; 7(5): e37395.
[169] Harrill AH, Harrill AH, Eaddy JS, Rose K, Cullen JM, Ramanathan L, Wanaski S, Collins S, Ho Y, Watkins PB, Lecluyse EL. Liver biomarker and in vitro assessment confirm the hepatic origin of aminotransferase elevations lacking histopathological correlate in beagle dogs treated with GABAA receptor antagonist NP260. Toxicology and applied pharmacology 2014; 277(2): 131-137.
[170] Andersson P, Gidlöf O, Braun OO, Götberg M, van der Pals J, Olde B, Erlinge D. Plasma levels of liver-specific miR-122 is massively increased in a porcine cardiogenic shock model and attenuated by hypothermia. Shock 2012; 37(2): 234-238.
[171] Rivoli L, Vliegenthart A, Potter CM, Bragt JJ, Tzoumas N, Gallacher P, Farrah TE, Dhaun N, Dear JW. The effect of renal dysfunction and haemodialysis on circulating liver specific miR-122. British journal of clinical pharmacology 2016.
[172] Bala S, Petrasek J, Mundkur S, Catalano D, Levin I, Ward J, Alao H, Kodys K, Szabo G. Circulating microRNAs in exosomes indicate hepatocyte injury and inflammation in alcoholic, drug-induced, and inflammatory liver diseases. Hepatology 2012; 56(5): 1946-1957.
[173] Esau C, Davis S, Murray SF, Yu XX, Pandey SK, Pear M, Watts L, Booten SL, Graham M, McKay R, Subramaniam A, Propp S, Lollo BA, Freier S, Bennett CF, Bhanot S, Monia BP. miR-122 regulation of lipid metabolism revealed by in vivo antisense targeting. Cell Metabolism 2006; 3(2): 87-98.
[174] Krützfeldt J, Rajewsky N, Braich R, Rajeev KG, Tuschl T, Manoharan M, Stoffel M. Silencing of microRNAs in vivo with 'antagomirs'. Nature 2005; 438(7068): 685-689.
[175] Laudadio I, Manfroid I, Achouri Y, Schmidt D, Wilson MD, Cordi S, Thorrez L, Knoops L, Jacquemin P, Schuit F, Pierreux CE, Odom DT, Peers B, Lemaigre FP. A Feedback Loop Between the Liver-Enriched Transcription Factor Network and Mir-122 Controls Hepatocyte Differentiation. Gastroenterology 2012; 142(1): 119-129.
[176] Tsai WC, Hsu SD, Hsu CS, Lai TC, Chen SJ, Shen R, Huang Y, Chen HC, Lee CH, Tsai TF, Hsu MT, Wu JC, Huang HD, Shiao MS, Hsiao M, Tsou AP. MicroRNA-122 plays a critical role in liver homeostasis and hepatocarcinogenesis. J Clin Invest 2012; 122(8): 2884-2897.

[177] Bai S, Nasser MW, Wang B, Hsu S-H, Datta J, Kutay H, Yadav A, Nuovo G, Kumar P, Ghoshal K. MicroRNA-122 inhibits tumorigenic properties of hepatocellular carcinoma cells and sensitizes these cells to sorafenib. Journal of Biological Chemistry 2009; 284(46): 32015-32027.
[178] Fornari F, Gramantieri L, Giovannini C, Veronese A, Ferracin M, Sabbioni S, Calin GA, Grazi GL, Croce CM, Tavolari S, Chieco P, Negrini M, Bolondi L. MiR-122/Cyclin G1 Interaction Modulates p53 Activity and Affects Doxorubicin Sensitivity of Human Hepatocarcinoma Cells. Cancer Research 2009; 69(14): 5761-5767.
[179] Zeng C, Wang R, Li D, Lin X-J, Wei Q-K, Yuan Y, Wang Q, Chen W, Zhuang S-M. A novel GSK-3 beta-C/EBP alpha-miR-122-insulin-like growth factor 1 receptor regulatory circuitry in human hepatocellular carcinoma. Hepatology 2010; 52(5): 1702-1712.
[180] Coulouarn C, Factor VM, Andersen JB, Durkin ME, Thorgeirsson SS. Loss of miR-122 expression in liver cancer correlates with suppression of the hepatic phenotype and gain of metastatic properties. Oncogene 2009; 28(40): 3526-3536.
[181] Hornby RJ, Starkey Lewis P, Dear J, Goldring C, Park BK. MicroRNAs as potential circulating biomarkers of drug-induced liver injury: key current and future issues for translation to humans. Expert Review of Clinical Pharmacology 2014; 7(3): 349-362.
[182] Bandiera S, Pfeffer S, Baumert TF, Zeisel MB. miR-122 – A key factor and therapeutic target in liver disease. Journal of Hepatology 2015; 62(2): 448-457.
[183] Li J, Ghazwani M, Zhang Y, Lu J, Li J, Fan J, Gandhi CR, Li S. miR-122 regulates collagen production via targeting hepatic stellate cells and suppressing P4HA1 expression. Journal of Hepatology 2013; 58(3): 522-528.
[184] Zeng C, Wang Y-L, Xie C, Sang Y, Li T-J, Zhang M, Wang R, Zhang Q, Zheng L, Zhuang S-M. Identification of a novel TGF-β-miR-122-fibronectin 1/serum response factor signaling cascade and its implication in hepatic fibrogenesis. Oncotarget 2015; 6(14): 12224-12233.
[185] Jopling CL. Modulation of Hepatitis C Virus RNA Abundance by a Liver-Specific MicroRNA. Science 2005; 309(5740): 1577-1581.
[186] Shimakami T, Yamane D, Welsch C, Hensley L, Jangra RK, Lemon SM. Base Pairing between Hepatitis C Virus RNA and MicroRNA 122 3' of Its Seed Sequence Is Essential for Genome Stabilization and Production of Infectious Virus. J Virol. 2012; 86(13): 7372-7383.
[187] Xu H, He J-H, Xiao Z-D, Zhang Q-Q, Chen Y-Q, Zhou H, Qu L-H. Liver-enriched transcription factors regulate MicroRNA-122 that targets CUTL1 during liver development. Hepatology 2010; 52(4): 1431-1442.
[188] Gatfield D, Le Martelot G, Vejnar CE, Gerlach D, Schaad O, Fleury-Olela F, Ruskeepaa AL, Oresic M, Esau CC, Zdobnov EM, Schibler U. Integration of microRNA miR-122 in hepatic circadian gene expression. Genes & Development 2009; 23(11): 1313-1326.
[189] Valdmanis PN, Kim HK, Chu K, Zhang F, Xu J, Munding EM, Shen J, Kay MA. miR-122 removal in the liver activates imprinted microRNAs and enables more effective microRNA-mediated gene repression. Nature Communications 2018; 9(1): 5321.

[190] Lou G, Song X, Yang F, Wu S, Wang J, Chen Z, Liu Y. Exosomes derived from miR-122-modified adipose tissue-derived MSCs increase chemosensitivity of hepatocellular carcinoma. Journal of Hematology & Oncology 2015; 8(1).
[191] Momen-Heravi F, Bala S, Kodys K, Szabo G. Exosomes derived from alcohol-treated hepatocytes horizontally transfer liver specific miRNA-122 and sensitize monocytes to LPS. Scientific Reports 2015; 5(1): 9991.
[192] Chai C, Rivkin M, Berkovits L, Simerzin A, Zorde-Khvalevsky E, Rosenberg N, Klein S, Yaish D, Durst R, Shpitzen S, Udi S, Tam J, Heeren J, Worthmann A, Schramm C, Kluwe J, Ravid R, Hornstein E, Giladi H, Galun E. Metabolic Circuit Involving Free Fatty Acids, microRNA 122, and Triglyceride Synthesis in Liver and Muscle Tissues. Gastroenterology 2017; 153(5): 1404-1415.
[193] Rivkin M, Simerzin A, Zorde-Khvalevsky E, Chai C, Yuval JB, Rosenberg N, Harari-Steinfeld R, Schneider R, Amir G, Condiotti R. Inflammation-Induced Expression and Secretion of MicroRNA 122 Leads to Reduced Blood Levels of Kidney-Derived Erythropoietin and Anemia. Gastroenterology 2016; 151(5): 999-1010. e1013.
[194] Brezis M, Rosen S. Hypoxia of the Renal Medulla — Its Implications for Disease. New England Journal of Medicine 1995; 332(10): 647-655.
[195] Lohr JW, Willsky GR, Acara MA. Renal Drug Metabolism. 1998; 50(1): 107-142.
[196] Lorz C. Paracetamol-Induced Renal Tubular Injury: A Role for ER Stress. Journal of the American Society of Nephrology 2004; 15(2): 380-389.
[197] Perazella MA. Renal vulnerability to drug toxicity. Clinical Journal of the American Society of Nephrology 2009; 4(7): 1275-1283.
[198] Miller RP, Tadagavadi RK, Ramesh G, Reeves WB. Mechanisms of cisplatin nephrotoxicity. Toxins 2010; 2(11): 2490-2518.
[199] Pabla N, Dong Z. Cisplatin nephrotoxicity: mechanisms and renoprotective strategies. Kidney international 2008; 73(9): 994-1007.
[200] Lee CG, Kim JG, Kim HJ, Kwon H-K, Cho IJ, Choi DW, Lee WH, Kim WD, Hwang SJ, Choi S. Discovery of an integrative network of microRNAs and transcriptomics changes for acute kidney injury. Kidney international 2014; 86(5): 943-953.
[201] Matthews O, Morrison EE, Tranter JD, Starkey Lewis P, Toor IS, Srivastava A, Sargeant R, Rollison H, Matchett KP, Kendall TJ, Gray GA, Goldring C, Park K, Denby L, Dhaun N, Bailey MA, Henderson NC, Williams D, Dear JW. Transfer of hepatocellular microRNA regulates cytochrome P450 2E1 in renal tubular cells. EBioMedicine 2020; 62: 103092.
[202] Malato Y, Naqvi S, Schürmann N, Ng R, Wang B, Zape J, Kay MA, Grimm D, Willenbring H. Fate tracing of mature hepatocytes in mouse liver homeostasis and regeneration. The Journal of clinical investigation 2011; 121(12): 4850-4860.
[203] Chowdhary V, Teng K-y, Thakral S, Zhang B, Lin C-h, Wani N, Bruschweiler-Li L, Zhang X, James L, Yang D. miRNA-122 Protects Mice and Human Hepatocytes from Acetaminophen Toxicity by Regulating Cytochrome P450 Family 1 Subfamily A Member 2 and Family 2 Subfamily E Member 1 Expression. The American journal of pathology 2017; 187(12): 2758-2774.
[204] Mossanen J, Tacke F. Acetaminophen-induced acute liver injury in mice. J Laboratory animals 2015; 49: 30-36.

[205] Antoine DJ, Williams DP, Kipar A, Laverty H, Park BK. Diet restriction inhibits apoptosis and HMGB1 oxidation and promotes inflammatory cell recruitment during acetaminophen hepatotoxicity. Molecular medicine 2010; 16(11-12): 479-490.
[206] Jensen TL, Kiersgaard MK, Sørensen DB, Mikkelsen LF. Fasting of mice: a review. Lab Anim 2013; 47(4): 225-240.
[207] Brillant N, Elmasry M, Burton NC, Rodriguez JM, Sharkey JW, Fenwick S, Poptani H, Kitteringham NR, Goldring CE, Kipar A. Dynamic and accurate assessment of acetaminophen-induced hepatotoxicity by integrated photoacoustic imaging and mechanistic biomarkers in vivo. Toxicology applied pharmacology 2017; 332: 64-74.
[208] Henderson NC, Arnold TD, Katamura Y, Giacomini MM, Rodriguez JD, McCarty JH, Pellicoro A, Raschperger E, Betsholtz C, Ruminski PG. Targeting of α v integrin identifies a core molecular pathway that regulates fibrosis in several organs. Nature medicine 2013; 19(12): 1617.
[209] Dobie R, Wilson-Kanamori JR, Henderson BE, Smith JR, Matchett KP, Portman JR, Wallenborg K, Picelli S, Zagorska A, Pendem SV. Single-Cell Transcriptomics Uncovers Zonation of Function in the Mesenchyme during Liver Fibrosis. Cell reports 2019; 29(7): 1832-1847. e1838.
[210] Henderson NC, Mackinnon AC, Farnworth SL, Poirier F, Russo FP, Iredale JP, Haslett C, Simpson KJ, Sethi T. Galectin-3 regulates myofibroblast activation and hepatic fibrosis. Proc Natl Acad Sci U S A 2006; 103(13): 5060-5065.
[211] Livak KJ, Schmittgen TD. Analysis of relative gene expression data using real-time quantitative PCR and the 2− ΔΔCT method. Methods 2001; 25(4): 402-408.
[212] Bergmeyer H, Scheibe P, Wahlefeld A. Optimization of methods for aspartate aminotransferase and alanine aminotransferase. Clinical chemistry 1978; 24(1): 58-73.
[213] Schindelin J, Arganda-Carreras I, Frise E, Kaynig V, Longair M, Pietzsch T, Preibisch S, Rueden C, Saalfeld S, Schmid B, Tinevez J-Y, White DJ, Hartenstein V, Eliceiri K, Tomancak P, Cardona A. Fiji: an open-source platform for biological-image analysis. Nature Methods 2012; 9(7): 676-682.
[214] Miller L. Analyzing gels and western blots with ImageJ. Blog Archive 2010; 2020(18/02/2020).
[215] Bieche I, Narjoz C, Asselah T, Vacher S, Marcellin P, Lidereau R, Beaune P, de Waziers I. Reverse transcriptase-PCR quantification of mRNA levels from cytochrome (CYP) 1, CYP2 and CYP3 families in 22 different human tissues. Pharmacogenetics genomics 2007; 17(9): 731-742.
[216] Foster AJ, Chouhan B, Regan SL, Rollison H, Amberntsson S, Andersson LC, Srivastava A, Darnell M, Cairns J, Lazic SE, Jang K-J, Petropolis DB, Kodella K, Rubins JE, Williams D, Hamilton GA, Ewart L, Morgan P. Integrated in vitro models for hepatic safety and metabolism: evaluation of a human Liver-Chip and liver spheroid. Archives of Toxicology 2019; 93(4): 1021-1037.
[217] Jang K-J, Otieno MA, Ronxhi J, Lim H-K, Ewart L, Kodella KR, Petropolis DB, Kulkarni G, Rubins JE, Conegliano D, Nawroth J, Simic D, Lam W, Singer M, Barale E, Singh B, Sonee M, Streeter AJ, Manthey C, Jones B, Srivastava A, Andersson LC, Williams D, Park H, Barrile R, Sliz J, Herland A, Haney S, Karalis K, Ingber DE, Hamilton

GA. Reproducing human and cross-species drug toxicities using a Liver-Chip. Science Translational Medicine 2019; 11(517): eaax5516.
[218] Morrison EE. Development of circulatory microRNAs as markers of organ injury and mediators of inter-organ signalling. Cardiovascular Science 2018; Doctor of Philosophy.
[219] Denli AM, Tops BB, Plasterk RH, Ketting RF, Hannon GJ. Processing of primary microRNAs by the Microprocessor complex. Nature 2004; 432(7014): 231-235.
[220] Murchison EP, Partridge JF, Tam OH, Cheloufi S, Hannon GJ. Characterization of Dicer-deficient murine embryonic stem cells. Proceedings of the National Academy of Sciences 2005; 102(34): 12135-12140.
[221] Kim Y-K, Kim B, Kim VN. Re-evaluation of the roles of DROSHA, Exportin 5, and DICER in microRNA biogenesis. Proc Natl Acad Sci USA 2016; 113(13): E1881-E1889.
[222] Kanellopoulou C, Muljo SA, Kung AL, Ganesan S, Drapkin R, Jenuwein T, Livingston DM, Rajewsky KJG, development. Dicer-deficient mouse embryonic stem cells are defective in differentiation and centromeric silencing. 2005; 19(4): 489-501.
[223] Bernstein E, Kim SY, Carmell MA, Murchison EP, Alcorn H, Li MZ, Mills AA, Elledge SJ, Anderson KV, Hannon GJ. Dicer is essential for mouse development. Nature genetics 2003; 35(3): 215-217.
[224] Fu G, Brkić J, Hayder H, Peng C. MicroRNAs in human placental development and pregnancy complications. International journal of molecular sciences 2013; 14(3): 5519-5544.
[225] Sekine S, Ogawa R, Ito R, Hiraoka N, McManus MT, Kanai Y, Hebrok M. Disruption of Dicer1 induces dysregulated fetal gene expression and promotes hepatocarcinogenesis. Gastroenterology 2009; 136(7): 2304-2315. e2304.
[226] Hand NJ, Master ZR, Le Lay J, Friedman JR. Hepatic function is preserved in the absence of mature microRNAs. Hepatology 2009; 49(2): 618-626.
[227] Mattis AN, Song G, Hitchner K, Kim RY, Lee AY, Sharma AD, Malato Y, McManus MT, Esau CC, Koller E. A screen in mice uncovers repression of lipoprotein lipase by microRNA-29a as a mechanism for lipid distribution away from the liver. Hepatology 2015; 61(1): 141-152.
[228] Nakai H, Fuess S, Storm TA, Muramatsu S-i, Nara Y, Kay MA. Unrestricted hepatocyte transduction with adeno-associated virus serotype 8 vectors in mice. Journal of virology 2005; 79(1): 214-224.
[229] Muzumdar MD, Tasic B, Miyamichi K, Li L, Luo L. A global double-fluorescent Cre reporter mouse. Genesis 2007; 45(9): 593-605.
[230] Boldin MP, Taganov KD, Rao DS, Yang L, Zhao JL, Kalwani M, Garcia-Flores Y, Luong M, Devrekanli A, Xu J. miR-146a is a significant brake on autoimmunity, myeloproliferation, and cancer in mice. The Journal of experimental medicine 2011; 208(6): 1189-1201.
[231] Guo Z, Maki M, Ding R, Yang Y, Xiong L. Genome-wide survey of tissue-specific microRNA and transcription factor regulatory networks in 12 tissues. Scientific reports 2014; 4: 5150.
[232] Zhang C, Liang S, Cheng S, Li W, Wang X, Zheng C, Zeng C, Shi S, Xie L, Zen K. Urinary miR-196a predicts disease progression in patients with chronic kidney disease. Journal of translational medicine 2018; 16(1): 91.

[233] Koscianska E, Starega-Roslan J, Krzyzosiak WJ. The role of Dicer protein partners in the processing of microRNA precursors. PloS one 2011; 6(12).
[234] Robles-Díaz M, Medina-Caliz I, Stephens C, Andrade RJ, Lucena MI. Biomarkers in DILI: one more step forward. Frontiers in pharmacology 2016; 7: 267.
[235] Wong FW-Y, Chan W-Y, Lee SS-T. Resistance to carbon tetrachloride-induced hepatotoxicity in mice which lack CYP2E1 expression. Toxicology applied pharmacology 1998; 153(1): 109-118.
[236] Xu J, Ma HY, Liang S, Sun M, Karin G, Koyama Y, Hu R, Quehenberger O, Davidson NO, Dennis EA, Kisseleva T, Brenner DA. The role of human cytochrome P450 2E1 in liver inflammation and fibrosis. Hepatol Commun 2017; 1(10): 1043-1057.
[237] Manibusan MK, Odin M, Eastmond DA. Postulated Carbon Tetrachloride Mode of Action: A Review. Journal of Environmental Science and Health, Part C 2007; 25(3): 185-209.
[238] Scholten D, Trebicka J, Liedtke C, Weiskirchen R. The carbon tetrachloride model in mice. Laboratory Animals 2015; 49(1_suppl): 4-11.
[239] Krauskopf J, Caiment F, Claessen SM, Johnson KJ, Warner RL, Schomaker SJ, Burt DA, Aubrecht J, Kleinjans JC. Application of High-Throughput Sequencing to Circulating microRNAs Reveals Novel Biomarkers for Drug-Induced Liver Injury. Toxicological Sciences 2015; 143(2): 268-276.
[240] Schueller F, Roy S, Vucur M, Trautwein C, Luedde T, Roderburg C. The role of miRNAs in the pathophysiology of liver diseases and toxicity. International journal of molecular sciences 2018; 19(1): 261.
[241] Roy S, Benz F, Alder J, Bantel H, Janssen J, Vucur M, Gautheron J, Schneider A, Schüller F, Loosen S, Luedde M, Koch A, Tacke F, Luedde T, Trautwein C, Roderburg C. Down-regulation of miR-192-5p protects from oxidative stress-induced acute liver injury. Clinical Science 2016; 130(14): 1197-1207.
[242] Wang Y-Q, Lan Y-Y, Guo Y-C, Yuan Q-W, Liu P. Down-regulation of microRNA-138 improves immunologic function via negatively targeting p53 by regulating liver macrophage in mice with acute liver failure. Bioscience reports 2019; 39(7).
[243] Zhang SY, Surapureddi S, Coulter S, Ferguson SS, Goldstein JA. Human CYP2C8 is post-transcriptionally regulated by microRNAs 103 and 107 in human liver. Mol Pharmacol 2012; 82(3): 529-540.
[244] Mohri T, Nakajima M, Fukami T, Takamiya M, Aoki Y, Yokoi T. Human CYP2E1 is regulated by miR-378. Biochem Pharmacol 2010; 79(7): 1045-1052.
[245] Tsuchiya Y, Nakajima M, Takagi S, Taniya T, Yokoi T. MicroRNA Regulates the Expression of Human Cytochrome P450 1B1. Cancer Research 2006; 66(18): 9090-9098.
[246] Gill P, Bhattacharyya S, McCullough S, Letzig L, Mishra PJ, Luo C, Dweep H, James L. MicroRNA regulation of CYP 1A2, CYP3A4 and CYP2E1 expression in acetaminophen toxicity. Scientific reports 2017; 7(1): 12331.
[247] Thummel KE, Lee CA, Kunze KL, Nelson SD, Slattery JT. Oxidation of acetaminophen to N-acetyl-p-aminobenzoquinone imine by human CYP3A4. Biochem Pharmacol 1993; 45(8): 1563-1569.

[248] Laine JE, Auriola S, Pasanen M, Juvonen RO. Acetaminophen bioactivation by human cytochrome P450 enzymes and animal microsomes. Xenobiotica 2009; 39(1): 11-21.
[249] Hinson JA, Roberts DW, James LP. Mechanisms of Acetaminophen-Induced Liver Necrosis. Adverse Drug Reactions 2010: 369-405.
[250] Pratt DS, Kaplan MM. Evaluation of Abnormal Liver-Enzyme Results in Asymptomatic Patients. N Engl J Med 2000; 342(17): 1266-1271.
[251] Soldin OP, Mattison DR. Sex Differences in Pharmacokinetics and Pharmacodynamics. Clinical Pharmacokinetics 2009; 48(3): 143-157.
[252] Dai G, He L, Chou N, Wan Y-JY. Acetaminophen Metabolism Does Not Contribute to Gender Difference in Its Hepatotoxicity in Mouse. Toxicological Sciences 2006; 92(1): 33-41.
[253] Mohar I, Stamper BD, Rademacher PM, White CC, Nelson SD, Kavanagh TJ. Acetaminophen-induced liver damage in mice is associated with gender-specific adduction of peroxiredoxin-6. Redox Biol 2014; 2: 377-387.
[254] Du K, Williams CD, McGill MR, Jaeschke H. Lower susceptibility of female mice to acetaminophen hepatotoxicity: Role of mitochondrial glutathione, oxidant stress and c-jun N-terminal kinase. Toxicol Appl Pharmacol 2014; 281(1): 58-66.
[255] Bhushan B, Walesky C, Manley M, Gallagher T, Borude P, Edwards G, Monga SP, Apte U. Pro-regenerative signaling after acetaminophen-induced acute liver injury in mice identified using a novel incremental dose model. Am J Pathol 2014; 184(11): 3013-3025.
[256] Jaeschke H, Williams CD, Ramachandran A, Bajt ML. Acetaminophen hepatotoxicity and repair: the role of sterile inflammation and innate immunity. Liver Int 2012; 32(1): 8-20.
[257] Cearley CN, Wolfe JH. Transduction characteristics of adeno-associated virus vectors expressing cap serotypes 7, 8, 9, and Rh10 in the mouse brain. Molecular Therapy 2006; 13(3): 528-537.
[258] Heymann F, Hamesch K, Weiskirchen R, Tacke F. The concanavalin A model of acute hepatitis in mice. Lab Anim 2015; 49: 12-20.
[259] Margalit M, Abu Gazala S, Alper R, Elinav E, Klein A, Doviner V, Sherman Y, Thalenfeld B, Engelhardt D, Rabbani E, Ilan Y. Glucocerebroside treatment ameliorates ConA hepatitis by inhibition of NKT lymphocytes. Am J Physiol Gastrointest Liver Physiol 2005; 289(5): G917-925.
[260] Mizuhara H, O'Neill E, Seki N, Ogawa T, Kusunoki C, Otsuka K, Satoh S, Niwa M, Senoh H, Fujiwara H. T cell activation-associated hepatic injury: mediation by tumor necrosis factors and protection by interleukin 6. J Exp Med 1994; 179(5): 1529-1537.
[261] Tiegs G, Hentschel J, Wendel A. A T cell-dependent experimental liver injury in mice inducible by concanavalin A. J Clin Invest 1992; 90(1): 196-203.
[262] Kagawa T, Shirai Y, Oda S, Yokoi T. Identification of Specific MicroRNA Biomarkers in Early Stages of Hepatocellular Injury, Cholestasis, and Steatosis in Rats. Toxicological Sciences 2018; 166(1): 228-239.
[263] Ono R, Yoshioka Y, Furukawa Y, Naruse M, Kuwagata M, Ochiya T, Kitajima S, Hirabayashi Y. Novel hepatotoxicity biomarkers of extracellular vesicle (EV)-associated miRNAs induced by CCl4. Toxicology Reports 2020; 7: 685-692.

[264] Wolenski FS, Shah P, Sano T, Shinozawa T, Bernard H, Gallacher MJ, Wyllie SD, Varrone G, Cicia LA, Carsillo ME, Fisher CD, Ottinger SE, Koenig E, Kirby PJ. Identification of microRNA biomarker candidates in urine and plasma from rats with kidney or liver damage. J Appl Toxicol 2017; 37(3): 278-286.
[265] Wienkers LC, Heath TG. Predicting in vivo drug interactions from in vitro drug discovery data. Nat Rev Drug Discov 2005; 4(10): 825-833.
[266] Nelson DR, Zeldin DC, Hoffman SM, Maltais LJ, Wain HM, Nebert DW. Comparison of cytochrome P450 (CYP) genes from the mouse and human genomes, including nomenclature recommendations for genes, pseudogenes and alternative-splice variants. Pharmacogenetics 2004; 14(1): 1-18.
[267] Lieber CS. Cytochrome P-4502E1: its physiological and pathological role. Physiol Rev. 1997; 77(2): 517-544.
[268] Guengerich FP. Characterization of human cytochrome P450 enzymes. The FASEB Journal 1992; 6(2): 745-748.
[269] Proteinatlas.org. Tissue Expression of CYP2E1.
[270] Boon R, Kumar M, Tricot T, Elia I, Ordovas L, Jacobs F, One J, De Smedt J, Eelen G, Bird M, Roelandt P, Doglioni G, Vriens K, Rossi M, Vazquez MA, Vanwelden T, Chesnais F, El Taghdouini A, Najimi M, Sokal E, Cassiman D, Snoeys J, Monshouwer M, Hu W-S, Lange C, Carmeliet P, Fendt S-M, Verfaillie CM. Amino acid levels determine metabolism and CYP450 function of hepatocytes and hepatoma cell lines. Nature Communications 2020; 11(1): 1393.
[271] Chen K, Guo N, Zhang R, Wei C, Guo R. CYP2E1 and miRNA-378a-3p contribute to acetaminophen- or tripterygium glycosides-induced hepatotoxicity. Basic & Clinical Pharmacology & Toxicology 2020; 126(2): 153-165.
[272] Kugler N, Klein K, Zanger UM. MiR-155 and other microRNAs downregulate drug metabolizing cytochromes P450 in inflammation. Biochemical Pharmacology 2020; 171: 113725.
[273] Elmen J, Lindow M, Silahtaroglu A, Bak M, Christensen M, Lind-Thomsen A, Hedtjärn M, Hansen JB, Hansen HF, Straarup EM. Antagonism of microRNA-122 in mice by systemically administered LNA-antimiR leads to up-regulation of a large set of predicted target mRNAs in the liver. Nucleic acids research 2008; 36(4): 1153-1162.
[274] Zeng Y, Lv Y, Tao L, Ma J, Zhang H, Xu H, Xiao B, Shi Q, Ma K, Chen L. G6PC3, ALDOA and CS induction accompanies mir-122 down-regulation in the mechanical asphyxia and can serve as hypoxia biomarkers. Oncotarget 2016; 7(46): 74526.
[275] Xie J, Ameres SL, Friedline R, Hung J-H, Zhang Y, Xie Q, Zhong L, Su Q, He R, Li M, Li H, Mu X, Zhang H, Broderick JA, Kim JK, Weng Z, Flotte TR, Zamore PD, Gao G. Long-term, efficient inhibition of microRNA function in mice using rAAV vectors. Nat Methods. 2012; 9(4): 403-409.
[276] Prozialeck WC, Edwards JR, Lamar PC, Liu J, Vaidya VS, Bonventre JV. Expression of kidney injury molecule-1 (Kim-1) in relation to necrosis and apoptosis during the early stages of Cd-induced proximal tubule injury. Toxicology and Applied Pharmacology 2009; 238(3): 306-314.
[277] Castoldi M, Spasic MV, Altamura S, Elmén J, Lindow M, Kiss J, Stolte J, Sparla R, D'Alessandro LA, Klingmüller U. The liver-specific microRNA miR-122 controls

systemic iron homeostasis in mice. The Journal of clinical investigation 2011; 121(4): 1386-1396.
[278] Zhou S-F, Wang B, Yang L-P, Liu J-P. Structure, function, regulation and polymorphism and the clinical significance of human cytochrome P450 1A2. Drug Metabolism Reviews 2010; 42(2): 268-354.
[279] Sarkar J, Qi C, Guo D, Ahmed MR, Jia Y, Usuda N, Viswakarma N, Rao MS, Reddy JK. Transcription Coactivator PRIP, the Peroxisome Proliferator-Activated Receptor (PPAR)-Interacting Protein, Is Redundant for the Function of Nuclear Receptors PPARα and CAR, the Constitutive Androstane Receptor, in Mouse Liver. Gene Expression 2006; 13(4): 255-269.
[280] Achour B, Barber J, Rostami-Hodjegan A. Expression of Hepatic Drug-Metabolizing Cytochrome P450 Enzymes and Their Intercorrelations: A Meta-Analysis. Drug Metabolism and Disposition 2014; 42(8): 1349-1356.
[281] McKinnon RA, Hall PDLM, Quattrochi LC, Tukey RH, McManus ME. Localization of CYP1A1 and CYP1A2 messenger RNA in normal human liver and in hepatocellular carcinoma byin situ hybridization. Hepatology 1991; 14(5): 848-856.
[282] Forkert PG, Massey TE, Jones AB, Park SS, Gelboin HV, Anderson LM. Distribution of cytochrome CYP2E1 in murine liver after ethanol and acetone administration. Carcinogenesis 1991; 12(12): 2259-2268.
[283] Sapone A, Affatato A, Canistro D, Broccoli M, Trespidi S, Pozzetti L, Biagi GL, Cantelli-Forti G, Paolini M. Induction and suppression of cytochrome P450 isoenzymes and generation of oxygen radicals by procymidone in liver, kidney and lung of CD1 mice. Mutation Research/Fundamental and Molecular Mechanisms of Mutagenesis 2003; 527(1-2): 67-80.
[284] Starkey JM, Zhao Y, Sadygov RG, Haidacher SJ, Lejeune WS, Dey N, Luxon BA, Kane MA, Napoli JL, Denner L, Tilton RG. Altered Retinoic Acid Metabolism in Diabetic Mouse Kidney Identified by 18O Isotopic Labeling and 2D Mass Spectrometry. PLoS ONE 2010; 5(6): e11095.
[285] Ronis MJ, Huang J, Longo V, Tindberg N, Ingelman-Sundberg M, Badger TM. Expression and distribution of cytochrome P450 enzymes in male rat kidney: effects of ethanol, acetone and dietary conditions. Biochem Pharmacol 1998; 55(2): 123-129.
[286] Lucas D, Ferrara R, Gonzalez E, Bodenez P, Albores A, Manno M, Berthou F. Chlorzoxazone, a selective probe for phenotyping CYP2E1 in humans. Pharmacogenetics 1999; 9(3): 377-388.
[287] John K, Hadem J, Krech T, Wahl K, Manns MP, Dooley S, Batkai S, Thum T, Schulze-Osthoff K, Bantel H. MicroRNAs play a role in spontaneous recovery from acute liver failure. Hepatology 2014; 60(4): 1346-1355.
[288] Prescott LF, Prescott L. Paracetamol (acetaminophen): a critical bibliographic review. Taylor & Francis London, 1996.
[289] Betrosian AP, Agarwal B, Douzinas EE. Acute renal dysfunction in liver diseases. World J Gastroenterol 2007; 13(42): 5552-5559.
[290] Sun Y, Koo S, White N, Peralta E, Esau C, Dean NM, Perera RJ. Development of a micro-array to detect human and mouse microRNAs and characterization of expression in human organs. Nucleic acids research 2004; 32(22): e188-e188.

[291] Valdmanis PN, Gu S, Chu K, Jin L, Zhang F, Munding EM, Zhang Y, Huang Y, Kutay H, Ghoshal K, Lisowski L, Kay MA. RNA interference–induced hepatotoxicity results from loss of the first synthesized isoform of microRNA-122 in mice. Nature Medicine 2016; 22(5): 557-562.
[292] Bellomo R, Kellum JA, Ronco C. Acute kidney injury. The Lancet 2012; 380(9843): 756-766.
[293] Molitoris BA, Reilly ES. Quantifying Glomerular Filtration Rates in Acute Kidney Injury: A Requirement for Translational Success. Seminars in Nephrology 2016; 36(1): 31-41.
[294] Woolbright B. The impact of sterile inflammation in acute liver injury. Journal of Clinical and Translational Research 2017.
[295] Wang M, You Q, Lor K, Chen F, Gao B, Ju C. Chronic alcohol ingestion modulates hepatic macrophage populations and functions in mice. Journal of Leukocyte Biology 2014; 96(4): 657-665.
[296] Moore JK, Mackinnon AC, Man TY, Manning JR, Forbes SJ, Simpson KJ. Patients with the worst outcomes after paracetamol (acetaminophen)-induced liver failure have an early monocytopenia. Alimentary Pharmacology & Therapeutics 2017; 45(3): 443-454.
[297] Williams CD, Bajt ML, Sharpe MR, McGill MR, Farhood A, Jaeschke H. Neutrophil activation during acetaminophen hepatotoxicity and repair in mice and humans. Toxicology and Applied Pharmacology 2014; 275(2): 122-133.

I Appendix

I.1 Dicer mRNA analysis

I.1.1 Dicer mRNA expression in the liver

Expression of Dicer mRNA was determined using RT-qPCR. Dicer was measured in the livers of the baseline, Null-AAV8 and Cre-AAV8 treated *Dicer1*$^{flox/flox}$ mice (Figure 6.1). Figure 6.1, shows both the Null-AAV8 and Cre-AAV8 mice have comparable expression to the baseline mice (week 0, dotted line). Statistical comparisions determined the Cre-AAV8 expression was not statistically different when compared to the Null-AAV8 mice (Linear regression: Cre Slope= 3.7 week^{-1}; Cre slope vs zero, p=0.5; Null vs Cre slope, p=0.5).

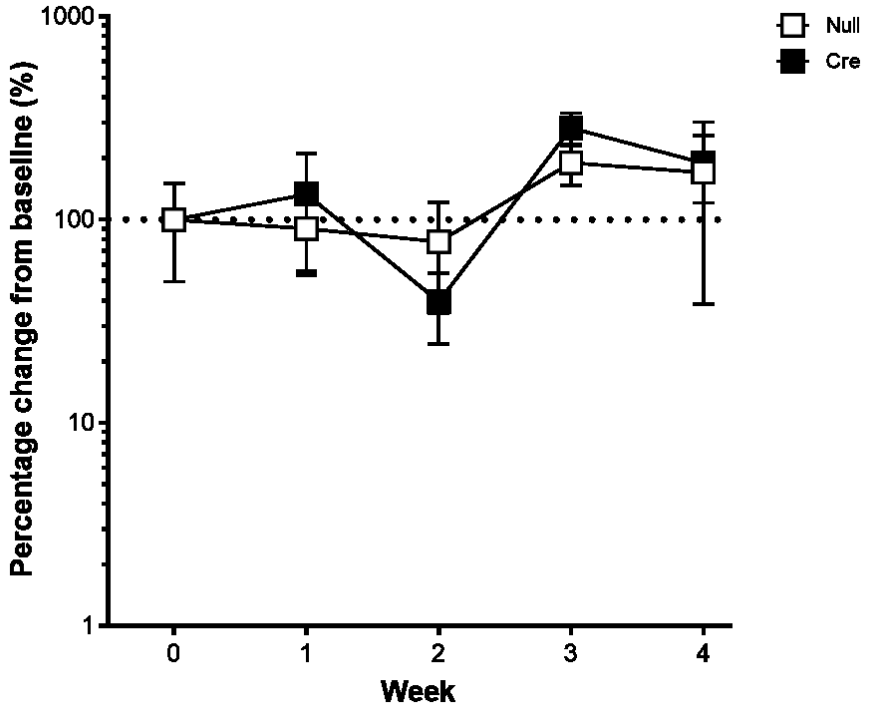

Figure 6.1 Dicer mRNA expression in the liver of the *Dicer1*$^{flox/flox}$ mice

Liver Dicer mRNA expression quantified by RT-qPCR. Dicer mRNA expression was measured in the baseline (untreated, week 0, dotted line), Null-AAV8 treated (white squares) and Cre-AAV8 treated (black squares) Dicer $^{flox/flox}$ *mice. MRNA measurements were carried out from week 1 to 4 in the Null and Cre-AAV8 treated mice. Each point was normalised to Hprt and then represented as a percentage in relation to the baseline mice. Error bars represent mean ±SD, n=5 (W0, Null W3, Cre W1 n=4). Linear regression was used to determine whether Cre-AAV8 treated mice have significantly different expression to the Null-AAV8 treated mice (p=0.5).Dicer mRNA is unchanged in the spleen following Null and Cre-AAV8 injection*

I.1.1 Dicer mRNA in the spleen

Dicer mRNA was determined in the spleen using RT-qPCR. Dicer was measured in the spleen of the baseline, Null-AAV8 and Cre-AAV8 treated *Dicer1*$^{flox/flox}$ mice (Figure 6.2). Figure 6.2 shows both the Null-AAV8 and Cre-AAV8 mice have similar expression to the baseline mice (week 0, dotted line). Statistical comparisions determined the Cre-AAV8 expression was not statistically different when compared to the Null-AAV8 mice (Linear regression: Cre Slope= 0.1 week^{-1}; Cre slope vs zero, p=0.1; Null vs Cre slope, p=0.9).

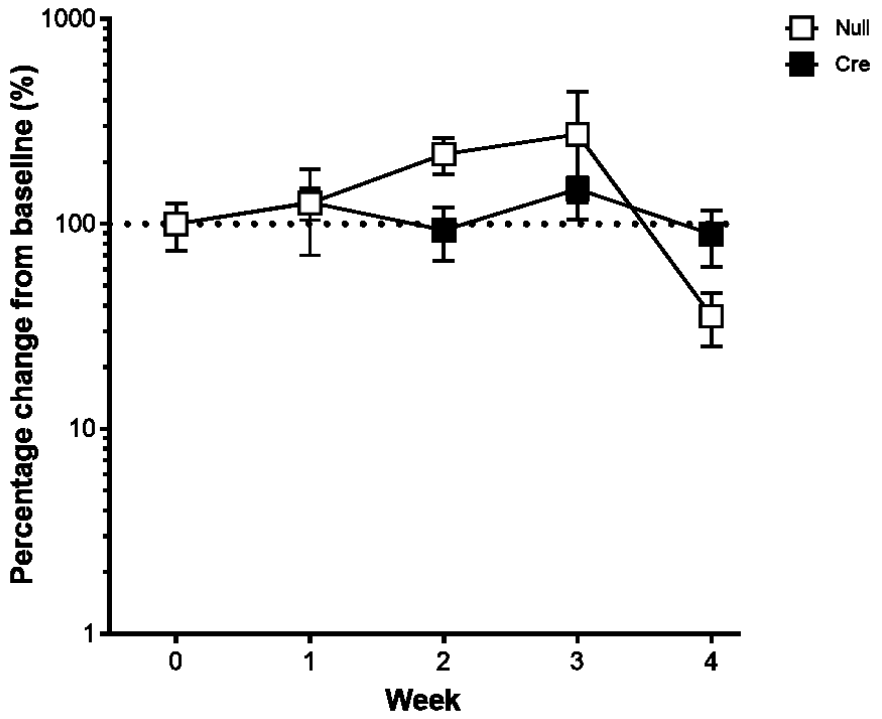

Figure 6.2 Dicer mRNA expression in the spleen in the Null and Cre-AAV8 treated mice

Dicer mRNA expression in the spleen was quantified through RT-qPCR. Dicer mRNA expression was measured in the baseline (untreated, week 0, dotted line), Null-AAV8 treated (white squares) and Cre-AAV8 treated (black squares) Dicer1$^{flox/flox}$ mice. MRNA measurements were carried out from week 1 to 4 in the Null and Cre-AAV8 treated mice. Each point was normalised to β-actin and then represented as a percentage in relation to the baseline mice. Error bars represent mean ±SD, n=5. Linear regression was used to determine whether Cre-AAV8 treated mice have significantly different expression to the Null-AAV8 treated mice (p=0.9)

I.2 Dicer mRNA in the kidney following AAV8 treatment

Dicer mRNA was measured in the kidney cortex and medulla of the baseline, Null-AAV8 and Cre-AAV8 treated *Dicer1*$^{flox/flox}$ mice (Figure 6.3A and B respectively). In the cortex, the Cre-AAV8 treated mice displayed a significantly lower mRNA expression than the Null-AAV8 (Linear regression: Cre Slope= -13.8 week^{-1}; Cre slope vs zero, p=0.003; Null vs Cre slope, p=0.005) (Figure 6.3A).

In contrast, the medulla of the Cre-AAV8 treated mice had comparable expression to the baseline (untreated) and Null-AAV8 treated mice (Linear regression: Cre Slope=-5.1 week^{-1}; Cre slope vs zero, p=0.43; Null vs Cre slope, p=0.9). (Figure 6.3B).

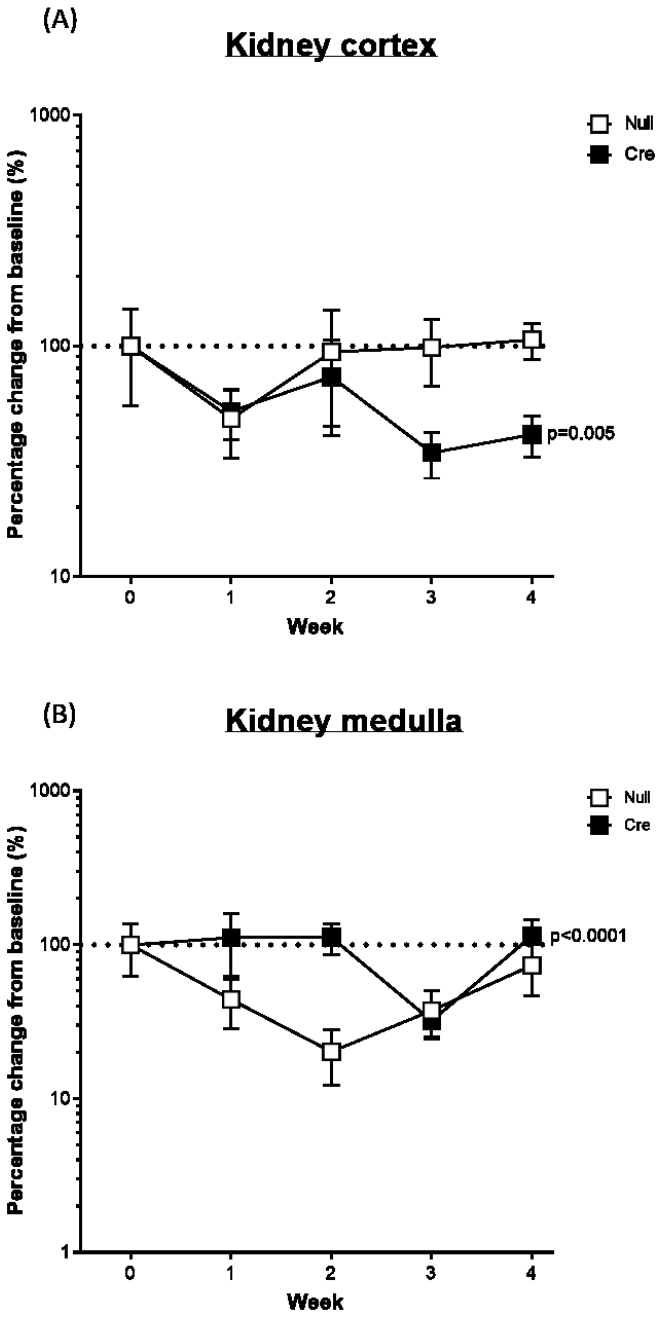

Figure 6.3 mRNA Dicer expression in the kidney following Null and Cre-AAV8 injection

Dicer mRNA expression in the kidney cortex (A) and medulla (B) quantified through RT-qPCR. Dicer mRNA expression was measured in the baseline (untreated, week 0, dotted line), Null-AAV8 treated (white squares) and Cre-AAV8 treated (black squares) Dicer1$^{flox/flox}$ mice. MRNA measurements were carried out from week 1 to 4 in the Null

and Cre-AAV8 treated mice. Each point was normalised to β-actin and then represented as a percentage in relation to the baseline mice. Error bars represent mean ±SD, n=5. Linear regression was used to determine whether Cre-AAV8 treated mice have significantly different expression to the Null-AAV8 treated mice (A: p=0.005; B: p=0.9).

I.3 Dicer mRNA expression in the brain, heart and lung

As before, Dicer mRNA expression was measured in the heart, lung and brain of the Null and Cre-AAV8 treated mice (Figure 6.4A, B and C respectively). In all three tissues, the Cre-AAV8 mice displayed a non-significant difference in Dicer mRNA expression, compared to the Null-AAV8 mice (Heart; linear regression: Cre Slope= 2.6 $week^{-1}$; Cre slope vs zero, p=0.4; Null vs Cre slope, p=0.5) (Lung; linear regression: Cre Slope=-12 $week^{-1}$; Cre slope vs zero, p=0.01; Null vs Cre slope, p=0.86) (Brain: Linear regression: Cre Slope=-16.39 $week^{-1}$; Cre slope vs zero, p=0<0.0001; Null vs Cre slope, p=0.07) (Figure 6.4C).

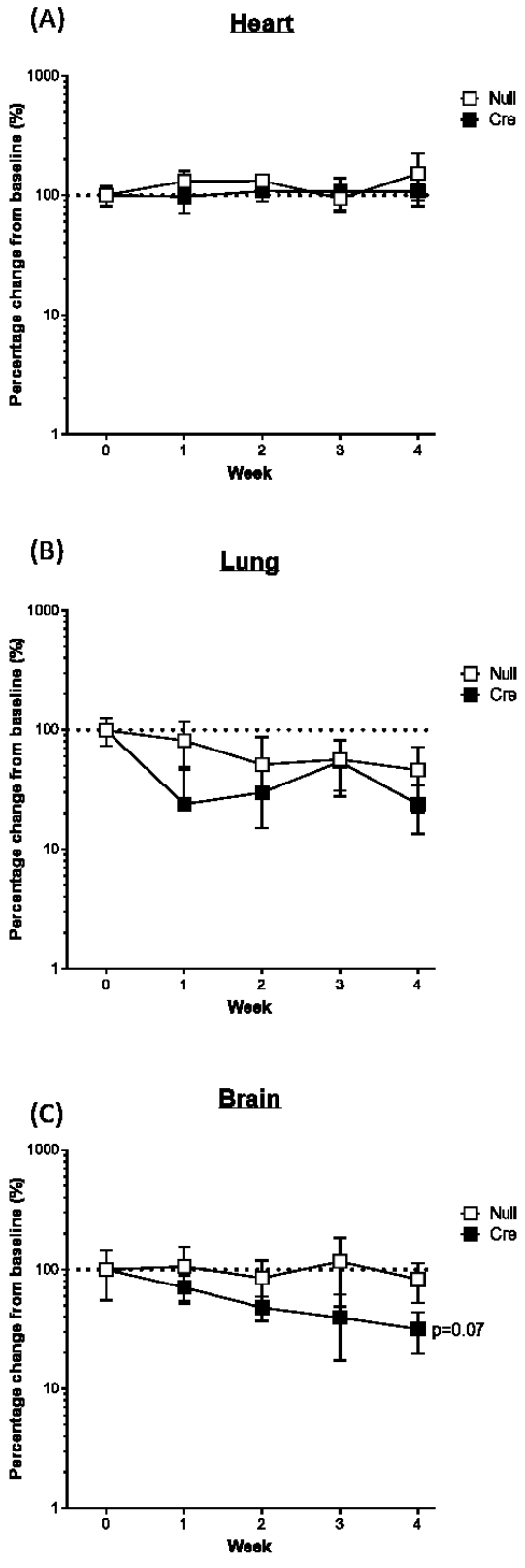

Figure 6.4 Dicer mRNA expression in the heart, lung and brain

Dicer mRNA expression in the heart (A), lung (B) and brain (C) quantified through RT-qPCR. Dicer mRNA expression was measured in the baseline (untreated, week 0, dotted line), Null-AAV8 treated (white squares) and Cre-AAV8 treated (black squares) Dicer1$^{flox/flox}$ mice. MRNA measurements were carried out from week 1 to 4 in the Null and Cre-AAV8 treated mice. In the heart, each point was normalised to GAPDH. In the lung and brain, each point was normalised to β-actin. Once normalised by the housekeeping gene, the data was then represented as a percentage in relation to the baseline mice. Error bars represent mean ±SD, n=5. Linear regression was used to determine whether Cre-AAV8 treated mice have significantly different expression to the Null-AAV8 treated mice (A: p=0.005; B: p=0.9, C: p=0.07).

I.4 MiR-122 is expression in all seven tissues analysed

Using RT-qPCR, Ct values of miRNA were measured in the liver (**Table 6.1**), spleen (**Table 6.2**), kidney cortex (**Table 6.3**) and medulla (**Table 6.4**), heart (**Table 6.5**), lung (**Table 6.6**) and brain (**Table 6.7**). For each tissue, miR-122-5p and its own tissue enriched miRNA were measured and assessed.

Table 6.1 Raw Ct miRNA values in the liver

		miR-122-5p					miR-192-5p					miR-151-3p				
W0	Baseline	12.21	12.12	12.425	11.89	12.31	17.3	17.03	17.57	17.455	17.675	22.885	22.81	22.875	22.825	23.265
W1	Null	11.89	12.235	12.46	11.785	11.64	17.635	17.73	17.97	17.54	17.035	22.99	22.85	23.065	22.58	22.57
	Cre	12.625	12.445	12.075	11.62	11.73	17.915	17.66	17.665	17.195	17.225	23.39	23.855	23.795	22.495	22.79
W2	Null	11.655	11.925	12.255	11.7	11.51	16.805	17.495	17.085	16.885	16.895	23.195	22.605	22.71	22.115	22.505
	Cre	13.045	12.88	12.945	13.105	13.135	18.595	18.935	19.135	18.92	18.69	23.78	23.06	22.975	23.135	22.87
W3	Null	13.215	11.805	12.24	11.635	11.64	17.47	18.635	17.675	16.96	16.995	22.655	23.79	23.05	22.345	22.57
	Cre	14.535	14.475	14.5	14.82	13.7	20.385	20.455	20.58	20.85	19.695	23.015	23.115	23.055	23.255	23.025
W4	Null	11.825	11.945	11.84	11.655	12.705	18.64	17.205	17.53	17.085	18.225	22.795	22.73	22.72	22.545	23.16
	Cre	15.875	15.8	16.875	14.93	15.53	22.09	21.99	22.835	21.135	20.93	23.045	23.25	23.45	22.985	22.89

MiRNA expression (miR-122-5p, miR-192-5p and miR-151-3p) in the liver of the baseline (untreated), Null-AAV8 and Cre-AAV8 treated Dicer1$^{flox/flox}$ mice. Measurements were taken from week 0-4 post AAV8 treatment. Each value represent an n=1 which is an average of the RT-qPCR duplicate reading.

Table 6.2 Raw Ct miRNA values in the spleen

		miR-122-5p					miR-146a-5p				
W0	Baseline	17.085	18.305	16.985	20.465	19.265	15.04	14.665	15.56	17.665	15.95
W1	Null	21.495	20.785	20.2	20.29	22.105	15.245	15.64	15.81	16.275	16.305
	Cre	23.565	21.045	21.725	23.075	20.725	16.75	16.885	16.345	16.24	15.76
W2	Null	21.89	20.835	20.44	21.355	22.25	16.09	16.09	15.955	14.97	14.775
	Cre	24.685	24.08	24.105	25.955	23.45	17.025	16.98	18.095	17.44	17.925
W3	Null	21.06	19.545	19.655	21.74	22.06	15.915	15.675	15.525	15.72	15.67
	Cre	24.67	24.395	25.39	25.49	23.815	15.665	15.605	15.69	15.8	14.77
W4	Null	22.59	18.965	22.095	22.385	22.22	15.795	15.62	15.12	15.52	14.93
	Cre	26.905	26.095	26.84	26.285	25.925	16.64	16.45	16.4	16.675	16.89

MiRNA expression (miR-122-5p and miR-146a-5p) in the spleen of the baseline (untreated), Null-AAV8 and Cre-AAV8 treated Dicer1$^{flox/flox}$ mice. Measurements were taken from week 0-4 post AAV8 treatment. Each value represent an n=1 which is an average of the RT-qPCR duplicate reading.

Table 6.3 Raw Ct miRNA values in the kidney cortex

		miR-122-5p					miR-192-5p					miR-196a-5p				
W0	Baseline	21.12	20.06	20.135	19.42	20.745	17.265	17.51	17.885	17.975	18.27	21.425	20.915	21.295	20.775	20.375
W1	Null	22.595	21.57	20.67	19.465	21.61	17.235	16.97	17.385	16.755	17.47	23.435	21.885	22.25	22.03	23.915
	Cre	21.835	22.49	21.085	20.125	21.64	16.98	16.905	16.325	16.035	17.15	22.475	22.265	22.31	22.025	22.745
W2	Null	20.125	21.04	18.955	21.79	19.115	16.895	17.79	17.815	17.525	16.73	23.34	21.855	22.01	21.59	22.89
	Cre	21.315	22.005	22.115	21.85	23.025	16.285	16.275	15.815	16.585	16.115	22.09	22.775	21.25	21.31	21.59
W3	Null	19.49	21.665	20.955	19.14	20.51	16.12	16.51	16.98	16.28	16.745	23.57	21.675	21.855	21.855	23.345
	Cre	22.99	23.155	22.935	23.695	22.465	16.86	16.405	16.495	16.87	16.355	22.375	22.01	21.905	21.72	20.935
W4	Null	19	20.39	22.02	20.565	19.57	16.43	16.83	16.875	16.685	16.835	21.785	22.17	21.13	21.7	21.37
	Cre	23.635	23.67	24.705	25.815	24.25	16.61	16.605	17.02	16.745	16.825	20.625	20.61	20.83	20.815	20.4

MiRNA expression (miR-122-5p, miR-192-5p and miR-196a-5p) in the kidney cortex of the baseline (untreated), Null-AAV8 and Cre-AAV8 treated Dicer1$^{flox/flox}$ mice. Measurements were taken from week 0-4 post AAV8 treatment. Each value represent an n=1 which is an average of the RT-qPCR duplicate reading.

Table 6.4 Raw Ct miRNA values in the kidney medulla

		miR-122-5p					miR-192-5p					miR-196a-5p				
W0	Baseline	20.21	20.68	18.7	19.6	18.79	17.425	17.31	17.32	17.93	17.965	21.925	21.68	22.07	21.915	21.875
W1	Null	20.555	22.095	20.715	17.605	20.525	17.105	17.135	17.305	16.83	16.95	22.415	23.115	23.145	22.245	22.49
	Cre	20.02	21.93	21.1	20.11	19.84	17.95	16.93	17.32	17.85	16.91	22.9	22.4	22.545	22.695	21.995
W2	Null	20.815	18.865	22.42	22.91	21.59	17.47	17.08	17.76	18.39	17.31	24.465	22.555	22.425	23.065	22.81
	Cre	24.495	23.715	22.38	23.09	21.93	17.21	17.775	17.76	17.53	17.47	22.85	22.69	22.395	22.38	22.925
W3	Null	19.135	20.88	20.875	17.965	18.95	17.105	17.995	17.55	17.41	17.26	22.175	21.96	22.5	22.14	21.75
	Cre	23.845	24.905	25.335	23.97	23.38	16.11	16.415	16.46	16.735	16.44	21.975	22.655	21.96	21.7	21.65
W4	Null	21.24	20.715	20.78	18.81	20.01	17.295	17.205	17.455	16.955	16.74	22.05	22.83	22.755	22.15	22.08
	Cre	24.37	22.675	23.59	24.865	22.705	19.245	16.51	17.09	16.565	16.255	23.755	21.88	21.75	21.46	21.365

MiRNA expression (miR-122-5p, miR-192-5p and miR-196-5p) in the kidney medulla of the baseline (untreated), Null-AAV8 and Cre-AAV8 treated Dicer1$^{flox/flox}$ mice. Measurements were taken from week 0-4 post AAV8 treatment. Each value represent an n=1 which is an average of the RT-qPCR duplicate reading.

Table 6.5 Raw Ct miRNA values in the heart

		miR-122-5p					miR-1-3p				
W0	Baseline	23.48	25.37	24.93	25.555	25.395	12.365	11.985	12.6	11.895	12.685
W1	Null	25.06	25.635	24.09	24.295	25.26	15.665	14.31	12.995	15.045	14.715
	Cre	27.195	25.025	26.735	25.14	26.75	14.555	13.19	12.63	14.835	12.2
W2	Null	25.94	25.825	26.01	25.725	25.92	14.42	13.65	13.685	13.925	14.08
	Cre	26.54	26.365	26.085	26.555	26.39	14.925	13.885	13.215	13.13	14.985
W3	Null	24.69	25.95	24.685	25.905	25.66	15.195	15.515	15.68	16.14	14.795
	Cre	26.155	27	26.625	26.455	26.65	13.915	13.66	13.455	11.835	13.725
W4	Null	25.6	26.195	24.62	26.135	24.7	14.36	14.34	14.415	14.74	14.29
	Cre	26.535	26.32	26.46	25.935	26.685	13.975	14.31	13.465	14	13.575

MiRNA expression (miR-122-5p and miR-1-3p) in the heart of the baseline (untreated), Null-AAV8 and Cre-AAV8 treated Dicer1$^{flox/flox}$ mice. Measurements were taken from week 0-4 post AAV8 treatment. Each value represent an n=1 which is an average of the RT-qPCR duplicate reading.

Table 6.6 Raw Ct miRNA values in the lung

		miR-122-5p					miR-195a-5p				
W0	Baseline	23.305	24.085	23.72	24.18	24.725	14.415	13.715	13.985	13.9	14.16
W1	Null	24.62	22.615	25.335	24.72	26.17	15.53	15.555	15.56	15.735	15.9
	Cre	23.755	23.62	24.14	24.04	24.76	13.555	14.4	14	14.135	14.185
W2	Null	25.2	24.64	25.34	24.81		14.605	14.67	14.9	14.745	
	Cre	25.015	24.7	24.55	24.37	24.585	14.385	14.555	14.575	14.005	14.075
W3	Null	22.55	24.4	24.025	24.555	24.225	13.935	14.415	14.1	14.28	14.07
	Cre	27.115	24.6	24.505	24.385	24.34	14.81	14.445	13.49	15.015	14.61
W4	Null	24.005	24.825	22.525	25.125	22.725	14.28	14.25	14.71	14.85	14.88
	Cre	24.935	25.175	25.73	25.425	26.245	13.61	14.475	15.475	15.415	15.65

MiRNA expression (miR-122-5p and miR-195a-5p) in the lung of the baseline (untreated), Null-AAV8 and Cre-AAV8 treated Dicer1$^{flox/flox}$ mice. Measurements were taken from week 0-4 post AAV8 treatment. Each value represent an n=1 which is an average of the RT-qPCR duplicate reading.

Table 6.7 Raw Ct miRNA values in the Brain

		miR-122-5p					miR-124-3p				
W0	Baseline	25.25	25.045	25.09	25.55		13.62	12.895	12.24	12.67	
W1	Null	25.935	25.385	25.62	25.58	25.6	14.52	14.015	13.47	13.775	14.505
	Cre	25.9	26.875	25.68	25.67	26.01	14.96	14.45	14.295	14.12	13.735
W2	Null	26.305	25.455	25.29	25.555	25.065	13.18	13.535	13.95	12.995	13.01
	Cre	25.99	25.805	25.8	25.995	26.03	14.26	14.305	14.11	14.575	13.875
W3	Null	25.855	25.57	26.295	25.675	25.315	14.395	14.58	14.965	13.985	14.865
	Cre	26.81	26.295	26.155	26.255	26.265	15.19	14.995	15.37	15.295	15.26
W4	Null	25.78	25.2	25.825	25.775	25.49	14.145	13.51	13.475	13.68	13.29
	Cre	26.015	26.805	25.755	26.165	25.97	14.98	15.03	13.43	14.08	13.64

MiRNA expression (miR-122-5p and miR-124-3p) in the brain of the baseline (untreated), Null-AAV8 and Cre-AAV8 treated Dicer1$^{flox/flox}$ mice. Measurements were taken from week 0-4 post AAV8 treatment. Each value represent an n=1 which is an average of the RT-qPCR duplicate reading.

Table 6.8 Raw Ct pri-miR-122 values of the liver and spleen

		Liver					Spleen				
W0	Baseline	25.24	25.765	26.84	26.105	27.205	35	35	35	35	35
W1	Null	25.125	26.495	26.335	26.765	27.405	35	35	35	35	35
	Cre	23.77	25.54	25.31	25.5	25.5	35	35	35	35	35
W2	Null	24.515	24.945	25.195	24.08	24.625	35	35	35	35	35
	Cre	24.135	24.32	24.135	25.395	24.62	35	35	35	35	35
W3	Null	23.165	23.25	23.335	23.36	23.86	35	35	35	35	35
	Cre	23.735	25.8	23.68	23.92	24.575	35	35	35	35	35
W4	Null	24.995	24.295	26.09	23.78	25.125	35	35	35	35	35
	Cre	26.835	23.05	24.52	22.855	24.845	35	35	35	35	35

Pri-miR-122 expression in the liver and spleen of the baseline (untreated), Null-AAV8 and Cre-AAV8 treated Dicer1$^{flox/flox}$ mice. Measurements were taken from week 0-4 post AAV8 treatment. Each value represent an n=1 which is an average of the RT-qPCR duplicate reading.

Table 6.9 Raw Ct pri-miR-122 values in the Kidney cortex and medulla

		Kidney cortex					**Kidney medulla**				
W0	Baseline	35	35	35	34.72	35	35	36.165	34.035	33.425	35
W1	Null	35	35	35	34.45	35	35	37.5	35	32.82	35
	Cre	37.5	37.5	40	35	35	35	35	35	35	35
W2	Null	35	35	35	35	35	35	35	35	35	35
	Cre	35	35	35	35	35	35	35	35	35	35
W3	Null	35	35	35	35	35	35	35	35	32.455	33.37
	Cre	35	35	35	35	35	35	35	35	34.23	33.875
W4	Null	35	35	35	35	35	35	35	40	37.15	35
	Cre	35	35	35	35	35	35	35	35	35	35

Pri-miR-122 expression in the kidney cortex and medulla of the baseline (untreated), Null-AAV8 and Cre-AAV8 treated Dicer1$^{flox/flox}$ mice. Measurements were taken from week 0-4 post AAV8 treatment. Each value represent an n=1 which is an average of the RT-qPCR duplicate reading.

Table 6.10 Raw Ct miRNA values in the plasma

		miR-122-5p					miR-192-5p					miR-196-5p				
W0	Baseline	26.17	26.44	26.53	25.5	26.07	26.91	26.67	27.76	27.26	26.54	29	30.07	30.095	29.625	28.975
W1	Null	16.89	23.145	18.57	26.245	26.075	20.83	24.755	22.21	26.315	27.065	27.065	27.12	27.41	28.65	29.095
	Cre	20.27	19.33	19.55	20.135		23.39	23.765	23.33	25.03		30.535	28.09	29.07	29.11	
W2	Null	24.81	23.825	21.14	23.25		24.205	28.865	25.22	25.53		27.5	29.4	29.34	28.505	
	Cre	23.515	26.115	19.91	25.14	21.84	26.975	25.075	23.46	26.62	24.55	30.06	29.155	28.095	30.74	29.195
W3	Null	17.38	15.635	19.92	19.255		22.21	20.06	22.83	23.675		27.69	28.605	28.31	28.005	
	Cre	19.97	23.76	25.41	22.035	20.34	22.59	22.715	23.96	23.74	24.56	28.06	27.795	27.425	28.34	27.555
W4	Null	19.925	25.65	15.34	23.425	16.43	23.665	26.43	19.41	26.315	20.565	29.94	30.07	26.185	30.605	27.28
	Cre	26.175	24.615	23.93	21.235	26.195	25.07	25	24.57	25.41	26.9	29.06	27.755	28.265	27.96	29.645

MiRNA expression (miR-122-5p, miR-192-5p and miR-151-3p) in the plasma of the baseline (untreated), Null-AAV8 and Cre-AAV8 treated Dicer1$^{flox/flox}$ mice. Measurements were taken from week 0-4 post AAV8 treatment. Each value represent an n=1 which is an average of the RT-qPCR duplicate reading.

I.5 Dicer mRNA expression is significantly lower following Cre-AAV8 treatment

To determine whether a lower dose of the Cre-AAV8 was effective at knocking down hepatic *Dicer1*, Dicer mRNA was assessed in the liver. The Cre-AAV8 treated *Dicer1* $^{flox/flox}$ mice displayed a significant loss of Dicer mRNA expression, compared to the Null-AAV8 treated group (ANOVA: saline Null vs Cre, p=0.0003)(**Figure 6.5**). With increasing doses of paracetamol, the expression of Dicer mRNA displays a non-significant increase in the baseline and Cre-AAV8 treated mice compared to the saline control (**Figure 6.5**).

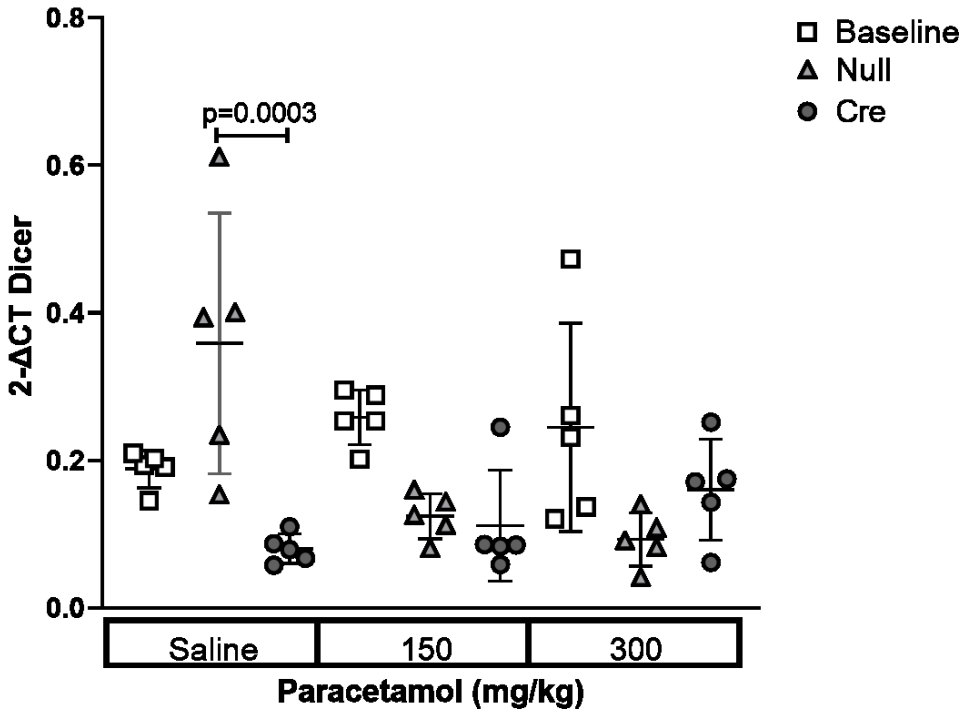

Figure 6.5 Dicer mRNA in the liver of the *Dicer* $^{flox/flox}$ mice following AAV8 injection

Dicer mRNA expression measured following saline, 150mg/kg paracetamol and 300mg/kg paracetamol in the liver of the baseline (untreated, white squares), Null-AAV8 (light grey triangles) and Cre-AAV8 (dark grey circles) treated Dicer1 $^{flox/flox}$ *mice. MRNA measurements were taken 3 weeks post AAV8 treatment and 6 hours following paracetamol dosing. Each point was normalised to β-actin, error bars represent mean ±SD, n=5. A multiple comparison two-way ANOVA was used to determine if expression was significant across all 9 sub-treatment groups. Dicer mRNA expression did not decrease in the spleen and kidney following Cre-AAV8 treatment.*

*Dicer mRNA was measured in the spleen, kidney cortex and medulla of the baseline, Null-AAV8 and Cre-AAV8 mice treated with saline, 150mg/kg paracetamol and 300mg/kg paracetamol (**Figure 6.6**). In all three tissues, Dicer mRNA expression did not significantly decrease following Cre-AAV8 injection in comparison to the baseline and Null-AAV8 mice (**Figure 6.6**A-C).*

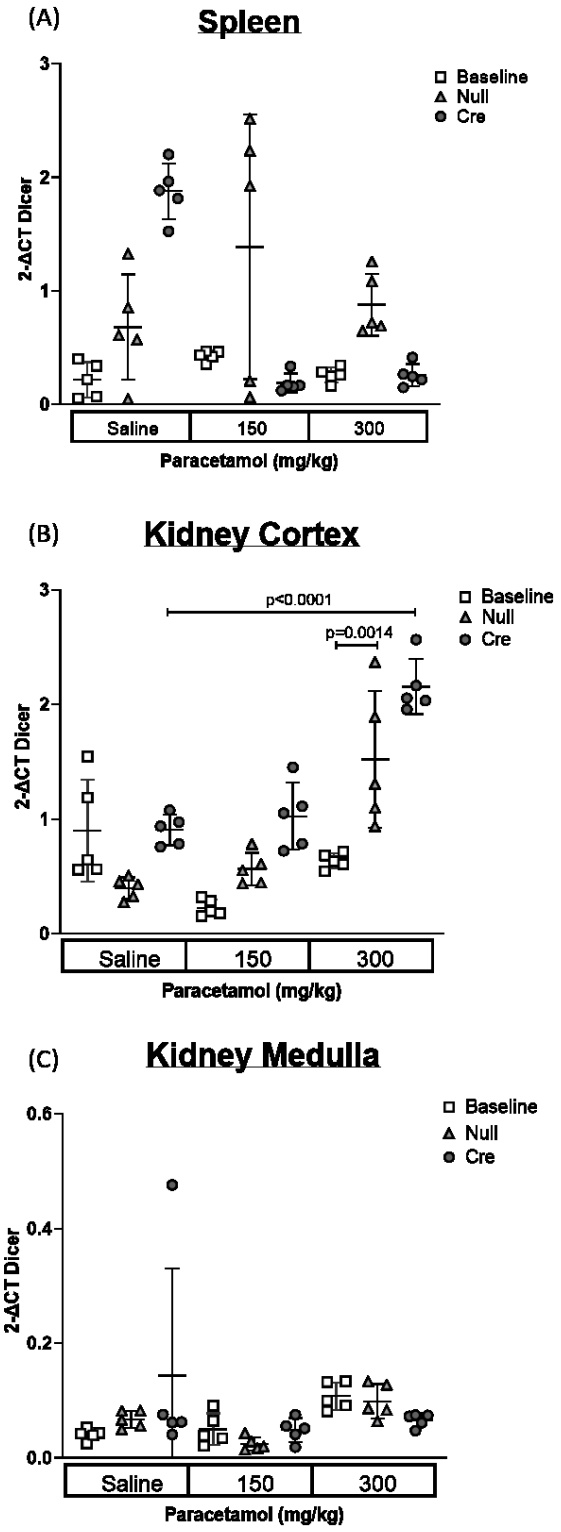

Figure 6.6 Dicer expression does not decrease in the spleen, kidney cortex and kidney medulla following Cre-AAV8 injection

Dicer mRNA was measured in the (A) spleen, (B) kidney cortex and (C) kidney medulla of the male Dicer-floxed mice. MRNA measurements were carried out via RT-qPCR 3 weeks following baseline (white squares), Null (light grey triangles) and Cre-AAV8 (dark grey circles) treatment and 6 hours after saline, 150mg/kg and 300mg/kg of paracetamol. In the spleen and kidney medulla, the data were normalised to GAPDH. In the kidney cortex, each point was normalised to β-actin, error bars represent mean ±SD, n=5. A multiple comparison two-way ANOVA was used to determine if the expression is significantly different between treatment groups.

I.6 Dicer mRNA expression in the heart, lung and brain

Again, Dicer mRNA was measured in baseline, Null-AAV8 and Cre-AAV8 mice treated with saline, 150mg/kg and 300mg/kg paracetamol. In the heart, lung and brain, Dicer mRNA expression did not significantly decrease following Null-AAV8 or Cre-AAV8 injection, when compared to the baseline mice (**Figure 6.7**)

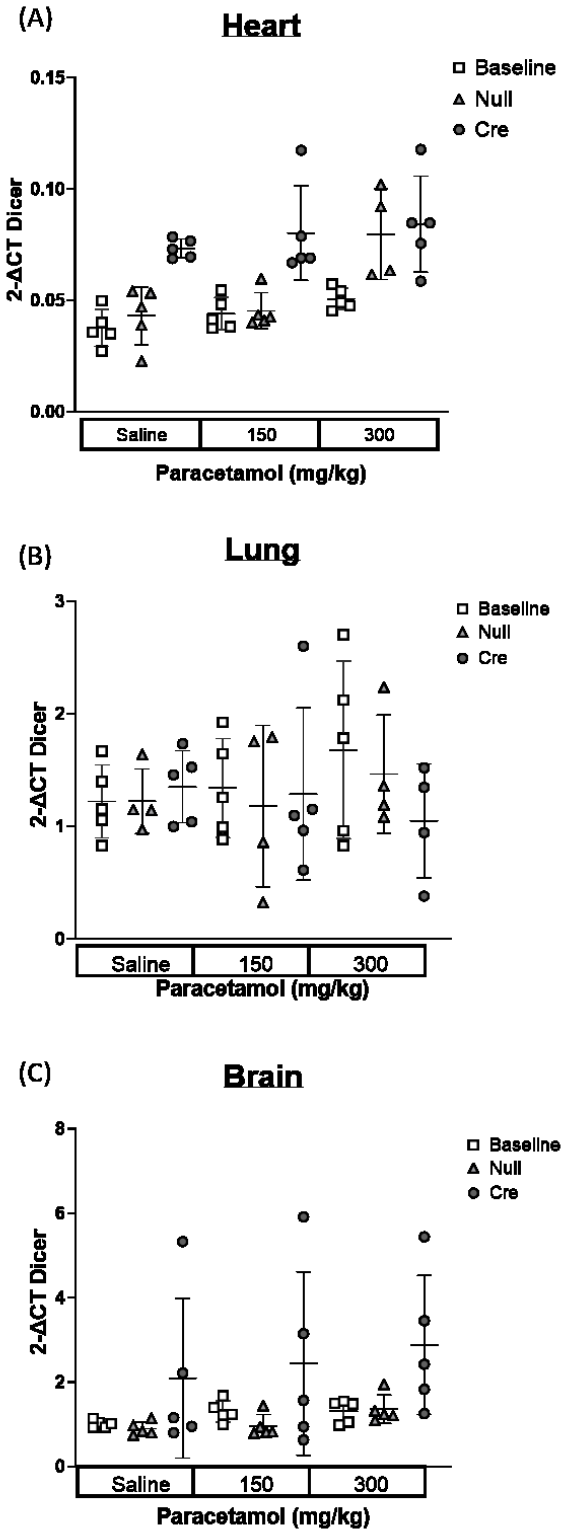

Figure 6.7 Dicer mRNA is unchanged the heart, lung and brain following Cre-AAV8 injection

Dicer mRNA was measured in the (A) heart, (B) lung and (C) brain of the male Dicer1 $^{flox/flox}$ mice. MiRNA measurements were carried out via RT-qPCR 3 weeks following baseline (white squares), Null-AAV8 (light grey triangles) and Cre-AAV8 (dark grey circles) treatment and 6 hours after saline, 150mg/kg and 300mg/kg of paracetamol. Data were normalised to β-actin in the lung and brain and in the heart, data were normalised to GAPDH. Error bars represent mean ±SD, n=5 (lung: Null saline, 150mg/kg and 300mg/kg and Cre 300mg/kg, n=4). Multiple comparison two-way ANOVA was used to determine if the expression is significantly different between treatment groups

I.6.1 Expression of cyp1a2 and cyp2e1 in the liver and kidney

Using RT-qPCR, Ct values of cyp1a2 and cyp2e1 mRNA were measured in the liver (**Table 6.11**), kidney cortex (**Table 6.12**) and medulla (**Table 6.13**). It was noted that both sections of the kidney had lower levels of cyp1a2 and cyp2e1 mRNA expression, compared to the liver.

Table 6.11 Raw Ct values of CYP450 enzymes in the liver of the healthy *Dicer1* $^{flox/flox}$ mice

		CYP1A2					CYP2E1				
W0	**Baseline**	**21.395**	**22.78**	**20.85**	**22.25**	**21.67**	**20.06**	**20.54**	**21.035**	**19.86**	**20.13**
W1	Null	21.77	20.93	21.56	21.13	22.335	20.16	19.91	20.01	20.065	20.08
	Cre	20.555	21.705	21.26	20.375	20.58	18.98	20.19	19.73	20.63	19.52
W2	Null	22.71	20.78	20.955	20.75	21.53	19.265	19.89	19.83	19.555	19.8
	Cre	19.955	20.34	19.735	20.595	21.21	19.63	18.86	18.63	19.5	20.005
W3	Null	20.97	21.715	22.285	23.47	21.575	19.675	20.415	20.665	19.845	19.905
	Cre	19.08	19.2	18.975	19.755	19.68	18.615	18.68	19.27	19.245	18.93
W4	Null	20.965	21.14	21.135	21.61	19.86	19.69	19.95	20.18	20.875	18.3
	Cre	18.63	19.205	19.69	18.945	19.065	18.24	18.91	19.25	19.15	19.545

MRNA expression (cyp1a2 and cyp2e1) in the liver of the baseline (untreated), Null-AAV8 and Cre-AAV8 treated Dicer1$^{flox/flox}$ mice. Measurements were taken from week 0-4 post AAV8 treatment. Each value represents an n=1 which is an average of the RT-qPCR duplicate reading.

Table 6.12 Raw Ct values of CYP450 enzymes in the kidney cortex of the healthy *Dicer1* $^{flox/flox}$ mice

		CYP1A2					CYP2E1				
W0	**Baseline**	**32.115**	**30.08**	**34.26**	**33.445**	**35**	**22.2**	**21.51**	**21.93**	**21.98**	**22.78**
W1	Null	40	40	40	40	40	21.415	21.025	21.005	23.375	23.87
	Cre	34.365	35	33.83	32.445	32.34	22.14	21.91	21.89	24.84	25.405
W2	Null	40	40	40	40	40	21.75	21.605	21.495	24.995	25.175
	Cre	32.815	32.26	35	33.95	34.74	22.415	22.265	21.61	23.415	25.83
W3	Null	35	34.48	35	31.875	33.89	22	21.075	20.67	24.375	24.965
	Cre	32.28	33.15	32.5	33.28	32.485	22.29	21.94	21.645	23.25	25.825
W4	Null	34.12	35	35	34.165	29.91	21	20.875	20.85	24.9	25.255
	Cre	32.48	31.235	33.81	31.935	31.775	22.045	21.685	21.755	25.795	26.125

MRNA expression (cyp1a2 and cyp2e1) in the kidney cortex of the baseline (untreated), Null-AAV8 and Cre-AAV8 treated Dicer1$^{flox/flox}$ mice. Measurements were taken from week 0-4 post AAV8 treatment. Each value represents an n=1 which is an average of the RT-qPCR duplicate reading.

Table 6.13 Raw Ct values of CYP450 enzymes in the kidney medulla of the healthy *Dicer1* $^{flox/flox}$ mice

		CYP1A2					CYP2E1				
W0	**Baseline**	**30.52**	**29.405**	**29.725**	**31.195**	**32.34**	**22.2**	**21.51**	**21.93**	**21.98**	**22.78**
W1	Null	32.4	33.375	31.725	28.305	30.855	21.415	21.025	21.005	23.375	23.87
	Cre	30.32	34	35	30.145	30.77	22.14	21.91	21.89	24.84	25.405
W2	Null	31.495	30.845	32.195	35	33.185	21.75	21.605	21.495	24.995	25.175
	Cre	30.31	32.18	32.015	32.37	33.965	22.415	22.265	21.61	23.415	25.83
W3	Null	32.665	32.81	31.325	28.205	30.26	22	21.075	20.67	24.375	24.965
	Cre	31.29	30.695	31.255	30.99	29.86	22.29	21.94	21.645	23.25	25.825
W4	Null	33.875	32.615	33.17	29.89	30.365	21	20.875	20.85	24.9	25.255
	Cre	29.475	29.275	30.39	34.62	29.7	22.045	21.685	21.755	25.795	26.125

MRNA expression (cyp1a2 and cyp2e1) in the kidney cortex of the baseline (untreated), Null-AAV8 and Cre-AAV8 treated Dicer1$^{flox/flox}$ mice. Measurements were taken from week 0-4 post AAV8 treatment. Each value represents an n=1 which is an average of the RT-qPCR duplicate reading.